Investigation of Carbon Capture Technology – Optimization of Microbial Electrochemical Cells:

A Study on Single-Chamber, Flow Cell, and Zero-Gap Reactor Configurations

Dissertation

der Mathematisch-Naturwissenschaftlichen Fakultät

der Eberhard Karls Universität Tübingen

zur Erlangung des Grades eines

Doktors der Naturwissenschaften

(Dr. rer. nat.)

vorgelegt von

Nils Rohbohm

aus Wesel

Tübingen

2024

Gedruckt mit Genehmigung der Mathematisch-Naturwissenschaftlichen Fakultät der Eberhard Karls Universität Tübingen.

Tag der mündlichen Qualifikation:	07.06.2024
Dekan:	Prof. Dr. Thilo Stehle
1. Berichterstatter/in:	Prof. Dr. Largus T. Angenent
2. Berichterstatter/in:	Prof. Dr. Uwe Schröder

Acknowledgments

Firstly, I would like to thank my advisor, Prof. Dr. Lars Angenent, for welcoming me into his lab and providing guidance throughout my PhD journey. I am grateful for his faith in my ability to pursue a PhD in biotechnology despite my background in chemistry. Lars has not only enhanced my scientific expertise by encouraging innovative thinking but has also believed in my potential, motivating me to excel. His push towards improving my scientific writing and speaker skills has also been invaluable. I thank the freedom and trust he granted me for conducting research, especially in tinkering, and the opportunity to engage in the creation of two DFG proposals, one of which was successfully funded.

Secondly, I extend my thanks to my thesis committee members, Prof. Dr. Uwe Schröder, Prof. Dr. Udo Weimar, and Prof. Dr. Andreas Kappler, for their time and reviews of my thesis. Special thanks to Prof. Dr. Andreas Kappler and his lab members for their assistance and support during my PhD. I thank Prof. Dr. Uwe Schröder for the discussions that led us to reevaluate the mechanisms of oxygen inhibition.

Thirdly, my gratitude goes to the bioelectrochemistry subgroup. Dr. Tianran Sun deserves special mention for his mentorship during the initial phase of my PhD, always making time and providing support whenever needed. I also appreciate his efforts to maintain biweekly meetings despite challenging time differences. I am also thankful to Dr. Ramiro Blasco Gómez for introducing me to bioelectrochemistry and to Ulrike Biehain for her continuous support and motivation.

Furthermore, I am grateful to all members of the Environmental Biotechnology group. Joining the lab in 2019, I have witnessed its growth and have had the privilege of contributing to its development while forming lasting friendships. I am particularly thankful to Dr. Christian Klask, Dr. Christian Fink, and Dr. Isabella Casini for their discussion and support at work and beyond work hours. Thank you, Dr. Saskia Baur and Nicolai Kreitli, for project-related discussions and for organizing the lab. I thank all of my other colleagues who helped during my PhD and whom I can call friends: Dr. Sarah Schulz, Dr. Pengfei Xia, Dr. Sebastian Beblawy, Lucas Mühling, Ulrike Biehain,

Dr. Han Wang, Patrick Schweizer, Caroline Schlaiß, Kurt Gemeinhardt, Dr. Laura Rovira Alsina, Julia Schumacher, Hiroki Yoshida, Antonio Velazquez, Mohamed Baboul, Aaron Zipperle, Garmani Thein, and Emma Jones.

Additionally, when I started my PhD at the Max-Planck institute for biology, I was welcomed by the Environmental Biotechnology group and colleagues from the MPI. For this, I thank Dr. Jaime Leonardo Moreno, Andrea Borbon, Dr. Liam Fitzstevens, Dr. Albane Ruaud, and Dr. Stacey Heaver.

I also acknowledge the funding from the Alexander von Humboldt Foundation and the Deutsche Forschungsgemeinschaft, which facilitated my research and provided opportunities to connect with fellow scientists, notably the DFG Ebiotech SPP.

Finally, my deepest appreciation goes to my friends and family for their understanding and support throughout this journey. I thank my parents, Petra and Dirk Rohbohm, and my brother Marco for their support in every life decision.

Summary

Rapid population growth is leading to increased resource demand, resulting in a surge of pollution and a raised need for energy. This situation highlights the need to transition from traditional energy sources, such as nuclear power and fossil fuels, to more sustainable and carbon-neutral options. Microbial electrochemical technologies have emerged as a possible solution to reduce environmental impact by turning industrial waste into valuable resources. At the heart of this innovation is a process known as microbial electrosynthesis, powered by preferably renewable electrical energy. This process harnesses renewable electrical power to transform carbon sources into complex, electron-rich organic molecules. These molecules can be used as sustainable fuels or raw materials for various chemical products. When powered by renewable energy, microbial electrosynthesis holds the potential to operate sustainably and help to achieve overall carbon neutrality. This is largely thanks to autotrophic microbes, which can reduce carbon dioxide, using it as their only carbon source.

Despite its potential, microbial electrosynthesis encounters several limitations and technical challenges that hinder its broader application. These challenges encompass low product yields, inefficient electron transfer between microbes and electrodes, a constrained variety of chemical products, and a pressing need for a more comprehensive understanding of microbial physiology. Addressing these obstacles requires a collaborative interdisciplinary approach, merging insights and methodologies from bioelectrochemistry, microbiology, and engineering.

This dissertation specifically targeted the advancement of microbial electrosynthesis for industrial use. Utilizing *Methanothermobacter thermautotrophicus*, which is known for its high methane production rates in the power-to-gas concept, my research focused on optimizing bioelectrochemical cell performance across different reactor designs. The first part involved developing a single-chamber bioelectrochemical cell that eliminated the need for ion-exchange membranes. This was achieved by substituting the oxygen evolution reaction with a carbon oxidation

reaction and employing a sacrificial carbon-based anode. The second part focused on a flow electrolyzer, examining various shutdown strategies using three different electrode materials (platinized titanium, nickel, and graphite) in collaboration with Electrochaea GmbH. Lastly, the final part studied a zero-gap bioelectrochemical cell to evaluate performance differences between a vapor-fed and a liquid-fed anode chamber, assessing which setup offers better operating efficiency.

Zusammenfassung

Das schnelle Wachstum der Weltbevölkerung treibt die Nachfrage nach Ressourcen in die Höhe, was zu einer verstärkten Umweltverschmutzung und einem gesteigerten Energiebedarf führt. Vor diesem Hintergrund wird die Notwendigkeit deutlich, von traditionellen Energiequellen wie Kernkraft und fossilen Brennstoffen auf umweltfreundlichere und kohlenstoffneutrale Alternativen umzusteigen. Hier bieten mikrobielle elektrochemische Technologien eine vielversprechende Möglichkeit, den ökologischen Fußabdruck zu verringern, indem sie industrielle Abfälle in wertvolle Ressourcen umwandeln. Im Zentrum dieser Innovation steht die mikrobielle Elektrosynthese, die durch erneuerbare elektrische Energie angetrieben wird und die Kraft dieser Energie nutzt, um Kohlenstoffquellen in komplexe organische Moleküle umzuwandeln. Diese Moleküle können dann als nachhaltige Treibstoffe oder als Grundstoffe für chemische Produkte genutzt werden. Wenn mikrobielle Elektrosynthese mit erneuerbarer Energie betrieben wird, kann der Prozess nachhaltig durchgeführt werden und zur Kohlenstoffneutralität beitragen, vor allem dank autotropher Mikroben, die Kohlendioxid als einzige Kohlenstoffquelle nutzen.

Trotz ihres Potenzials stößt die mikrobielle Elektrosynthese auf mehrere Einschränkungen und technische Herausforderungen, die ihre breite Anwendung verhindern. Zu diesen Herausforderungen gehören geringe Produktausbeuten, ineffizienter Elektronentransfer zwischen Mikroben und Elektroden, eine begrenzte Vielfalt an chemischen Produkten und die dringende Notwendigkeit eines umfassenderen Verständnisses der mikrobiellen Physiologie. Um diese Herausforderungen zu überwinden, ist ein interdisziplinärer Ansatz erforderlich, bei dem Erkenntnisse und Methoden aus der Bioelektrochemie, der Mikrobiologie und dem Ingenieurwesen zusammengeführt werden.

Meine Dissertation untersucht die Optimierung der mikrobiellen Elektrosynthese für den industriellen Einsatz. Unter Verwendung von *Methanothermobacter thermautotrophicus*, der für seine hohen Methanproduktionsraten im Power-to-Gas-Konzept bekannt ist, konzentrierte sich meine Forschung auf die Optimierung der

Leistung bioelektrochemischer Zellen in verschiedenen Reaktordesigns. Im ersten Teil ging es um die Entwicklung einer Einkammer bioelektrochemischen Zelle, bei der keine Ionenaustauschmembran benötigt wurde. Dies wurde erreicht, indem die Sauerstoffbildungsreaktion durch eine Kohlenstoffoxidationsreaktion ersetzt wurde und eine Opferanode auf Kohlenstoffbasis verwendet wurde. Der zweite Teil konzentrierte sich auf einen Durchflusselektrolyseur, wobei in Zusammenarbeit mit der Electrochaea GmbH verschiedene Abschaltstrategien unter Verwendung von drei verschiedenen Elektrodenmaterialien (platiniertes Titan, Nickel und Graphit) untersucht wurden. Im letzten Teil wurde eine *Zero-Gap* bioelektrochemische Zelle untersucht, um die Leistungsunterschiede zwischen einer dampfgespeisten und einer flüssigkeitsgespeisten Anodenkammer zu bewerten und festzustellen, welche Anordnung die höhere Effizienz bietet.

Table of Contents

Acknowledgments iii
Summary v
Zusammenfassung vii
Table of Contents ix
Chapter 1 Introduction 1
1.1. Motivation 1
1.2. Organization and summary of chapters 4
Chapter 2 Literature review 7
2.1. Microbial fuel cell 8
2.2. Microbial electrosynthesis 8
2.3. Ion Exchange Membranes in Microbial Fuel Cells and Microbial Electrosynthesis Systems 12
2.4. Single-chamber systems 14
2.5. The need to change the electrode material 15
2.6. Carbon-assisted water electrolysis (CAWE) 17
2.7. Magnetite mineral as electrode material 18
2.8. Redox-active organic electrodes 22
2.9. Reactor designs of microbial electrosynthesis 23
2.10. Microbe of choice: *M. thermautotrophicus* 25
Chapter 3 Carbon oxidation with sacrificial anodes to inhibit O2 evolution in membrane-less bioelectrochemical systems for microbial electrosynthesis 27
3.1. Author Contributions 27
3.2. Abstract 27
3.3. Broader context 29
3.4. Introduction 29
3.5. Results and discussion 34
3.5.1. The minimal required cell potential is lower for carbon oxidation than for O_2 evolution at the anode, while the kinetics of the carbon oxidation reaction is higher 34
3.5.2. Carbon-based anodes with and without iron species circumvented the need for a membrane, opening the possibility of a membrane-less system 35

3.5.3. Different carbon materials as the anode affected the CH_4 production duration of microbial electrosynthesis, and competitive methane production rates were achieved to other BES studies. 38

3.5.4. The duration of methane production in the single-chamber bioelectrochemical system was only a few days due to oxidation of reduced sulfur compounds at the anode and a resulting sulfur limitation. 43

3.5.5. Soluble iron elongated the optimum-performance period for reasons that are related to sulfide oxidation 46

3.5.6. Magnetite, which is an alternative redox mediator to soluble iron, shortened the optimum performance period. 49

3.5.7. When sulfur source limitations are overcome, carbon at the anode would become a limiting factor 49

3.5.8. A final limitation would be the impact of carbon corrosion on the CH_4 production rates 50

3.5.9. Carbon oxidation with sacrificial anodes for single-chamber BES is ready for research purposes within the field of microbial electrosynthesis 53

3.5.10. Before the industrial application of carbon oxidation with sacrificial anodes in BES for microbial electrosynthesis can commence, several breakthroughs are required. 54

3.6. Conclusion 55

3.7. Experimental section 55

3.7.1. Chemicals, strain, and medium 55

3.7.2. Preparation of carbon-based electrodes 56

3.7.3. Measurement of dissolved O_2 57

3.7.4. Sample analyses 57

3.7.5. Electrochemical system 58

3.7.6. Immobilization of magnetite 59

3.7.7. SEM, EDX, X-ray diffraction, and FTIR 59

3.8. Acknowledgements 60

Chapter 4 Performance effect on different shutdown methods of three electrode materials for power-to-gas with electromethanogenesis 61

4.1. Author Contributions 61

4.2. Abstract 61

4.3. Introduction 62

4.4. Materials and methods 65

4.4.1. Chemicals, strain, and medium 65

4.4.2. Analytics 65

4.4.3. Operating conditions 66

4.4.4. Startup and shutdown procedure 67
4.4.5. Equations 68
4.5. Results and Discussion 69
4.5.1. The microbial electrolysis cell using a platinized titanium cathode exhibited higher production rates compared to those with graphite and nickel cathodes during interrupted power supply 69
4.5.2. Recovery of CH_4 is influenced by the pH after power supply interruption and leads to nickel dissolution 71
4.5.3. Nickel cathode effectiveness is compromised by elevated nickel concentrations following power supply interruptions, impacting CH_4 production and recovery times. 74
4.5.4. Gradual degradation of the nickel electrode in a microbial electrolysis cell over ten weeks is less impacted by the different shutdown modes but by other factors 77
4.5.5. More prolonged power interruption influences the recovery of CH_4 production 79
4.5.6. Short-term O_2 exposure did not harm the CH_4 recovery time of the microbe 80
4.5.7. The operating conditions of the microbial electrochemical cell promote water and gas crossover through the ion-exchange membrane 81
4.5.8. The flow rate influences the current generation and has a higher effect on the microbial electrochemical cell performance 83
4.6. Limitations of the study 84
4.7. Conclusion 86
4.8. Acknowledgements 87
Chapter 5 A comparison study between liquid- and vapor-fed Zero-gap bioelectrolysis cells 89
5.1. Author contributions 89
5.2. Abstract 90
5.3. Introduction 90
5.4. Results 93
5.4.1. Nafion 117 membrane outperformed Htec-PFSA membrane in terms of volumetric CH_4 production within liquid-fed zero-gap bioelectrochemical cells, thereby guiding the selection of Nafion 117 for subsequent experimentation in a vapor-fed system 93
5.4.2. Nafion 117 membrane exhibits better stability and efficiency compared to the Htec-PFSA membrane, evidenced by lower increases in cell voltage and better H_2 production efficiency 96

5.4.3. Electromethanogenesis in a vapor-fed zero-gap bioelectrochemical cell is influenced by pressure adjustments in the anodic chamber, affecting CH_4 production rates and conversion efficiency 97

5.4.4. Vapor-fed zero gap bioelectrochemical cell maintains a lower cell voltage and reduces electrocatalyst degradation 100

5.4.5. Metal compound concentrations did not change during liquid- and vapor-fed bioelectrochemical experiments 101

5.5. Discussion 103

5.6. Limitations of the study 106

5.7. Experimental Details 107

5.7.1. Strain and medium 107

5.7.2. Bioelectrochemical setup 108

5.7.3. Analytical analysis 111

5.7.4. Calculations 111

5.8. Acknowledgments 112

Chapter 6 113

6.1. Closing summary 113

6.2. Recommendations for future work 114

6.2.1. Single-chamber membrane-less bioelectrochemical system: a tool for basic research 115

6.2.2. Recommendations for future studies in microbial electrosynthesis 117

Supplementary for Chapter 3 123

Supplementary for Chapter 4 145

Supplementary for Chapter 5 157

References 161

Chapter 1

Introduction

1.1. Motivation

Carbon dioxide (CO_2) is a greenhouse gas that is fundamental in the global carbon cycle. CO_2 is vital in controlling the Earth's climate, making it central to the discourse on climate change (Mac Dowell et al. 2017). The current CO_2 levels, exceeding pre-industrial era benchmarks, pose a challenge that needs to be solved globally. The primary sources of this increase include industrial activities, emissions from transportation, and the combustion of fossil fuels in day-to-day life, with deforestation further intensifying the problem. The resulting CO_2 accumulation triggers a greenhouse effect, thus, increasing global temperatures (Baker et al. 2018). This increase in CO_2 level and the resulting heat is linked to more frequent and intense weather events, sea-level rise, and enhanced global desertification, adversely affecting agricultural production and leading to more frequent heatwaves and floods. The impact of these events on human welfare and the global economy is profound, and an urgent need to reduce global CO_2 emissions is imminent.

The global consensus on the need to diminish CO_2 emissions has led governments worldwide to prioritize this goal, necessitating a receptiveness to innovative technologies designed to curb and mitigate future CO_2 emissions. Efforts to decrease the surplus CO_2 released into the atmosphere, referred to as CO_2 capture technologies, fall into two primary categories: storage and reutilization or revalorization (McLaughlin et al. 2023). One storage approach involves sequestering CO_2 underground as carbonates (Chen et al. 2023). Despite its efficacy in immobilizing large quantities of CO_2, the long-term geological impacts of this method remain largely unexplored. Other storage solutions include oceanic CO_2 sequestration (Kumar and Sangwai 2023) and afforestation (Ménard et al. 2023), which is aimed at natural carbon absorption. Yet, the sheer volume of CO_2 emissions necessitates additional

strategies beyond storage. Because fossil fuel consumption is a principal driver of CO_2 emissions, the shift towards renewable energy sources, such as wind and solar, has become increasingly critical.

Nonetheless, the challenge of intermittency, whereby energy generation does not always align with demand, presents a considerable hurdle (Yekini Suberu, Wazir Mustafa, and Bashir 2014). This gap necessitates energy storage solutions to harness surplus renewable energy for later use. While battery storage offers a straightforward approach, its capacity limitations underscore the need for alternative solutions. The power-to-X concept emerges as an innovative solution, converting excess renewable electricity into chemical forms such as hydrogen (H_2) (Luna et al. 2019). When this process is integrated with CO_2 capture, it facilitates the electrochemical production of higher-value chemicals. This power-to-X addresses the issue of renewable energy's intermittency. It contributes to CO_2 mitigation by creating products with a net negative carbon footprint, effectively turning CO_2 from a waste product into a valuable resource (Luna et al. 2019). Such CO_2 capture technologies are pivotal in the transition to a sustainable energy economy, offering the benefit of enhancing renewable energy utilization and contributing to global CO_2 reduction efforts.

The chemical stability of CO_2, which is characterized by its high activation energies required for conversion into value-added chemicals, presents challenges for traditional chemical processes. Consequently, the biological facet of the power-to-X strategy has attracted increasing attention, leveraging microbes to transform CO_2 into valuable chemical products (Mishra et al. 2020). This process involves using surplus electrical energy to electrolyze water, generating H_2 and oxygen (O_2), which are then introduced into a bioreactor. Within this environment, microbes facilitate the conversion of CO_2 into targeted chemical outputs. This approach offers a dual benefit for industries such as chemical and cement production, which are notorious for their substantial greenhouse gas emissions. It enables them to sequester and add value to their waste emissions.

Electrochaea GmbH employs a process called biomethanation, utilizing excess electrical energy and CO_2 to produce methane (CH_4) through a method known as power-to-gas strategy (Shima and Thauer 2021). This approach is particularly relevant

for the gas infrastructure, which faces limitations on the concentration of H_2 that can be introduced into the gas grid. The power-to-gas strategy not only offers a solution to the storage and utilization of renewable energy but also aligns with efforts to decarbonize gas networks, providing a sustainable pathway for integrating renewable energy sources into existing energy systems. Unfortunately, the biomethanation process for the power-to-gas strategy has an energy efficiency of 50% during the two-step process that hampers the economic viability of the power-to-CH_4 conversion (Contreras et al. 2022). A possible upgrade to the two-step biomethanation process is microbial electrochemical technologies, which combine biology and electrochemistry in a one-step process (Schröder, Harnisch, and Angenent 2015). Microbial electrochemical technologies investigate how microbes interact with electrodes and harness the electrical energy for different processes. Within microbial electrochemical technologies, microbial electrosynthesis utilizes microbes to facilitate chemical reactions by harnessing electrons in the form of H_2 directly from the electrode (Schröder, Harnisch, and Angenent 2015). In combination with a methanogen, this process is called electromethanogenesis. Microbial electrosynthesis presents the opportunity to address environmental concerns by converting CO_2 into valuable products while potentially reducing capital costs through the integration of biological processes into electrochemical cells. However, microbial electrosynthesis faces several challenges, including low yields, inefficiencies in electron transfer mechanisms, a limited diversity of chemical outputs, and a need for a comprehensive understanding of microbial metabolic pathways (Prévoteau et al. 2020). Addressing these issues requires a multidisciplinary approach, merging insights from bioelectrochemistry, microbiology, and engineering to refine and economically scale microbial electrosynthesis technologies.

My dissertation focuses on optimizing microbial electrochemical technologies, particularly enhancing microbial electrosynthesis for its broader application in industry. Contrary to initial assumptions, I discovered that the primary obstacles to effective microbial electrochemical technology deployment were not microbial efficiency but rather the operating capabilities of the bioelectrochemical cells. Notable research indicates that the methanogen *Methanothermobacter thermautotrophicus*

can produce CH_4 at high volumetric rates and is used in an industrial setting (Rusmanis et al. 2019). Therefore, this methanogen is a prime candidate to use as a benchmark for microbial electrochemical technology research. A critical challenge facing microbial electrochemical technology is its suboptimal energy efficiency, which is closely related to the design and operation of the bioelectrochemical cell. My work focused on optimizing the performance of the bioelectrochemical cell in various reactor designs using the methanogen *M. thermautotrophicus*. In a broader context, my dissertation seeks to overcome the technological hurdles that currently limit the industrial scalability of microbial electrosynthesis, paving the way for its wider adoption and application. The first part was the development of a single-chamber bioelectrochemical cell that bypasses the need for an ion-exchange membrane, which is traditionally required to separate gases during electrosynthesis. This separation is crucial for cultivating strictly anaerobic microbes without producing O_2, which was achieved by replacing the O_2 evolution reaction with carbon oxidation, thus, enabling microbial electrosynthesis in a membrane-less setup. The second part of my work was a collaborative work with Electrochaea GmbH, where we investigated the implications of different shutdown methods and the frequency of shutdown on the bioelectrochemical cell with *M. thermautotrophicus*. The aim was to identify the electrode material with the fastest CH_4 recovery post-shutdown, with an additional focus on how different shutdown strategies affected the dissolution rates of a nickel cathode and, consequently, the CH_4 recovery time. The third part focuses on the implementation of a zero-gap bioelectrochemical cell, experimenting with both liquid-fed and vapor-fed anode chambers. This strategy was designed to enhance cell performance by preventing the formation of a pH gradient and reducing potential catalyst abrasion due to liquid flow.

1.2. Organization and summary of chapters

Chapter 2 is a literature review of the necessary information for this dissertation. An emphasis was made on: 1) bioelectrochemical systems; 2) the different reactor designs; 3) the problems an ion-exchange membrane creates and possible solutions; and 4) the microbe of choice.

Chapter 3 presents carbon oxidation and the use of sacrificial anodes as a method to prevent O_2 evolution in membrane-less bioelectrochemical systems for microbial electrosynthesis. The study first explored various carbon-based materials for their ability to inhibit O_2 evolution, with graphite requiring additional carbon oxidation time to become dominant. Subsequent tests with *M. thermautotrophicus* ΔH evaluated how these anodes influenced CH_4 production. Results indicated that carbon-based anodes supplemented with soluble iron extended the optimal performance duration (defined by an empirical cathode-based geometric CH_4 production rate exceeding 25 L m^{-2} d^{-1}) by one day. Iron notably prolonged CH_4 production periods, yet the oxidation of sulfur sources emerged as a primary constraint, presenting a considerable challenge for future research endeavors. Besides sulfur source limitations, anode performance was also potentially hindered by carbon availability or corrosion. Nonetheless, these findings underscore the viability of employing a single-chamber bioelectrochemical system for laboratory-scale applications.

Chapter 4 contains the influence of various shutdown strategies on the operating efficiency of three electrode materials—platinized titanium, graphite, and nickel—in power-to-gas systems utilizing electromethanogenesis. Employing a scaled-up flow electrolyzer that was configured as a microbial electrolysis cell within a laboratory-modified strain of *M. thermautotrophicus*, the study evaluated the recovery of CH_4 production following simulated maintenance-induced shutdowns. Among the materials tested, the microbial electrolysis cell that was equipped with platinized titanium electrodes exhibited greater efficiency and performance, followed by those with nickel and graphite electrodes. Further analysis of microbial electrolysis cell using nickel electrode, which were subjected to different shutdown protocols, revealed that the short-circuit method led to the biggest nickel degradation. However, this did not critically impact the volumetric CH_4 production rate or the recovery time of CH_4 production post-shutdown.

Chapter 5 examines liquid- and vapor-fed zero-gap bioelectrolysis cells. I conducted experiments with two liquid-fed zero-gap bioelectrolysis cells, each utilizing a different ion-exchange membrane. These experiments involved the recirculation of pure water within the anodic chamber. Among these, the cell equipped with the Nafion 117 ion-

exchange membrane exhibited better stability in performance when compared to the one using the Htec-PFSA (perfluorosulfonic acid) ion-exchange membrane. Following this, I explored the operation of a vapor-fed zero-gap bioelectrolysis cell with the Nafion 117 ion-exchange membrane to address the pH gradients introduced by liquid recirculation. This modification enhanced cell performance, primarily due to reduced catalyst degradation, thereby, improving the cell voltage. However, issues arose when the overpressure in the anodic chamber was relieved, leading to the end of stable cell voltage. I hypothesized that this might have caused an irreversible alteration to the ion-exchange membrane, resulting in inefficient H_2 production or crossover. Another observation was that the bioreactor, serving as the glass recirculation vessel, was the major source of efficiency loss in these experiments. Over 30% of H_2 was detected in the headspace, leading to substantial losses without being converted to CH_4.

Chapter 6 summarizes the different findings in electromethanogenesis with three different reactor types. A larger portion of this section discusses the limitations of the current work and recommendations for future work.

Chapter 2

Literature review

The current era is marked by increasing population growth, leading to escalated resource demands. This trend increases pollution and energy demand (Solomon et al. 2009). Transitioning from fossil fuels and nuclear power to sustainable, carbon-neutral energy sources is gaining importance (Tosun, Mišić, and Schmidt 2018). Among sustainable technologies, such as solar and wind energy, microbial electrochemical technologies have emerged as promising solutions to reduce the carbon footprint (Jhong, Ma, and Kenis 2013).

Generally, microbial electrochemical technologies are bioelectrochemical systems (BESs) comprising two electrodes, with microbes facilitating reactions at one or more electrodes (Schröder, Harnisch, and Angenent 2015). Electrode reactions typically occur in single- and double-chamber reactors, with the latter being more common due to its ability to separate anodic and cathodic reactions via an ion-exchange membrane. This separation into two chambers helps mitigate power losses, albeit introducing membrane-associated power losses. The membrane will lead to osmotic fluxes, pH gradients, and biofouling and will affect the overall performance of the BES (Leong et al. 2013).

Microbes that are capable of electron transfer to or from electrodes are electroactive and fall into two categories: (i) those degrading organic matter to donate electrons and (ii) those accepting electrons for synthesizing value-added chemicals (Yee et al. 2020). Within BESs, these microbes can convert organic matter into energy or chemicals (Schröder, Harnisch, and Angenent 2015). These microbes are applied in various microbial electrochemical technology forms, including microbial fuel cells, microbial electrolysis cells, and microbial electrochemical desalination systems (Hallenbeck, Grogger, and Veverka 2014).

2.1. Microbial fuel cell

One of the most studied BESs is a microbial fuel cell, a galvanic cell that converts organic substances into electrical energy through redox reactions (Logan et al. 2006). Here, microbes metabolize biodegradable substrates at the bioanode, generating energy. Concurrently, the cathode chamber functions as a chemical fuel cell, reducing O_2 to hydroxide ions (Santoro et al. 2017). Key to this process is exoelectrogens, such as the soil microbe *Geobacter sulfurreducens*, known for forming biofilms on electrodes and exhibiting high power densities in microbial fuel cells (Logan 2009; Logan et al. 2019; Yi et al. 2009). Another widely studied exoelectrogen is *Shewanella oneidensis*. Rosenbaum et al. demonstrated an aerated BES combining a microbial electrolysis cell and microbial fuel cell, where aerated *S. oneidensis* enhanced H_2 production and electrical power generation (Rosenbaum, Cotta, and Angenent 2010). This study highlighted that aerobic conditions increased H_2 production and electrical output due to augmented active biomass formation.

While chemical fuel cells can generate electrical energy up to megawatts, microbial fuel cells typically produce milliwatts to a few watts (Logan et al. 2015). Nonetheless, their ability to biodegrade pollutants, such as in wastewater treatment, presents an opportunity and an alternative clean water technology. Although high anodic current and coulombic efficiencies (CE) are achievable, scaling this technology for industrial profitability remains a challenge (Wang and Ren 2013). Therefore, the promise of microbial fuel cells as an energy source hinges on advancements in reactor designs, material cost reductions, and microbial efficiency enhancements (Angenent and Rosenbaum 2013; Santoro et al. 2016).

2.2. Microbial electrosynthesis

In microbial electrolysis cells, electric power serves as the driving force for the microbial reduction of carbon sources at the cathode, which produces multi-carbon and electron-dense organic molecules that can serve as fuels and terminal chemical products (**Figure 2.1**). This idea is called microbial electrosynthesis, and combined with renewable energy to generate electrical energy makes this technology sustainable (Nevin et al. 2010; Rabaey and Rozendal 2010). Furthermore, autotrophic microbes

and their ability to uptake CO_2 as sole carbon source can make this technology carbon neutral (Bajracharya et al. 2015).

Microbial electrosynthesis utilizes microbes to synthesize fuels and chemicals by applying an external power supply as an electron donor (Moscoviz et al. 2016). The efficiency of this electrically driven microbial reduction depends on various operating conditions, including pH, temperature, organic feed source, electrode material, and the microbial species used. Different microbes have been identified for producing a variety of chemical compounds, such as H_2 (Rozendal et al. 2006), acetate (Nevin et al. 2010), alcohols (Steinbusch et al. 2010), polymers (Hegner et al. 2020), and CH_4 (Geppert et al. 2019). In this dissertation, we will mainly focus on the CH4 production of methanogens to understand the microbe used in this thesis.

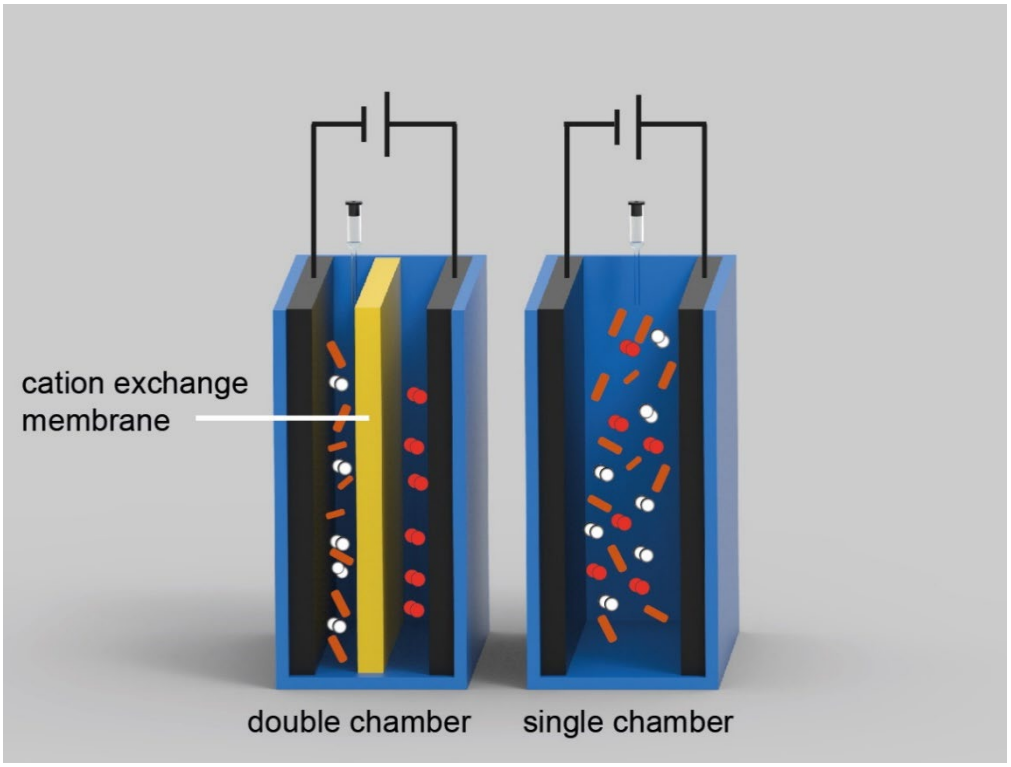


Figure 2.1: conversion of electrical energy and CO_2 to value-added chemicals. The cathode and anode splits water into H_2 and O_2, respectively. A cation exchange membrane separates the evolved O_2 from the microbes in a double-chamber reactor. The H_2 acts as a mediator for the microbial reduction reaction of CO_2.

The concept of electromethanogenesis was pioneered in 1999 by Park et al., who first demonstrated CH_4 synthesis in a BES by converting CO_2 into CH_4 (Park et al. 1999). They reported electrically reduced neutral red that served as a mediator and electron

source for the bacteria. The term electromethanogenesis was then used to describe the electrically driven microbial reduction to CH_4 (Cheng et al. 2009). This initiated a debate on how methanogens convert current into CH_4. Cheng et al. observed that *Methanobacterium spp*. could produce higher CH_4 yields through direct electron transfer compared to H_2-mediated electromethanogenesis. Conversely, other studies indicated that hydrogenotrophic methanogens were primarily responsible for electromethanogenesis (Villano et al. 2010). Villano and coworkers deduced that H_2-mediated electromethanogenesis relies on the applied cathode potential, with direct electron transfer occurring predominantly at lower potentials.

We can distinguish three types of electromethanogenesis: 1) direct via outer-membrane redox proteins; 2) indirect through electrochemically (Van Eerten-Jansen et al. 2013) and enzymatically mediated compounds (Deutzmann, Sahin, and Spormann 2015); and 3) interspecies electron transfer (Rotaru et al. 2014), which employs microbial syntrophy to conduct electrons for electromethanogenesis. Understanding the mechanisms of these electron transfers is pivotal for enhancing microbial electrosynthesis by focusing on biologically catalyzed cathodic reactions (Rosenbaum et al. 2011). For instance, c-type cytochromes have been shown to catalyze the O_2 reduction reaction in *Shewanella putrefaciens* (Freguia, Tsujimura, and Kano 2010), offering the potential for improved anoxic conditions. The combination of c-type cytochromes and hydrogenase in *Methanobacterium*-like archaea has demonstrated higher electron acceptance compared to H_2 gas (Dinh et al. 2004). However, the hypothesis that c-type cytochromes enhance electron uptake efficiency remains to be conclusively proven. In a more recent study, methanogens have the ability to lower the activation overpotential for the reduction reaction at the cathode (Deutzmann, Sahin, and Spormann 2015). Particularly noting that hydrogenase from *Methanococcus maripaludis* facilitates electron uptake, thus, reducing the overpotential for H_2 generation. Additionally, research has focused on artificial redox mediators, such as methyl viologen and neutral red, to improve microbial growth and metabolism in biocathodes (Rosenbaum et al. 2011; Park and Zeikus 1999; Aulenta et al. 2007).

In contrast to the traditional thermochemical methanation processes, such as the Sabatier process, which require high temperatures and pressures for effective carbon conversion (Walspurger et al. 2014), electromethanogenesis presents a less energy-intensive alternative. It aligns with the power-to-gas concept, utilizing excess (predominantly renewable) energy to convert CO_2 into CH_4 (Geppert et al. 2016). Most research on electromethanogenesis remains in the proof-of-principle phase, focusing on optimizing reactor design, electrode materials, and culture inocula to make the process industrially viable. However, the reported CH_4 production rates vary considerably from a few hundred mL CH_4 m^{-2} d^{-1} (in volume of CH_4 produced per cathode surface area per day) to 30.3 L CH_4 m^{-2} d^{-1} (Cheng et al. 2009; Clauwaert and Verstraete 2009) and recently to 669 L CH_4 m^{-2} d^{-1}(Rad et al. 2023). Each study is influenced by factors such as applied potential, temperature, electrode materials, medium, and inoculum type. A comparison of the studies solely through the production rate is, in fact, difficult. Pure culture inoculums perform far worse than enriched or non-enriched cultures (Mayer et al. 2019). Mayer and coworkers achieved a maximum volumetric CH_4 production rate of 0.21 L CH_4 m^{-2} d^{-1} using *M. maripaludis*, which is a well-established methanogen (Lohner et al. 2014). However, these studies served as proof-of-principle, and their interest was to establish new methanogens and the possibility of using them for industrial purposes. Kracke et al. used *M. maripaludis* as well to report the biocathode performance with three different transition-metal-based cathodes (Kracke et al. 2019) as proof-of-principle concepts for alternative electrode materials. Further studies have concentrated on modifying the cathode to enhance microbe-electrode interactions, which is crucial for effectively reducing the power generation in microbial electrosynthesis. Deutzmann et al. demonstrated that enzymes, such as hydrogenase from *M. maripaludis,* could lower activation overpotential at the cathode (Deutzmann, Sahin, and Spormann 2015). Therefore, choosing electrode material is critical in microbial electrosynthesis, as it has desirable characteristics, including biocompatibility, hydrophilicity, and high surface area. Carbon-based materials, such as carbon nanotubes or reticulated carbon with three-dimensional structures, perform better than metal-based electrodes due to increased surface area (Jourdin et al. 2014). Enhancing these electrodes with a catalyst, be it

metal such as platinum or conductive polymers, further increases their current densities (Guzman et al. 2017).

Assessing the performance of newly developed electrodes is vital. Cyclic voltammetry, which is an analytical electrochemical technique, is employed to identify various processes at the electrode (Bard and Faulkner 2000), including redox reactions, stability of reactants or the electrode(Chen, Patil, and Schröder 2018), reaction kinetics (Sun et al. 2017), and analyte concentration determination (Yuan, Renock, et al. 2015). Differential pulsed voltammetry, which is an adjunct to cyclic voltammetry, uses small pulses to enhance the selectivity and visibility of redox reactions (Puig et al. 2017). Electrochemical Impedance Spectroscopy further elucidates electrode properties, providing insights into charge and mass transfer at the electrode's surface or bulk (He et al. 2021). These techniques collectively enable a comprehensive assessment of electrode performance.

Current research in microbial electrosynthesis focuses on developing new electrode materials (de Smit et al. 2023; Sharma et al. 2019), genetically modifying organisms (Rosenbaum and Henrich 2014), and innovating reactor designs (Giddings et al. 2015). Most reactor designs incorporate an ion exchange membrane to segregate the anodic and cathodic chambers, thus, separating microbes from O_2 evolving at the anode. Nevertheless, the highest reported CH_4 production was an open-culture single-chamber reactor (Clauwaert and Verstraete 2009) capable of surviving oxic conditions. While mixed cultures may introduce interfering processes that inhibit chemical compound production rates, pure cultures are more controllable but more costly and challenging to maintain in sterile conditions, making open cultures more appealing for large-scale industrial reactors (Bajracharya et al. 2015). In both cases, including a membrane is a desired solution to avoid contact with O_2, but it comes with disadvantages, which will be addressed in the next section.

2.3. Ion Exchange Membranes in Microbial Fuel Cells and Microbial Electrosynthesis Systems

Microbial fuel cells and electrolysis cells need ion exchange membranes when anaerobic microbes are used to produce electrical energy or chemical compounds. An

ideal membrane for such applications should possess attributes such as high ionic conductivity, low internal resistance, and selective permeability, and it should exhibit mechanical, chemical, and thermal stability. Additionally, it should have minimal biofouling tendencies and be cost-effective (Davis, Genders, and Pletcher 1997). However, fulfilling all these requirements simultaneously is challenging, and trade-offs are often necessary. Ion exchange membranes can be classified into three types: cation exchange membranes (CEMs), anion exchange membranes (AEMs), and bipolar membranes (BPMs). These membranes are typically polymer-based, with CEMs containing negative charges ($-SO^{3-}$, $-COO^{-}$, $-PO_3^{2-}$) to allow the passage of positively charged ions, whereas AEMs possess positive charges ($-NH_3^{+}$, $-NHR_2^{+}$, $-NRH_2^{+}$) to facilitate the movement of negatively charged ions (Davis, Genders, and Pletcher 1997). The most common membranes for microbial electrosynthesis are CEM, and the sulfonated tetrafluoroethylene-based fluoropolymer-copolymer with the brand name Nafion is extensively used in research (Heitner-Wirguin 1996). Nafion is primarily employed in fuel cells as a proton exchange membrane, promoting proton transport.

The first technical barrier for CEM is the proton permeability. The transport of protons from the anode to the cathode depends on the applied electrical field and diffusion rate. If the CEM exhibits low proton permeability, the supply of protons on the cathode would eventually be depleted and would cause a higher pH gradient between the chambers. Consequently, the electro-osmotic flux, which carries all ionic and non-ionic solutes, would transfer all cations (Na^{+}, Ca^{2+}, K^{+}) through the membrane to establish charge neutrality (Rozendal, Hamelers, and Buisman 2006). On the other hand, high proton concentrations in the anolyte are desired to facilitate the transport of protons from the anode to the cathode. In the case of low proton concentration in the anolyte, cations other than protons will be transported to maintain electroneutrality (Rozendal et al. 2007). These transferred cations can also precipitate at the membrane to hinder mass transport and further increase the internal resistance (Długołęcki et al. 2010).

As a result, the pH in the cathode chamber increases, and a higher pH gradient is reached, which will cause performance loss in H_2 production through higher thermodynamic cell potentials (Baek et al. 2022). Despite the primary role of

membranes being to prevent O_2 contact with anaerobes, O_2 diffusion through them is often unavoidable. For instance, Nafion membranes exhibit one of the highest O_2 diffusion coefficients, making them particularly susceptible to fouling (Kim et al. 1996; Xu et al. 2012). Membrane resistance, which is a critical factor influencing ion transport and overall internal resistance in BES, can be measured through electrical impedance spectroscopy (Leong et al. 2013). The membrane resistance has a high impact on the BES internal resistance. It can be lowered by increasing the surface area of the membrane while keeping the electrode surface area fixed. Oh and Logan demonstrated that increasing the surface area of the membrane can considerably enhance the power densities of microbial fuel cells. However, this effect may not scale effectively in larger systems (Oh and Logan 2006). They claimed that the reactor size limits this effect and would not work at a larger scale. Lastly, it is important to note that membranes add to operating costs through maintenance needs such as cleaning or replacement.

2.4. Single-chamber systems

The issues that comprise a membrane could be avoided by removing the membrane and establishing a membrane-less reactor design. Eliminating the membrane reduces the internal resistance of the cell, thus, addressing many issues inherent to membrane-based systems (Rozendal et al. 2007). However, membrane-less microbial fuel cells present their own set of challenges. Notably, the diffusion of O_2 and the formation of biofilms on electrodes have been observed to reduce performance, particularly at higher power densities, when compared to membrane-equipped microbial fuel cells (Leong et al. 2013). The term single-chamber is sometimes used to describe designs where the membrane is placed adjacent to the electrode, which may lead to confusion (Zhang et al. 2010). While only a limited number of studies have reported on membrane-less reactors, most of these have been in the context of microbial fuel cells. Typically, these reactors operate using microbes that are not sensitive to O_2 (Cheng et al. 2009; Call and Logan 2008). However, Giddings and coworkers designed a membrane-less reactor for microbial electrosynthesis, situating the anode at the boundary of the reactor's liquid interface (Giddings et al. 2015). To mitigate O_2 diffusion within the reactor, a gassing cannula was strategically placed

between the anode and cathode. Their study compared acetate production using *Sporomusa ovata*, which is a strict anaerobe, in both an H-type cell and the membrane-less reactor. The H-type cells were operated with applied voltages between 3 and 5 V, resulting in 69 to 164 mmol day^{-1} m^{-2} acetate. Although the acetate with the membrane-less reactor was between 28 to 36 mmol day^{-1} m^{-2}, the applied voltages were considerably lower, resulting in a higher reactor performance than with H-type cells. Key benefits of a membrane-less design include the absence of biofouling, reduced membrane resistance, and lower operating costs. However, the presence of O_2 evolution at the anode in such systems presents a considerable limitation, particularly for anaerobic cultures in microbial electrosynthesis setups. This factor alone can render the membrane-less design impractical for certain applications where anaerobic conditions are essential.

2.5. The need to change the electrode material

While a microbial fuel cell has the O_2 reduction reaction at the cathode, a microbial electrolysis cell has the O_2 evolution reaction (OER) at the anode. In both cases, a membrane will be needed. The membrane disadvantages described in the previous section, such as biofouling, pH gradient, osmotic fluxes, and ohmic resistances, make membranes less attractive. Moving towards a single-chamber system without a membrane is desirable. While some single-chamber BES designs exist, they are set up with a microbial community that survives oxic conditions by spatial removal of O_2 (Call and Logan 2008). For strict anaerobic microbes in a pure culture, separating the anode and cathode is the utmost priority (Liu et al. 2019). For this purpose, a new method to inhibit the OER at the anode needs to be investigated. Halley et al. investigated magnetite as a new material and showed promising results in inhibiting OER in an abiotic electrochemical system (Halley, Schofield, and Berntson 2012). They hypothesized a pathway through cyclic voltammogram measurements by employing magnetite, which is a redox-active iron mineral. Their study showed a consumable electrode using magnetite (Fe_3O_4) for an electrolysis cell with a net reaction,

$$\mathrm{Fe_3O_4 + H_2O \rightarrow Fe_2O_3 + H_2 \uparrow} \quad (1)$$

where magnetite gets oxidized to maghemite (Fe_2O_3). While they state that the formation of maghemite occurred through an intermediate step of ferric

oxyhydroxide (FeOOH), there is a possibility that Fe_3O_4 gets oxidized through molecular O_2 formed at the anode. Even if the findings showed the possibility of inhibiting OER, they also showed low current densities of 400 mA g^{-1} Fe_3O_4. The lack of O_2 gas measurements and cyclic voltammograms stopped before +1 V, diminished the reliability of inhibiting the OER. Similar results were also studied for pyrite (Lalvani and Shami 1985), which is an iron(II) disulfide. They reported H_2 production at the cathode with an anode potential that is half of the OER potential. From an economic point of view, they produced H_2 with less energy, which can be cost-beneficial. Unfortunately, the current generation was lower than typical water electrolysis cells due to its higher bandgap of 0.95 eV (Ennaoui et al. 1993) compared to 0.1 eV for magnetite (Cornell and Schwertmann 2003).

Another interesting idea to avoid the membrane during the electrolysis is the electrochemical gasification of carbons, also known as carbon-assisted water electrolysis (Sabareeswaran et al. 2013), where carbon gets oxidized to CO_2. Although the method provides H_2 with an applied potential six times less than a classic water electrolysis cell, CO_2 as a by-product prevents its use on an industrial scale (Ju, Badwal, and Giddey 2018). It is especially interesting for microbial electrosynthesis because the products of carbon-assisted water electrolysis (H_2 and CO_2) are the substrates for microbial electrosynthesis. However, up to now, coal is the primary carbon source with a high efficiency. It is possible to use other sources, such as alcohol, but using valuable chemicals as sources to produce CO_2 is not cost-beneficial. There is a possibility to use biomass as a source of carbon (Yahiro et al. 2019). Yet, the efficiency and the reaction kinetics are low, which makes the applicability of carbon-assisted water electrolysis for now irrelevant to microbial electrosynthesis.

If we consider that the inhibiting OER from magnetite is because of the more favorable redox reaction compared to OER ($\mathrm{E}_{\mathrm{Fe_2O_3/Fe_3O_4}} < \mathrm{E}_{\mathrm{O_2}}$) (White, Peterson, and Hochella 1994), it opens the possibility of a larger variety of redox-active materials. However, we also need to consider the reaction kinetics. While magnetite is thermodynamically more favorable, it is not relevant once the applied potential reaches the OER potential. In this case, the kinetics of the redox reactions is the rate-determining step (Hu et al. 2021). Different iron minerals could be used. However, the accessibility of some

minerals, such as vivianite, is more difficult than magnetite (Cornell and Schwertmann 2003). Even though magnetite exhibits the highest conductivity among all iron oxides (Cornell and Schwertmann 2003), it is lower compared to metals or graphite (Pierson 1994; Matula 1979). One possibility would be to dope magnetite with transition metals (Walz et al. 1997). Another possibility would be using organic compounds in exchange for inorganic materials, which are synthesized by depletable mineral resources (Song and Zhou 2013). There are different types of electroactive organic compounds, such as conducting polymers (Zhou et al. 2011), organosulfur compounds (Weng et al. 2009), organic free radical compounds (Guo et al. 2012), and organic carbonyl compounds (Renault et al. 2011). While conducting polymers enhance the conductivity of inorganic compounds (Guzman et al. 2017), organic carbonyl compounds are highly redox active, making them an ideal replacement for magnetite. Therefore, in the follow-up sections, we will present carbon-assisted water electrolysis in more detail, explain why magnetite is an interesting mineral, and state which electroactive organic compounds are the most promising in inhibiting the OER.

2.6. Carbon-assisted water electrolysis (CAWE)

The ideal configuration for bioelectrochemical systems should supposedly be a single-chamber, membrane-less design. Such a setup not only improves current generation but also enhances synthesis efficiency. In the anodic chamber of conventional systems, the primary gases produced are chlorine (Cl_2) and O_2. Cl_2, which is a strong oxidizing and highly toxic agent, poses considerable challenges. Although Cl_2 production can be mitigated by removing chlorine ions from the medium, O_2 generation from water splitting remains an issue, particularly as it hinders the growth of anaerobic microbes when used for microbial electrosynthesis.

An alternative to water splitting, which involves O_2 evolution at the anode, is CAWE. CAWE oxidizes carbon at the anode, replacing the OER. CAWE comprises two primary mechanisms: (1) oxidation of carbon-based electrodes, which is referred to as carbon oxidation with sacrificial anodes; and (2) oxidation of soluble or non-soluble carbon materials in the anolyte. CAWE offers several advantages compared to conventional water electrolysis. For instance, the standard electrode cell potential for the four-electron process in CAWE is −0.21 V, which is lower than the −1.23 V that is required

for conventional water electrolysis. The carbon-oxidation rate is higher than the OER rate, making it kinetically more advantageous (Ju, Badwal, and Giddey 2018; Carmo et al. 2013).

Additionally, CAWE generates CO_2 and CO, which can be used as substrates for microbial electrosynthesis. Most studies involving CAWE have focused on oxidizing soluble and non-soluble carbon materials to generate H_2 (Ju, Badwal, and Giddey 2018). This process typically involves incorporating a concentrated carbon solution into the electrolyte. However, such an addition poses potential challenges for BES, as the carbon solution might be toxic to microbes and could lead to undesirable side reactions. Consequently, carbon-based electrodes emerge as a more suitable alternative for integration into BES. Holubowitch and coworkers developed an abiotic, membrane-less electrochemical cell capable of reducing O_2 to deoxygenate water (Holubowitch et al. 2019), which is a promising approach for implementing it in BES. CAWE has already been applied, albeit inadvertently, in a BES context. Zeppilli et al. utilized graphite granules in a membrane-less BES configured for the removal of perchloroethylene. This application effectively reduced O_2 production, demonstrating the feasibility and effectiveness of CAWE in BES applications (Zeppilli et al. 2019). Despite these advancements, the use of CAWE specifically for microbial electrosynthesis has yet to be explored and remains an area ripe for future research.

2.7. Magnetite mineral as electrode material

Magnetite has an inverse spinel structure where Fe^{2+}-ions and half of the Fe^{3+}-ions occupy the octahedral sites, whereas the other half of the Fe^{3+}-ions occupy tetrahedral sites. It has a Verwey temperature of 118K (Verwey 1939) at which fast electron transfer between the Fe^{2+}-ions and Fe^{3+}-ions occurs above this temperature at the octahedral sites. This delocalization permits magnetite its conductivity, which is around 10^4 S m^{-1} (Coey et al. 1998) and 1000 times lower than the conductivity of copper (Matula 1979). The ideal magnetite stoichiometric ratio Fe^{2+}/Fe^{3+} is $\chi = 0.5$. However, magnetite can be easily oxidized so that the Fe^{2+}/Fe^{3+} ratio decreases, and a fully oxidized magnetite ($\chi = 0$) would result in maghemite. The best way to measure the stoichiometry of magnetite is either by ^{57}Mössbauer spectroscopy or colorimetric iron assay (Gorski and Scherer 2010; Stookey 1970).

Magnetite has a variety of applications, especially in biotechnology (Viggi et al. 2020), medical applications (Soleymani et al. 2020), biosensors (Moreira, Santana, and Spinelli 2020), supercapacitor (Mao, Zhou, and Peng 2020), and environmental studies (Yuan, Ilton, et al. 2015). Different synthesis methods apply for each application, and chemical coprecipitation is the most widely used technique for synthesizing magnetite nanoparticles (Sorwat et al. 2020). The reaction involves a mixture of Fe^{3+} and Fe^{2+} with a stoichiometric ratio of 2:1 in an anoxic environment at basic pH. Another technique is the hydrothermal reaction using an autoclaved steel reactor at high-pressure conditions (Chen and Xu 1998). The hydrothermal process allows to control nucleation and grain growth by changing the temperature or the reaction time. In the same way, the electrochemical method regulates the particle to a certain size by shifting the current density or potential (Cabrera et al. 2008), while avoiding particle aggregation. Control of particle size is an important characteristic of magnetite. By reducing the particle size, the surface area not only becomes much larger and more reactive but can also develop peculiar properties, such as superparamagnetism, below a particle size of 30 nm (Lu, Salabas, and Schüth 2007). The biomineralization of magnetite through magnetotactic bacteria also showed unique magnetic properties of magnetite, which can be applied for biotechnological applications (Faivre and Schuler 2008). These bacteria have magnetosomes, which are organelles with magnetic iron crystals, such as magnetite, enclosed in their membranes to navigate through the water. However, the biomineralization mechanism must be understood before biomineralized magnetite can be produced on a large scale.

Magnetite is known for its high sensitivity to oxidation reactions, which influence its magnetic properties. Byrne et al. explored this aspect, studying the interaction of magnetite with iron cycling processes in the presence of Fe(III)-reducing bacteria (*G. sulfurreducens*) and phototrophic Fe(II)-oxidizing bacteria (*Rhodopseudomonas palustris* TIE-1) (Byrne et al. 2015). The study was carried out by alternating a period of oxidation through illumination followed by a reduction step from an acetate feed in dark conditions. Notably, they observed fluctuating magnetic susceptibility, which decreased during oxidation and increased during reduction. This pattern underscores the potential to use magnetic susceptibility as a tool to assess the reversibility and

redox state of magnetite. A subsequent study by the same group extended this research to examine the effects of these bacteria on both the surface and bulk of magnetite (Byrne et al. 2016). They found that while the bulk of magnetite could be reduced by Fe(III)-reducing bacteria, the surface was only oxidizable by Fe(II)-oxidizing bacteria.

To a certain extent, magnetite was used as an alternative material for supercapacitors or detectors. In some cases, magnetite electrodes could not be used purely, and they were dispersed with a carbon-based material such as graphite or conductive polymer (Al-Zahrani et al. 2016; Liu et al. 2008; Janáky et al. 2009). A field of interest for magnetite electrodes is the identification of harmful ions in aqueous environments. Yuan et al. used magnetite electrodes to recognize the intermediate U(V)O22+ reaction on the surface (Yuan, Renock, et al. 2015). They could directly confirm the one-electron reduction from UO_2^{2+} to UO^{2+} while measuring the total number of electrons transferred during the reduction process. Interestingly, bulk and powder magnetite were used as electrodes, and differences in the detection of uranium ions were found. While both powder and bulk magnetite could identify the one-electron reduction from UO_2^{2+} to UO^{2+}, only the electrode with powder magnetite was able to show the disproportionation product U^{4+} *via* the oxidation reaction to UO_2^{2+} at 0.42 V vs. Ag/AgCl. Furthermore, adding graphite powder to the powder magnetite electrode improved the signal for the redox reactions. Although Yuan et al. showed that bulk magnetite was less effective in their application than powdered magnetite, it can be used in other applications.

Zebardast et al. built a bulk electrode rod of pure magnetite by cold isostatic pressing and sintering under an argon atmosphere followed by hot isostatic pressing (Zebardast, Rogak, and Asselin 2012) for the decomposition of H_2O_2. An analysis of the composition of the magnetite rod revealed 11 wt% of hematite. This means a stoichiometric ratio of $\chi \approx 0.45$, consistent with other post-magnetite synthesis analyses. The fact that the ratio of $\chi \approx 0.45$ could not be improved by sintering under an argon atmosphere shows the high sensitivity of magnetite to undergo oxidation reactions. Likewise, the rapid magnetite depletion during the removal of pertechnetate concerned Farrell and coworkers (Farrell et al. 1999). Subsequently,

they analyzed the electrode stability. As expected, magnetite wear strongly depends on the strength of the anodic polarization and less on the concentration of pertechnetate. Moreover, the oxidation of magnetite would inevitably increase the internal resistance due to the lower conductivity of hematite. In their case, electrode oxidation was less of a problem due to the higher affinity of the solution species to be oxidized.

While high-weight percentages of magnetite to carbon were used in the above publications, magnetite can also be dispersed in a smaller magnetite-to-carbon ratio where it acts as a catalyst. For example, a carbon paste electrode with 15 wt% magnetite content was prepared to detect chlorite ions in an aqueous medium (Al-Zahrani et al. 2016). A carbon paste electrode is already capable of detecting chlorite. However, the addition of magnetite exhibited an enhancement in the current signal and enabled the detection of chlorite in the nanomolar range.

As mentioned in the previous section, magnetite has a low conductivity (Halley, Schofield, and Berntson 2012), and a carbon-based material has to be added to increase its conductivity. However, in the above-mentioned publications, their interest in using magnetite as an electrode did not rely on its low conductivity and the desire to improve it. High conductivities are desirable for industrial purposes where cost efficiencies are more important. Therefore, magnetite is still in the need of improvement for applications in microbial electrosynthesis. A handful of publications use magnetite in microbial electrosynthesis (Zhu et al. 2019; Vu, Noori, and Min ; Viggi et al. ; Ren et al.). However, none of them used magnetite as an anode to inhibit the OER. Improvements in methanogenesis were observed by Vu et al. when magnetite was added as a supplement in the medium. Zhu et al. built a magnetite/granular activated carbon cathode, where an increase in the production rate of acetate was also observed. In contrast, a recent study with *M. thermoautotrophicus* fed with H_2 and CO_2 showed the influence of Fe nanoparticles on the growth and production rate in an anaerobic digester (Cheng et al. 2020). An increase in CH_4 production was found by adding 1.5g L^{-1} of Fe nanoparticles to the medium. Yet, it is known that microbes found in soils or wastewater have a high affinity to sustain high iron concentrations

(Sandy and Butler 2009). Therefore, the increased production rate with added magnetite could result from dissolved iron rather than magnetite.

2.8. Redox-active organic electrodes

The lack of improvement in energy densities and concerns about resource depletion have paved the way for organic electrodes as an alternative to lithium-ion electrodes (Song and Zhou 2013). To be considered an alternative electrode material for microbial electrosynthesis, the organic molecule must be electroactive and, most importantly, redox-active. While conductive polymers show high conductivities, they do not undergo reversible electrochemical redox reactions (Shirakawa et al. 1977). Another possible candidate is organic free radicals that can be used as anode with redox potentials above +0 V. However, stabilized organic free radicals, such as 2,2,6,6-Tetramethylpiperidinyloxyl (TEMPO), show high chemical reactivity and can, in some cases be toxic (Oyaizu and Nishide 2009). Organosulfur molecules have also been researched. The slow reaction reversibility due to high activation energies and the possible dissolution made it a complex material to handle (Liang, Tao, and Chen 2012). Finally, organic carbonyl compounds possess high energy densities and low redox potentials, which are good candidates for microbial electrosynthesis electrodes (Wu et al. 2017).

Quinone materials are emerging as up-and-coming electrode materials in battery research and may present a viable alternative to redox-active electrodes. Known for their ability to undergo redox reactions at positive redox potential values, quinones are broadly categorized into two types: small quinones and polymer quinones. Small quinone molecules are characterized by their high capacities and power densities, making them attractive for high-performance applications. However, they are hindered by challenges, such as dissolution and low conductivities, with their conductivity being approximately 100 times lower than that of magnetite. Polymer quinones have been the subject of extensive research to address these limitations. These compounds exhibit similar properties to their small quinone counterparts but with the added benefits of higher conductivity and insolubility, resolving some key issues (Wu et al. 2017). Another noteworthy class of materials is non-conjugated organic polymers, such as poly(vinylferrocene). These polymers demonstrate redox

potentials around +0.5V and boast high energy densities. Despite these advantages, they tend to exhibit insulating properties, necessitating their dispersion with a conductive material for optimal functionality (Iwakura et al. 1987).

In summary, organic electrodes, such as quinones and non-conjugated organic polymers, represent alternatives to traditional inorganic materials, such as magnetite, especially due to their redox reaction capabilities. However, it is important to note that the application of organic electrodes has primarily been within battery research. Their suitability for use in microbial electrosynthesis remains an area that warrants further investigation. A critical aspect of this research will be to evaluate the toxicity of these electrodes in the presence of microbes, ensuring their compatibility and safety in microbial electrosynthesis applications.

2.9. Reactor designs of microbial electrosynthesis

A widely utilized configuration in BES is the H-cell, comprising two half-cells separated by an ion-exchange membrane. This setup has been extensively employed in fundamental research for investigating biofilm formation, electron transfer mechanisms, and the initial stages of microbial electrosynthesis (Sandfeld et al. 2024). Despite its widespread use (Boto et al. 2023; Kracke et al. 2021), the H-cell design presents several drawbacks: (i) increased internal resistance from the large distance between the anode and cathode, which can impede efficient electron transfer; (ii) suboptimal electrolyte mixing, which affects mass transport within the system; and (iii) limited surface-to-volume ratio, which restricts the overall reaction efficiency and capacity. Nonetheless, the simplicity and cost-effectiveness of setting up an H-cell make it a convenient choice for conducting studies in laboratory-scale settings. However, its design falls short in terms of industrial scalability.

Flow-type electrolyzer designs have marked a considerable improvement in electrolysis technology, primarily through optimizing internal components and operating dynamics. These designs offer a lowered internal resistance by reducing the distance between the anode and cathode, enhancing mixing through flow chambers, and utilizing electrodes that span the entire flow cell to maximize the surface-to-volume ratio. This approach improves the traditional H-cell-type reactor designs,

opening potential industrial applications. There exists a variety of flow electrolyzer types, such as a tubular bioelectrochemical fixed-bed reactor (Ceballos-Escalera, Pous, Balaguer, et al. 2024), rotating disc reactor (Hackbarth et al. 2023), or plate reactor (Rovira-Alsina, Dolors Balaguer, and Puig 2022). A comparison between the reactors would show an increase in performance compared to less optimal reactor designs. However, despite these advancements, the production rates still lag behind those of gas fermenters, particularly in lab-scale applications. Techno-economic analyses reveal a critical efficiency threshold; microbial electrosynthesis could be deemed viable for industrial purposes if they achieve over 50% energy efficiency (Jourdin et al. 2020; Jourdin and Burdyny 2021). A notable experiment by Van Eerten-Jansen et al. utilized a plate reactor for microbial electrosynthesis, employing anaerobic sludge as an inoculum. This setup achieved a maximum energy efficiency of 51%, albeit with a low current density, resulting in reduced volumetric production rates (Van Eerten-Jansen et al. 2012). While advancements have been made, achieving a balance between energy efficiency and production rate remains a pivotal challenge.

In a stride for industrial applicability, Geppert et al. (Geppert et al. 2019) leveraged an electrochemical configuration inspired by redox-flow batteries to produce CH_4 with an energy efficiency of around 30% at a current density of 3.5 mA cm^{-2}. Their experimental setup, characterized by a zero-gap design that positions electrodes close to the membrane, demonstrated increased current density from 1.0 to 3.5 mA cm^{-2} and reduced resistance during CH_4 production. The potential for scaling this design is underscored by the possibility of stacking multiple individual cells, similar to the approach in abiotic electrolyzers, suggesting a promising route for larger-scale implementations. Additionally, Rad et al. set a new benchmark by enhancing the current density to 30 mA cm^{-2} with notably low cell voltages in a hybrid bioelectrochemical system (Rad et al. 2023) while the energy efficiency was 43 ±3%. This advancement was facilitated by shielding the cathodic catalysts with a porous transport layer to prevent direct contact with the catholyte, showcasing an innovative strategy to optimize performance. The biggest improvement was found in copying abiotic electrolyzer setups, and the future of microbial electrosynthesis seems to lie in

membrane electrode assemblies (MEA), which consist of catalysts-coated membrane and gas diffusion electrodes.

2.10. Microbe of choice: *M. thermautotrophicus*

M. thermautotrophicus ΔH, which is a rod-shaped thermophile, is a hydrogenotrophic methanogen with an optimal growth temperature of 65 °C. It utilizes H_2 as an electron donor and CO_2 as an electron acceptor and a carbon source for growth (Thauer et al. 2008). *M. thermautotrophicus* ΔH have emerged as particularly effective, converting CO_2 and H_2 into CH_4 at high volumetric rates of 700-800 L L^{-1} day^{-1} in both bench-scale and pilot-scale gas fermentation systems (Nishimura et al. 1992; Rusmanis et al. 2019). Furthermore, an evolved strain of *M. thermautotrophicus* was successfully implemented for commercial purposes of Electrochaea GmbH and underscored the potential in the power-to-gas sector. It has demonstrated higher production rates, reduced risk of microbial contamination, lesser cooling needs for the fermentation broth, and the flexibility to modulate operations based on the availability of electrical energy (Thema, Bauer, and Sterner 2019). Notably, hydrogen sulfide, which damages catalysts in thermochemical methanation, serves as a sulfur source for *M. thermautotrophicus*, making its presence in industrial off-gases or biogas beneficial for biomethanation.

Deutzmann and coworkers demonstrated through targeted genetic modifications—specifically, the deletion of genes encoding hydrogenase and formate dehydrogenase in methanogens—that direct electron transfer does not play a key role in electron transfer within BES (Deutzmann, Sahin, and Spormann 2015). Instead, H_2 acts as the primary mediator of electron transfer, which is generated at the cathode and serves as an electron donor for *M. thermautotrophicus* ΔH. The robustness of *M. thermautotrophicus* ΔH and its high production rate in gas fermenters make it an ideal candidate for several applications in BES.

Chapter 3

Carbon oxidation with sacrificial anodes to inhibit O2 evolution in membrane-less bioelectrochemical systems for microbial electrosynthesis

Reproduced and adapted with permission from: Rohbohm N., Sun T., Blasco-Gómez R., Byrne J. M., Kappler A. and Angenent L. T. (2023). Carbon oxidation with sacrificial anodes to inhibit O_2 evolution in membrane-less bioelectrochemical systems for microbial electrosynthesis. *EES Catalysis*, Vol. 1, No. 6, pp. 972-986. Copyright 2023 EES catalysis.

3.1. Author Contributions

L.T.A., T.S., and R.B.-G. initiated the work. N.R., T.S., and L.T.A. designed the experiments. N.R. performed the laboratory experiments and analyzed the data. L.T.A. and T.S. supervised the project. N.R. and L.T.A. wrote the manuscript. All edited the paper and approved the final version.

3.2. Abstract

Microbial electrosynthesis is an emerging biosynthesis technology that produces value-added chemicals and fuels and, at the same time, reduces the environmental carbon footprint. However, constraints, such as low current densities and high inner resistance, disfavor this technology for industrial-scale purposes. The cathode performance has been strongly improved in recent years, while the anode performance has not been given enough attention despite its importance in closing the electric circuit. For traditional water electrolysis, O_2 is produced at the anode, which is toxic to the anaerobic autotrophs that engage in microbial electrosynthesis. To overcome O_2 toxicity in conventional microbial electrosynthesis, the anode and the cathode chamber have been separated by an ion-exchange membrane to avoid contact between the microbes and O_2. However, ion-exchange membranes increase the maintenance costs and compromise the production efficiency by introducing an

additional internal resistance. Furthermore, O_2 is inevitably transferred to the catholyte due to diffusion and electro-osmotic fluxes that occur within the membrane. Here, we proved the concept of integrating carbon oxidation with sacrificial anodes and microbes to simultaneously inhibit the O_2 evolution reaction (OER) and circumvent membrane application, which allows microbial electrosynthesis to proceed in a single chamber. The carbon-based anodes performed carbon oxidation as the alternative reaction to the OER. This enables microbial electrosynthesis to be performed with cell voltages as low as 1.8-2.1 V at 10 $A \cdot m^{-2}$. We utilized *Methanothermobacter thermautotrophicus* ΔH in a single-chamber Bioelectrochemical system (BES) with the best performing carbon-based anode (*i.e.*, activated-carbon anode with soluble iron) to achieve a maximum cathode-geometric CH_4 production rate of 27.3 $L \cdot m^{-2} \cdot d^{-1}$, which is equal to a volumetric methane production rate of 0.11 $L \cdot L^{-1} \cdot d^{-1}$ in our BES, at a coulombic efficiency of 99.4%. In this study, *Methanothermobacter thermautotrophicus* ΔH was majorly limited by the sulfur source that inhibited electromethanogenesis. However, this proof-of-concept study allows microbial electrosynthesis to be performed more energy-efficiently and can be immediately utilized for research purposes in microbial electrosynthesis.

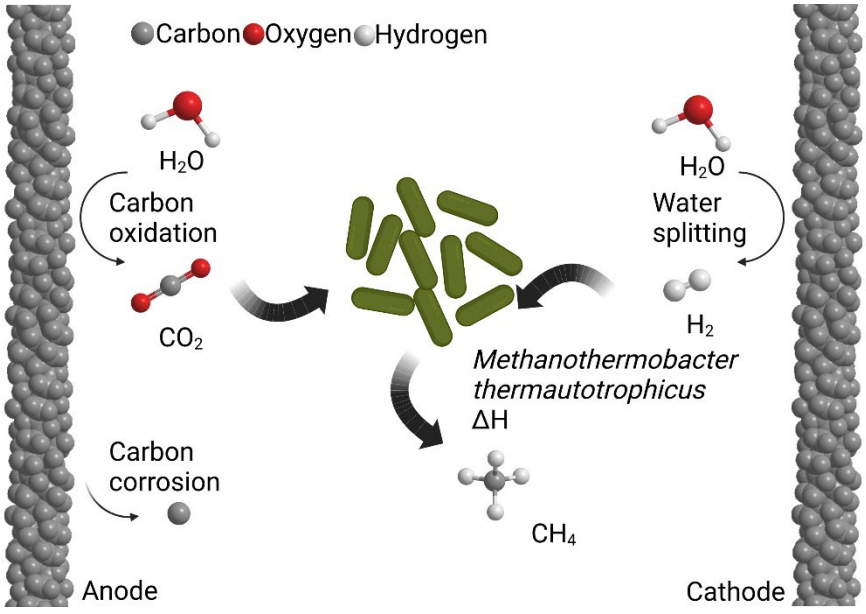


Figure 3.1: Graphical abstract showcasing the carbon oxidation for microbial electrosynthesis.

3.3. Broader context

In microbial electrolysis cells, electric power serves as the driving force for microbial reduction of CO_2 at the cathode to produce multi-carbon and electron-dense organic molecules that can serve as fuels and terminal chemical products. This idea is called microbial electrosynthesis and, combined with renewable energy to generate electrical power, makes it an emerging technology for sustainable chemical production. Microbial activity and electrode performance are critical factors in determining the overall efficiency of microbial electrosynthesis. Several studies have focused on modifying the cathode to improve the microbe-electrode interaction and compatibility due to its importance in generating reducing power for microbial electrosynthesis. However, so far, the focus was rarely on the anode performance. Here, we employed a sacrificial carbon-based anode that enabled us to remove the ion-exchange membrane in the electrochemical cell. We proved the concept of a single chamber bioelectrochemical cell using *Methanothermobacter thermautotrophicus* ΔH with this sacrificial carbon-based anode. This study shows a different path forward to perform microbial electrosynthesis, especially in the laboratory for basic research.

3.4. Introduction

Globally increasing demands for value-added chemicals and fuels require innovative chemical and biochemical synthesis strategies to proceed in a more cost-efficient and environmentally friendly manner. Microbial electrosynthesis is a bioprocess with bioelectrochemical systems to convert inorganic gases into valuable, multi-carbon compounds to store excessive renewable energy such as wind or solar energy (Nevin et al. 2010; Rabaey and Rozendal 2010). This makes it an attractive technology for achieving the goal of a carbon-neutral society. Microbial activity and electrode performance are critical factors in determining the overall efficiency of microbial electrosynthesis. However, the inherent problem of scaling-up microbial electrosynthesis is the currently low current density of the bioelectrochemical system, which results in a considerably lower production rate compared to chemical electrosynthesis that produces the same compounds (**Table S1**). To increase the current density, the electrochemical performance must be increased by, for example,

improving the cathode performance. Indeed, several studies have focused on the modification of the cathode to improve microbe-electrode interactions and its biocompatibility (Tremblay, Angenent, and Zhang 2017; Kracke et al. 2020).

Besides the biocompatibility problems, another troublesome part of bioelectrochemical systems is the ion-exchange membrane. Classically, the anode is separated from the cathode by an ion-exchange membrane to avoid interaction of the O_2 evolving at the anode with the strict anaerobic microbes in the cathodic chamber (Giddings et al. 2015). However, applying an ion-exchange membrane in bioelectrochemical systems has several disadvantages. By including an ion-exchange membrane, the internal resistance is increased (Długołęcki et al. 2010). This will lead to decreased ion transport, which consequently limits electron transfer and reduces the current generation. Ideally, protons are primarily transported from the anodic to the cathodic chamber using cation exchange membrane to maintain hydrogen production. However, the transfer of other cations, such as sodium or potassium, to the cathode chamber cannot be neglected and reduces the ionic transport number of protons. Consequently, the slower mass transfer rate of protons leads to a pH gradient (Rozendal, Hamelers, and Buisman 2006). In addition, the ion-exchange membrane also generates an electro-osmotic flow that allows all ionic and non-ionic solutes, including O_2, to pass through membrane into the cathode chamber, thus, making its purpose ineffective (Kim et al. 1996). The pore size of the membrane in addition to O_2 permeation, which allows biofilm formation, makes it vulnerable to fouling (Jourdin et al. 2018). Finally, the combination of all the disadvantages will result in high maintenance and operating costs (Fornero, Rosenbaum, and Angenent 2010).

The ideal bioelectrochemical system would, therefore, be a single-chamber system in which the ion-exchange membrane has been removed (Mano, Mao, and Heller 2004). This would improve not only the current generation but also the synthesis efficiency. Cl_2 and O_2 are the main gases produced on the anode side, with Cl_2 being not only a strong oxidizing agent to many elements but also very toxic. While Cl_2 can be avoided by removing the chlorine-ions from the anodic chamber, O_2 would still be produced without modifications at the anode through water splitting and hinder anaerobic microbes from growing for microbial electrosynthesis to proceed. Thus far, few

reports have been published showing membrane-less bioelectrochemical systems, and most reports are about microbial fuel cells and enzymatic fuel cells. Furthermore, most membrane-less, single-chamber systems were operated without O_2-sensitive microbes (Call and Logan 2008; Cheng et al. 2009). Giddings and coworkers designed a membrane-less system for microbial electrosynthesis in which the anode was placed at the boundary of the liquid interface to avoid O_2 from mixing (Giddings et al. 2015). Besides, different patent applications for single-chamber bioelectrochemical systems were filed with setups to capture and remove O_2 away from the cathode (Kumar et al. 2020; Lovley and Nevin 2012). However, none of these innovations had tried to circumvent the O_2-evolution reaction (OER) at the anode.

An appealing approach to avoid O_2 formation at the anode is carbon-assisted water electrolysis (CAWE) for which carbon is oxidized at the anode instead of the OER in conventional electrolysis (Ju, Badwal, and Giddey 2018; Holubowitch et al. 2019). The classical hydrogen-evolution reaction (HER) is not disturbed and proceeds at CAWE. CAWE can include: **(1)** the oxidation of carbon-based electrodes, which we refer to as carbon oxidation with sacrificial anodes; and **(2)** the oxidation of soluble carbon materials (which we did not study) or non-soluble carbon materials in the anolyte. Here, we address carbon oxidation of sacrificial anodes, forming CO_2, CO, and oxygenated surface-functional groups. The desired two chemical reactions can be described as follows (**Eq. 2** and **Eq. 3**):

$$C + 2H_2O \rightarrow CO_2 + 4H^+ + 4e^- \qquad E^0 = +0.21\ V \quad (2)$$

$$C + H_2O \rightarrow CO + 2H^+ + 2e^- \qquad E^0 = +0.51\ V \quad (3)$$

A major advantage of using CAWE instead of conventional water electrolysis with O_2 evolution at the anode is the lower operating cell voltage, resulting in lower energy consumption rates. For example, the standard electrode cell potential for the four-electron process (Eq. 2) for CAWE is $E^0_{cell,CAWE} = -0.21$ V, while the conventional water electrolysis reaction requires $E^0_{cell,water\ electrolysis} = -1.23$ V (Ju, Badwal, and Giddey 2018). Another advantage of CAWE compared to conventional water electrolysis is the higher carbon-oxidation reaction rate than the OER rate at the anode (exchange current density: $j_{0,CAWE} = 10^{-6}$ A·cm^{-2} *vs.* $j_{0,OER} = 10^{-7}$ A·cm^{-2}).(Ju, Badwal, and Giddey

2018) Albeit, the carbon-oxidation reaction at the anode is still slower than the HER rate at the cathode ($j_{0,HER}$ = 10^{-3} A·cm^{-2}) (Carmo et al. 2013). Finally, a necessary substrate for microbial electrosynthesis is CO_2 or CO, which is the desired product of carbon oxidation with sacrificial anodes. Thus, the matching product formation as extra carbon source for the microbes is another pertinent advantage of carbon oxidation with sacrificial anodes for microbial electrosynthesis.

An example of carbon oxidation with carbon-based anodes was shown by Holubowitch et al., who demonstrated an abiotic membrane-less electrochemical cell that was capable of reducing O_2 to deoxygenate water (Holubowitch et al. 2019). While their main focus was on reducing O_2, we identified with their data that either no O_2 was produced or O_2 production was decreased at the anode and that O_2 was electrochemically reduced at the cathode. Carbon oxidation with carbon-based anodes was not only tested abiotically but also for bioelectrochemical systems. Lai et al. found a lower O_2 content and a higher CO_2 content in their anodic compartment using graphite (Lai et al. 2017). They concluded that carbon oxidation with the graphite anode was the main cause of the lower O_2 formation. A follow-up study for the removal of perchloroethylene in a membrane-less bioelectrochemical system used graphite granules as a single anode to avoid O_2 production (Zeppilli et al. 2019). To our knowledge, carbon oxidation with sacrificial anodes has not been tested for microbial electrosynthesis.

The objective of this work was a proof of concept to show that carbon oxidation can be utilized in a single-chamber bioelectrochemical system to specifically perform microbial electrosynthesis. We used different types of carbon electrodes as anodes and assessed whether O_2 formation was inhibited or just decreased. In addition, we tested iron (soluble and coated) materials with carbon electrodes to further circumvent the OER by including a parallel Faradaic reaction. After we had studied the feasibility of our carbon electrodes and deciphered the mechanism of the inhibition, we operated our carbon electrodes in bioelectrochemical systems to evaluate their potential for microbial electrosynthesis. Here, we report the successful implementation of carbon oxidation with a sacrificial anode for microbial electrosynthesis using *Methanothermobacter thermautotrophicus* ΔH, which is an

autotrophic and anaerobic microbe, and which is being used in the power-to-gas concept to store renewable electric power into CH_4 gas (Martin et al. 2013).

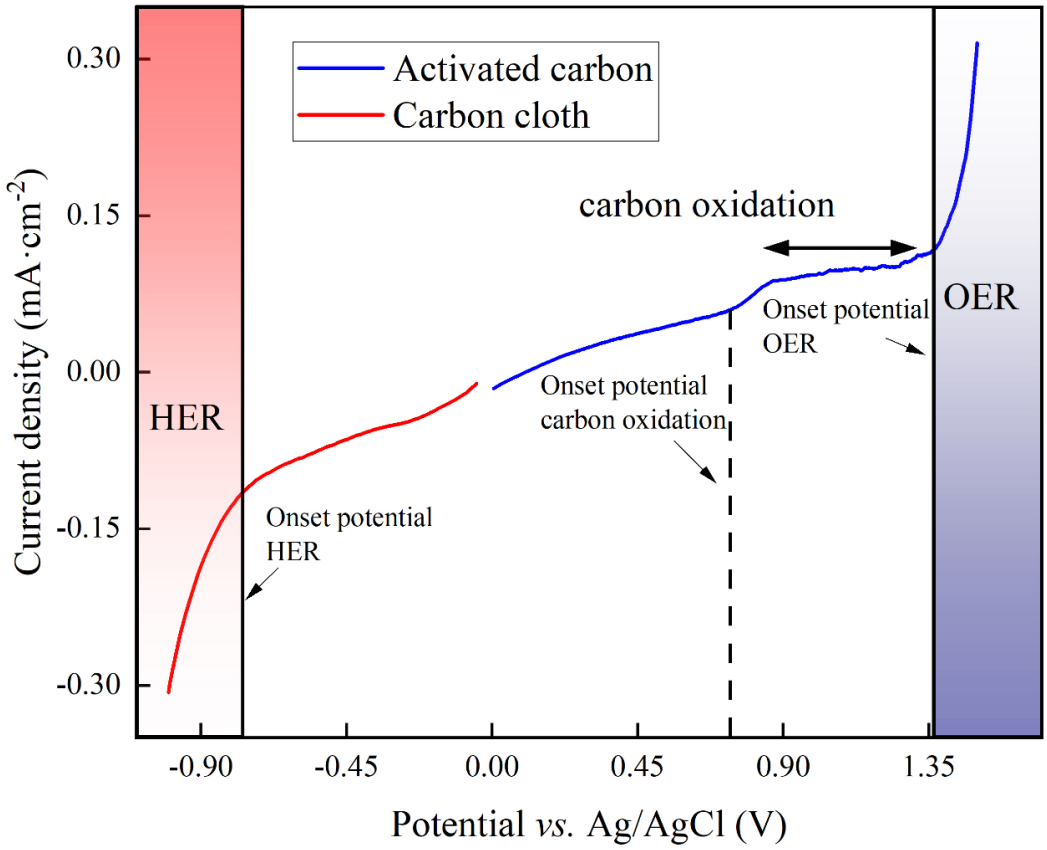


Figure 3.2: Linear sweep voltammogram of the activated-carbon anode (blue line) and the carbon-cloth cathode (red line) in 66 mM phosphate buffer (pH = 7.2) at a scan rate of 20 $mV \cdot s^{-1}$.

3.5. Results and discussion

3.5.1. The minimal required cell potential is lower for carbon oxidation than for O_2 evolution at the anode, while the kinetics of the carbon oxidation reaction is higher

For our proof-of-concept process, we used the two carbon-oxidation reactions from CAWE compared to the OER from conventional water electrolysis. The two carbon-oxidation reactions have a theoretically more favorable thermodynamic potential of +0.21 V *vs.* RHE (reversible hydrogen electrode which depends on the solution pH) for CO_2 production (four electrons in Eq. 2) and +0.51 V *vs.* RHE for CO production (two electrons in Eq. 3), respectively(Ji et al. 2021), than the OER, with a standard potential of +1.23 V *vs.* RHE. For conventional water electrolysis with the OER, the overall cell potential would be -1.23 V. However, electrode materials have properties that introduce an overpotential. In the case of carbon electrodes, the overpotential can be up to 500 mV or higher (Yi et al. 2017).

To measure the overpotentials (η) for our specific BES for carbon oxidation with carbon-based anodes, OER, and HER, we performed linear sweep voltammetry on the activated carbon (as the anode) and carbon cloth (as the cathode). Linear sweep voltammograms demonstrated that the measured overpotential ($|\eta| = [E_{\text{onset potential}} + E_{\text{reference electrode correction}}] - [E^0 - 0.059 \cdot \text{pH}]$) of carbon oxidation with activated carbon was +1.16 V, while the HER for carbon cloth had an overpotential of +0.190 V (**Figure 3.2**). Thus, the minimum required cell potential for CAWE anodes would be -1.56 V ($E^0_{HER} - \eta_{HER} - [E^0_{\text{carbon oxdiation}} + \eta_{\text{carbon oxidation}}]$), which is -1.37 V greater than the theoretical value ($E^0_{\text{cell, carbon oxidation}} = E^0_{HER} - E^0_{\text{carbon oxidation}} = -0.21$ V). The OER with the activated carbon had an overpotential of +0.86 V (**Figure 3.2**). Therefore, the minimal required cell potential for conventional water electrolysis would be equivalent to -2.28 V ($E_{\text{cell, water electrolysis}} = E^0_{HER} - \eta_{HER} - [E^0_{OER} + \eta_{OER}]$), which is -1.05 V greater than the theoretical value. The considerably less negative overall cell potential for CAWE compared to conventional water electrolysis should lower the energy consumption in our system as well.

However, besides the cell potentials, the kinetics of the different electrochemical reactions are also important. The linear-sweep voltammogram of activated carbon did not show any pristine carbon-oxidation peaks to compare the kinetic value of the carbon oxidation to the OER (**Figure 3.2**). However, the exchange current density, which is a dimension of the reaction rate, can be deduced from the linear-sweep voltammograms by means of the Butler-Volmer equation (Eq. S1 in supporting note 1 of the SI) (Bard and Faulkner 2000). The exchange current density for carbon oxidation was 10^{-5} A·cm^{-2} and was one magnitude higher than the OER at 10^{-6} A·cm^{-2}. Therefore, the carbon oxidation reaction with sacrificial anodes is a faster electrochemical reaction than OER.

3.5.2. Carbon-based anodes with and without iron species circumvented the need for a membrane, opening the possibility of a membrane-less system

To identify whether O_2 production is inhibited by carbon oxidation, we measured the O_2 content of an abiotic, two-electrode electrochemical system for five days. The O_2 content measurement was performed abiotically to circumvent using L-cysteine, which would be the preferred sulfur source and reducing agent in our medium for the BES experiments, and which would have removed O_2 from the electrolyte. The abiotic experiments were performed in triplicate for two temperature conditions: room temperature and 60°C, which is the optimal growth temperature of *Methanothermobacter thermautotrophicus* ΔH. We used a graphite rod, thermally activated graphite felt, carbon cloth, and activated carbon as our carbon anodes for four out of seven treatments and included a platinum anode that was poised at 10 A·m^{-2} in 0.066 M phosphate buffer as the positive control to compare the results of the carbon oxidation with sacrificial anodes to the OER (**Figure 3.3**).

We added Fe^{2+} species in the form of: **(1)** soluble Fe^{2+} species (0.1 g·L^{-1} of Fe^{2+}, corresponding to 0.27 g·L^{-1} $FeSO_4$); and **(2)** coated magnetite for three out of seven treatments to this abiotic O_2 evolution study. We added Fe^{2+} species because abiotic electrochemical systems increased the current density for carbon oxidation with sacrificial anodes without reducing the Coulombic efficiency (Yin et al. 2009). Soluble

Fe^{2+} is directly reduced at the carbon-based anode to Fe^{3+} at electrochemical rates that are higher than carbon oxidation and the OER (**Eq. 4**).

$$\text{At the anode: } Fe^{2+} \rightarrow Fe^{3+} + e^{-} \quad (4)$$

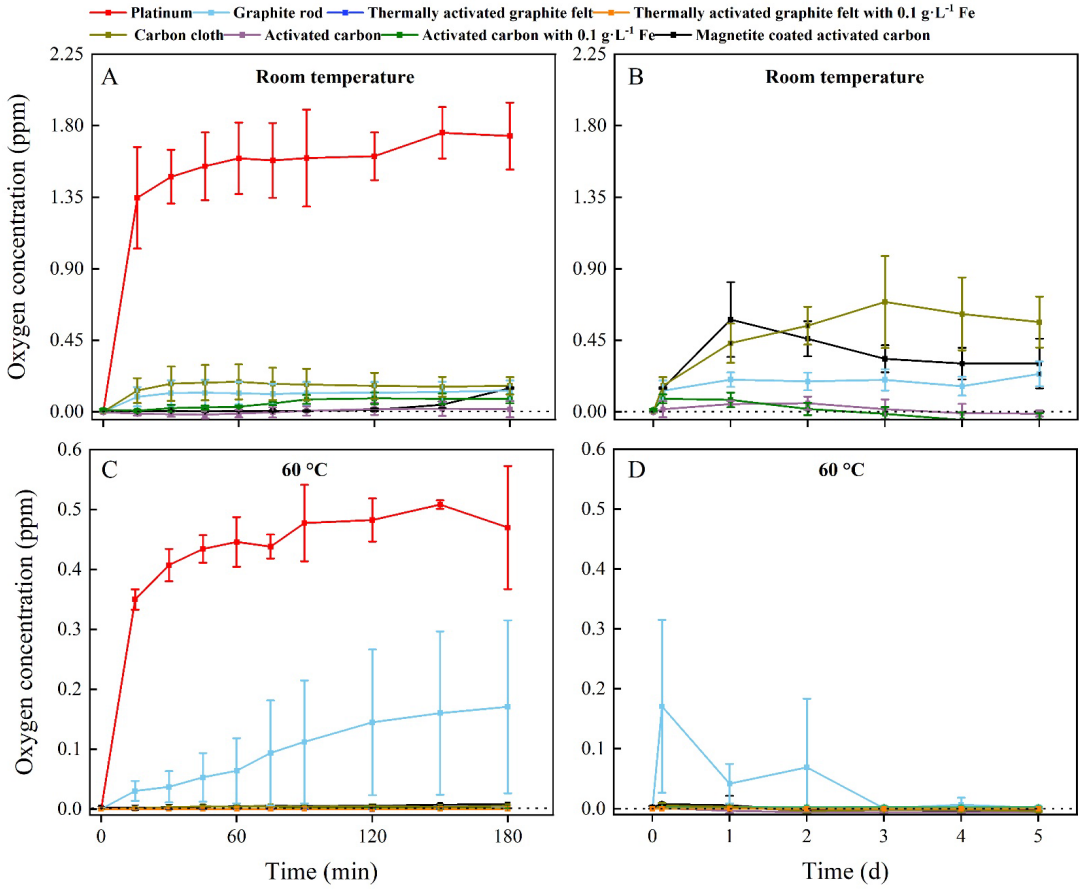


Figure 3.3: O_2 concentration in the electrolyte of platinum, graphite-rod, thermally activated graphite felt, carbon-cloth, and activated-carbon anodes over time. Two temperature conditions were included. Two treatments with thermally activated graphite felt and three treatments with activated carbon were included, including iron additions. The error bars show the standard deviation for the average values from triplicate systems: **(A)** the O_2 concentration at room temperature for 180 min; **(B)** the O_2 concentration at room temperature for 5 days; **(C)** the O_2 concentration at 60°C for 180 min; and **(D)** the O_2 concentration at 60°C for 5 days. We omitted the data for the first 180 min from panels B and D for clarity reasons. No L-cysteine was added to these abiotic experiments.

Therefore, soluble Fe^{2+} is an ultimate electron donor in addition to the carbon-based anodes when Fe^{2+} is continuously added to the system. Soluble Fe^{2+} was added to the thermally activated-graphite-felt and activated-carbon anodes. Magnetite is another biocompatible Fe^{2+} source. We coated magnetite on the activated carbon to form the anode after performing a magnetite-to-carbon ratio analysis (supporting information

note 2 of the SI). Magnetite is a mixed-valent Fe(II), Fe(III) magnetic iron mineral that oxidizes to maghemite (γ-Fe_2O_3), donating one electron (**Eq. 5**):

$$3Fe_3O_4 \rightarrow 4\,\gamma - Fe_2O_3 + Fe^{2+} + 2e^- \quad (5)$$

All carbon-based anodes with and without Fe^{2+} species showed an inhibitory effect on the O_2 production compared to the positive control for the first 180 min at room temperature, with the graphite-rod and carbon-cloth anodes producing more O_2 compared to the thermally activated-graphite-felt and activated-carbon anodes (**Figure 3.3A**). Thus, a pretreatment to activate the graphite or carbon will permit a faster inhibition of O_2 synthesis. We turned off the electrochemical system with the platinum anode after 180 min to avoid accumulating O_2 and H_2 and creating a *Knallgas* reaction. For the next 5 days, the accumulated O_2 concentration of all the carbon-based anodes was relatively low (<1 ppm), but activated-carbon anodes with and without soluble Fe^{2+} could sustain a nearly O_2-free environment (**Figure 3.3B**). However, magnetite-coated activated-carbon anodes showed a higher O_2 concentration at room temperature compared to the other activated carbon-based electrodes for unknown reasons (**Figure 3.3B**). A possibility is a change of the composition and reactivity of the activated carbon after synthesis of magnetite (pH change from acidic to basic).

In contrast, all the experiments with carbon-based anodes at 60°C inhibited O_2 production during the first 180 min, except for the graphite-rod anode (sky-blue line, **Figure 3.3C**). In addition, no O_2 was produced at 60°C for the thermally activated-graphite-felt and activated-carbon anodes with and without soluble Fe^{2+} and activated-carbon anodes with magnetite (**Figure 3.3D**). Because the kinetics of a reaction are directly related to the temperature, the increase in the temperature, therefore, increased the carbon-oxidation rate. Likewise, the kinetics of the OER were also affected by the increase in temperature. However, our results show that no production of O_2 occurred and that carbon oxidation was the dominating reaction in our system (**Figure 3.3D**).

During the five-day operating period, the O_2 concentration in the electrolyte with the graphite-rod anode gradually decreased, suggesting that graphite needs an activation

time to oxidize its surface and efficiently perform carbon oxidation (**Figure 3.3D**). Indeed, the thermally activated-graphite-felt and activated-carbon anodes did not show O_2 evolution during the first couple of days of the operating period (**Figure 3.3D**). The concentrations of CO_2 and CO were measured for the two temperature conditions and the seven treatments, but the concentrations were very low for both gases due to the low applied current of up to 1 mA cm^{-2} and were not further monitored. In summary, the carbon-based anodes circumvented O_2 production at 60°C and were used for further thermophilic BES experiments. Because we completely inhibited O_2 evolution at the anode, we can remove the membranes from the bioelectrochemical system to perform microbial electrosynthesis. When comparing these abiotic results to the BES experiments, the abiotic O_2 evolution results will be conservative because we added reducing agents only to the microbial medium.

3.5.3. Different carbon materials as the anode affected the CH_4 production duration of microbial electrosynthesis, and competitive methane production rates were achieved to other BES studies.

In our proof-of-concept BES for microbial electrosynthesis, we opted for the microbe *M. thermautotrophicus* ΔH due to its high growth rate (doubling time of 120 min) and relatively high CH_4 production rate (Martin et al. 2013). This archaeal strain grows anoxically at 60°C and shows a resilient behavior in the presence of O_2 by having the ability to grow after exposure to air for several hours (Kiener and Leisinger 1983). However, as a strict anaerobic methanogen, it is still sensitive to O_2 for longer operating periods, resulting in the absence of growth when prolonged O_2 is present. The BES experiments were performed at 60°C and close to neutral-pH conditions with graphite-rod, thermally activated-graphite-felt, and activated-carbon anodes in an experimental design with six treatments including soluble Fe^{2+} and magnetite. We set the current at 2 mA and with a 1x1 cathode-surface area the cathode-based geometric current density was 1 mA cm^{-2} (**Figure 3.4**).

M. thermautotrophicus ΔH produced CH_4 with CO_2 as the sole carbon source during carbon oxidation with sacrificial anodes for all treatments (**Figure 3.4A**). After an

operating period of one day, the maximum cathode-based geometric CH_4 production rates for the BESs with the graphite-rod, the thermally activated graphite felt, the activated-carbon anode were 18.97 ± 2.84, 25.13 ± 2.34, and 26.75 ± 2.38 $L \cdot m^{-2} \cdot d^{-1}$, respectively (**Table 1**). This resulted in a maximum volumetric CH_4 production rate of 0.1 ± 0.001 $L \cdot L^{-1} \cdot d^{-1}$ for the BES with the activated-carbon anode. Coulombic efficiencies of 97.96 ± 8.71% for the BES with the activated-carbon anodes suggest an efficient H_2 uptake by the microbes at the cathode (**Figure 3.4)**.

By adding soluble Fe^{2+} to thermally activate-graphite-felt and activated-carbon anodes at 60°C with *M. thermautotrophicus* ΔH, we achieved a higher maximum cathode-based geometric CH_4 production rate of 27.48 ± 0.26 and 27.30 ± 0.29 $L \cdot m^{-2} \cdot d^{-1}$, respectively, resulting in a volumetric CH_4 production rate of 0.11 $L \cdot L^{-1} \cdot d^{-1}$ for both and a higher Coulombic efficiency of 100.61 ± 0.01% and 99.36 ± 0.57% with the added soluble Fe^{2+} than without (**Table 1**, **Figure 3.4A**). However, with magnetite-coated activated-carbon anode material, the methane production was lower compared to activated-carbon anode material. The maximum cathode-based geometric CH_4 production rate was 27.15 ± 0.65 $L \cdot m^{-2} \cdot d^{-1}$m with a Coulombic efficiency of 99.40 ± 0.02% (**Table 1** and **Figure 3.4)**.

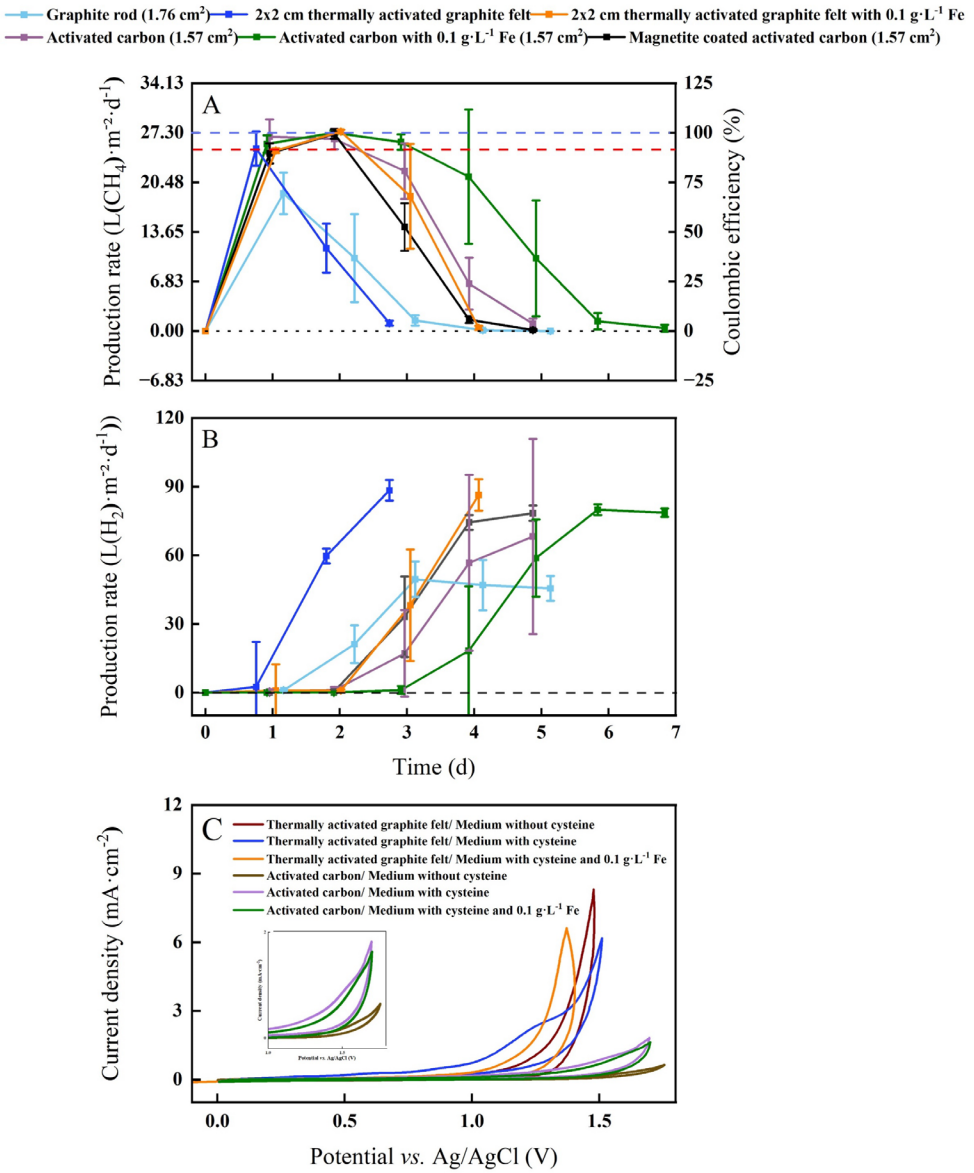


Figure 3.4: Membrane-less BES performance for electromethanogenesis and cyclic voltammetry analysis with L-cysteine: **(A)** CH_4 production rates corrected to the cathode surface area and Coulombic efficiencies (at I = 10 $A \cdot m^{-2}$); **(B)** H_2 production rate corrected to the cathode surface area during batch experiments over time with the thermophilic archaeon M. thermautotrophicus ΔH. Graphite-rod, thermally activated graphite felt and activated-carbon anodes were included with two treatments and three treatments for thermally activated graphite felt and activated carbon, respectively, including iron additions (soluble iron and magnetite). The error bars show the standard deviation for the average data from triplicate systems. For **(A)** and **(B)** Carbon cloth was used as the cathode: (Y-axis 1) cathode-based geometric CH_4 production rates and H_2 production rates for six treatments; and (Y-axis 2) for **(A)** Coulombic efficiencies for six treatments. After reaching a maximum H_2 production rate, we stopped the current to not accumulate excessive amounts of H_2 in our BESs. While the blue-dotted line represents 100% Coulombic efficiency at a 27.30 $L \cdot m^{-2} \cdot d^{-1}$ methane production rate, the red-dotted line shows the empirical cathode-based geometric CH_4 production rate of > 25 $L \cdot m^{-2} \cdot d^{-1}$ to determine the duration of the optimum performance period; and **(C)** cyclic voltammograms of thermally activated graphite felt and activated carbon at a scan rate of 5 mVs^{-1} in MS-medium. In total 6 cyclic voltammogramms were recorded where the MS-medium for each carbon-based electrode contained L-cysteine without soluble Fe^{2+}; L-cysteine with soluble Fe^{2+}; and without L-cysteine and without soluble Fe^{2+}

Table 1 | Performance data of the carbon-based anodes.

Carbon-based anode	Maximum geometric CH_4 production rate in $L \cdot m^{-2} \cdot d^{-1}$	Maximum volumetric CH_4 production rate in $L \cdot L^{-1} \cdot d^{-1}$	Optimum performance period in d
Graphite rod	18.97 ± 2.84	0.07 ± 0.01	0
Thermally activated graphite felt	25.13 ± 2.34	0.10 ± 0.009	1
Thermally activated graphite felt with 0.1 $g \cdot L^{-1}$ of Fe^{2+}	27.48 ± 0.26	0.11 ± 0.001	2
Activated carbon	26.75 ± 2.38	0.10 ± 0.009	2
Activated carbon with 0.1 $g \cdot L^{-1}$ of Fe^{2+}	27.30 ± 0.29	0.11 ± 0.001	3
Magnetite-coated activated carbon	27.15 ± 0.65	0.11 ± 0.002	2

To compare the different experimental conditions in our study, we choose an empirical cathode-based geometric CH_4 production rate of > 25 $L \cdot m^{-2} \cdot d^{-1}$ to determine the duration of the optimum-performance period for each treatment. Under this definition of the optimum performance period, the graphite-rod anode never reached this CH_4 production rate, resulting in an optimum performance period of zero (**Table 1**). We achieved an optimum-performance period of 1 day for the thermally activated-graphite-felt anode. After an operating period of two days, the cathode-based geometric CH_4 production rates for the BESs with the activated-carbon anode was 26.44 ± 1.40 $L \cdot m^{-2} \cdot d^{-1}$ after which it decreased, resulting in an optimum-performance period of two days (**Table 1**). By adding soluble Fe^{2+} to thermally activated-graphite-

felt and activated-carbon anodes, the optimum-performance period was elongated to two and three days at an average cathode-based geometric CH_4 production rate of 26.17 ± 0.29 and 26.36 ± 0.84 $L \cdot m^{-2} \cdot d^{-1}$, respectively (**Table 1**). However, with magnetite, the optimum performance period was shortened to two days at an average cathode-based geometric CH_4 production rate of 25.81 ± 1.01 $L \cdot m^{-2} \cdot d^{-1}$, which is one day shorter than for the activated-carbon anodes with soluble Fe^{2+} (**Table 1**). For the activated-carbon anodes as an example, the pH remained between 7.3 and 7.8 (**Figure S1**), and CO_2 was never limited (**Figure S2)**.

We achieved a maximum cathode-based geometric CH_4 production rate of 27.48 $L \cdot m^{-2} \cdot d^{-1}$ with thermally activated graphite felt and 0.1 g L^{-1} soluble Fe^{2+}, which was slightly higher than Kracke et al., who achieved a maximum of 26.76 $L \cdot m^{-2} \cdot d^{-1}$ at a cathode-based geometric current density of 1 mA cm^{-2} (Kracke et al. 2020). The authors utilized a mesophilic methanogen (*i.e.*, *Methanococcus maripaludis*) in a BES with membranes and a NiMo cathode. However, the reported maximum volumetric CH_4 production rate by Kracke et al. was 1.38 $L \cdot L^{-1} \cdot d^{-1}$, which was 12.5 times higher than the 0.11 $L \cdot L^{-1} \cdot d^{-1}$ for our study due to a more optimum electrode-surface-to-reactor-volume ratio (Kracke et al. 2020). An even higher volumetric CH_4 production rate of 2.9 ± 1.2 $L \cdot L^{-1} \cdot d^{-1}$ compared to Kracke et al. (Kracke et al. 2020) was achieved by Baek et al., using a zero-gap electrochemical cell (Baek et al. 2022). Despite its lower geometric CH_4 production rate of 18.25 $L \cdot m^{-2} \cdot d^{-1}$ and side-products of acetate and propionate (at a cathode-based geometric current density of 1.74 mA cm^{-2}), the zero-gap electrochemical cell has an optimized electrode-surface-to-reactor-volume ratio and has the propensity to increase the production rates for microbial electrosynthesis, including for our system (Baek et al. 2022). Even higher volumetric CH_4 production rates of 12 $L \cdot L^{-1} \cdot d^{-1}$ were achieved by Geppert et al. (Geppert et al. 2019).

Noteworthy is the considerably lower volumetric CH_4 production rates for all BES studies compared to gas fermentation by sparging H_2 and CO_2, for which CH_4 production rates of 688 $L \cdot L^{-1} \cdot d^{-1}$ (using the standard molar volume of CH_4 from 1.28 $mol \cdot L^{-1} \cdot h^{-1}$) had already been achieved in the 1990s (Nishimura et al. 1992). It is clear that several breakthroughs are necessary to close the gap between microbial electrosynthesis and gas fermentation for CH_4 production. Regardless, our proof-of-

concept was successful for which we could produce the highest cathode-based geometric CH_4 production rate of 27.48 $L \cdot m^{-2} \cdot d^{-1}$ with our membrane-less BES with sacrificial anodes.

3.5.4. The duration of methane production in the single-chamber bioelectrochemical system was only a few days due to oxidation of reduced sulfur compounds at the anode and a resulting sulfur limitation.

Our abiotic O_2 measurements with graphite-rod anodes showed O_2 production at 60°C (**Figure 3.3D**), identifying that O_2 inhibition to the thermophilic methanogen was a reason for a zero-day optimum-performance period during our BES experiment with graphite-rod anodes (**Figure 3.4A**). The thermally activated-graphite-felt anodes and activated-carbon anodes during abiotic experiments exhibited no O_2 production after an operating period of five days (**Figure 3.3D**), explaining the longer optimum-performance period for these anodes than the graphite-rod anodes (**Figure 3.4A**). Still, we could only maintain a longest optimum-performance period of three days for the BES with activated-carbon anodes and soluble Fe^{2+} (**Table 1**). By comparing the CH_4 production rate (**Figure 3.4A**) with the H_2 production rate (**Figure 3.4B**), we observed different onsets of H_2 production after the CH_4 production had peaked for graphite-rod, thermally activated-graphite-felt, and activated-carbon anodes (with and without iron). This indicated that the electrochemical system was not limiting (H_2 production did not stop). Thus, carbon oxidation had not diminished the available carbon at the anode to maintain a working electrochemical system.

This also became clear when we increased the size of the anode surface areas and observed a similar optimum-performance period of one day for each of the BESs with the 1x1 cm-, 1x2 cm-, and 2x2 cm-thermally activated-graphite-felt anodes and with L-cysteine as the sulfur source and reducing agent in our growth medium (**Figure S3**). While the larger electrode provided a larger surface area for the carbon oxidation to occur and a more stable cell voltage (**Figure S4**), it did not improve the performance. Such a similar performance showed that, indeed, the carbon material was not limiting but that something else was limiting the methanogens to produce CH_4. Without a

membrane, L-cysteine oxidizes to L-cystine, which may render L-cysteine unavailable as a sulfur source and reducing agent (Zhou et al. 2007). Therefore, we investigated whether the relatively fast oxidation of reducing sulfur components in the growth medium would diminish our sulfur source for methanogenic growth and activity.

Instead of L-cysteine, we added 0.1 $g \cdot L^{-1}$ Na_2S as a sulfur source and reducing agent to our treatment for the BESs to have a measurable sulfur source and a more potent reducing agent to lower the oxygen redox potential (ORP) without harming the microbes (Fink et al. 2021). We used thermally activated-graphite-felt anodes with 0.1 g L^{-1} Fe^{2+} because this resulted in the maximum cathode-based geometric CH_4 production rate (**Table 1**). However, we increased the anode size from 1x1 to 2x2 cm and also increased the number of methanogenic cells during inoculation by 10 times compared to previous experiments. We compared the treatment with Na_2S and soluble Fe^{2+} to the control with L-cysteine and soluble Fe^{2+}, and obtained a similar: (1) CH_4 production pattern; and (2) optimum-performance period of two days compared to previous results (**Figure 3.4A**), and between the treatment and the control (**Figure S5A**).

To determine whether sulfide was oxidized and limiting the methanogens in our BESs, the sulfide concentration of each sampling point was measured for the treatment BESs through a photometric assay. The sulfide concentration decreased rapidly after the first day, proving that sulfide was removed, likely by oxidation (**Figure S5B**). After three days, sulfide was nearly depleted (**Figure S5B**). In addition, the ORP value increased from -375 mV to -100 mV showing that the reducing power of sulfide was removed at the same time (**Figure S5C**). These results suggest that the previous experiments were all limited in sulfur compounds, such that the sulfur source and/or the reducing power became limiting to the methanogens (**Table 1**).

A potential inhibiting factor for *M. thermautotrophicus* ΔH is an ORP value that is not negative enough to provide reducing power. In fact, electromethanogenesis would already be inhibited at a minimum ORP of -200 mV (Hirano et al. 2013). Because both sulfur compounds were oxidized during the BES operating conditions, the reducing power and, subsequently, the ORP value for methanogenesis should worsen. To find out whether the depletion of the sulfur source or the increase in the ORP due to the

absence of the reducing agent limited the methanogens after oxidation of reduced sulfur compounds, we added another treatment. Besides the Na_2S and soluble Fe^{2+}, we added Ti-NTA, L-cysteine, and soluble Fe^{2+}. In fact, we introduced Ti-NTA at the beginning of the experiment and after every sampling point. However, no difference in the cathode-based geometric CH_4 production rate was observed between Ti-NTA and the control (L-cysteine) (**Figure S5A**). In addition, the ORP values were similar throughout the operating period and had crossed the minimum value of -200 mV between Day 1 and Day 3 (**Figure S5C**). Thus, adding Ti-NTA did not lower the ORP because Ti^{3+} was also oxidized at the anode, preventing its reducing power from being effective. Therefore, we could not distinguish whether the depletion of the sulfur source or the increase in the ORP due to the absence of the reducing agent limited the methanogens.

Regardless, reduced sulfur compound was the limiting factor of the single-chamber BES. Therefore, the recovery of sulfide *in situ* after sulfur oxidation is a desirable objective to circumvent the continuous supply of sulfide to the electrochemical system. For a recent study by Izadi et al., sulfide was oxidized at the anode to elemental sulfur after which the sulfide was recovered at the cathode by switching the polarity of the electrodes (Izadi et al. 2021). Based on their study, we performed a BES experiment using thermally activated graphite felt as both anode and cathode while adding 0.1 $g \cdot L^{-1}$ Na_2S as an additional sulfur source. The polarity of the electrodes was switched every 4 h to reduce the elemental sulfur to sulfide. However, our study did not have a desirable outcome because the cathode-based geometric CH_4 production rate was lower than in all other BES experiments, possibly due to a stressed environment (**Figure S6A**). In addition, the sulfide concentration was depleted faster, limiting CH_4 production (**Figure S6B**). We cannot rule out that sulfide was oxidized to higher charged sulfur oxides, such as sulfate or thiosulfate, which are more difficult to reduce back to sulfide, preventing the capability to recover sulfide.

3.5.5. Soluble iron elongated the optimum-performance period for reasons that are related to sulfide oxidation

We performed cyclic voltammetry (CV) measurements with two carbon materials at the anode in an abiotic experiment with 6 treatments of which with and without L-cysteine and with and without soluble Fe^{2+} were included (**Figure 3.4C**). We were interested in observing the onset potential of the oxidation of reduced sulfur compounds during the forward electrochemical scan (5 mV s^{-1}). The thermally activated graphite felt with L-cysteine and without soluble Fe^{2+}, showed the earliest onset potential of the six cyclic voltammograms and an electrochemical shoulder with a mid-point potential of +1.25 V *vs.* Ag/AgCl (**Figure 3.4C**). The resulting faster oxidation of L-cysteine rate, explains why the optimum-performance period for the BES was the shortest between the thermally activated graphite felt and activated carbon anode treatments (one day in **Table 1**). Adding soluble Fe^{2+} to the thermally activated graphite felt anode with L-cysteine clearly shifted the onset potential to a higher voltage (**Figure 3.4C**), reducing the oxidation of L-cysteine rate in our BES, and explaining the longer optimum-performance period (two days in **Table 1**). The no-L-cysteine control (*i.e.*, no-sulfur control) shifted the onset potential further to a higher voltage, which was anticipated (**Figure 3.4C**).

Even though the current densities for the three cyclic voltammograms with activated carbon were approximately four times lower than with thermally activated graphite felt (**Figure 3.4C**), we observed the same order of first onset potentials (L-cysteine without soluble Fe^{2+}; L-cysteine with soluble Fe^{2+}; and without L-cysteine and without soluble Fe^{2+} [control]). We found a mid-point potential of +1.5 V *vs.* Ag/AgCl with the activated carbon with L-cysteine and without soluble Fe^{2+} (**Figure 3.4C**). The higher mid-point potential of L-cysteine oxidation (1.5 *vs*. 1.25 V) and the lower current densities explain why the activated carbon with L-cysteine but without iron showed a longer optimum-performance period for the BES compared to the thermally activated graphite felt (two days *vs*. 1 day in **Table 1**) – the slower L-cysteine oxidation rate elongated the growth period of methanogens. The addition of soluble Fe^{2+} to the activated carbon with L-cysteine, showed the same result as with thermally activated graphite felt: **(1)** a slower onset potential; and **(2)** a higher mid-point potential (1.6 V

vs. Ag/AgCl in **Figure 3.4C**), explaining the higher optimum-performance period (three days in **Table 1**). Thus, the addition of soluble Fe^{2+}, reduced the L-cysteine oxidation rate.

We suspect that the formation of iron sulfide (FeS) in the electrolyte and/or at the anode slowed the oxidation of reduced sulfur compounds, allowing the methanogens a longer growth period before the sulfur source became limiting. Indeed, the activated carbon-based anodes with soluble Fe^{2+} showed a decreased overall iron concentration throughout time (**Figure S7**). The initial iron concentration was 0.1 $g \cdot L^{-1}$, continuously decreasing until it stabilized after three days (**Figure S7**). In addition, we observed the precipitation of FeS, which persisted as a black precipitate. The removal of sulfide through FeS is a desired outcome in water treatment (Lin et al. 2017). Fortunately, it has been shown to benefit *M. thermautotrophicus* ΔH by improving CH_4 production after adding Fe (Cheng et al. 2020). Here, the formation of FeS benefited the microbe by lowering the oxidation of reduced sulfur compounds rate. However, FeS is still redox active with sulfide oxidation as an ultimate result, explaining that the maximum optimum-performance period was still only three days (**Table 1**).

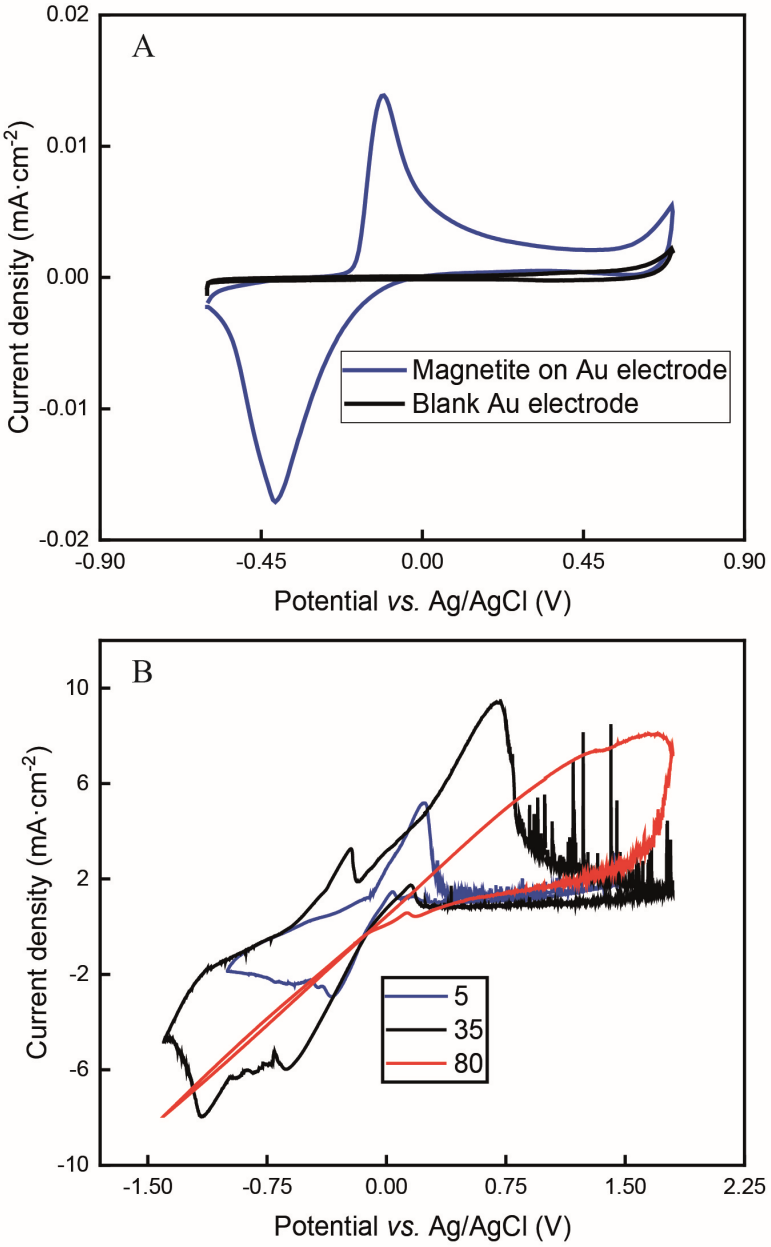


Figure 3.5: Electrochemical analysis of magnetite: **(A)** cyclic voltammogram of magnetite nanoparticles that were drop-casted on an Au electrode at a scan rate of 20 mVs^{-1} in 66 mM phosphate buffer; and **(B)** cyclic voltammograms of bulk magnetite at cycle 5, 35, and 80 at a scan rate of 20 mVs^{-1} in 50 mM PBS.

3.5.6. Magnetite, which is an alternative redox mediator to soluble iron, shortened the optimum performance period.

The cyclic voltammogram of synthesized magnetite nanoparticles that were immobilized on an Au electrode featured two peaks with a peak splitting of +0.28 V, representing the oxidative peak at -0.12 V *vs.* Ag/AgCl and the reductive peak at -0.41 V *vs.* Ag/AgCl (**Figure 3.5A**). The comparison of the standard potential of both magnetite-oxidation reactions with the literature exhibited that the two-electron oxidation of magnetite to maghemite (**Eq. 5**) occurred for our system (Bradley and Tratnyek 2019). Roberts et al. had shown that magnetite is prone to develop this irreversible reaction, which would have a negative impact on long-duration BES experiments (Roberts et al. 2014). Indeed, the cyclic voltammograms of bulk magnetite showed decreasing reaction rates with increasing cycles (**Figure 3.5B**), which can be explained by the formation of maghemite (**Eq. 5**).

To quantify the reaction rates, Tafel slopes were calculated from bulk magnetite during different cycles of the cyclic voltammogram (**Supporting Information note 1** and **Figure 3.5B**). Bulk magnetite electrodes achieved 187 mV/dec at cycle 5. It transitioned to 617 mV/dec and 1310 mV/dec at cycles 35 and 80, respectively (**Figure 3.5B**). The formation of maghemite increased the inner resistance of the anode material to decrease its reaction rate by forming a resistor-type cyclic voltammogram (Fig. 4B), which likely would constrain the BES. This is one possible reason why we observed the shorter optimum performance period of two days *vs*. three days for magnetite-coated activated carbon anodes and activated-carbon anodes, respectively. However, more work would be necessary to exclude other possible reasons.

3.5.7. When sulfur source limitations are overcome, carbon at the anode would become a limiting factor

The oxidation and the removal of the carbon anode itself due to its sacrificing nature, would likely be the next liming factor of our BES due to a lack of accessible carbon to be oxidized. Our proof-of-concept BESs used relatively small geometric anode surfaces of 1.57 cm^2. For our calculation, we used the ideal reaction of donating four electrons

and producing CO_2 during carbon oxidation (**Eq. 2**). To calculate the radius change (Δr) during the two-day optimum performance period of the activated carbon anode (as one example anode), we first calculated the volume (V) of carbon that was consumed (Eqs. 6-9), which was equivalent to $1.10 \cdot 10^{-2}$ cm^3 ($8.95 \cdot 10^{-4}$ mol carbon), using the equation of the Coulombic efficiency (Kracke et al. 2020). The exposed surface of the activated carbon anode corresponded to a halved cylinder so that the volume after the optimum performance period and its corresponding radius change would be:

$$V_{after\ optimum\ performance} = V_{start} - V_{consumed} = \frac{1}{2} \cdot \pi \cdot {r_{start}}^2 h - 1.10 \cdot 10^{-2}\ cm^3 \quad (6)$$

$$\frac{1}{2} \cdot \pi {r_{after\ optimum\ performance}}^2 h = V_{start} - V_{consumed} \quad (7)$$

$$r_{after\ optimum\ performance} = \sqrt[2]{\frac{(V_{start} - V_{consumed}) \cdot 2}{\pi \cdot h}} \quad (8)$$

$$\Delta r = r_{start} - r_{after\ optimum\ performance} \approx 34\ \mu m \quad (9)$$

With r_{start} = 0.475 cm and h = 2.175 cm. The relatively small change in the radius of 34 µm shows that the accessible carbon did not limit the system's performance yet. We could not determine when the carbon would become limiting due to the sulfur source limitations. If this occurs, the accessibility of carbon should be increased. This can be achieved by adding more carbon after increasing the ratio of anode surface area to reactor volume or improving the reactivity of the carbon. In addition, anodes could be replaced periodically.

3.5.8. A final limitation would be the impact of carbon corrosion on the CH_4 production rates

We observed that the activated carbon-based electrodes started to disintegrate, and small carbon particles were found in suspension (**Figure S8**) that might impact the CH_4 production rate during long-term operating conditions (considerably longer than three days). We refer to this as carbon corrosion, which could impact the CH_4 production rate mostly negatively due to: (1) the exfoliation of carbon material at the

anode, limiting carbon oxidation; and (2) the toxicity of a tar-like solution to methanogens. On the other hand, there is a mechanism known from abiotic carbon oxidation systems that could improve CH_4 production, which we refer to as indirect carbon oxidation by Fe^{3+} (described below). Therefore, we examined carbon corrosion by investigating the surface and the bulk of the anodes with FTIR to track the change of functional groups exhibited at the carbon material. We used the activated-carbon anodes from our abiotic experiments during the measurements of the liquid O_2 concentration (no soluble iron was added).

Several oxidized functional groups from the initial activated carbon material, such as ketones and phenol groups, were identified by the C=O stretching bond at 1700-1800 cm^{-1} and -OH stretching bonds at 3300-3600 cm^{-1}, respectively (**Figure S9**). The absorbance peak at 2500-3000 cm^{-1} represented the C-H stretching bond of the paraffin oil, which we had added to produce the anodes. The larger absorbance of -OH bonds suggested an alkaline chemical activation of the carbon from the manufacturer. Almost all the -OH stretches disappeared after five days of anode oxidation. The phenol functional group can act as a catalyst for carbon oxidation and facilitate the CO_2 reaction at the anode. Once the functional group was consumed, the electrode exfoliated in small carbon particles.

While small concentrations of carbon particles in solution might not have a big influence, higher concentrations have been shown to influence methanogenesis. Cavalcante et al. identified that adding conductive material of carbon particles to a culture of methanogens enhanced methanogenesis (Cavalcante, Gehring, and Zaiat 2021). However, inhibition of methanogenesis occurred even at lower carbon material concentrations when the inoculation was performed at a relatively low cell density. In addition, Umetsu et al. showed that *M. thermautotrophicus* ΔH adsorbed on -OH and -COOH functional groups and prevented hydrogen or mineral uptake, inhibiting methanogenesis (Umetsu et al. 2020).

We also found that carbon corrosion and the reaction of the released carbon with Fe^{3+} (**Eq. 10**) could explain another stimulation of the CH_4 production rate besides: **(1)** reducing the oxidation of reduced sulfur compounds rate due to FeS formation; and **(2)** the presence of conductive particles. Iron would need to be present in our

membrane-less BES for this other stimulation, and we refer to this mechanism as indirect carbon oxidation by Fe^{3+}. The continuous addition of soluble Fe^{2+} stimulated abiotic carbon oxidation systems because Fe^{2+} is directly reduced at the carbon-based anode to Fe^{3+} (**Eq. 4**). However, even without continuous soluble Fe^{2+} addition, a current increase can be anticipated due to the circular nature of the electron-mediating process, with the ultimate electron donor coming from the carbon-based anode material than the continuously added Fe^{2+}. This is due to indirect carbon oxidation by Fe^{3+} using carbon in the solution that originated from carbon corrosion at the anode (**Figure 3.6**). Indirect carbon oxidation reduces Fe^{3+} back to Fe^{2+} in the solution, while carbon is oxidized to CO_2 (**Eq. 10** and **Figure 3.6**). The reactions of the electron-mediating process can be described as follows:

$$\mathrm{C} + 4\mathrm{Fe}^{3+} + 2\mathrm{H_2O} \rightarrow \mathrm{CO_2} + 4\mathrm{Fe}^{2+} + 4\mathrm{H}^{+} \quad (10)$$

Because the reduction and oxidation of soluble iron species occur at the anode and with carbon in solution in the electrolyte, respectively, there is a continuous reformation of Fe^{2+} to maintain a higher current density for the electrochemical cell. An advantage of the circular nature of this electron-mediating process is that Fe^{3+} is oxidized in the electrolyte with carbon and not at the cathode, which, as a competing process, would have reduced the Coulombic efficiency for methane production.

We do not know whether carbon corrosion would have positive or negative effects on the CH_4 production rate and the duration of the optimum-performance period for our BES. We would first need to solve the reduced sulfur compound oxidation problem. Likely, there may be an initial positive effect when carbon corrosion is only starting to occur, but when more and more carbon particles accumulate, we may observe a negative effect of carbon corrosion. Therefore, measures should be taken to reduce the negative effects of carbon corrosion on the anode activity and microbial activity to lengthen the optimum performance period of anode oxidation with sacrificial anodes.

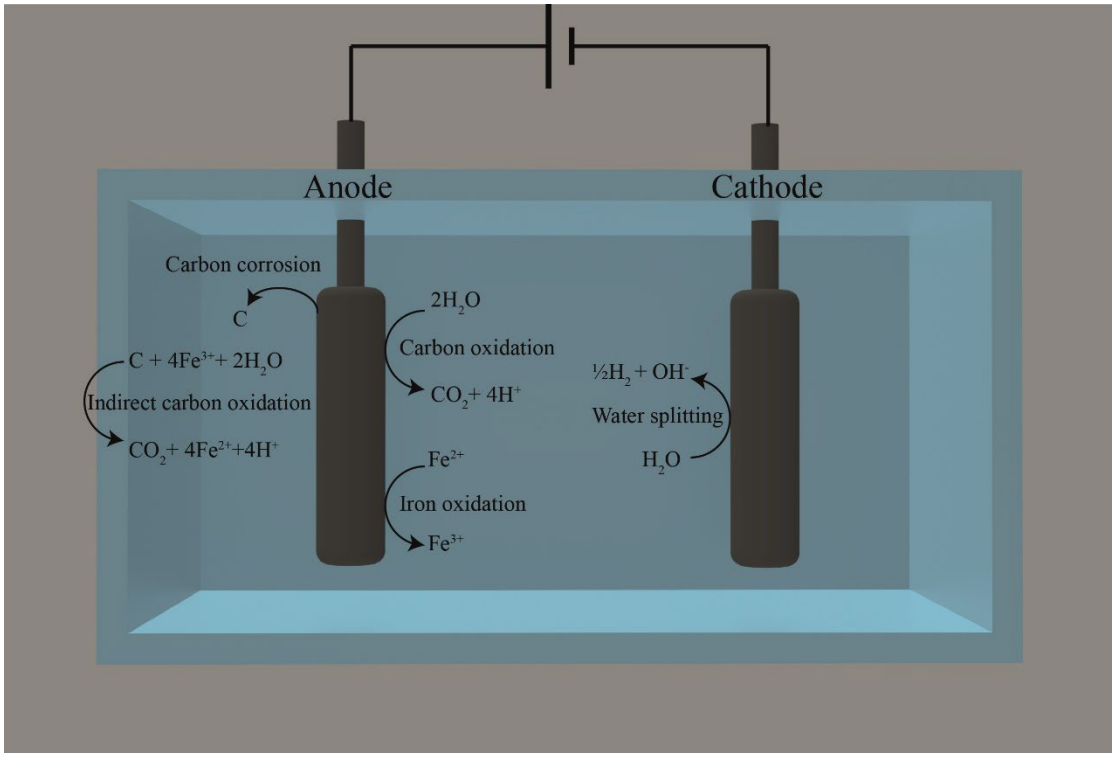


Figure 3.6 : Overview of the reactions that occur at the anode and cathode during the carbon oxidation using thermally activated graphite felt and activated carbon anodes with 0.1 $g \cdot L^{-1}$ of Fe^{2+}. Water splitting takes place at the cathode to produce H_2. The main reaction at the anode is carbon oxidation, followed by the oxidation of Fe^{2+} and indirect carbon oxidation by the formed Fe^{3+}. For more information, see section on the impact of carbon corrosion on the CH_4 production rates.

3.5.9. Carbon oxidation with sacrificial anodes for single-chamber BES is ready for research purposes within the field of microbial electrosynthesis

We showed that implementing carbon oxidation with sacrificial anodes in a single-chamber BES can perform microbial electrosynthesis. We cultivated *M. thermautotrophicus* ΔH with *in-situ* produced H_2 at the cathode under constant pH and temperature conditions to produce CH_4 for an optimum performance period of three days. The growth behavior followed a similar trend for all BESs until the amount of sulfur source limited the CH_4 production rates. Our maximum cathode-based geometric CH_4 production rate was already compatible with other studies due to similarly set current densities (Kracke et al. 2020). Further optimizations of our system should not only increase the geometric CH_4 production rate but also prolong the production days to several weeks. With the relatively low current densities of microbial electrosynthesis, our system is already useful for research purposes because

the sulfur source will not become limiting that fast with lower current densities. Our work can also inform the earlier studies with a single-chamber BES in the field of perchlorate removal (Zeppilli et al. 2019). We advise the authors to replace the graphite anode materials with activated-carbon anode materials and to add soluble iron to increase the performance.

3.5.10. Before the industrial application of carbon oxidation with sacrificial anodes in BES for microbial electrosynthesis can commence, several breakthroughs are required.

Our system would have a considerably lower theoretical power consumption than membrane-based two-compartment cells due to the lower potential to operate the BES (**Figure S4** and **S10**). After optimizing the single-chamber BES and making it continuous, a direct comparison between the production rates and power consumption rates should be performed with a conventional membrane-based cell for microbial electrosynthesis. Another advantage of the single-chamber cell compared to a membrane-based cell would be the lower capital costs due to the absence of ion-exchange membranes, albeit a full techno-economic analysis would be necessary to be conclusive. These advantages make our system a desirable opportunity for scale-up. However, several problems must be overcome.

We must prolong the optimum performance period to several months rather than a few days before scale-up can commence. We observed the limiting factor of sulfur source availability in our membrane-less BES, which had a promising current density. Utilizing a microbe that is not reliant on a redox-active sulfur compound as either a sulfur source for growth or to provide reducing power would be one route to overcome the utilization of a single-chamber BES. If this problem can be overcome, we predict two additional limitations for our membrane-less BES: **(1)** the availability of accessible carbon; and **(2)** carbon corrosion. Because carbon gets consumed over time, innovative BESs must be designed to refill the consumed carbon at the anode.

Undoubtedly, carbon corrosion would inhibit the growth of microbial cells during operating periods of several weeks, depending on the current densities. In addition, carbon corrosion would introduce a higher content of -OH, -C=O, and -COOH

functional groups, increasing the charge transfer resistance of the carbon material and decreasing the electrochemical performance.(Liu et al. 2020) Consequently, the carbon anode decreases its conductivity and current density, while deteriorating. Ideally, carbon corrosion is avoided by efficiently transforming carbon into CO_2 or CO. Studies to mitigate carbon corrosion currently tend to use either expensive catalysts to protect the carbon material or structurally stronger carbon, such as graphene or carbon nanotubes (Zhao, Tu, and Chan 2021). In our case, excessive carbon corrosion has to be avoided, and a continuous system rather than our batch system could remove the by-products. Furthermore, mesoporous carbon would enlarge the surface area and the porosity, allowing more reaction sites for carbon oxidation rather than carbon corrosion.

3.6. Conclusion

We have proven the concept that microbial electrosynthesis is possible in a BES without membranes by utilizing carbon oxidation with sacrificial anodes. Our BES produced CH_4 with an O_2-sensitive thermophilic methanogen at a cathode-based geometric current density of 1 mA cm^{-2} for 3 days after which reduced sulfur compounds became limiting in the growth medium due to sulfur oxidation at the anode. The system is ready for microbial electrosynthesis experiments with relatively low current densities to perform basic research. However, for industrial applications, several breakthroughs are necessary to overcome limitations at the anode, such as sulfur oxidation, refilling of carbon, and protecting against carbon corrosion.

3.7. Experimental section

3.7.1. Chemicals, strain, and medium

All chemicals were used as received unless otherwise noted in the text. These chemicals were of technical or analytical grade and were purchased from Sigma-Aldrich (St. Louis, USA), Alfa Aeser (Haverhill, USA), Merck (Darmstadt, Germany), Thermo-Fischer (Waltham, USA), VWR (Radnor, USA), and Carl Roth (Karlsruhe, Germany). The strain *M. thermautotrophicus Δ*H (DSM 1053) was obtained from the DSMZ (Braunschweig, Germany). A pre-culture was grown at 60°C in 100-mL serum bottles with 20 mL of modified anaerobic MS-Medium containing (per liter): 6.77 g

$NaHCO_3$; 0.17 g K_2HPO_4; 0.235 g $(NH_4)_2SO_4$; 0.09 g $MgSO_4$; 0.06 g $CaCl_2$ x 2 H_2O; 0.23 g KH_2PO_4; 1 mL trace elements (10x); 1 mL of 4 M H_2SO_4; 0.5 g L-cysteine hydrochloride (Fink et al. 2021). The trace-element solution was a 10x stock solution containing (per 100 mL): 0.2 g nitrilotriacetic acid; 3 g $MgSO_4$ x 7 H_2O; 0.5 g $MnSO_4$; 0.3 g $FeSO_4$ x 7 H_2O; 0.11 g $CoSO_4$ x 7 H_2O; 0.068 g $CaCO_3$; 0.18 g $ZnSO_4$; 0.01 g $CuSO_4$ x 5 H_2O; 0.018 g $KAl(SO_4)_2$ x 12 H_2O; 0.01 g H_3BO_3; 0.01 g Na_2MoO_4 x 2 H_2O; 0.48 g $(NH_4)_2Ni(SO_4)_2$ x 6 H_2O; 0.01 g Na_2WO_4 x 2 H_2O; 0.01 g Na_2SeO_4. The trace-element solution was adjusted to a pH value of 1 with H_2SO_4. The MS-Medium was buffered only in the bioelectrochemical system by adding 2.5 M 3-(*N*-morpholino)propanesulfonic acid (MOPS) at pH = 7.2 for a final media concentration of 25 mM. 25mM Ti-NTA was prepared according to Moench et al.(Moench and Zeikus 1983). All solutions were sterilized either through a sterile filter or autoclaved and made anaerobic by sparging with N_2 or N_2/CO_2.

3.7.2. Preparation of carbon-based electrodes

The activated carbon served not only as active material but also as a conductive and surface enlarging material and was used as purchased (~100 mesh particle size (~150 µm), DARCO®, Cabot Norit Americas Inc, Marshall, USA). The activated carbon and paraffin oil (Sigma-Aldrich) was homogeneously mixed in a mortar at 70%:30% to form a paste (Zhang et al. 2017). The resulting paste was pelleted into a self-made electrode holder and cured in an 80°C vacuum oven for 4 h. Activated-carbon-associated magnetite was synthesized through a co-precipitation method by mixing activated carbon with 2 M $FeCl_3$ and 1 M $FeCl_2$ (Sorwat et al. 2020). Then, 20 % NH_4OH was slowly dropped into the solution until pH 9. The solution was stirred for 1 h to complete the synthesis of magnetite. The precipitate was centrifuged, cleaned with deionized water until pH 7, and dried in a vacuum oven at 80°C for 4 h. Different amounts of activated carbon to magnetite were used during the synthesis ranging from 0% to 60% of activated carbon. In this study, activated carbon that was co-precipitated with magnetite is called magnetite-coated activated carbon (**Supporting Information**). The 60% activated carbon and 40% maghemite mixture was synthesized by adding 60 % activated carbon and 40% magnetite mixture into an aerated oven at 80°C for 24 h.

3.7.3. Measurement of dissolved O_2

The O_2 measurements were carried out in a self-designed five-neck round flask. To measure the dissolved O_2, an O_2-sensitive foil (0-100% O_2, PreSens Precision sensing, Regensburg, Germany) was glued at the mid-height of the flask. The electrochemical cell was operated as a two-electrode setup with a 1x1-cm carbon cloth electrode as the cathode. A platinum wire, a graphite rod, a thermally activated graphite felt, a carbon cloth, activated carbon, and activated carbon that was coated with magnetite were used as anodes. Thermally activated graphite felt and activated carbon anodes were used with addition of soluble iron. The measurements were carried out in 0.066 M phosphate buffer at room temperature and 60°C. The phosphate solution was buffered at 7.2 to mimic the pH of the MS medium used in the bioelectrochemical system. Before each experiment, the cells were purged with N_2 gas for 1 h to secure an O_2-free solution.

3.7.4. Sample analyses

The bioelectrochemical systems were sampled once per day. The gas compositions of the bioelectrochemical systems were sampled with a 500-µL gastight syringe (Hamilton, Reno, USA) and analyzed using a gas chromatograph (SRI GC, Torrance, USA). The gas chromatograph used a Haysep D column (length 3m, outer diameter 1/8”, SRI GC) and a Molsieve 13X column (length 3m, outer diameter 1/8”, SRI GC). It was equipped with a thermal coupled detector and a flame ionization detector to measure N_2, O_2, H_2, and CO_2, and CH_4, respectively. N_2 and H_2 were used as carrier gas. Coulombic efficiencies for CH_4 were calculated according to Kracke and coworkers (Kracke et al. 2020). Cell growth was measured by cell counting with a light microscope (X41, Olympus, Shinjuku, Japan). The anodes were collected after the experiment and stored anoxically at -20°C for further analyses. The outer layer and the bulk of magnetite particles were analyzed through a sequential extraction. First, the outer layer of magnetite particles was dissolved by acidifying with 1 M HCl for 1 h. It was followed by a complete dissolution of the magnetite particle by acidifying with 6 M HCl for 24 h. The iron content from the liquid samples and the oxidation state of iron in the magnetite electrodes were further analyzed *via* the Ferrozine assay (Stookey 1970; Sorwat et al. 2020). Sulfide concentrations were determined photometrically

based on a modified version of Cline and Gilboa-Garber (CLINE 1969; Gilboa-Garber 1971). Sulfide samples were stabilized with $Zn(ac)_2$ and stored at -20°C. The diamine reagent (N,N-Dimethyl-p-phenylenediamine sulfate salt and $FeCl_3$) was mixed with the stabilized sample at a 1:1 ratio and kept in the dark for 30 min for the reagents to react. The samples were measured at 565 nm. The ORP was measured with an ORP electrode (Hanna Instruments, Vöhringen, Germany) connected to an ORP controller (Alpha pH 800, Eutech Instruments, Singapore).

3.7.5. Electrochemical system

All electrochemical measurements (cyclic voltammetry, linear sweep voltammetry, and chronopotentiometry) were conducted in a five-neck round flask with a working volume of 50 mL. The electrochemical cells were operated as a two-electrode or a three-electrode setup and controlled *via* a potentiostat (VMP3, Bio-Logic, Grenoble, France). An Ag/AgCl (3M KCl, 0.210 V *vs*. SHE) in-house-made reference electrode was used for the three-electrode setup. All measurements with a reference electrode were ohmic-drop corrected and were determined by potentiostatic electrochemical-impedance spectroscopy. Ohmic-drop-corrected potentials were calculated following the method of Sun and coworkers (Sun et al. 2017). The reaction kinetics of carbon and magnetite were calculated with the Butler-Volmer equation, using linear sweep voltammetry and cyclic voltammetry measurements (Supporting Information). The 1x1-cm carbon cloth electrode (PANEX 30-PW06, Zoltek, St. Louis, USA), thermally activated graphite felt (Sigracell, SGL carbon, Bonn, Germany) and the platinum wire (Bioanalytical Systems, Inc., West Lafayette, USA) were used as cathodes, and the carbon-based electrode, graphite rod (Mersen, Suhl, Germany), carbon cloth (Zoltek), thermally activated graphite felt (SGL carbon), the carbon paste electrode holder (Bio-Logic), and the gold electrode (Bio-Logic) were used as anodes depending on their intended application, which is described in the results part. A titanium wire (Sigma Aldrich, St. Louis, USA) was threaded through the carbon cloth and thermally activated graphite felt, and glued with carbon conductive cement (Thermo-Fischer, Waltham, USA) for better conductivity. The temperature was either room temperature or controlled by a water bath at 60°C (ICC basic IB R RO 15 eco, IKA, Staufen im Breisgau, Germany). The supporting electrolyte for the abiotic experiments was phosphate

buffer (0.066 M) or phosphate buffered saline (0.05 M), with the pH buffered at 7.2. Before each abiotic electrochemical experiment, a high-purity N_2 gas was introduced to remove O_2. The bioelectrochemical systems were either autoclaved or chemically sterilized before the beginning of each experiment. The reactors were filled with 50-mL MS-Medium, were made anaerobic by sparging with 80:20 (*v/v*) N_2/CO_2 through a sterile filter, and were continuously stirred with a magnetic stir bar. The reactors were operated in batch mode and were fed for 5 min with pure CO_2 as the sole carbon source *prior* to the experiment and every day for 1 min after liquid sampling to exchange the headspace. After feeding, an overpressure of 80 mbar of CO_2 was kept in the headspace. The electrochemical cells were submerged in a water bath to prevent heat loss for optimal growth of *M. thermautotrophicus* ΔH at 60°C.

3.7.6. Immobilization of magnetite

Magnetite was immobilized by dispersing magnetite nanoparticles onto an Au electrode (Biologic) to test its electrochemical behavior. The protocol is an adjusted version from Sun and coworkers (Sun et al. 2017). Briefly, ten milligrams of the active powder and 40 µL of Nafion were mixed with 960 µL 70% ethanol and sonicated for 15 min. Then, 10 µL were drop casted onto the surface of the Au electrode and dried at room temperature. To avoid iron from oxidizing, the preparations for the drop casted magnetite were performed inside a glovebox (mBraun, Garching, Germany).

3.7.7. SEM, EDX, X-ray diffraction, and FTIR

A 50-µL aliquot of 0.1% poly-L-lysine solution was placed onto a glass slide and was dried for 1 h in a 60°C incubator. The samples were placed onto a poly-L-lysine coated glass slide that was attached to aluminum stubs, using carbon adhesive tabs. The sample was coated with a 10-nm deposition of platinum, using a BAL-TEC^{TM} SCD 005 sputter coater (Leica biosystems, Nussloch, Germany). The purpose of the coating was to reduce any charging effects during scanning electron microscope (SEM) analysis. All images were taken in secondary-electron (SE) mode using a Zeiss Crossbeam 550L focused ion beam (FIB) SEM (Zeiss, Wetzlar, Germany), which was operated with an acceleration voltage of 2 kV. The SEM was equipped with an Oxford Instrument energy dispersive spectrometry detector (Ultim Max, Oxford Instrument, Abingdon, United

Kingdom). Elemental maps of iron and carbon were obtained along with corresponding spot analysis.

X-ray diffraction (XRD) was carried out on dry material using Bruker's D8 Discover GADDS XRD2 micro-diffractometer that was equipped with a Co-anode (Cu Kα radiation, λ = 0.154 nm) at parameters of 30 kV/30mA (Billerica, USA). The total measurement time was 240 s at two detector positions, which were 15° and 40°. Fourier transform infrared (FTIR) spectroscopy was performed on a Vertex 80v equipped with an RT-DLaTGS detector (Bruker, Billerica, USA). 0.5 mg of sample was mixed homogenously with 250 mg KBr (FTIR grade, Carl Roth, Karlsruhe, Germany) and compressed at 10T to form a pellet. Samples were scanned 32 times in the range of 400-4500 cm^{-1}.

3.8. Acknowledgements

This work was supported by the Deutsche Forschungsgemeinschaft (DFG, German Research Foundation, EBiotech, SPP2240; L.T.A.) – project number 445506379, the Alexander von Humboldt Foundation in the framework of the Alexander von Humboldt Professorship (L.T.A.), and The Novo Nordisk Foundation CO_2 Research Center with grant number NNF21SA0072700 (L.T.A.). L.T.A and A.K. are also grateful to funding from the Deutsche Forschungsgemeinschaft under Germany´s Excellence Strategy – EXC 2124 – 390838134. R.B-G. was supported by an FPI grant (BES-2015-074229) from the Spanish Ministry of Economy and Competitiveness (MINECO) within the research project CTQ2014-53718R. The authors gratefully acknowledge the Tübingen Structural Microscopy Core Facility (Funded by the Federal Ministry of Education and Research (BMBF) and the Baden-Württemberg Ministry of Science as part of the Excellence Strategy of the German Federal and State Governments) for their support and assistance in this work. The authors also thank the German Research Foundation DFG (INST 37/1027-1 FUGG) for the financial support provided for the acquisition of the cryogenic focused ion beam scanning electron microscope. We thank Prof. Dr. Uwe Schröder (University of Greifswald) for helpful and insightful discussions.

Chapter 4

Performance effect on different shutdown methods of three electrode materials for power-to-gas with electromethanogenesis

This chapter is a preliminary manuscript in collaboration with the company Electrochaea GmbH. The list of authors are: Nils Rohbohm, Maren Lang, Johannes Erben, Kurt Gemeinhardt, Nitant Patel, Ivan Ilic, Doris Hafenbradl, Jose Rodrigo, and Largus T. Angenent.

4.1. Author Contributions

D.H., J.R., and L.T.A. initiated the work. M.L., J.E., J.R., N.P., and N.R. designed the experiments. M.L., N.R., J.E., and K.G. performed the laboratory experiments and analyzed the data. L.T.A. and J.R. supervised the project. N.R. wrote the manuscript. L.T.A. edited this chapter.

4.2. Abstract

In the prospect of industrial bioelectrochemical systems, regular maintenance shutdowns are essential for optimal performance, involving inspections and component replacements to extend the system lifespan. This study examines the impact of such shutdowns on three electrode materials (platinized titanium, graphite, and nickel) in a microbial electrolysis cell that is used for electromethanogenesis in power-to-gas applications. The focus is on methane (CH_4) production from hydrogen (H_2) and carbon dioxide (CO_2) using *Methanothermobacter thermautotrophicus*. Our study exhibited that the platinized titanium electrode, which balances efficiency and cost, had a high volumetric CH_4 production rate and coulombic efficiency. The microbial electrolysis cell using graphite electrode is cost-effective but was less efficient due to lower catalytic activity. The microbial electrolysis cell with the nickel electrode showed moderate improvements compared to the graphite experiment. Additionally, the nickel electrode experiment demonstrated the fastest recovery

during a shutdown experiment, followed by experiments involving platinized titanium and graphite electrodes. Notably, fluctuations in pH and nickel concentrations during power interruptions considerably affect CH_4 production recovery in the nickel electrode microbial electrolysis cell. This research enhances understanding of the integration of biological and electrochemical processes in microbial electrolysis cells, providing valuable insights into electrode selection and operating strategies for effective and sustainable CH_4 production.

4.3. Introduction

The power-to-gas (such as hydrogen [H_2], ammonia, or methane [CH_4]) concept harnesses surplus electrical energy to generate grid-compatible gas. Electrochaea GmbH has adopted this concept with biomethanation, harnessing excess electrical energy and CO_2 to generate CH_4 using *Methanothermobacter thermautotrophicus*, as detailed in work by Martin and coworkers (Martin et al. 2013). While it is possible to achieve high volumetric CH_4 production rates (Nishimura et al. 1992), the process faces challenges, as all the other green methanation processes, due to the high capital costs of conventional water electrolysis. This underscores the pressing need for an alternative method to realize power-to-CH4 conversion more effectively (Contreras et al. 2022).

Microbial electrochemistry is an interdisciplinary field that combines principles from biology and electrochemistry. It explores the ability of living microbes to interact with electrodes and utilize electrical energy for various processes. Microbial electrochemical systems have garnered considerable attention due to their potential applications in diverse fields, including energy generation (Christgen et al. 2023), environmental remediation (Ceballos-Escalera, Pous, Korth, et al. 2024), and biotechnology (Boto et al. 2023). Microbial electrosynthesis has emerged as a promising approach for sustainable chemical production within microbial electrochemistry. Microbial electrosynthesis involves the utilization of microbes to catalyze chemical reactions by accepting electrons in the form of H_2 from an electrode (Schröder, Harnisch, and Angenent 2015). These electrons are then used to drive

desired metabolic pathways, including reducing CO_2 to valuable compounds. By harnessing this unique capability, microbial electrosynthesis enables the conversion of CO_2, which is a greenhouse gas, into valuable chemicals and fuels, providing a potential solution for environmental and economic challenges. Ideally, all the generated H_2 at the cathode is transformed into CH_4, generating a fully grid-compatible gas. Furthermore, it could reduce capital expenditures by integrating biology into electrochemical cells. However, microbial electrosynthesis also faces certain limitations and technical obstacles. These challenges include low product yields, inefficient electron transfer, a limited range of products, and the need for a deeper understanding of microbial physiology (Prévoteau et al. 2020). Overcoming these hurdles necessitates interdisciplinary collaborations, combining bioelectrochemistry, microbiology, and engineering expertise to develop efficient and economically viable microbial electrosynthesis technologies.

Current density is pivotal, serving as a crucial metric that directly influences the efficiency and effectiveness of bioelectrochemical systems processes. It quantifies the amount of electric current passing through a unit area of the surface of an electrode, thus, dictating reaction rates, product selectivity, and overall performance. Enhancing current densities will result in improved reaction kinetics and yields. Recent studies have explored various approaches to enhance microbial electrosynthesis performance, focusing on either the cathode (Kracke et al. 2020) or the anode (Rohbohm et al. 2023), as well as optimizing cell configurations (Geppert et al. 2019; Baek et al. 2022; Rad et al. 2023). A crucial parameter in establishing a system is ensuring practical energy efficiencies (EE). Achieving high current densities at low operating cell potentials is essential for practical EE. Rad et al. demonstrated considerable progress with a hybrid microbial electrosynthesis system, achieving 42% EE over 160 days and a maximum CH_4 production rate of 669 LN(CH4) m^{-2} d^{-1} with an average current density of 30 mA cm^{-2} at 2.2 V, bringing us closer to a marketable microbial electrosynthesis (Rad et al. 2023). However, it was not well shown how much implication the porous Teflon membrane has on its performance. In addition, because the microbial community and catholyte are separated completely from the

cathode, it is not clear whether there is a real advantage to integrating them into one system.

It is worth noting that none of these studies have explored the challenges posed by industrial operating conditions, where operating cost (OPEX) and capital cost (CAPEX) considerably affect the feasibility of a technology, here microbial electrosynthesis (Jourdin et al. 2020). Embracing industrial conditions is crucial for replicating real-world settings, enabling rigorous testing and validation of processes, products, and technologies. Rovira-Alsina and coworkers have achieved acetate production parity with pure CO_2 gas, which used an H-type cell to simulate industrial off-gases with 14% CO_2 and 12% O_2 (Rovira-Alsina, Dolors Balaguer, and Puig 2022). Nonetheless, limitations such as non-continuous gas feed and open culture conditions may have impacted microbe survival. In another study, Deutzmann et al. demonstrated an effective microbial electrosynthesis powered by intermittent electricity, mirroring a solar energy grid's power profile (Deutzmann, Kracke, and Spormann 2023). They achieved >96% Coulombic efficiency (CE) in CH_4 production using *Methanococcus maripaludis*, showing the compatibility of BES with renewable energy fluctuations.

Here, we report a microbial electrolysis cell for simulated maintenance-induced intermittent shutdowns. We tested three types of electrodes, platinized titanium, graphite, and nickel, for scale-up processes relevant in terms of availability and cost-effectiveness. Platinized titanium electrodes strike a balance between efficiency and cost. By depositing a thin layer of platinum on titanium, these electrodes retain the catalytic prowess of platinum while mitigating the cost concerns associated with using pure platinum electrodes. This compromise makes platinized titanium electrodes a practical choice and served us as the control electrode. Graphite is economical and readily available, making it an attractive option for cost-conscious projects. Similarly, nickel, which is widely recognized for its role in abiotic H_2 electrosynthesis, presents an additional catalytic effect compared to graphite. We investigated how shutdown methods affect the electrode performance. All three electrodes were tested by comparing their performance in producing efficiently CH_4 from H_2 and CO_2 using *M. thermautotrophicus*.

4.4. Materials and methods

4.4.1. Chemicals, strain, and medium

All chemicals were used as received unless otherwise noted in the text. These chemicals were of technical or analytical grade. The used strain is an adapted laboratory strain of *M. thermautotrophicus* from Martin and coworkers (2013). The medium was a modified version of Martin et al. (2013). The inoculum for the BES was taken from a CH_4-producing continuous stirred-tank bioreactor.

4.4.2. Analytics

Sampling of the bioelectrochemical system occurred twice daily. Evolved gases from the reservoirs were collected in gas bags, and their composition was determined using a gas chromatograph (Agilent micro GC 490, Agilent Technologies, Sanata Clara, California). The gas chromatograph was equipped with two molsieve 5A and one pora PLOT U column. A thermal coupled detector measured N_2, O_2, CH_4, H_2, and CO_2. Argon was the carrier gas for one molsieve 5A column, while He was the carrier gas for the other two columns. Trace and major element analysis was conducted using an ion-coupled plasma mass spectrometer (Agilent 7900) with 1% HNO_3 as the matrix. The samples were centrifuged for 5 min at 25001 relative centrifugal force (Centrifuge 5427 R, Eppendorf; Hamburg, Germany). Every sample was diluted 1:100 in 1% HNO_3.

All scanning electron microscopy (SEM) images were taken in secondary-electron mode using a Zeiss Crossbeam 550L focused ion beam SEM (Zeiss, Wetzlar, Germany), which was operated with an acceleration voltage of 2 kV. The SEM was equipped with an Oxford Instrument energy dispersive spectrometry detector (Ultim Max, Oxford Instrument, Abingdon, United Kingdom). Elemental maps of iron and carbon were obtained along with corresponding spot analysis. The Nafion 117 samples were coated with a 10-nm deposition of platinum using a BAL-TEC^{TM} SCD 005 sputter coater (Leica Biosystems, Nussloch, Germany). The purpose of the coating was to reduce any charging effects during scanning electron microscope (SEM) analysis.

4.4.3. Operating conditions

The electrochemical cell employed was a two-chamber "flow-cell" from Electrocell (Electro MP Cell, Electrocell, Skjern, Denmark). This cell was divided into cathodic and anodic compartments, separated by a proton exchange membrane (Nafion 117, FuelCellsEtc, College Station, TX). The cathode (working electrode) materials included flat graphite (SGL Carbon, Wiesbaden, Germany), nickel (Electrocell, Skjern, Denmark), and platinized titanium (Electrocell, Skjern, Denmark), while the anode (counter electrode) material was iridium oxide (16 g m^{-2}) on titanium (Electrocell, Skjern, Denmark). The total surface area of the membrane, cathode, and anode was 100 cm^2. Both compartments were connected to glass reservoirs *via* tubing (Cole-Parmer Instrument Company, Vernon Hill, IL). The cathodic compartment was filled with the medium during experiments, and the anodic compartment contained Milli-Q water. Anolyte and catholyte were recirculated between the glass reservoirs and the electrochemical cell using two peristaltic pumps (Masterflex, Cole-Parmer Instrument Company, Vernon Hill, IL).

The glass reservoirs featured several openings. One opening served as outgas and was connected to a collection bag (Supel™ Inert foil gas sampling bag, Supelco, Pennsylvania, USA). A tube filled with silica beads preceded the gas bag to dry the off-gas. The pH was measured with a handheld pH meter (Mettler Toledo, Columbus, Ohio). The oxidation-reduction potential (ORP) and conductivity measurements were performed using an ORP probe (Hanna Instruments, Vöhringen, Germany) and a conductivity sensor (Endress + Hauser, Reinach, Switzerland). OD_{650} was measured through a photometer (Lovibond MD 610, Tintometer GmbH, Dortmund, Germany). A water jacket and a recirculating water thermostat (KISS 104A, Huber, Raleigh, NC) were used to heat the water jacket of the reservoirs to 62 °C. The temperature distribution was assumed to be uniform due to the high electrolyte recirculation between the glass reservoirs and the electrochemical cell. The total and wet volume of both cathodic and anodic compartments, including glass reservoirs and tubing, was 350 mL for each compartment. The catholyte volume inside the electrochemical cell was 60 mL.

The cathode and anode were connected to a power supply (EA-PS 3040-10 C, EA-Elektroautomatik, Viersen, Germany) with a preset potential of 3V as a two-electrode setup. The current was recorded using a multimeter (Agilent 34972A, Agilent Technologies, Santa Clara, California) with data acquisition through Labview (National Instruments, Austin, Texas). The CO_2 flow rate was controlled using a mass flow controller (EL-Flow Prestige, Bronkhorst, Kamen, Germany) and adjusted according to the current generated in the electrochemical cell using Labview. A dampening system (R1016823S4000000, Varem, Bovalenta, Italy) was installed downstream of the pump and upstream of the electrochemical cell to reduce pressure fluctuations caused by the peristaltic pump during electrolyte recirculation. For abiotic electrochemical experiments, a similar setup was employed as described above. A reference electrode (3M Ag/AgCl) was introduced into the cathode chamber for the three-electrode setup. The cathode, anode, and reference electrode were connected to a potentiostat (VSP, Bio-logic, Claix, France) that was controlled *via* EC-lab software (Bio-logic, Claix, France).

4.4.4. Startup and shutdown procedure

When starting the electrochemical cell, the power source was set to 3V, the water thermostat was adjusted to achieve a temperature of 62°C within the glass reservoirs, and the recirculation pump was set to 120 ml min^{-1} (100 rounds *per* min). The outgas were collected each day and analyzed twice. pH, temperature, and OD_{650} were measured at least once a day. OD_{650}, conductivity, and pH of the anolyte and catholyte were analyzed daily by sampling 10 ml. Initially, the cell was inoculated with a starting OD_{650} of 1.

Each experiment was run for multiple weeks, and one week comprised of 5 days with operating conditions followed by 2 days of shutdown. Anolyte and catholyte levels were adjusted on the third day of every week during the graphite and nickel experiments and on the second and fourth days during the platinized titanium experiment. The anolyte was refilled with distilled water, and the catholyte was extracted to reach the original liquid volumes. A concentrated medium was added to compensate for the loss of nutrients due to catholyte extraction and sampling. The

setup was started at the beginning of each week by starting the heating and the peristaltic pump. Once the operating temperature was reached, the power source was set to 3V, and the CO_2 supply started. During the nickel experiment, a liquid sample for trace element analysis was taken right before switching on the power source, 2h after switching on the power source, and on days 3 and 5 of each week. On day 5, the system was shut down with the following procedure: the heating and power source was switched off, the electrical circuit between the power source and the cell was interrupted, and the CO_2 supply stopped. Once the temperature in the reservoirs fell below 40°C, the pump was shut off. During the nickel experiment, the procedure was altered in some weeks because the electrical circuit was closed, and the power source was switched off or set to 0.9 V.

4.4.5. Equations

The Coulombic efficiency (CE) was calculated according to Kracke and colleagues (Kracke et al. 2020):

$$\mathbf{CE} = \frac{\mathbf{n \cdot F \cdot z}}{\int \mathbf{Idt}} \tag{11}$$

Where n is the molar quantity of produced CH_4 and H_2, F the Faraday constant, z number of electrons to form CH_4 or H_2, and I the current of the microbial electrolysis cell. The EE was calculated as follows (Geppert et al. 2016):

$$\mathbf{EE} = \frac{\mathbf{\Delta G_{CH4} \cdot n}}{\mathbf{E_{cell}} \cdot \int \mathbf{Idt}} \tag{12}$$

With $\Delta G_{CH4,}$ the Gibbs free energy of CH_4 (890.4 kJ/mol), and $E_{cell,}$ the applied cell voltage (3 V)

4.5. Results and Discussion

4.5.1. The microbial electrolysis cell using a platinized titanium cathode exhibited higher production rates compared to those with graphite and nickel cathodes during interrupted power supply

Three-electrode types were run in a BES with defined electrolyte flow rates (120 mL min^{-1}). Given the importance of pH control as a cost determinant, pH monitoring was undertaken without concurrent pH regulation. The overarching concept was establishing an equilibrium state between catholyte and anolyte pH, obviating the need for bidirectional pH control measures even if a pH gradient would be created. At first, the experiment ran for three weeks with consecutive 5 days of runtime and 2 days without current. During the two power supply interruptions, the microbial electrochemical cell was disconnected from the power source (open-circuit).

In the comparative analysis of electrode materials, platinized titanium as cathode, serving as a benchmark for this study, demonstrated a higher volumetric CH_4 production rate and CH_4-CE performance. It achieved a peak volumetric CH_4 production rate of 16.98 L L^{-1} d^{-1} (volume of CH_4 per BES cell volume per day) and a CH_4-CE of 92.6% (**Figure 4.1A**). This high volumetric production rate is attributable to its enhanced catalytic properties, which increased the overall current that other materials lacked (**Figure 4.1**). In the first week, the production rate steadily increased with the current ramp-up during the start phase, reaching a maximum of 16.82 L L^{-1} d^{-1} at 90.2% CH_4-CE (**Figure 4.1A**). Following the first shutdown, the production rate progressively climbed, peaking at 16.98 L L^{-1} d^{-1} by the end of the second week. The microbes responded better to the interruptions after the second shutdown, achieving a volumetric CH_4 production rate of 16.69 L L^{-1} d^{-1} within two days (**Figure 4.1A**).

The microbial electrolysis cell using graphite as cathode, while cost-effective and accessible, underperformed in comparison. The graphite cathode microbial

electrolysis cell achieved a lower maximum volumetric CH_4 production rate of 10.47 L L^{-1} d^{-1} and CH_4-CE of 71.8% (**Figure 4.1B**). The lower production rate can be attributed to a lower current because of the missing catalyst. The graphite cathode exhibited its highest average current after the second shutdown with 349.5 mA, while the platinized titanium cathode generated an average current of 498.1 mA, which is 1.4 fold higher (**Figure 4.1A** and **B**). Initially, the average current for the graphite cathode was 263.9 mA at the end of the first week (**Figure 4.1A**). After the first shutdown, the average current rose from 263.9 mA to 335.7 mA, reaching a maximum volumetric CH_4 production rate of 10.07 L L^{-1} d^{-1} with a CH_4-CE of 75.8%. A continuous increase of the volumetric CH_4 production rate post-shutdown without a stable phase would mean that *M. thermautotrophicus* required a second week of adaptation due to the power supply interruption. Post-second shutdown, the volumetric CH_4 production rate stabilized at a maximum of 10.48 L L^{-1} d^{-1}, but the CH_4-CE never surpassed 75.5% (**Figure 4.1B**) compared to the >90% CH_4-CE of the platinized titanium cathode (**Figure 4.1A**).

The nickel cathode microbial electrolysis cell showed moderate improvement compared to the graphite cathode in terms of average current, which is attributed to higher conductivity and catalytic effect (**Figure 4.1C**). The average current reached a maximum of 405.5 mA, which is 15.5% higher than the graphite cathode and 18.5% lower than the platinized titanium cathode (**Figure 4.1**). The microbial electrolysis cell with the nickel cathode had a maximum volumetric CH_4 production rate and CH_4-CE of 12.78 L L^{-1} d^{-1} and 84.4%, respectively (**Figure 4.1C**). However, it fell short of matching the performance of the platinized titanium cathode microbial electrolysis cell. After an initial 4-day current ramp-up, the nickel cathode reached stable volumetric CH_4 production rates pre-shutdown at 11.16 L L^{-1} d^{-1} and 78.8% CH_4-CE (**Figure 4.1C**). Post-shutdown, it took only a day to return to pre-shutdown production levels, achieving a maximum of 12.32 L L^{-1} d^{-1} with a CH_4-CE of 79.4%. A similar pattern was observed in the third week, peaking at 12.78 L L^{-1} d^{-1} and 84.4% CH_4-CE (**Figure 4.1C**).

Another critical factor for industrial readiness is energy efficiency (EE). In this study, the average EEs for graphite, nickel, and platinized titanium were 22.19%, 21.17%, and

23.76%, respectively, with their maximum efficiencies reaching 29.16%, 32.45%, and 35.83% (**Figure 4.1**). These values align closely with existing literature under similar current densities and cell voltages (Cai et al. 2022; Geppert et al. 2019; Gomez Vidales et al. 2021). When comparing graphite, nickel, and platinized titanium electrodes (**Figure 4.1**), it is apparent that each material has its unique strengths and weaknesses. However, platinized titanium consistently surpassed the performance of the other electrodes in this study. The reason for the overall lower CH_4-CE of the graphite and nickel cathodes during the microbial electrolysis cell experiments was the lower H_2 production or the H_2 loss through a suboptimal system. The average CEs of H_2 were 80.4% and 69.8% for the nickel and the graphite microbial electrolysis cell experiments, respectively (**Figure S17**). The platinized titanium cathode microbial electrolysis cell experiment achieved an H_2 CE of 91.3%, showing higher available H_2 in the system and higher efficiency in producing H_2 (**Figure S17**). A better comparison would be the conversion efficiency of H_2 to CH_4. In this case, the graphite cathode microbial electrolysis cell showed the highest conversion efficiency at 83.1%, followed by the nickel cathode at 80.6% and the platinized titanium cathode at 77.2% (**Figure 4.1**). Despite interruptions in the power supply, the microbial electrolysis cell with platinized titanium as cathode consistently showed higher performance, attributing its success to the higher catalytic properties.

4.5.2. Recovery of CH_4 is influenced by the pH after power supply interruption and leads to nickel dissolution

Deutzmann and colleagues demonstrated that *M. maripaludis* exhibited robust CH_4 recovery despite varying shutdown times (Deutzmann, Kracke, and Spormann 2023). In scenarios with intermittent power supply for electrochemical CH_4 production, the choice of electrode material considerably impacts the recovery process. We compared the three electrode materials and assessed which electrode material was able to recover CH_4 production with an H_2 to CH_4 conversion efficiency goal of >80%. The nickel electrode showed a rapid recovery response (1.9 days), platinized titanium recovered in 2 days, and graphite slightly lagged, taking 2.4 days to reach 80% H_2 to CH_4 conversion efficiency. Notably, after the second power shutdown, all three

electrodes reached >80% conversion efficiency within 1 day, with platinized titanium achieving the highest (89.9%, **Figure 4.1A**). Graphite and platinized titanium had similar average H_2 to CH_4 conversion efficiencies (90.3% and 93.1%, respectively, **Figure 4.1A** and **B**), while the nickel electrode averaged 84% (**Figure 4.1C**).

While operating conditions for all three electrodes remained consistent, a considerable pH difference emerged, especially for the nickel electrode. Initially, pH values for all microbial electrolysis cells ranged from 6.7 to 7.5 in the catholyte (**Figure S18**). However, a shift towards higher pH values occurred for the microbial electrolysis cells using graphite and platinized titanium cathodes. In contrast, the microbial electrolysis cell with the nickel cathode experienced a pH decrease to 5.9 and 6.3 during the first and second power supply shutdowns. This pH shift, lowering the pH from the optimal growth range, led to an elevated nickel concentration in the medium, potentially affecting CH_4 production recovery. The initial nickel content (**Figure S19A**) was 0.29 ppm, increased to 3.11 ppm before the shutdown, further elevated to 5.15 ppm after the shutdown, and decreased to 2.38 ppm before the second shutdown. After the microbial electrolysis cell was reactivated after the second shutdown, the nickel concentration had a modest increase to 3.46 ppm, potentially influencing the observed accelerated recovery in CH_4 production. In summary, the CH_4 recovery for all three electrode materials was less than a day after an adaptation to the power shutdowns. The lower conversion efficiency for the microbial electrolysis cell with the nickel cathode could be explained by the higher nickel concentration due to the lower pH, but more evidence is needed.

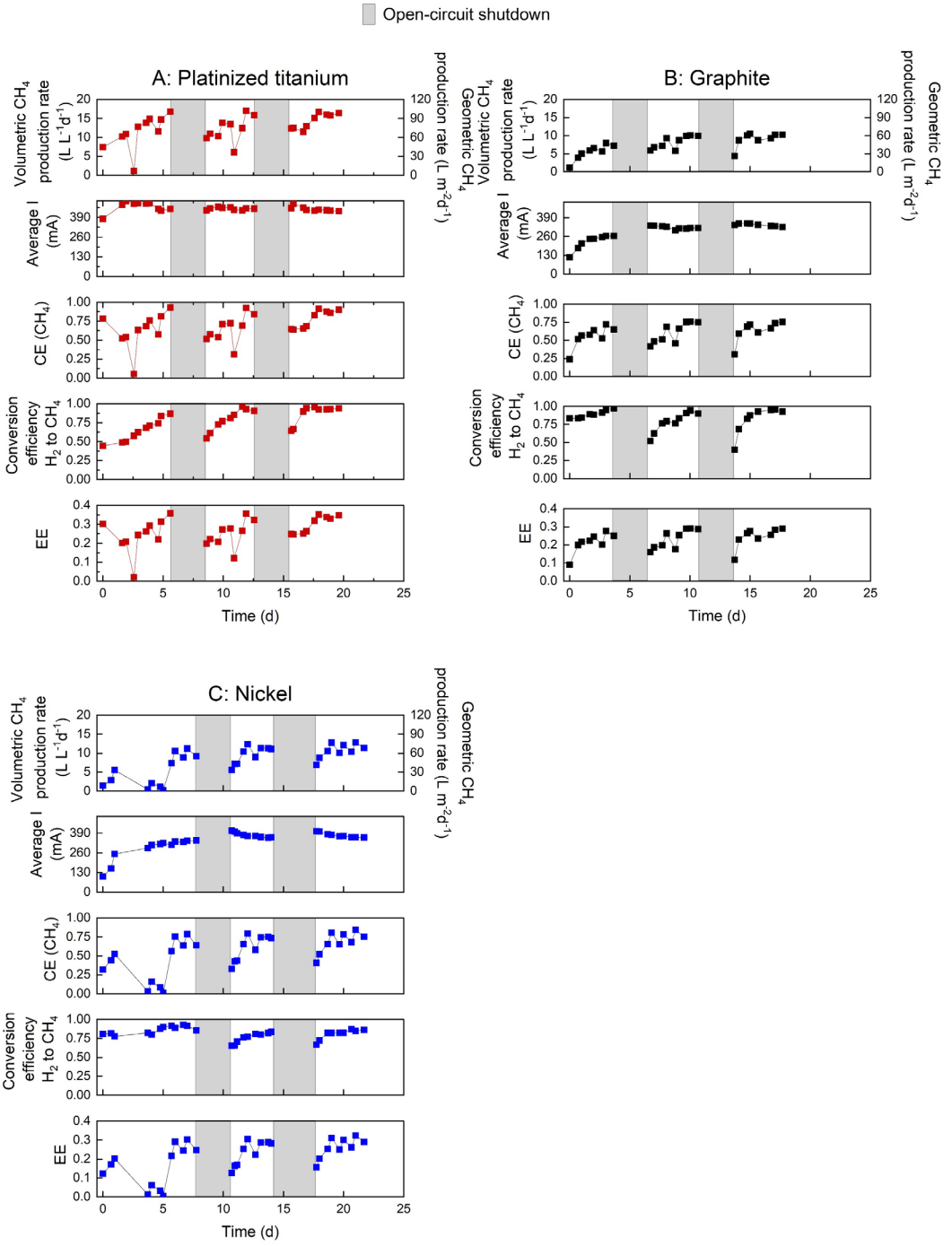


Figure 4.1: Effect of different electrode materials during 3 days shutdowns with (A) platinized titanium, (B) graphite and (C) nickel electrodes. Shown are for each electrode: the volumetric CH_4 production rate (Y1 Axis top), the geometric production rate (Y2-axis top graph); average current of a sample period; the coulombic efficiency of CH_4, the conversion efficiency of H_2 to CH_4; and the energy efficiency.

4.5.3. Nickel cathode effectiveness is compromised by elevated nickel concentrations following power supply interruptions, impacting CH_4 production and recovery times.

Nickel electrodes have the benefit to be durable and stable while having good catalytic properties to produce H_2. It is, therefore, an ideal candidate for large-scale applications. Additionally, nickel supports the growth of *M. thermautotrophicus* in electromethanogenesis via Ni-enzymes (Thauer et al. 2010; Schönheit, Moll, and Thauer 1979). Therefore, using nickel electrodes in electromethanogenesis offers a favorable environment for their growth, ensuring that nickel availability does not become a limiting factor. However, similar to many other compounds, an upper concentration limit exists beyond which it becomes toxic. In the preceding section, we demonstrated that elevated nickel concentrations slowed CH_4 production recovery, although the differences observed after the second interruption period were relatively minor. To comprehensively assess the impact of nickel concentrations on electromethanogenesis, the microbial electrolysis cell with the nickel cathode experiments involving repeated power supply interruptions was extended. The experiment was continued following the same experimental procedure. This involved a 5-day run time followed by a 2-day power supply interruption with the power supply cable disconnected from the cell. Additionally, we explored the potential occurrence of side reactions depending on the electrical connectivity of the microbial electrolysis cell. Three interruption modes were employed: 1) complete disconnection (open-circuit), where all cables were disconnected; 2) short-circuit, for which the anode and cathode were directly linked, but no current was set, allowing electrons to flow freely between cathode and anode; and 3) polarization, involving the application of an external potential of 0.9 V.

Following the nickel experiment, which consisted of 2 open-circuit shutdown periods (**Figure 4.1C** and **4.2A**), we started with another open-circuit shutdown during week 3. The open-circuit shutdown method proved optimal during the first two shutdowns, and the power supply interruption time was kept to 2-days. Following the third shutdown (open-circuit), the nickel concentration was 2.13 ppm with a CH_4 recovery

period of one day and a maximum volumetric CH_4 production rate at 12.4 L L^{-1} d^{-1} (**Figure S19** and **4.2A**). While polarized and open-circuit shutdowns in weeks 4 and 5 showed no considerable differences in nickel concentrations (3.02 and 2.56 ppm, respectively), a notable increase occurred after a short-circuit shutdown (7.95 ppm). A higher nickel concentration was reached despite a pH of 7.86 (Figure 4.2A) after the first short-circuit shutdown in week 6 (anode and cathode connected), which is typically unfavorable for nickel dissolution. However, a short-circuit event enhances nickel dissolution, as demonstrated by the elevated nickel concentration post the first short-circuit shutdown. It affected the recovery time to achieve at least 80% CH_4 conversion efficiency (**Figure 4.2E**). After the week 6 short-circuit shutdown, the microbial electrolysis cell took a half-day to reach more than 80% H_2 to CH_4 conversion efficiency. Despite the higher initial nickel concentrations, the microbial electrolysis cell reached its highest volumetric CH_4 production rate of 15.11 L L^{-1} d^{-1} (**Figure 4.2A**).

Two polarized and open-circuit shutdowns followed the short-circuit shutdown through weeks 7 to 9, decreasing nickel concentrations (**Figure S19A**) and restoring nickel concentrations to values before the week 6 short-circuit shutdown. The idea was to investigate the impact of short-circuit shutdowns on nickel dissolution. Interestingly, H_2 to CH_4 conversion efficiency returned to pre-short circuit shutdown levels. During week 10, another short-circuit shutdown resulted in a higher nickel concentration (7.36 ppm), but it did not affect CH_4 conversion efficiency, recovering within half a day. In contrast to the first short-circuit shutdown, the volumetric CH_4 production rates did not exceed other previous shutdown methods (**Figure 4.2** and **S19A**). While the open-circuit shutdown method is optimal to avoid excessive nickel concentration increases, all shutdown methods were viable because increased nickel concentrations do not impair CH_4 conversion efficiency. It is crucial to note that a higher frequency of short circuit shutdowns could potentially harm the nickel electrode, leading to degradation and a loss of catalytic efficiency in H_2 production. This can be clearly seen in our study, where short-circuit had a higher impact on nickel dissolution than other shutdown methods (**Figure S19A**). It is advantageous to avoid shutting down the microbial electrolysis cell using the short-circuit interruption mode and use the open-circuit or polarized modes instead.

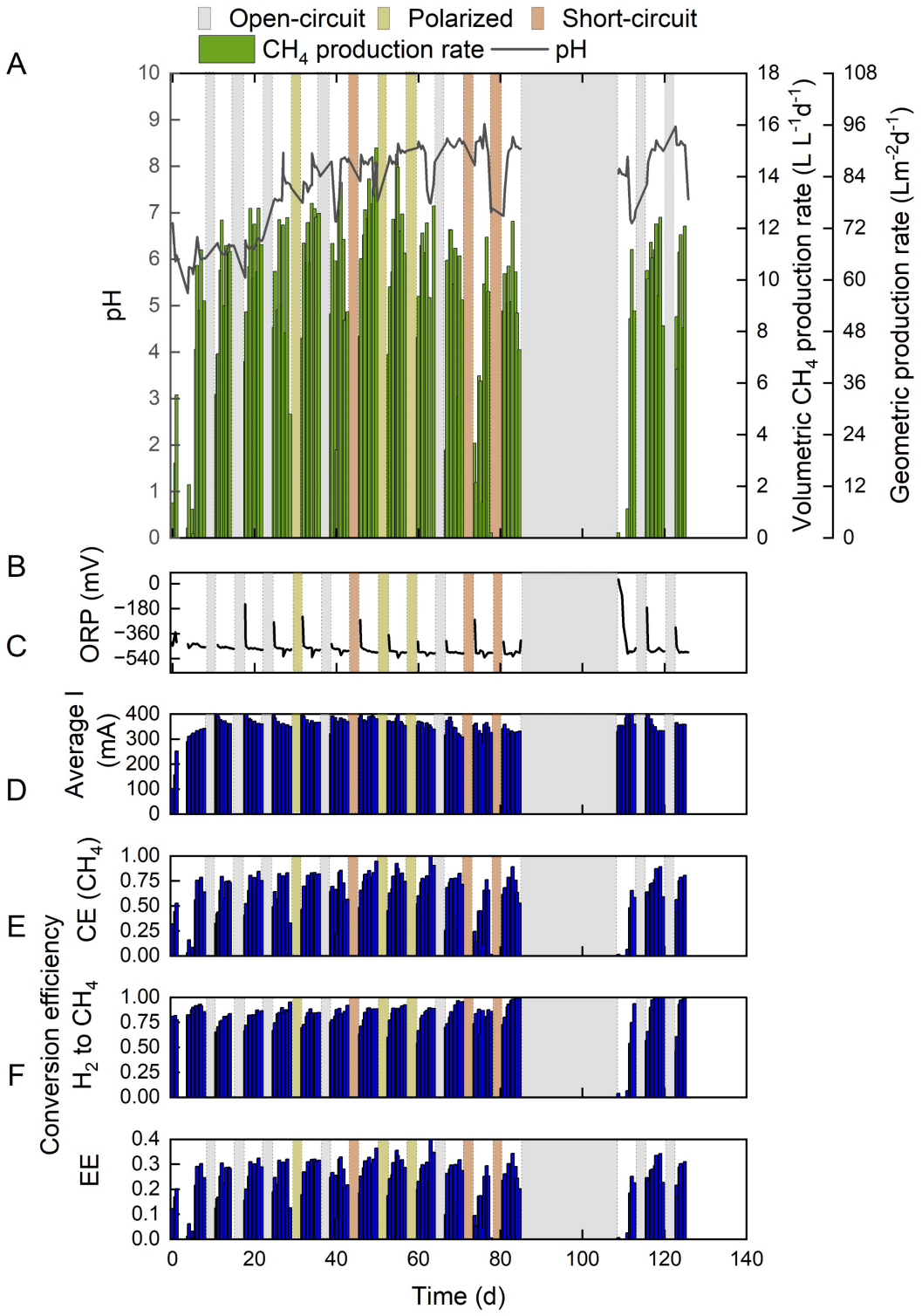


Figure 4.2: Period of the nickel electrode experiment with different shutdown methods coded in grey open-circuit shutdown, light yellow polarized shutdown, and light red short-circuit shutdown. The different graphs show (A) the BES cell volumetric (Y2-axis) and geometric (Y3-axis) CH_4 production rate as well as the pH, (B) the oxidation-reduction potential (ORP), (C) the average current of a sample period, (D) the Coulombic efficiency (CE) of CH_4, (E) the conversion efficiency of H_2 to CH_4, and (F) the energy efficiency (EE) of the BES.

4.5.4. Gradual degradation of the nickel electrode in a microbial electrolysis cell over ten weeks is less impacted by the different shutdown modes but by other factors

We anticipated that the performance of the nickel electrode would gradually decline throughout the operating period due to: 1) morphology changes of the catalysts; 2) electrolyte impurities; and 3) corrosion. During 10 weeks of the microbial electrolysis cell with nickel cathode experiment, the average current decreased from 377.75 mA for week 1 to 334.44 mA for week 10, corresponding to 11.6% degradation. To further measure the deterioration of the nickel electrode, we assessed the reduction in current throughout the operating period. Therefore, a linear regression was used at the restart of the microbial electrolysis cell until the shutdown occurred. The regression revealed that there is no trend indicating that a particular shutdown method is accountable for a more pronounced degradation. The observed current degradation spanned a range from -8.54 mAd^{-1} to -29.70 mAd^{-1} and occurred without any shutdown method, impacting the decrease in current throughout time (**Figure S20**). The nickel electrode shows signs of degradation throughout the operating period, but the shutdown modes do not seem to have the biggest effect.

One of the degradation issues that can arise is electroplating the electrode with metals from the electrolyte. This would be seen by the decreased electrolyte concentration of the electroplated compound. To address this concern, we monitored the electrolyte/medium throughout the experiment and assessed the concentration of metal compounds (Mg, Ca, Mn, Fe, Co, Zn, Se, and Mo), excluding nickel (refer to **Figure S19**). Among these elements, calcium (Ca) and selenium (Se) displayed no considerable change in concentrations. The detected calcium was not added to the medium; we assume contamination from an unknown source. Similarly, zinc (Zn) was detected, potentially indicating contamination from a reactor component containing zinc (**Figure S19G**). Nevertheless, this contamination did not appear to have a discernible impact on the operation of the microbial electrolysis cell.

The most notable effects were observed with magnesium (Mg) and iron (Fe), which showed a near depletion of these metals in the electrolyte (**Figure S19H**), which could indicate electroplating of the cathode. Intriguingly, despite the importance of iron in iron-sulfur clusters and magnesium in ATP and ADP-dependent reactions (Kaster et al. 2011), this depletion did not appear to impede CH_4 production. A study that used a concentrated trace element solution as a catalyst showed a decreased deposition of the metals on the electrode when a chelating agent was used. (de Smit et al. 2023). In our study, we utilized nitrilotriacetic acid as a chelating agent, and except for magnesium and iron, all other elements did not seem to be influenced by the applied electric field (**Figure S19**). Finally, manganese (Mn), cobalt (Co), and molybdenum (Mo) exhibited a sharp initial decrease in their concentration, which later stabilized. The concentration of the elements was measured using cell-free effluent, and the decrease in concentration could also have resulted from M. thermautotrophicus taking the elements for nutrition instead of electroplating. Furthermore, once per week the electrolyte level was adjusted with medium that resulted in an increase in the concentration and a decrease throughout the running of the microbial electrolysis cell.

If electroplating is not the clear cause of the decrease in current density, it suggests that other potentially harmful reactions may have occurred. These potential reactions may have occurred on the electrode surface or during the shutdown period, corroding the nickel electrode and decreasing its performance. A degradation possibility occurs during self-discharge and open-circuit voltage, where the nickel electrode may have corroded, leaching either Ni^{2+} or $Ni(OH)_2$ into the solution, which we observed after each shutdown method (**Figure S19**). Furthermore, further oxidation to β-$Ni(OH)_2$ or NiO could have occurred due to the elevated O_2 content during the initial phase (**Figures. S21** and **S22**). An abiotic study conducted by Kim and colleagues (Kim et al. 2022) explored the recyclability of nickel electrodes through successive shutdown and startup cycles of the electrochemical cell, and an increased degradation of the nickel electrode was observed. In this study, the corroded Ni^{2+} could be electroplated on the bare nickel electrode, reducing the reaction sites for the H_2 evolution reaction. However, substantial proof for these side reactions could not be given. Overall, the

microbial electrolysis cell should not be interrupted frequently to avoid corrosion. In case of an interruption and leaching of nickel into the electrolyte, the O_2 contamination should be prevented to avoid further corrosion reactions.

4.5.5. More prolonged power interruption influences the recovery of CH_4 production

In a circumstance where a more extended interruption of the system occurs, such as a breakdown of components, a speedy recovery of the system is the desired outcome. We showed that after an initial adaption of three consecutive shutdowns, *M. thermautotrophicus* could quickly recover to >80% H_2 to CH_4 conversion efficiencies within a day. We then examined if our system could sustain CH_4 production after 24 days. The shutdown mode was open-circuit (**Figure 4.2**), and no additional prevention methods were used to ensure the survivability of the microbe. After restarting the microbial electrolysis cell, the H_2 level showed near 100% H_2-CE (**Figure S23**); consequently, no CH_4 was produced. *M. thermautotrophicus* grows fast, with a doubling time of 3 h. In this case, after 3 days, the conversion efficiency to CH_4 was still below 10%, and recovery seemed unlikely.

A long-term shutdown can increase the likelihood of O_2 contamination. Even if the microbe could survive long exposures to O_2 (Kiener and Leisinger 1983), in our study, the extended shutdown and the increased ORP value harmed the microbes. The ORP of the BES was 32.2 mV at the restart of the microbial electrolysis cell, at which point no methanogenesis could occur (**Figure 4.2B**) (Hirano et al. 2013) and could indicate O_2 exposure. Only after 1 day did the ORP reach -304.2 mV, which is beneficial for methanogenesis. However, the ORP further decreased to -504 mV without *M. thermautotrophicus* being able to produce CH_4. The microbial electrolysis cell was then reinoculated with fresh inoculum from a continuous stirred-tank bioreactor, which reestablished CH_4 production. The conversion efficiency of H_2 to CH_4 of the microbial electrolysis cell reached 75% after 1 day and 94% after 1.7 days (**Figure 4.2E**). The subsequent open-circuit shutdowns did not impact the recovery of CH_4. For future applications, the glass recirculating vessel should be built to prevent O_2 contamination, which increases the ORP for long-term shutdowns. The above-

mentioned O_2 problem was due to the relatively small experimental setup and should be avoided in large-scale applications.

4.5.6. Short-term O_2 exposure did not harm the CH_4 recovery time of the microbe

To facilitate the growth of methanogens, the system must maintain anoxic conditions, primarily due to the absence of mechanisms for O_2 detoxification. Fortunately, *M. thermautotrophicus* exhibits a higher O_2 exposure tolerance than other methanogens (Kiener and Leisinger 1983). However, given the setup (customized drying tube for the off-gas), there was O_2 contamination, which could have impeded the methanation process. During our experiments, we monitored O_2 concentrations, yet we did not observe a substantial reduction in the methanation process, even with extended exposure to O_2 (**Figures S21** and **S22**). Notably, high O_2 concentrations were detected at the beginning and after restart of the experiment with all three electrodes (**Figure S21**). While it took several days to achieve high H_2 conversion into CH_4, the O_2 levels remained consistently low and sometimes exhibited spikes, which, interestingly, did not seem to affect the production rates (**Figures 4.2** and **S22**). In the case of the more extended nickel experiment, high percentages of O_2 were observed as well, with negligible impact on the conversion efficiency (**Figure 4.2E**). Because the temperature was switched off during the shutdown periods, it could have put the microbes in a hibernation mode, which might have extended their survival.

However, it is worth noting that in some instances, O_2 levels spiked (**Figure S22**), adversely affecting the overall production rate and reducing both the EE and CE of H_2 and CH_4 (**Figures 4.2F and S23**). When these O_2 spikes occurred, the O_2 to N_2 ratio corresponded to air, suggesting a possible system leak, likely stemming from the customized drying tube (for further explanation, see material and methods) connected before the collection bag used in this study. Nevertheless, *M. thermautotrophicus* demonstrated its capacity to sustain the electromethanation process even during such leakages. In summary, despite the potential challenges posed by O_2 contamination and the associated variability in production efficiency, the

resilience of *M. thermautotrophicus* and the ability of the system to maintain anoxic conditions underscore the robustness of the electromethanation process, even in the face of unexpected environmental or system fluctuations.

4.5.7. The operating conditions of the microbial electrochemical cell promote water and gas crossover through the ion-exchange membrane

In general, one of the performance losses in electrochemical cells arises from the ion exchange membrane (Liu et al. 2023), which poses a challenge that must be addressed for successful implementation in an industrial setting. When electrodes are polarized, three modes of mass transport become relevant: convection, migration, and diffusion. While diffusion through the ion exchange membrane is restricted, mass transport via migration and convection can occur when an electric field is applied and a pressure difference exists between the two chambers. Notably, during the nickel microbial electrolysis cell experiment, the catholyte volume increased by 53.9 mL on average, while the anolyte volume decreased by 100.7 mL. The reduction in anolyte volume can be attributed to the fast migration of produced H^+-ions (Grotthuss' mechanism), leading to a decrease in the overall anolyte volume. These H^+-ions can cross the cation-exchange membrane and become neutralized in the catholyte, resulting in the dilution of the catholyte. Another plausible explanation is that water transport is driven by hydraulic pressure due to a slight overpressure on the anolyte side. Despite our efforts to minimize overpressure by maintaining identical liquid flow rates in both chambers and using a dampening system, it cannot be ruled out that overpressure might have occurred.

The occurrence of water crossover is unsurprising, given the proton migration. However, it was observed that CO_2 also crossed over from the catholyte to the anolyte during operation (**Figure S24**). In an anion-exchange membrane, CO_2 crossover occurs due to the formation of carbonate species, which can migrate under the influence of the applied electric field. The presence of CO_2 in the anode chamber is counterintuitive, as the Nafion 117 membrane should ideally prevent anion crossover.

We suspect three potential explanations for this phenomenon: (i) the precipitation of carbonate species on the membrane; (ii) hydrophobic property loss of the membrane; and (iii) swelling of the membrane from increased temperature exposure. Because CO_2 crossover was evident from the beginning, it is unlikely that the Nafion 117 membrane was obstructed. However, we observed undefined precipitates on the Nafion membrane after the experiment, which we analyzed with SEM and EDX. Suspected carbonate precipitates from continuous CO_2 feeding could clog the membrane, while the acidic anolyte (monitored, not continuously tracked, pH of 1.6 ± 0.2) may counteract this by dissolving the precipitates, enabling CO_2 crossover. Simultaneously, the temperature-sensitive swelling of Nafion 117 might further influence carbonate behavior, contributing to both precipitation and transmembrane crossing (Martin et al. 2022; Mališ et al. 2018).

The SEM analysis of the Nafion 117 membrane, post-experimentation, revealed the formation of precipitates during the microbial electrolysis cell operations (**Figure S25**). Compared to an unused Nafion 117 membrane (**Figures S25A** and **B**), the post-experiment Nafion 117 exhibited a uniformly distributed layer of precipitate (**Figures S25C** and **D**). Upon closer inspection at higher magnifications, the precipitate appeared amorphous (**Figures S25E** and **F**). EDX spectroscopy analysis identified peaks corresponding to sulfur, fluorine, carbon, phosphorus, and iron within this amorphous precipitate (**Figure S26**). The presence of sulfur and fluorine aligns with the composition of Nafion, while phosphorus and iron are likely constituents of the precipitate. Although carbonate species were not directly detectable, their involvement in the precipitation, driven by substantial CO_2 crossover, should not be disregarded. Carbonate presence was measured by acidifying a 1 cm^2 Nafion 117 segment placed in a sealed serum vial, with GC measurements indicating a CO_2 concentration of 1.9 ± 0.6 mmol cm^{-2}, affirming carbonate accumulation on the membrane. Calcinating the Nafion 117 membrane and subsequent ICP-MS analysis of the residue confirmed the detection of all elements present in the medium (**Figure S27**). Despite attempts to mitigate mass transport effects through a dampening system, water and CO_2 crossover phenomena underscore the challenges in achieving optimal operating efficiency. Future research should address these membrane-related

challenges to enhance the industrial applicability of microbial electrochemical technologies.

4.5.8. The flow rate influences the current generation and has a higher effect on the microbial electrochemical cell performance

Resistance considerably influences bioelectrochemical system performance, with solution, charge transfer, and diffusion resistance being the primary factors (Sleutels et al. 2012; Ter Heijne et al. 2011). These resistances, resulting from ohmic limitations, kinetic constraints, and mass transport phenomena, respectively, can be modulated by adjusting the flow rate of the electrolyte. However, finding the optimal flow rate is crucial, as it is pivotal in removing gas bubbles and maintaining active reaction sites.

To determine the optimal flow rate for our setup, we conducted experiments using graphite cathodes under three different recirculation flow rates: 100 mL min^{-1}, 200 mL min^{-1}, and 300 mL min^{-1}. *Prior* to the experiments, we preconditioned the abiotic electrochemical cell for 20 h at 3 V to ensure uniform conditions across tests. We maintained the anolyte and catholyte pH during the flow rate experiments at 2 and 7, respectively. We employed cyclic voltammetry, sweeping potentials from -0.7 to -1.15 V vs. Ag/AgCl (3M KCl), at a scan rate of 25 mV s^{-1} to assess the impact of flow rates on system performance. The results indicated that the highest current (**Figure 4.3**), -250.5 mA, was achieved at the lowest flow rate (100 mL min^{-1}), while the lowest current, -156.9 mA, was observed at the highest flow rate (300 mL min^{-1}) at -1.15 V. Interestingly, the intermediate flow rate (200 mL min^{-1}) presented a moderate reduction in current density, indicating a potential optimal middle ground. The relationship between flow rate and system efficiency is not linear, as excessively high flow rates can adversely affect efficiency despite reducing resistive losses from bubble formation. Our empirical findings hint at an optimal flow rate below the 4 L min^{-1} maximum recommended by the manufacturer (Electrocell, Denmark), underscoring the importance of tailored operating adjustments based on specific system performance. This suggests that an optimal current generation in our

bioelectrochemical system is achieved with a flow rate that is neither too low nor too high, ideally around 100 to 200 mL min^{-1}. Unfortunately, this observation also suggests that previous biotic experiments may have been conducted under suboptimal flow conditions, potentially limiting their performance.

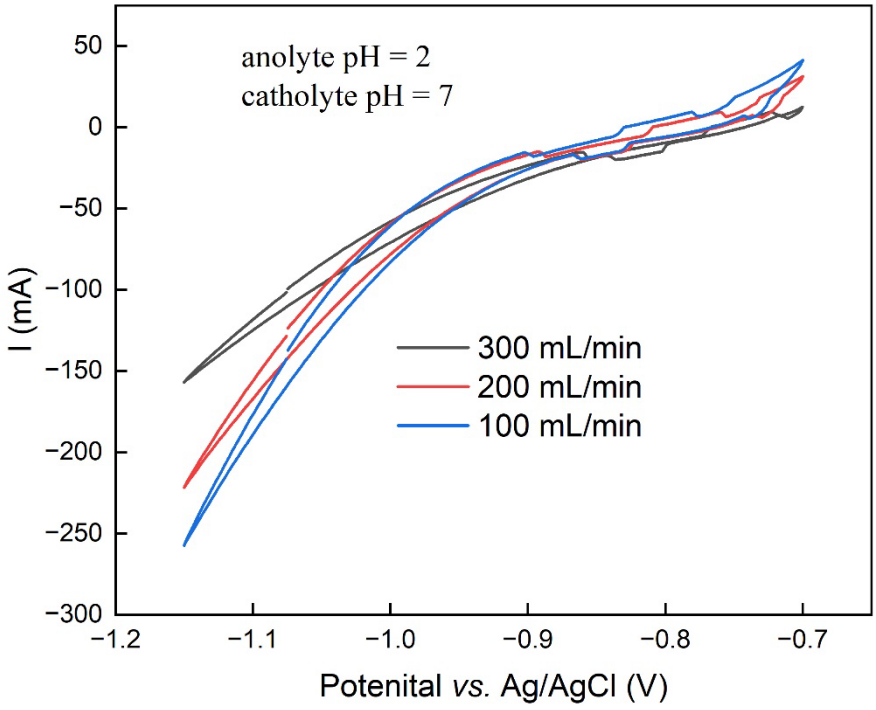


Figure 4.3: Cyclic voltammograms on the microbial electrolysis cell performance influence of flow rate at constant pH. The microbial electrolysis cell ran 20 h *prior* to the experiment to reach an equilibrium state. The potential was scanned from -0.7 V to -1.15 V vs Ag/AgCl (3M KCl) at a scan rate of 25 mV s^{-1}.

4.6. Limitations of the study

Microbial electrosynthesis confronts a hurdle in achieving industrial viability, primarily attributed to its low EE. Despite achieving a CH_4-CE exceeding 90%, the overall EE remains at a modest 20-35%, which is an improvement compared to other studies but still distant from commercial feasibility. A techno-economic analysis recommends a minimum EE of 50% for microbial electrosynthesis industrial applications (Jourdin et al. 2020). Furthermore, for abiotic CO_2 reduction to value-added chemicals, an EE exceeding 60% is preferable (Luna et al. 2019). Assuming that a constant EE of 50% was achieved in the platinized titanium microbial electrolysis cell experiment, the peak volumetric CH_4 production rate on day 12 would require a cell voltage of 2.13 V (**Figure**

S28). This suggests that a cell voltage of 2 V or lower would be essential for the optimal operation of the system in question. Optimizing the microbial electrolysis cell design, including reducing the anode-cathode distance in a zero-gap configuration using a membrane electrode assembly, is imperative to attain this target. Furthermore, H_2 and CH_4 CE fluctuations during experiments underscore the need for a more leak-proof reactor design to minimize losses and enhance H_2 conversion to CH_4. This is a general problem when using lab-scale setups and would be mitigated using a large steel bioreactor for industrial applications.

The nickel experiment in this study reveals an average H_2 volumetric percentage of 32.54% in the headspace, indicating low mass transfer and a challenge to overcome. To enhance soluble H_2 and align with the microbial electrosynthesis concept of producing H_2 directly assimilable by microbes, a well-designed bioreactor setup is necessary to prolong H_2 retention before outgassing. Furthermore, the increased H_2 bubble formation with rising current density (target of >50 $mAcm^{-2}$) will not allow microbes to directly uptake H_2 unless the cell density is high enough. Two effective strategies for optimizing H_2 conversion to CH_4 involve either pressurizing the bioreactor or recirculating the off-gas. Both of which should be implemented in the future.

Because heating incurs considerable costs, especially when scaling up for industrial purposes, utilizing the unique heat production capabilities of *M. thermautotrophicus*, which is a hydrogenotrophic methanogen with entropy-retarded growth, is crucial (von Stockar and Liu 1999). During methanogenesis, *M. thermautotrophicus* produces heat (negative enthalpy) to offset entropy reduction by producing 1 mole of CH_4 and 2 moles of water from 5 moles of gas. Unfortunately, exploiting this metabolism advantage for a microbial electrosynthesis system is currently unattainable and is achievable only at higher productivities (current densities). A larger surface-to-volume ratio between electrode and electrolyte would also be necessary to achieve higher productivities.

Another limitation is the occurrence of a pH gradient. The anolyte pH was around 2 for all three electrodes, while the catholyte ranged between 7 and 8.5. When both

chambers have equal pHs, the thermodynamic potential difference between the O_2 and H_2 evolution reactions is 1.23 V (Rossi et al. 2021). In this study, we had a pH gradient that increased the thermodynamic cell voltage to 1.62 V, a 0.39 V increase to equal pH conditions. It has been shown that using a vapor-fed anode reduces the pH gradient by not allowing the accumulation of protons (Rossi et al. 2021; Baek et al. 2022). Ideally, the protons will migrate to the cathode chamber, and the large pH difference across the cell will be mitigated. Consequently, a new electrochemical cell, such as a zero-gap electrochemical cell, should be used to optimize the system (Rad et al. 2023). Furthermore, the ion-exchange membrane should be upgraded to avoid gas and water crossovers.

4.7. Conclusion

Despite the inherent low current densities of our study, we observed that intermittent power shutdowns initially affected the microbes, but they quickly adapted to the new experimental conditions. High absolute currents were attained using three electrode materials (platinized titanium, graphite, and nickel), resulting in elevated volumetric CH_4 production rates. In an extended microbial electrolysis cell experiment with nickel as the cathode, incorporating three shutdown types showed minimal influence on overall performance. Specifically, only the short-circuit method led to higher nickel dissolution, potentially causing increased degradation if employed as the sole shutdown approach. The open-circuit shutdown method stands out as the optimal strategy for system preservation, offering a straightforward approach with minimal disruptive effects, and is recommended as the primary shutdown. To enhance future studies, addressing the influences of O_2 and CO_2 crossover is crucial to optimizing both the cell and the recirculating vessel. Platinized titanium electrode outperformed nickel and graphite electrodes. Because the cost of platinum is high and the possible sulfide contamination throughout time, nickel-based electrodes could be the better option. Especially when nickel-based catalysts, such as NiMo, outperform platinum (McCrory et al. 2015). Therefore, nickel-based electrodes should be further investigated, emphasizing changing their morphology.

4.8. Acknowledgements

This work was supported by the Deutsche Forschungsgemeinschaft (DFG, German Research Foundation, EBiotech, SPP2240; L.T.A.) – project number 445506379, the Alexander von Humboldt Foundation in the framework of the Alexander von Humboldt Professorship (L.T.A.), and The Novo Nordisk Foundation CO_2 Research Center with grant number NNF21SA0072700 (L.T.A.). Authors acknowledge funding from the central innovation program for small and medium-sized enterprises (Zentrales Innovationsprogramm Mittelstand [ZIM]), a cooperation project of the ministry of economic affairs and energy (Bundesministeriums für Wirtschaft und Energie [BMWi]) project number 16KN066610 (D.H. and J.R.). The authors gratefully acknowledge the Tübingen Structural Microscopy Core Facility (Funded by the Federal Ministry of Education and Research (BMBF) and the Baden-Württemberg Ministry of Science as part of the Excellence Strategy of the German Federal and State Governments) for their support and assistance in this work.

Chapter 5

A comparison study between liquid- and vapor-fed Zero-gap bioelectrolysis cells

5.1. Author contributions

Nils Rohbohm: Conceptualization, Methodology, Formal Analysis, Investigation, Data Curation, Writing – Original Draft, Review, and Editing, Visualization, Project Administration; **Largus T. Angenent.**: Conceptualization, Writing – Original Draft, Review, and Editing, Supervision, Project Administration, Funding Acquisition.

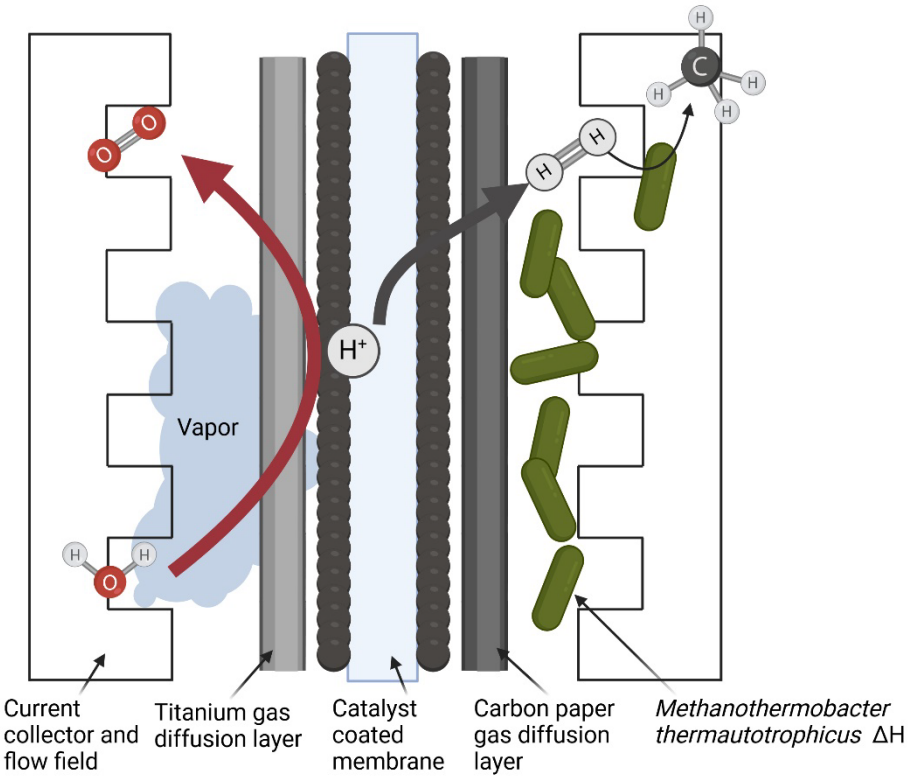


Figure 5.1: Graphical abstract of a vapor-fed bioelectrochemical cell.

5.2. Abstract

Improving microbial electrosynthesis could be one solution for transitioning towards sustainable chemical production, offering a pathway to convert CO_2 into valuable commodities using renewable energy sources. Therefore, we examined the performance differences between liquid- and vapor-fed zero-gap bioelectrochemical cells for electromethanogenesis, utilizing a membrane electrode assembly to enhance mass and ohmic transport. Focusing on CH_4 and H_2 production, it compares two ion-exchange membranes under varied conditions. Vapor-fed systems demonstrated advantages in reducing electrocatalyst degradation and maintaining stable cell voltages, although they did not considerably outperform liquid-fed systems in volumetric CH_4 production rates. The research underscores the need for further optimization to address performance losses and suggests potential for industrial applications of microbial electrosynthesis, highlighting the importance of system catalyst protection.

5.3. Introduction

Renewable sources, such as solar and wind, offer an economically viable alternative to fossil fuels for electricity generation. However, their intermittent nature necessitates extensive energy storage, achievable through methods including hydropower, underground pressure storage, or conversion into chemical energy, such as with batteries. Another approach involves converting electrical energy into chemical energy carriers, such as methane gas (CH_4) or acetate, through the synergy of electrochemistry and biology. This dual approach holds the potential to mitigate major greenhouse gas emissions while facilitating the storage of renewable energy.

Electrochemistry collaborates with biology in a dual-phase approach: water electrolysis splits water into H_2 and O_2 in the initial step. Subsequently, microbes utilize H_2 to reduce CO_2 into CH_4 or commodity chemicals in a distinct bioprocess, which is known as a gas-fermentation system. The amalgamation of these steps occurs within bioelectrochemical cells, defining the field as microbial electrochemistry (Schröder, Harnisch, and Angenent 2015). The specific term for the CO_2 upgrading at the biocathode is microbial electrosynthesis. While integration streamlines the

process economically by eliminating a unit process, it is noteworthy that H_2 and O_2 are still generated within the bioelectrochemical cell *via* water electrolysis. The integrated bioelectrochemical cell holds potential advantages compared to abiotic electrosynthesis cells utilizing metal catalysts at electrodes, such as CO_2 electrolyzers, given the current limitations in efficient electrocatalysts for CO_2-reducing abiotic systems concerning selectivity, stability, and abundance (Gawel et al. 2022).

Geppert and colleagues achieved an industrial breakthrough by implementing the electrochemical design of a redox-flow battery, achieving a current density of 3.5 mA cm^{-2} with approximately 30% energy efficiency in CH_4 production (Geppert et al. 2019). Despite a short operating period of only one day, their zero-gap design, where electrodes are closely attached to the membrane, effectively reduced resistance and increased current density from 1.0 to 3.5 mA cm^{-2} during CH_4 production compared to other studies (Kracke et al. 2020). Scaling up the zero-gap design by stacking individual cells represents potential for industrial applications akin to electrolyzers or fuel cells. Rad et al. were the first to improve the current density to 30 mA cm^{-2} with low cell voltages using a hybrid bioelectrochemical system (Rad et al. 2023). It must be noted that they protected their cathodic catalysts with a porous transport layer to avoid contact with the catholyte and microbes.

The membrane electrode assembly comprises gas diffusion electrodes and a catalyst-coated membrane used for a zero-gap design, which is readily commercially available. The membrane electrode assembly ensures optimal mass and ohmic transport while reducing cell ohmic losses. For an efficient electrochemical cell, it is imperative to protect the electrocatalysts from contaminants. Rad and coworkers protected their catalysts with a porous transport layer (Rad et al. 2023). However, there exists also other approaches. While abiotic liquid-fed electrolyzers necessitate ultra-pure water not to degrade the electrocatalyst, vapor-fed electrolyzers only need humid air to resolve a possible source of contamination. This simplifies the overall setup and allows the application of electrolyzers in areas where clean water is not readily available. Using contaminated water or seawater that exhibits low efficiencies with liquid-fed electrolyzers would also be possible. Vapor-fed electrolyzer cells are being studied more and more abiotically but not so much in bioelectrochemical systems. However,

Rossi and colleagues enhanced the zero-gap design by introducing vapor into the cathode chamber, using only a phosphate buffer at the anode chamber and utilizing an anion-exchange membrane (Rossi et al. 2021). Their abiotic system achieved 4.3 mA cm^{-2} in H_2 production without considerably altering the pH gradient between the anode and cathode chambers. Baek and coworkers used a bioelectrochemical system that adopted the vapor-feed system at the anode (Baek et al. 2022), employing a cation exchange membrane (Nafion) for sustained CH_4 production throughout a couple of weeks at 1.7 mA cm^{-2}, surpassing the duration achieved by Geppert et al. (2019). However, using a platinized titanium felt at the cathode in both studies hinders economic viability at an industrial scale. The relatively low current density was also achieved at a high cell voltage (2.8 V) that would also not have commercial viability. Furthermore, their study did not show considerable improvements in the current density using the zero-gap design because higher current densities were reached using a flow electrolyzer or an H-cell, disproving the benefit of a vapor-fed zero-gap electrolyzer.

Here, we aimed to enhance the efficiency of a liquid-fed zero-gap cell and to ascertain the optimal ion-exchange membrane for its operation. Initially, the study focused on testing two distinct ion-exchange membranes within the liquid-fed zero-gap cell to identify which one exhibited better performance. Subsequently, the investigation extended to a vapor-fed anode zero-gap cell, utilizing the previously identified optimal ion-exchange membrane. The core objective was to compare between the liquid-fed and vapor-fed systems, assessing their respective performances. The comparison between the two systems aimed to highlight the benefits of employing a vapor-fed anode, particularly emphasizing its possible potential to prevent pH gradient development and reduce the risk of catalyst wear caused by the liquid flow within the cell.

5.4. Results

5.4.1. Nafion 117 membrane outperformed Htec-PFSA membrane in terms of volumetric CH_4 production within liquid-fed zero-gap bioelectrochemical cells, thereby guiding the selection of Nafion 117 for subsequent experimentation in a vapor-fed system

The first aim was to increase the efficiency of bioelectrochemical systems for electromethanogenesis, with a particular focus on optimizing the performance of liquid-fed zero-gap cells. We evaluated the effectiveness of two distinct ion-exchange membranes—Nafion 117 and Htec-PFSA (perfluoro sulfonic acid)—within these cells, aiming to ascertain which membrane facilitates the electromethanogenic process. This initial investigation serves as a foundational step, guiding the selection of an optimal membrane for further experimentation within a vapor-fed system.

The experimental procedure involved operating two identical bioelectrochemical cells under liquid-fed, zero-gap conditions, with each cell incorporating one of the two selected membranes, Nafion 117 or Htec-PFSA. These bioelectrochemical systems were operated under the fed-batch mode, receiving a continuous supply of CO_2 as the only carbon substrate for the electromethanogenesis process. By employing chronopotentiometric control, we ensured a consistent electrical current of 120 mA across the cell, achieving a geometric current density of 7.5 mA cm^{-2}. Preliminary findings (not included in this study) indicated that such a current density initially produced a cell voltage below 2 V, aligning with one criteria for industrial scalability and efficiency. Each reactor started with an optical density (OD_{600}) of 0.04, inoculated with *M. thermautotrophicus* ΔH. The inoculation process for the controls followed a sequential approach: first, the reactor with the Htec-PFSA membrane was inoculated, which then served as the inoculum source for the subsequent Nafion 117 membrane reactor.

Upon inoculating the zero-gap bioelectrochemical cell with the Htec-PFSA membrane, a brief one-day lag phase preceded the initiation of electromethanogenesis (**Figure**

5.2). Notably, the cell exhibited efficient H_2 production, achieving a H_2 Coulombic efficiency (H_2-CE) of 94.3% (**Figure S29**). Subsequent volumetric CH_4 production rate (volume of CH_4 per bioelectrochemical cell catholyte volume per day), commencing post-lag phase, peaked at 59.86 L L^{-1} d^{-1} by day 10, accompanied by a 74.3% CH_4 Coulombic efficiency (CH_4-CE) (**Figure 5.2A** and **B**). Overall, the reactor had a stable phase, displaying minor fluctuations until day 17, maintaining an average volumetric CH_4 production rate of 47.29 L L^{-1} d^{-1} at a 58.7% CH_4-CE. The overall average volumetric CH_4 production rate throughout the 28-day experimental period, excluding the lag phase, was 42.96 L L^{-1} d^{-1} with a 50.8% CH_4-CE. The maximum energy efficiency (EE) obtained was 36.8% (**Figure 5.2B**).

In contrast, the bioelectrochemical cell inoculated with the Nafion 117 membrane experienced no lag phase, likely due to the *prior* adaptation of microbes to electromethanogenesis. The system demonstrated efficient volumetric CH_4 production, attaining a peaked volumetric CH_4 production rate at 68.01 L L^{-1} d^{-1} on day 20, with a CH_4-CE of 84.4% and a 44.4% EE (**Figure 5.2A** and **B**). The reactor had a stable production phase with minor fluctuations, maintaining an average volumetric CH_4 production rate of 55.93 L L^{-1} d^{-1} at 69.4% CH_4-CE, excluding day 28 when the reactor leaked (drop of volumetric CH_4 production rate, **Figure 5.2**), which also finalized the experiment. Comparing the performance of Nafion 117 and Htec-PFSA ion-exchange membranes in volumetric CH_4 production reveals an advantage for Nafion 117. Nafion 117 outperformed the Htec-PFSA membrane, showing an 11.9% higher peak volumetric CH_4 production rate and a 23.1% increase in the average volumetric CH_4 production rate. This outcome suggests that Nafion 117 has an advantageous application compared to the Htec-PFSA membrane in this study and was further used for the vapor-fed experiment.

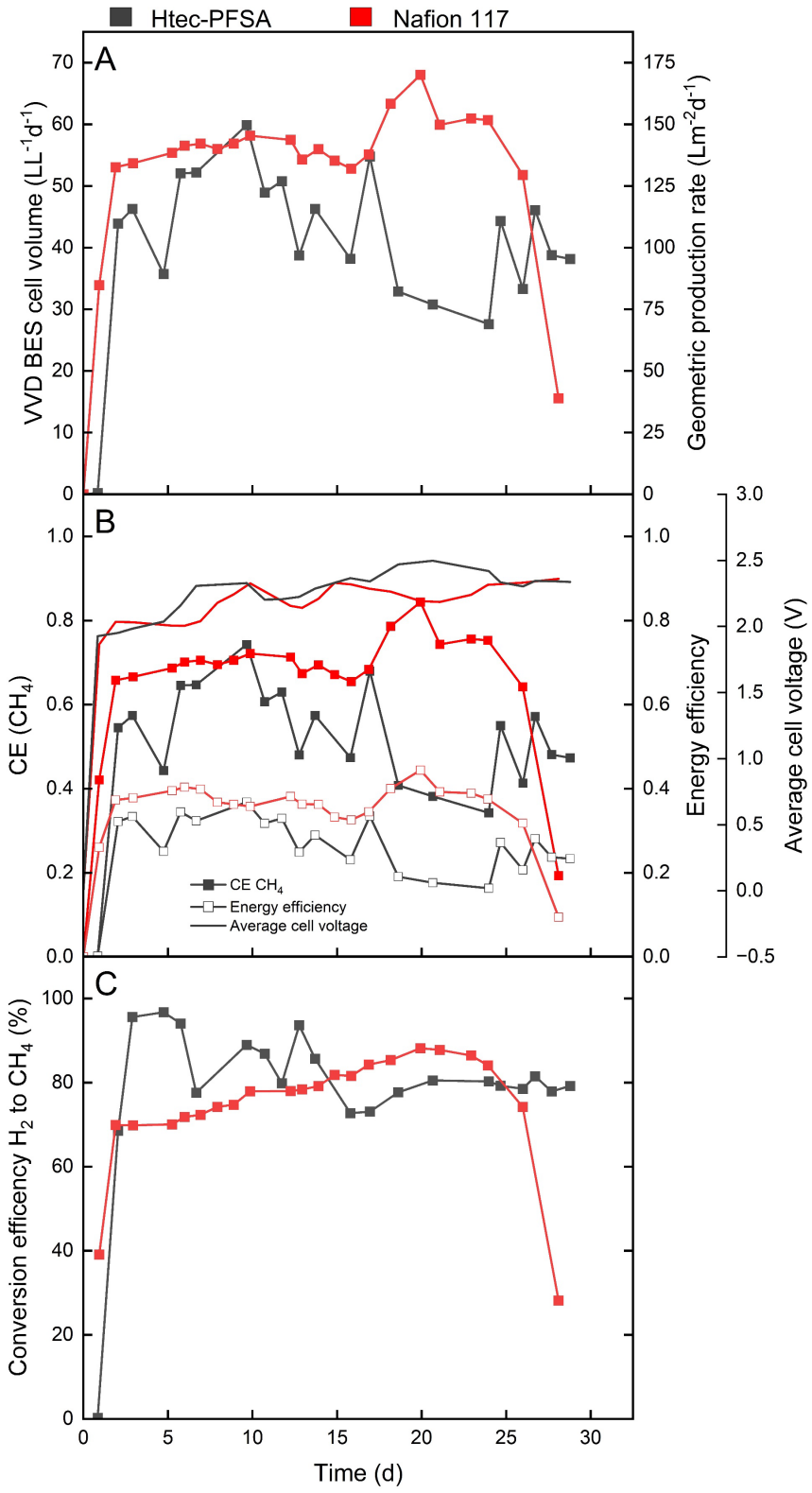


Figure 5.2: Zero-gap bioelectrochemical liquid-fed experiment using two ion-exchange membranes, Htec-PFSA and Nafion 117, which are coded in dark grey and red, respectively. The different graphs show: (A) the BES cell volumetric (Y1-axis) and geometric (Y2-axis) CH_4 production rate; (B) the CEs (Y1-axis), energy efficiencies (Y2-axis), and average cell voltage (Y3-axis); and (C) the conversion efficiency of H_2 to CH_4. The sudden performance drop for the bioelectrochemical cell using Nafion 117 corresponded to a leakage of the glass recirculating vessel.

5.4.2. Nafion 117 membrane exhibits better stability and efficiency compared to the Htec-PFSA membrane, evidenced by lower increases in cell voltage and better H_2 production efficiency

One of the biggest flaws in bioelectrochemistry is the lack of protection of the electrocatalysts, which are susceptible to degradation throughout time due to harsh environmental conditions. These conditions often involve exposure to a medium enriched with metals essential for microbial growth, adversely affecting the integrity of the electrocatalysts. While anode degradation can be somewhat mitigated through the utilization of pure water, the inevitable wear and the potential crossover of ions from the cathode to the anode chamber can compromise the performance of anodic electrocatalysts. However, a predominant source of catalyst degradation is attributed to the catholyte, which contains the growth medium for the microbes. In this study, the electrocatalyst was Pt/C, which is particularly vulnerable to poisoning by sulfides present in the medium. A key indicator of this degradation is the increase in the cell voltage needed to sustain a constant applied current, where an increase in cell voltage is inversely related to the activity of the catalyst. Throughout the duration of the liquid-fed experiments, both the Htec-PFSA and Nafion 117 membranes exhibited a decline in catalytic activity, shown by an increase in cell voltages. Specifically, the Htec-PFSA membrane experiment recorded a cell voltage rise from 1.92 V to 2.49 V (**Figure 5.2B**). Conversely, the setup with the Nafion 117 membrane demonstrated a more modest increase, from 1.86 V to 2.36 V. This lesser increase in cell voltage, observed with the Nafion 117 membrane, is an advantage for the H_2 production efficiency.

The ideal scenario involves producing H_2 without byproducts or losses. However, as cell voltages increase, there is a discernible decrease in catalytic activity, impacting H_2 production. In this study, the Htec membrane exhibited an overall subpar performance, with an average cell voltage increase to 2.30 V (**Figure 5.2B**), which was a higher cell voltage compared to Nafion 117, leading to a steady decline in H_2-CE and limiting CH_4 production. Conversely, Nafion 117 demonstrated a more stable H_2-CE at 91.2% versus 66.5% of the Htec membrane (**Figure S29**). While both membranes

experienced periods of elevated cell voltages, the bioelectrochemical cell with Nafion 117 had an overall lower cell voltage throughout the experiment compared to the cell using the Htec-PFSA membrane, resulting in less disruption to H_2 production. Notably, at an average cell voltage of 2.47 V, the H_2-CE of the Htec membrane irreversibly crashed. Assessing overall reactor performance, the conversion efficiency of available H_2 to CH_4 was similar for both membranes, with the Htec membrane slightly outperforming Nafion 117 at 82.4% compared to 76.6% (**Figure 5.2C**). As a consequence of the liquid-fed zero-gap bioelectrochemical cell performance, the vapor-fed experiment was conducted with the membrane electrode assembly using the Nafion 117 ion-exchange membrane.

5.4.3. Electromethanogenesis in a vapor-fed zero-gap bioelectrochemical cell is influenced by pressure adjustments in the anodic chamber, affecting CH_4 production rates and conversion efficiency

Here, a vapor-fed zero-gap bioelectrochemical cell was operated, paralleling previous liquid-fed experiments at the anode. The introduction of vapor into the anode chamber was controlled at 3 mL min^{-1}, following a 10-min equilibration period, to ensure system stability before commencing measurements. The inoculation strategy adopted for this experiment was consistent with that used in the liquid-fed experiment involving the Nafion 117 membrane. Similar to the liquid-fed experiment utilizing the Htec-PFSA membrane, a one-day lag phase was observed before the onset of electromethanogenesis. During the initial 5 days, without pressurization at the anode, the cell averaged a volumetric CH_4 production rate of 45.60 L L^{-1} d^{-1}, peaking at 49.14 L L^{-1} d^{-1} (**Figure 5.3A**). The CH_4-CE averaged 56.6%, reaching a maximum of 60.9% (**Figure 5.3B**). This performance was comparable to that observed with the Htec membrane experiment. To address the issue of back pressure from the cathodic chamber and to reduce H_2 crossover, the anode chamber was subsequently pressurized to 100 mbar. This adjustment maintained an average volumetric CH_4 production rate of 47.43 L L^{-1} d^{-1} with an average CH_4-CE of 58.8%. The peak volumetric CH_4 production rate and CH_4-CE were 52.23 L L^{-1} d^{-1} and 64.8%, respectively. The

highest EE was 39.1% on day 1. On day 43, the pressure relief valve was removed to assess its impact on system performance. Post-removal, the average H_2-CE was 91.4%, with a H_2-to-CH_4 conversion efficiency of 65.5% (**Figure 5.3C** and **S28**). This indicated that H_2 availability was not a limiting factor, with the primary losses attributed to outgassing. However, removing the pressure relief valve resulted in a performance decline. Despite an initial high H_2-CE of 92.7%, it decreased to 75.9% by the end of the observation period, with an average of 78.7% (**Figure S30**). Although there was an excess of H_2, the volumetric CH_4 production rate was sustained at 49.73 L L^{-1} d^{-1}. Repressurization of the anodic compartment resulted in a stabilization of the H_2-CE at 77.1%. Yet, damage to the Nafion 117 membrane was irreversible, preventing recovery to initial H_2 production levels. Upon repressurizing the anolyte compartment of the bioelectrochemical cell, the H_2-CE stabilized below 90% until the end of the experiment. The average EE was 33.8% during the experiment (**Figure 5.3B**).

On day 51, coinciding with the highest observed optical density (O.D.) of 0.85 (**Figure S31**), a considerable drop in the volumetric CH_4 production rate occurred (**Figure 5.3A**). We suggested a nutrient deficiency for the microbes. Transitioning to continuous operation at a hydraulic retention time of 7 led to a decrease and subsequent stabilization in O.D. (**Figure S31**). Removal of the pressure relief valve during continuous operation resulted in an average volumetric CH_4 production rate increase to 51.56 L L^{-1} d^{-1}, which is a marked improvement compared to the semi-batch operation. Reintroducing the pressure relief valve further enhanced the average volumetric CH_4 production rate to 55.68 L L^{-1} d^{-1}, reaching a 62.48 L L^{-1} d^{-1} peak. It also reached its highest EE with 39.7%. Notably, the conversion efficiency of H_2 to CH_4 also improved, averaging 80.3% before and rising to 89.84% post-pressurization of the anodic compartment (**Figure 5.3C**). This increase in conversion efficiency throughout the initial 43 days of the operating period was attributed to reduced H_2 production and less overall H_2 excess in the headspace. Overall, continuous operation with a pressurized anodic compartment positively impacted both CE and volumetric CH_4 production rates.

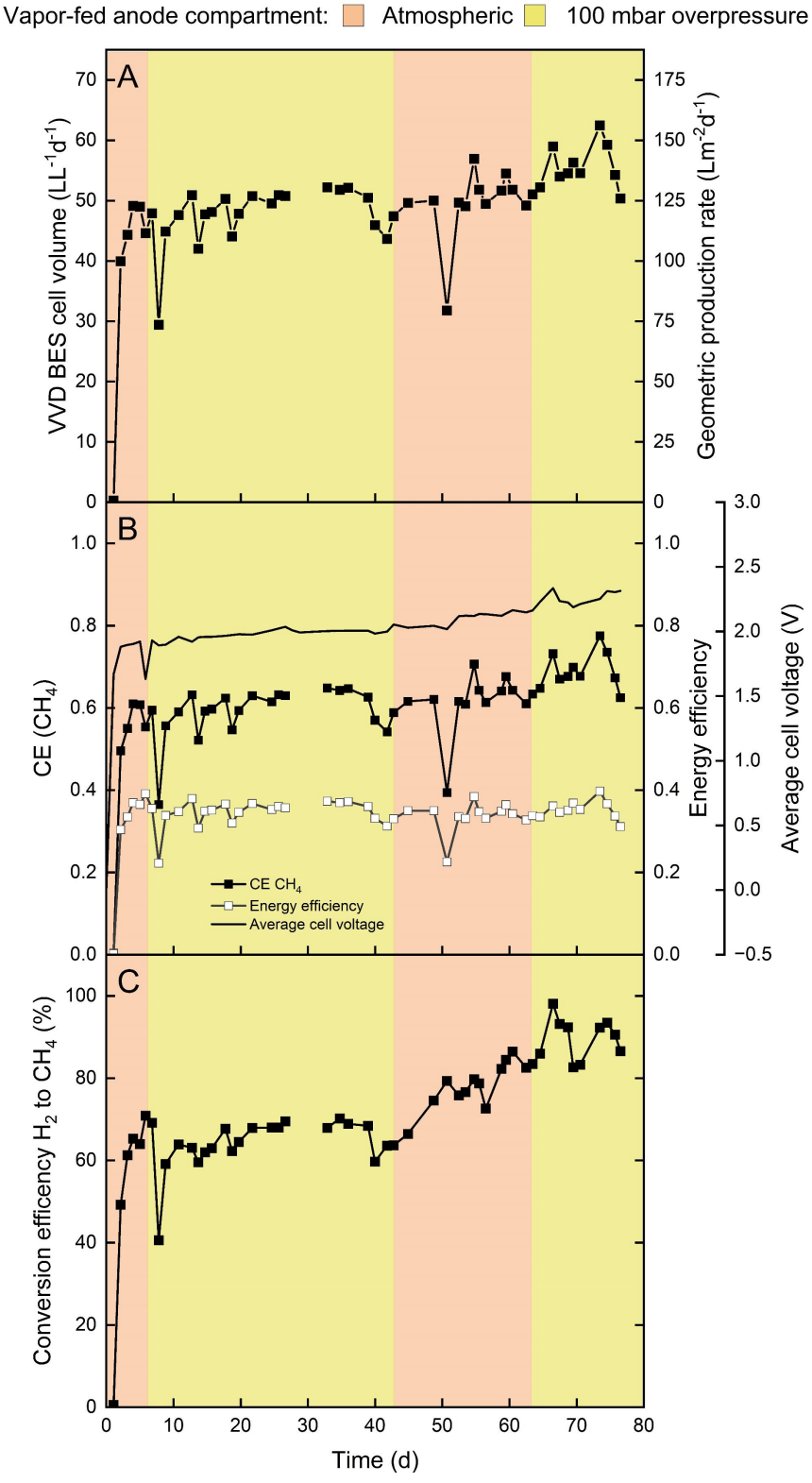


Figure 5.3: Zero-gap bioelectrochemical vapor-fed experiment using Nafion 117. The anode compartment of the bioelectrochemical cell was kept at atmospheric pressure (orange) or 100 mbar overpressure (yellow). The different graphs show (A) the BES cell volumetric (Y1-axis) and geometric (Y2-axis) CH_4 production rate; (B) the CEs (Y1-axis), energy efficiencies (Y2-axis), and average cell voltage (Y3-axis); and (C) the conversion efficiency of H_2 to CH_4. The decrease in H_2 production(**Figure S30**) decreased the excess H_2 in the system, which resulted in the steady increase in the conversion efficiency of H_2 to CH_4.

5.4.4. Vapor-fed zero gap bioelectrochemical cell maintains a lower cell voltage and reduces electrocatalyst degradation

In the introductory section, we highlighted the advantages of using a vapor-fed bioelectrochemical cell, particularly in circumventing the pH gradient, which contributes to an elevated thermodynamic cell voltage. Additionally, this approach considerably reduces the degradation of the electrocatalyst, which is a notable advantage compared to the liquid-fed system, where electrocatalyst degradation is more pronounced. In comparison, the liquid-fed bioelectrochemical cell demonstrated a marked increase in cell voltage, from 1.86 V to 2.36 V throughout 28 days (**Figure 5.2B**). In contrast, the vapor-fed cell exhibited voltage stability, maintaining a consistent cell voltage of 1.96 V for 42 days (**Figure 5.3B**). This stability persisted until the overpressure was removed from the anode compartment. Subsequent to the adjustment, the cell had a decline in H_2 production efficiency accompanied by an increase in cell voltage, which peaked at an average maximum of 2.33 V. The stability of the catalyst, which is a factor in the long-term performance of bioelectrochemical systems, was assessed by monitoring the change in cell voltage throughout the operating period and was 172 $\mu V\ h^{-1}$.

The degradation of catalysts can change the resistance of the electrolyzer. We evaluated the ohmic resistance involving various contributors such as contact resistance, catalyst resistance, and solution resistance. We employed the current interrupt method to measure the ohmic resistance of the bioelectrochemical cell, as inserting a reference electrode for impedance measurements in the bioelectrochemical cell was not feasible. An increase in bioelectrochemical cell voltage of 500 mV theoretically indicates a rise in ohmic resistance. Our findings corroborate this theory: the initial area-specific ohmic resistance was measured at 18 ± 0.46 Ω cm^2 at the onset of the experiment and increased to 46 ± 0.06 Ω cm^2 by its conclusion, a 2.6-fold increase. This rise in area-specific ohmic resistance suggests that the membrane electrode assembly has become less efficient. Given that the electrolyte composition remained unchanged (**Figure 5.4**), suggesting minimal impact from solution resistance, we hypothesize that the catalyst and contact resistance are the primary contributors. In conclusion, vapor-fed bioelectrochemical cells offer

advantages in terms of voltage stability and reduced electrocatalyst degradation compared to liquid-fed bioelectrochemical systems.

5.4.5. Metal compound concentrations did not change during liquid- and vapor-fed bioelectrochemical experiments

The zero-gap bioelectrochemical cell experiments observed a consistent decline in H_2 production, concurrently impeding CH_4 conversion. This reduction in H_2 generation indicates reduced electrocatalytic activity at the cathode. Concurrently, increasing cell voltage across all experiments further suggests a decline in H_2 evolution reaction efficacy. The possibility of cathode poisoning *via* electroplating of metal compounds is considered, which was shown by another study that electroplated metal compounds onto cathodes using concentrated trace element solutions (de Smit et al. 2023). Consequently, in our study, analytical measurements of various elements, namely ^{23}Na, ^{24}Mg, ^{39}K, ^{55}Mn, ^{59}Co, ^{60}Ni, and ^{95}Mo, were conducted (**Figure 5.4**). No deficiencies in the medium were noted, and element concentrations remained stable throughout the experiments. Notably, despite no initial deficiency, a decline in ^{60}Ni concentration was observed, suggesting an increased uptake by *M. thermautotrophicus* ΔH compared to other elements. Nickel is used in the Ni-enzymes of *M. thermautotrophicus* ΔH to enhance growth (Thauer et al. 2010; Schönheit, Moll, and Thauer 1979). While the electroplating of nickel cannot be excluded, the absence of similar trends in other elements challenges this hypothesis. Therefore, the vapor-fed bioelectrochemical system is the optimal setup for this study, but measures should be taken to prevent element deficiencies during the operation, especially from nickel and magnesium.

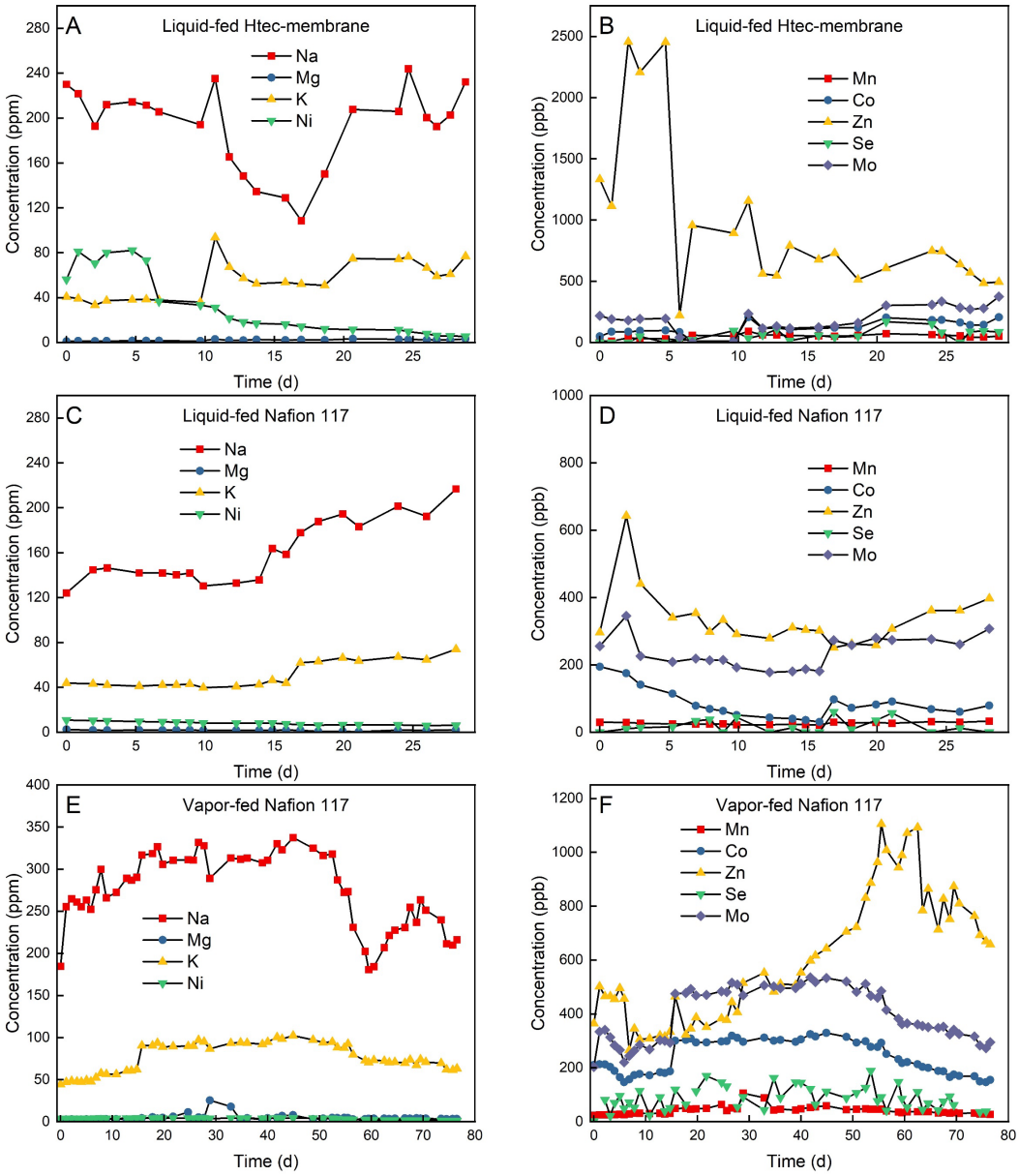


Figure 5.4*:* Element concentrations Na, Mg, K, Ni, Mn, Co, Zn, Se, and Mo in the catholyte measured with ICP-MS during the liquid- and vapor-fed bioelectrochemical experiments. (A) and (B) shows the liquid-fed experiment using the Htec-PFSA membrane, (C) and (D) demonstrate the liquid-fed experiment using the Nafion 117 membrane, and (E) and (F) exhibit the vapor-fed experiment using the Nafion 117 membrane.

5.5. Discussion

The zero-gap bioelectrochemical experiments successfully ran with *M. thermautotrophicus* ΔH under two operating modes, liquid- and vapor-feeding at the anode compartment. While both operating modes have shown comparable volumetric CH_4 production rates, differences in cell voltages, notably for the vapor-feeding experiment, could make vapor-feeding an option for future studies. The liquid-feeding experiment had a higher volumetric CH_4 production rate than the vapor-feeding experiment. Furthermore, the liquid-feeding experiment reached the highest volumetric CH_4 production rate and EE, making vapor-feeding the less optimal solution in our study. However, the observations with the liquid-feeding experiments indicate that degradation is inevitable, and vapor-feeding showed more stable cell voltages and degradation rates. Comparing the volumetric CH_4 production rate with a similar zero-gap design using vapor-fed systems, we had a much higher volumetric CH_4 production rate while the cell voltage was also lower in our study (Baek et al. 2022). However, Rad and coworkers managed a higher overall volumetric CH_4 production rate by protecting their electrocatalyst efficiently (Rad et al. 2023). It is, therefore, necessary to find the main contributors to the degradation of the electrocatalysts and to the setup of the system in both operating modes (liquid- and vapor-feeding) to optimize the zero-gap bioelectrochemical cell for future studies.

The low H_2 to CH_4 conversion efficiency observed in this study is largely attributed to a higher current density. When low current densities are used, H_2 is easier miscible in the electrolyte and can be uptaken by the microbes without forming gas bubbles and outgas. Geppert and colleagues showed this observation when running a redox flow battery type reactor, which we would classify as a zero-gap cell (Geppert et al. 2019). They observed that the outgas concentration of H_2 increased with higher current densities. However, H_2 is not an excellent soluble gas, so with higher current densities, more gas bubbles would be formed and are less likely to be uptaken by the microbes. Once the diffusion layer is saturated with dissolved H_2, H_2 bubble formation will occur (Kracke et al. 2021). Due to the low solubility of H_2, the absolute current needed to saturate the diffusion layer would be reached at low current densities. In this study, bubble formation was inevitable since, assuming Fick's law at 60°C and atmospheric

pressure, the minimum current density is 1.37 mA cm^{-2} at which bubble formation would occur (Kracke et al. 2021; Verhallen et al. 1984). In general, *M. thermautotrophicus* is an efficient microbe that converts H_2 and CO_2 at a very high conversion efficiency and yield and Electrochaea GmbH now uses it in a commercial setting (Martin et al. 2013; Contreras et al. 2022). Therefore, the study was not limited by the microbe. As for all gas fermentation processes, the low dissolution of H_2 is the limiting step in efficiently converting H_2 into any value-added chemical (Contreras et al. 2022). Therefore, our reactor setup presents major flaws in efficiently retaining H_2 to convert H_2 and CO_2 into CH_4. A solution would be to pressurize the system to dissolve more H_2 or to recirculate the gas phase to increase the mass transfer rate of dissolved H_2 (Cai et al. 2022).

PFSA ion-exchange membranes are widely used in electrochemical systems. However, the use of Nafion 117 in this study is not only one of the most studied ion-exchange membranes, it also has a disadvantage. Once the ion-exchange membrane encounters stress, its performance decreases, and H_2 crossover occurs (Stucki et al. 1998). Here, the ion-exchange membrane can encounter swelling through exposure to higher operating temperatures, loss of cation-selectivity, mechanical stress from electrolyte recirculation, and ion precipitation on the membrane. While the disadvantages and problems of PFSA ion-exchange membranes are known, it is unclear which ones are the main reason for the performance loss of both liquid- and vapor-fed systems. H_2 crossed over to the anode side (measured qualitatively) in both anodic operating modes, and we hypothesize that the swelling of the membrane is the main contributor to the H_2 crossover. We recommend testing new ion-exchange membranes that could prevent the above-mentioned disadvantages for future studies.

Furthermore, it has been shown that at higher current densities, more H_2 crosses through the ion-exchange membrane (Trinke et al. 2018; Martin et al. 2022; de Groot, Kraakman, and Garcia Barros 2022). The main contributor to H_2 crossover is the diffusion of supersaturated H_2. Supersaturated H_2 is dissolved H_2 at the boundary layer of the electrode that exceeds the average possible solubility of H_2, which can be calculated through Henry's law. Another possibility of H_2 crossover is convection through electro-osmotic drag or pressure difference. None of all possible H_2 crossover

mechanisms could be shown as a major contributor to both operating modes. While it was impossible to mitigate the H_2 loss/crossover for the liquid-fed bioelectrochemical experiments, we slowed down the H_2 crossover during the vapor-fed experiment by pressurizing the anode compartment to 100 mBar. It was noticeable that the system was stable through the high H_2-CE and the more or less constant cell voltage until the anodic compartment was set back to atmospheric pressure. However, there is no substantial proof that pressurizing the anodic compartment always improves the performance of the cell. Because pressurizing the anodic compartment improved the humidity levels observed by condensation, the anode might have lacked water for the O_2 evolution reaction.

A major contributor to performance loss is the poisoning of the catalyst layer itself. While the Htec-PFSA ion-exchange membrane generally underperformed, the Nafion 117 experiments showed stable H_2 production in both liquid- and vapor-fed operating modes. The difference between the modes is the increased cell voltage, where the vapor-feeding shows its major benefit with its lower and more stable cell voltage during the first 42 days. Several studies have shown that catalyst poisoning is a major contributor to decreased current densities in which the catalyst layer is blocked by precipitate or the constant electrolyte flow causes abrasion (Rad et al. 2023). The catalyst itself can react with the electrolyte to deactivate its catalytic ability. In this study, Pt was inevitably poisoned through sulfide that adsorbs on the active sites of Pt and inhibits the H_2 evolution reaction (Chen et al. 2018). Other elements that might have been electroplated on the cathode layer showed no concentration reduction except for Ni, which is needed for the methanogen to grow. The other measured elements were protected by a chelating agent (NTA). De Smit and coworkers showed that metals electroplated less on the cathode when a chelating agent was used (de Smit et al. 2023). It is, therefore, necessary to protect the catalyst layer by separating it from the electrolyte or using an improved catalyst inert to the electrolyte.

NiMo has been shown to be stable with methanogen medium while having the same catalytic prowess as Pt (Kracke et al. 2019; Deutzmann, Kracke, and Spormann 2023). Pentlandite-type catalysts ($Fe_3Co_3Ni_3S_8$) also show good catalytic activity and biocompatibility with elevated stability in the presence of H_2S (Rad et al. 2023). Rad

and colleagues who used pentlandite in their hybrid zero-gap bioelectrochemical cell showcased high current densities. However, they protected their catalysts with a porous transport layer, which is composed of a PTFE-coated titanium mesh and is commonly used in abiotic electrolyzers to protect the catalysts layer. The idea of bioelectrochemistry is not to protect the catalyst with a hydrophobic layer to prevent contact between the catalyst layer and electrolyte and to have the miscible H_2 directly uptaken by the microbes. In their study, the porous transport layer protected the catalysts efficiently by delivering the highest current density at low cell voltages. In this case, is microbial electrosynthesis even an option? If high current densities can only be achieved by including a hydrophobic layer between the catalyst layer and electrolyte, an abiotic electrochemical cell can be used instead, and the evolved H_2 gas can be transported to the bioreactor through a hydrophobic membrane to generate smaller H_2 bubble size. However, a yet unexplored prospect in microbial electrochemistry is using biofilm at which high current densities without protecting the electrode are theoretically possible (Jourdin and Burdyny 2021).

In theory, the benefit of using vapor-fed bioelectrochemical cells is the circumvention of a pH gradient that alters the thermodynamic cell potential of water splitting. Ideally, the water vapor at the anode is split into O_2 and protons. The protons are then transported to the cathode to form H_2, leaving the anode compartment at a neutral pH (Fornaciari et al. 2020). Our study showed no improvement in the cell voltage during the vapor-fed experiment compared to the liquid-fed experiment. Both operating modes had similar starting cell voltages, which diverged to similar final higher cell voltages. The supposedly faster degradation of the electrocatalysts for the liquid-fed experiment compared to the vapor-fed experiment makes vapor-feeding a better option to protect the catalysts from, for example, abrasion. However, a proof of circumventing a pH gradient could not be shown.

5.6. Limitations of the study

The study presents a viable approach for the industrial application of microbial electrosynthesis. However, a considerable challenge remains in the form of low current density and the consequent low EE. Jourdin et al. (2020) postulated that microbial electrosynthesis becomes economically feasible only when the EE exceeds

50%. In our study, the peak EEs recorded were 44.4% for liquid-fed and 39.7% for vapor-fed experiments (**Figure 5.2B and 5.3B**), falling short of the desired threshold. A contributing factor to this inefficiency is the excess H_2 in the headspace, which results in less H_2 being converted to CH_4. Recirculating the headspace gas could increase the solubility of H_2 and increase the EE to more than 50%, making microbial electrosynthesis an option for industrial applications (Cai et al. 2022). Moreover, vapor-fed electrolyzers encounter a specific limitation concerning the water content within the membrane (Fornaciari et al. 2020). Low water content in the membrane can lead to increased ohmic resistance. In our experiments, we consistently supplied water vapor to the anodic compartment to maintain high humidity levels inside the cell. However, the humidity levels were not measured, which should be the aim of future studies.

5.7. Experimental Details

5.7.1. Strain and medium

M. thermautotrophicus ΔH (DSM 1053) was purchased from DSMZ (Braunschweig, Germany). The medium was adjusted from Martin et al.(2013) and contained (*per* liter): KH_2PO_4, 1.36 g; sodium sulfate, 0.71 g; trisodium nitrilotriacetate, 0.21 g; nitrilotriacetic acid (NTA), 0.076 g; ammonium nickel(II) sulfate, 1.97 mg; cobalt(II) sulfate heptahydrate, 0.71 mg; sodium molybdate dihydrate, 0.61 mg; magnesium sulfate heptahydrate, 0.25 mg; iron(II) sulfate, 0.05 g; ammonium sulfate, 0.06 g; sodium selenate, 0.26 mg; and sodium tungstate dihydrate, 0.32 mg. *M. thermautotrophicus* ΔH was cultivated for the inoculum in serum bottles containing 6 g/L sodium bicarbonate as a pH buffer and 0.5 g/L L-cysteine hydrochloride as a reducing agent and sulfur source. The serum bottles were sparged with N_2/CO_2 (80/20%, v/v) to create an anoxic environment. Subsequently, the headspace was replaced with H_2/CO_2 (80/20%, v/v) at 1 bar overpressure and autoclaved. Incubation of *M. thermautotrophicus* ΔH occurred at 60°C and 150 rpm. The bioelectrochemical system underwent a similar anoxic treatment by sparging with pure CO_2 before supplementation and inoculation. Following the establishment of anoxic conditions,

the sulfur source (0.3 g/L sodium sulfide) was added, and the pH was adjusted to 7.2 using 1M NaOH, which was diluted in the medium instead of water.

5.7.2. Bioelectrochemical setup

The electrochemical cell was a commercially available zero-gap electrolysis cell (**Figure 5.5 B** and **C**, H-tec Systems GmbH, Augsburg, Germany) composed of a membrane electrode assembly. The perfluorosulfonic acid (PFSA) ion-exchange membrane was coated with 0.5 mg/cm² Pt on the cathode side and 2 mg/cm² IrRu mix on the anode side. A carbon paper with a mesoporous carbon layer and Ti-felt was placed on top of the catalyst and contacted by the current collector. In subsequent experiments, the frame of the electrolysis cell was kept. However, the catalysts-coated ion-exchange membrane and the gas diffusion layer were exchanged with a Nafion 117 ion-exchange membrane coated with 1mg/cm² Pt/C on the cathode and 2 mg/cm² Ir on the anode (CCM-E25-N117, Quintech, Göppingen, Germany). The gas diffusion electrodes were carbon paper with a mesoporous layer and Ti-felt for the cathode and anode side (Quintech, Göppingen, Germany), respectively. The total geometric surface area of the zero-gap bioelectrochemical cell was 16 cm², and a constant current of 120 mA was applied *via* a potentiostat (VMP3, Bio-logic, Claix, France) and controlled through EC-lab software (Bio-logic, Claix, France). The anode and cathode compartments were connected to glass recirculation vessels (**Figure 5.5 A**). The catholyte glass recirculation vessel contained multiple ports for pH measurement, gas feed, outgas, in/out ports for the glass recirculation, gas sampling, base feed for pH control, medium feed, and medium out. The anolyte recirculation vessel only contained ports to monitor the pH and recirculate the water to the electrochemical cell.

During vapor-fed operation, water recirculation was replaced by the humid air of the anolyte forced by a N_2 gas flow rate of 3 mL/min. The anolyte and catholyte were run at 65°C using a water thermostat (KISS 104A, Huber, Raleigh, USA). A multi-channel pump (Masterflex L/S pump equipped with a multi-channel pump head model 7519-20, Cole Parmer, Germany) was used as medium feed in and out during continuous operation (**Figure 5.5 A**). CO_2 was used as a carbon source, and the flow rate was controlled using the Bronkhorst EL-Flow® Prestige mass flow controller (Bronkhorst

Deutschland NORD GmbH, Kamen, Germany). The CO_2 flow rate was adjusted from 0.6 mL min^{-1} to 0.3 mL min^{-1} to ensure that carbon is not limited. The outgas volume was measured offline using a MilliGascounter MGC-1 V3.4 PMMA (Dr.-Ing. RITTER Apparatebau GmbH& Co. KG, Bochum, Germany).

Three experiments were conducted with different operating conditions. The first experiment was the commercial electrochemical cell with MilliQ water as an anolyte. The second experiment replaced the ion-exchange membrane with the Pt/Ir-coated Nafion 117 and used MilliQ water as an anolyte. The third experiment was similar to the second experiment, with vapor feeding the anode side. Vapor-feeding was realized by pumping humid air from the anolyte vessel to the anodic side of the bioelectrochemical cell. The cathodic vessel was first sparged with pure CO_2 for each experiment to make the catholyte/medium anoxic. Before inoculation, the catholyte medium was reduced with 0.3 g L^{-1} sodium sulfide, and the pH was set to 7.2. The inoculation was performed with pre-grown *M. thermautotrophicus* ΔH in serum bottles to an OD_{600} of approx. 0.04. The bioelectrochemical cells were operated in fed-batch mode. After two weeks, 3 mL of a 100x medium was added. 0.5 mL of 40 g L^{-1} Na_2S was added every week. The continuous mode operation was exclusively applied to the third experiment and was initiated only after completing the fed-batch phase to compare it with the liquid-fed bioelectrochemical cell experiments. The hydraulic retention time (HRT) was 7 days, corresponding to a constant feed rate of 0.03 mL min^{-1}. The pH of the catholyte and anolyte was monitored (Bluelab, Gisborne, New Zealand). A sample day consisted of measuring OD_{600}, pH, and out gas composition. The liquid sample was stored at -20 °C until further analysis. The ohmic resistance of the zero-gap bioelectrochemical cell was measured using the current interrupt method using the potentiostat (Bio-logic, Claix, France). A current of 120 mA, which was the applied current during the zero-gap bioelectrochemical experiments, was used during the current interrupt with 1 s intervals repeated 10 times.

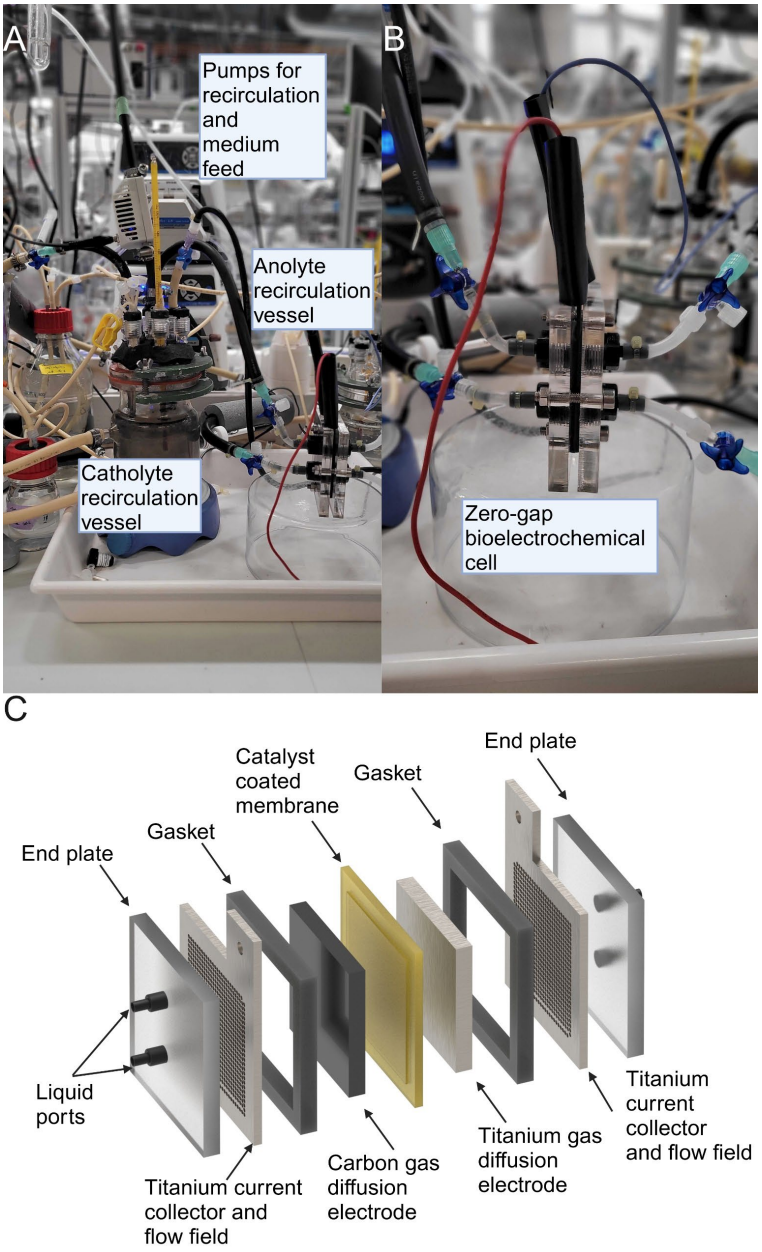


Figure 5.5: Lab views: (A) Image of the zero-gap bioelectrochemical cell in operation; (B) Close-up view of the zero-gap bioelectrochemical cell; and (C) exploded view of the zero-gap bioelectrochemical cell. The catholyte glass recirculation vessel contained ports to monitor and control the pH and to sample gas. Two ports were used to recirculate the electrolyte/medium. Liquid samples were taken from a three-way valve at the recirculation tubing line. Two ports were used for the gas-in and the gas-out. The gas-out tubing line contained a condenser to avoid water loss. The ports for the anolyte glass recirculation vessel consisted of the recirculation tubing and a pH probe for pH monitoring. During the vapor-fed experiment, ports for N_2 gas-in and a tubing connected to the anodic compartment were used.

5.7.3. Analytical analysis

A gas chromatograph (SRI GC, Torrance, USA) was used to analyze the headspace gas composition. The gas chromatograph was equipped with a Haysep D column (length 3m, outer diameter 1/8", SRI GC). A thermal coupled detector and a flame ionization detector were used to measure H_2, CH_4, and CO_2 with N_2 as the carrier gas. The column temperatures and pressures were set at 70°C and 20 psi, respectively. 500 µL was taken from the gas headspace with a gastight syringe (Hamilton, Reno, USA) for each sample point. The OD_{600} was measured with a UV/VIS-Spectrophotometer at 600 nm absorbance (BioMate™ 160, ThermoFischer Scientific, Waltham, USA). All liquid samples were analyzed on an Agilent 7900 ion-coupled plasma mass spectrometer instrument (Agilent, Santa Clara, USA) to quantify ^{23}Na, ^{24}Mg, ^{39}K, ^{44}Ca, ^{55}Mn, ^{56}Fe, ^{59}Co, ^{60}Ni, ^{66}Zn, ^{78}Se, and ^{95}Mo. The samples were diluted 1:100 in 1% HNO_3, which was also the matrix.

5.7.4. Calculations

Coulombic efficiency was calculated by dividing the produced CH_4 or H_2 in number of electrons by the number of electrons supplied to the electrochemical cell. The equation is as follows:

$$\mathrm{CE} = \frac{\mathrm{n} \cdot \mathrm{F} \cdot \mathrm{z}}{\int \mathrm{Idt}} \tag{13}$$

Where n is the molar quantity of produced CH_4 or H_2, F the Faraday constant, z number of electrons to form CH_4 or H_2 , and I the current of the bioelectrochemical cell (7.5 mA cm^{-2}). The energy efficiency was calculated as follows:(Geppert et al. 2016)

$$\mathrm{EE} = \frac{\Delta \mathrm{G}_{\mathrm{CH4}} \cdot \mathrm{n}}{\mathrm{E}_{\mathrm{cell}} \cdot \int \mathrm{Idt}} \tag{14}$$

With ΔG_{CH4} the Gibbs free energy of CH_4 (890.4 kJ/mol), and E_{cell} the measured cell voltage.

The conversion efficiency of H_2 to CH_4 was calculated as follows:

$$\text{Conversion efficiency } \mathrm{H_2} \text{ to } \mathrm{CH_4} = \frac{4\mathrm{n}_{\mathrm{CH_4}}}{4\mathrm{n}_{\mathrm{CH_4}} + \mathrm{n}_{\mathrm{H_2}}} \tag{15}$$

With n_{CH4} the quantity of mole of CH_4 and n_{H2} the quantity of mole of H_2.

5.8. Acknowledgments

This work was supported by the Deutsche Forschungsgemeinschaft (DFG, German Research Foundation, EBiotech, SPP2240; L.T.A.) – project number 445506379, the Alexander von Humboldt Foundation in the framework of the Alexander von Humboldt Professorship (L.T.A.), and The Novo Nordisk Foundation CO_2 Research Center with grant number NNF21SA0072700 (L.T.A.).

Chapter 6

6.1. Closing summary

The results of this dissertation showed three different microbial electrolysis cell systems that were successfully run with *M. thermautotrophicus* to improve the bioelectrochemical systems for microbial electrosynthesis. Each of the presented systems showcased an improvement or has given new insights into the bioelectrochemical cells. However, further research needs to be performed to achieve an unwritten current density target of 50 mA cm^{-2} and have microbial electrosynthesis as a possibility for industrial application. In Chapter 3, we successfully proved the concept of a membrane-less BES by leveraging carbon oxidation alongside sacrificial anodes. In our experiments, the BES facilitated the production of CH_4 utilizing an O_2-sensitive thermophilic methanogen at the cathode, achieving high CE at a geometric current density of 1 mA cm^{-2} for 3 days. Subsequently, the production faced limitations due to the depletion of reduced sulfur compounds in the growth medium, which resulted from sulfur oxidation occurring at the anode. Transitioning these findings towards industrial-scale applications demands considerable innovations to address, including the avoidance of sulfur oxidation, carbon recycling, and the prevention of carbon corrosion. However, a membrane-less single-chamber BES is ready for further studies that run BES at relatively low current densities for research purposes.

In Chapter 4, three microbial electrolysis cells were run in a scaled-up BES but at relatively low current densities. We observed that *M. thermautotrophicus* quickly adjusted to intermittent power shutdowns, showing good CH_4 recovery times post-shutdown. Three electrode materials were used in a microbial electrolysis cell, platinized titanium, graphite, and nickel, that attained high absolute currents, with platinized titanium reaching the highest volumetric CH_4 production rate followed by the microbial electrolysis cell using nickel and graphite electrodes, respectively. An extended investigation into the use of nickel electrodes within microbial electrolysis cells, exploring three shutdown procedures, revealed minimal effects on performance, except for the short-circuit approach, which increased nickel dissolution

and could lead to accelerated degradation. Overall, it showed that the methanogen, which is run in an industrial setting, can adjust to harsh environments and adapt to produce efficiently CH_4 post-shutdowns. However, the study identified limitations on the glass recirculating vessel, which introduced O_2 during long shutdown periods and did not efficiently retain H_2.

In Chapter 5, the investigation into zero-gap bioelectrolysis cell technologies focused on two liquid-fed and one vapor-fed anode configurations. Among these, the setup featuring the Nafion 117 ion-exchange membrane outperformed its counterpart in liquid feed mode and was further tested under vapor feed conditions. The transition to a vapor-fed anode aimed at circumventing pH gradient formation and improving catalyst performance yielded positive outcomes, with the vapor-fed cell exhibiting prolonged stability in cell voltage. Another discovery was the importance of anode chamber pressurization; its absence negatively impacted the ion-exchange membrane, causing irreversible harm. It resulted in an H_2 crossover and a decline in catalyst performance. Similar to the limitation in Chapter 4, H_2 was not fully converted to CH_4 because H_2 could not be retained long enough in the glass recirculating vessel. In the next section, I will present my ideas on optimizing every study of each chapter presented in this dissertation. I also discuss future studies that I think are interesting and could bring microbial electrosynthesis closer to industrial application.

6.2. Recommendations for future work

Three different bioelectrochemical cells were investigated and improved in this dissertation. However, improvements need to be made, and this section provides a personal opinion on how this could be done. Chapters 4 and 5 are connected and have higher chances for industrial readiness, and recommendations for future work will be included in both chapters. The proof-of-concept presented in Chapter 3 needs ample optimization. However, it is a great tool for basic research, which will be discussed in the next section.

6.2.1. Single-chamber membrane-less bioelectrochemical system: a tool for basic research

The single-chamber BES is anticipated to be more energy-efficient than traditional two-chamber, membrane-based systems due to its lower operating cell voltage, as discussed in section 3.4.10. It is necessary for future research to conduct a direct comparison of performance and power consumption between membrane-less and membrane-based microbial electrolysis cells, particularly considering that the zero-gap design in membrane-based systems could narrow the performance gap with membrane-less designs. However, empirical evidence is required to substantiate this hypothesis. The design without ion-exchange membranes implies reduced initial costs for the membrane-less system, yet a detailed techno-economic analysis is essential to assess its economic viability conclusively. For broader applications, a crucial objective is to extend the optimal performance period of the system from a short span of days to several months. A considerable challenge in this regard is the reliance on sulfur compounds within the membrane-less BES; these compounds are oxidized at the anode, making them inaccessible to the microbes. A potential solution to this limitation involves transitioning to microbes that do not rely on redox-active sulfur compounds, such as the commonly utilized *Sporomusa ovata*. In preliminary experiments, thiosulfate was successfully used as a sulfur source with *S. ovata* grown heterotrophically. Further adaptation experiments are necessary to explore the growth of *S. ovata* under autotrophic conditions. Sulfate-reducing microbes, which are capable of converting sulfate back to sulfide, are particularly promising for membrane-less BES applications. This regeneration of oxidized redox-active sulfur compounds by sulfate-reducing bacteria, when paired with microbes that require sulfide and produce chemical outputs from H_2 and CO_2, could establish a self-sustaining circular reaction system.

However, as mentioned in section 3.4.10, I anticipate further obstacles related to carbon availability and corrosion, both of which are interconnected and must be addressed in tandem. Identifying a sustainable carbon source, ideally sourced from processes that generate carbon as a by-product, is necessary. An example of such a source is the carbon waste generated during the industrial production of grey H_2. This

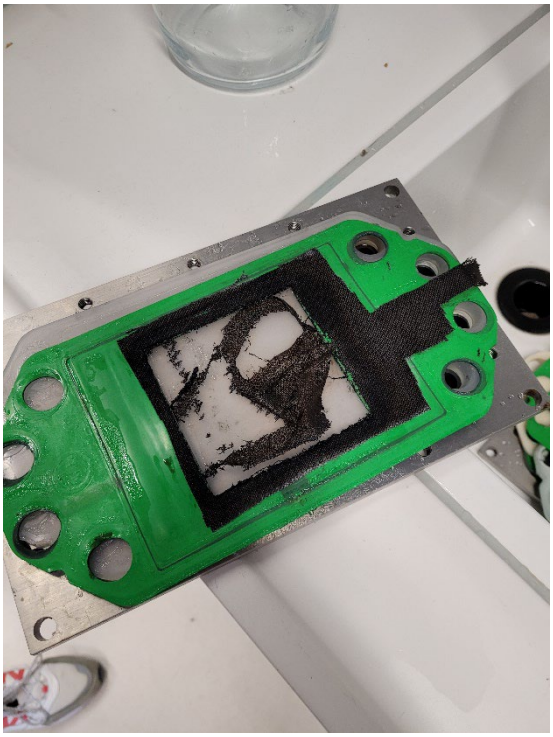


Figure 6.1: the single-chamber BES was scaled-up using a plate reactor design. The projected geometric surface area was 100 cm^2. The anode was activated carbon cloth. It shows the dissolution of the anode after applying a voltage for 6 h.

approach not only addresses the need for a sustainable carbon supply but also contributes to the circular economy by repurposing waste products. The next challenge is to circumvent excessive carbon corrosion or dissolution. When I tried to scale-up the membrane-less BES with a 100 cm^2 activated carbon cloth, the anode completely dissolved and the system was short-circuited (**Figure 6.1**). The experiment would have lasted longer if other materials, such as granular-activated graphite, had been used. However, it corroded the surface, leading to increased charge transfer resistance due to the accumulation of functional groups on the carbon surface. The result is a less conductive anode, which decreases the current density. Minimizing carbon corrosion through the use of either costly protective catalysts or more robust carbon forms, such as graphene or carbon nanotubes, might be necessary. Finally, transitioning to a continuous system could mitigate by-product accumulation, and employing mesoporous carbon increases the number of reactive sites, reducing the risk of carbon corrosion while enhancing surface area and porosity for improved carbon oxidation.

Classic CAWE is not performed as a membrane-less single-chamber system. It is mainly used as a replacement reaction for the OER since carbon oxidation is faster than the OER (Ju, Badwal, and Giddey 2018). It is, therefore, interesting to use a classic plate reactor BES with an ion-exchange membrane and perform CAWE instead of water electrolysis in microbial electrosynthesis. Some reviews suggested alternative oxidation, such as glycerol to formic acid or glucose to gluconic acid (Jourdin and Burdyny 2021; Abdollahi et al. 2022). These alternative reactions showed theoretical cell voltages lower than water electrolysis. However, using glucose or glycerol is not an economical solution. Another alternative reaction is the oxidation of Fe^{2+} to Fe^{3+} at the anode and regenerating the Fe^{2+} through indirect carbon oxidation, as mentioned in section 3.4.8.

I believe that the biggest application of a membrane-less single-chamber with carbon oxidation lies in basic research of BES. Many studies that investigate extracellular electron transfer could benefit from the simplicity of the setup. For example, the extracellular electron transfer study using *Candidatus* Methanoperedens by Ouboter and coworkers poised their bioanode at 0 V, which is below the theoretical potential of the OER (Ouboter et al. 2022). The aim was to oxidize CH_4 with the microbe. Therefore, separating the anodic and cathodic chambers is unnecessary since H_2, which should not be generated at the applied potential, should also not introduce additional interaction with the microbe. However, replacing their H-cell setup with a membrane-less design has not been performed before, and possible side reactions that hamper biological growth are not known.

6.2.2. Recommendations for future studies in microbial electrosynthesis

The presented microbial electrochemical technologies in chapters 4 and 5 have room for improvement, and this section elucidates which improvements I would suggest for future research. In general, electrochemical cells should have low internal resistances. A key recommendation for advancing microbial electrosynthesis is the adoption of a zero-gap design in electrochemical cells to minimize internal resistances. The zero-gap configuration, which positions the anode and cathode in close proximity, effectively

reduces ohmic losses. Although successfully implemented in Chapter 5, the low conductivity of the medium in comparison to traditional electrochemical cells is a limitation to achieving higher current densities (Prévoteau et al. 2020). Future research should prioritize the development of durable, reliable catalysts that are less prone to degradation. Contamination and deactivation of catalysts remain considerable hurdles, as illustrated in Chapter 5. A promising solution, Rad and colleagues used a porous transport layer, specifically a PTFE-coated titanium mesh, to protect the catalysts (Rad et al. 2023). This approach, which is common in abiotic electrochemical cells, could extend catalyst longevity in microbial electrosynthesis applications. However, the bioelectrochemical consensus suggests that microbes directly uptake miscible H_2 from the cathode, complicating the goal of reaching target current densities of 50 mA cm^{-2} without encountering issues such as bubble formation at high current densities. Bubble formation at high current densities is unavoidable unless the surface area of the electrodes is large enough not to saturate the diffusion layer of the electrode with H_2 (Kracke et al. 2021). Future studies could explore altering catalyst morphology, such as electrodepositing catalysts onto metal foams instead of flat electrodes. This adaptation could enhance the efficiency and scalability of microbial electrosynthesis by increasing the electrode surface area and improving gas diffusion. Yet, if protecting the catalysts remains a prerequisite for achieving high current densities, the feasibility of microbial electrosynthesis for scaling up is, for me, questioned. An alternative approach, which is the old approach, involves the two-unit process combining an abiotic electrolyzer with a bioreactor, offering higher efficiency. This is supported by advancements in classical electrochemical cells, such as those by Hysata, which reports EE up to 95% (Hodges et al. 2022).

The potential of biofilms to increase current densities in microbial electrosynthesis has been a topic of interest, with studies suggesting that the positioning of microbes such as *M. thermautotrophicus* close to the cathode, ideally in the form of a biofilm, could considerably improve extracellular electron transfer, and thereby enhance CO_2 conversion to CH_4 efficiency (Jourdin and Burdyny 2021). Jourdin and coworkers demonstrated that a biofilm thickness of 400 µm could augment current production throughout time. Further theoretical analysis by the same author suggested that

current densities could range between 750 to 1100 mA cm^{-2} if the biofilm is integrated within the 3D structure of the electrode (Jourdin and Burdyny 2021; Jourdin et al. 2018). Even if just 10% of this theoretical range were achievable, microbial electrosynthesis might become a viable option for industrial applications. The choice of microbe is crucial for such biofilm-based enhancements to be realized. Wildtype strains of *M. thermautotrophicus*, known for their ability to adhere and form biofilms *via* cell surface structures such as fimbriae, are promising microbes for future studies. Specifically, strains of *M. thermautotrophicus* that possess functional fimbriae have been shown to develop biofilms on nickel grids (Thoma et al. 2008). The production of fimbriae is directly correlated with the formation of cell-cell structures, with higher fimbriae expression promoting biofilm growth and lower levels favoring planktonic cell growth. Genetically modified strains of *M. thermautotrophicus* ΔH that either lack or overexpress fimbriae genes (*e.g.*, Mth60 fimbriae gene) offer an opportunity to explore further the impact of biofilm formation on current densities (Fink et al. 2023). However, the effect of high current densities on cellular stress within these biofilms remains to be investigated. Future research should aim to compare the performance and stress levels of planktonic cells versus biofilm-based systems of *M. thermautotrophicus* in microbial electrolysis cells. I hypothesize that planktonic cells may experience less stress than biofilm cells. This assessment could pave the way for developing microbial electrosynthesis technologies that are both effective and adaptable for industrial use, highlighting the importance of biofilm formation in enhancing electrochemical processes.

In Chapters 4 and 5, a challenge to solve was the high proportion of H_2 in the headspace, indicating inefficiencies in H_2 utilization. The above-proposed solutions to enhance conversion efficiencies include developing thicker biofilms or using larger 3D electrodes to increase the miscibility of H_2. Particularly in Chapter 5, a hypothetical achievement of near 100 % conversion efficiency of H_2 to CH_4 would mean an EE exceeding 50% at a current density of 7.5 mA cm^{-2}, which is a minimum EE goal postulated elsewhere (Jourdin and Burdyny 2021). Fortunately, addressing the retention of H_2 within the bioreactor presents a known but solvable problem. One straightforward solution is recirculating the headspace gas to improve H_2 solubility.

Cai and coworkers demonstrated a ninefold increase in the mass transfer rate of H_2 by implementing gas recirculation (Cai et al. 2022). Additionally, optimizing the design of the glass recirculation vessel to allow for pressurization could further improve gas solubility, although the current glass vessels limit overpressure to a maximum of 400 mBar. Another challenge concerns gas diffusion issues, such as CO_2 in Chapter 4 and H_2 in Chapter 5. Both studies employed a Nafion 117 ion-exchange membrane, suggesting that shifting toward membranes with higher selectivity and lower permeability could yield better results. Given that most ion-exchange membrane research focuses on abiotic systems, future studies should carefully consider membrane thickness and material composition to suit bioelectrochemical applications. Moreover, general system enhancements should be explored to optimize performance, including an improved flow field for enhanced mass transport, online gas measurement to monitor gas concentrations accurately, a leak-proof glass recirculation vessel to prevent gas loss, online ORP control for maintaining optimal redox conditions, and a leveling control to ensure consistent medium supply.

The overarching goal for microbial electrosynthesis lies in its application within industrial settings. A fundamental economic principle applies here: if the cost of producing a product exceeds its market value, further research and development into the process become economically unjustifiable. However, should microbial electrosynthesis achieve the necessary EE and current density benchmarks, its integration into industrial environments should be considered. A critical aspect of scaling microbial electrosynthesis for industrial use involves utilizing carbon sources that are readily available as industrial by-products rather than relying on pure CO_2. These by-products often comprise a mixture of gases, potentially including toxic compounds. Recent studies have shown promising outcomes when using industrial off-gases as feedstocks (Rovira-Alsina, Dolors Balaguer, and Puig 2022).

Moreover, the operating resilience of microbial electrosynthesis to fluctuations in the electrical energy supply has been studied with both acetogens and methanogens showing adaptability to intermittent energy sources (Deutzmann, Kracke, and Spormann 2023; Deutzmann et al. 2022). This resilience is crucial for integrating microbial electrosynthesis processes in real-world industrial environments, where

energy supply can be variable. Therefore, future research directions should encompass a broader spectrum of industrial applications, but this should only proceed once microbial electrosynthesis has met its EE and current density targets. Achieving these targets is essential to ensure that the technology is technically viable and economically feasible. Without meeting these baseline criteria, pursuing industrial-scale applications of microbial electrosynthesis would not be practical.

Supplementary for Chapter 3

Supplementary note 1:

Determination of the exchange current density and Tafel slope

For the determination of the exchange current density for the carbon oxidation, OER, and HER, the Butler-Volmer equation (**Eq. S1**) was used and transformed to determine j_0 from its interception at the y-axis.(Bard and Faulkner 2000) The Butler-Volmer equation (**Eq. S1**) is described as followed:

$$j = j_0 \left\{ exp\left[\frac{\alpha_a z F}{RT}\eta\right] - exp\left[\frac{\alpha_c z F}{RT}\eta\right]\right\} \quad \text{(S1)}$$

With j the current density, j_0 the exchange current density, α_a and α_c the anodic and cathodic charge transfer coefficient, respectively, z the number of electrons involved in the reaction, F the Faraday constant, R the universal gas constant, T the temperature, and η the activation overpotential.

When η>>0, the **Eq. S1** simplifies to **Eq. S2** :

$$\eta = \frac{2.3\ RT}{\alpha F} log j_0 - \frac{2.3\ RT}{\alpha F} log j \quad \text{(S2)}$$

Eq. S2 can be transformed into the Tafel equation to calculate the Tafel slope, which was used to calculate the Tafel slopes of magnetite:

$$\eta = \pm \frac{2.3\ RT}{\alpha F} log \frac{j}{j_0} + A \quad \text{(S3)}$$

$$\eta = B log \frac{j}{j_0} + A \quad \text{(S4)}$$

With B the Tafel slope, and A the symmetry factor. The exchange current density j_0 and the Tafel slope are calculated from $\log|j|$ *vs.* η by the interception of the y-axis and the slope, respectively.

Supplementary note 2:

Magnetite analyses

We investigated magnetite as a possible redox mediator. We fabricated magnetite anodes with activated carbon, which is our carbon source for carbon oxidation, to increase the conductivity of magnetite, which is a semi-conductor.(Cornell and Schwertmann 2003) Since the conductivity of the electrode can vary depending on the amount of activated carbon used, we investigated which ratio of magnetite to activated carbon is suitable for higher current generation, longevity, and inhibition of O_2 evolution. Therefore, we performed abiotic tests with different ratios of magnetite and activated carbon ranging from 20% to 100% of the total activated carbon. We used the chronoamperometric method to determine the electronic conductivity of our mixtures and set the WE at +0.6 V *vs*. Ag/AgCl. The current of a chronoamperometric graph decreased exponentially to reach an asymptotic value, which was used to calculate the conductivity (**Fig. S11**). The specific electronic conductivity σ was calculated (**Eq. S5**).

$$\sigma = \frac{I \cdot D}{E \cdot A} \quad \text{(S5)}$$

Where I is the asymptotic current, D is the thickness of the electrode (D = 0.4 cm), E is the applied potential, and A is the surface area of the electrode (A = 0.28 cm^2). The calculated specific electronic conductivities of 40% magnetite and 60% activated carbon showed the highest electronic conductivity with 3.89 × 10^{-4} S·cm^{-1} and was further analyzed for its ability to inhibit O_2 (**Table S2**).

A critical aspect of sufficient electrical conductivity is a homogenous distribution of magnetite on activated carbon particles. Ideally, only a thin layer of magnetite is adsorbed on the surface of the activated carbon. To analyze the distribution of magnetite on activated carbon, we characterized synthesized magnetite on activated carbon with X-ray diffraction (XRD). We compared synthesized magnetite with the following materials: **(1)** pure magnetite; **(2)** pure activated carbon; and **(3)** commercial magnetite (**Fig. S12**). The XRD patterns of magnetite, magnetite on activated carbon, and commercial magnetite show overlapping diffraction peaks for the whole

spectrum, confirming that our synthesis contains magnetite. Further comparison of the XRD peaks shows a good agreement with standard patterns, indicating high crystalline quality. However, because maghemite's XRD pattern is virtually indistinguishable from the XRD pattern of magnetite, we analyzed the Fe(II)/Fe(III) ratio with the ferrozine assay. The ratio of Fe(II)/Fe(III) found in our samples corresponded to 0.40 ± 0.1, which is 20% lower than the ideal ratio of 0.5 for magnetite. This means that 20% of our material was oxidized, likely to maghemite. The XRD pattern of the activated carbon can be attributed to amorphous carbon that is also observed in magnetite coated activated carbon.

Scanning electron micrograph of magnetite on activated carbon demonstrated a rough and porous particle (**Fig. S13A**). Furthermore, close-up views of the particle showed that magnetite was synthesized as round-shaped nanoparticles (**Fig. S13B,C**). However, it was not possible to identify whether magnetite was homogeneously coated on activated carbon. To underline the homogenous distribution of magnetite, we performed EDX to detect the iron on the surface. By detecting the Fe with Fe Kα energy-dispersive X-ray spectroscopy (EDX) elemental mapping of magnetite-coated activated carbon, we detected the distribution of Fe. The overlay of a magnetite-coated activated carbon particle SEM micrograph with the elemental mapping of Fe confirmed that Fe was very well dispersed on top of the activated carbon particle (**Fig. S14** and **S15**).

The stability of magnetite anodes is primarily determined by the crystal structure and purity of the magnetite mineral

We calculated the conductivity of different magnetite to activated carbon ratios and found that the ratio of 40%:60% magnetite to activated carbon obtained higher conductivities for our electrodes (**Eq. S5** and **Fig. S11**). To understand how this ratio functions in stability and longevity, we prepared triplicates of 40%:60% magnetite to activated carbon electrodes as our counter electrodes and poised the carbon cloth WE at -0.8 V *vs.* Ag/AgCl. After 7 days, the liquid/electrode interface developed an orange precipitate of Fe(III) at each electrode. After the experiment, we analyzed each Fe(II)/Fe(III) electrode ratio with a sequential extraction. We compared them with the starting material (**Fig. S16**) and analyzed the abundance of Fe(II) and Fe(III) for each

section (electrode liquid interface, middle section, upper section). Here, the starting material was partially oxidized with a stoichiometric ratio of around 0.44. After 7 days of oxidation, the outer layer of the magnetite particle was nearly completed oxidized, while the stoichiometric ratio of the bulk was similar to the initial stoichiometric ratio of magnetite. In conclusion, activated carbon coated magnetite showed nearly complete oxidation at the outer layer that might prevent a stable and durable anode. Refer to the main text for further informations on the durability of magnetite anodes under section “Magnetite, which is an alternative redox mediator to soluble iron, shortened the optimum performance period”

Table S1| Comparison of abiotic and biotic current densities with their respective coulombic efficiencies and references

Product	Current density [mA cm^{-2}]	Coulombic Efficiency [%]
Abiotic		
H_2	Up to 2000	99 (Lee et al. 2020)
Ethanol	250	46 (Ma et al. 2016)
CH_4	200	70 (Zhang et al. 2021)
Biotic		
Acetate	10	100 (Jourdin et al. 2015)
CH_4	1	99 (Kracke et al. 2020)

Table S2 | The electronic conductivity of different activated carbon to magnetite and hematite percentages calculated by chronoamperometry (CA) method.

Activated carbon to magnetite	Electronic conductivity [S/cm]
100% activated carbon	5.08×10^{-8}
60% activated carbon, 40% magnetite	3.89×10^{-4}
40% activated carbon, 60% magnetite	2.91×10^{-4}
20% activated carbon, 80% magnetite	1.91×10^{-4}
60% activated carbon, 40% maghemite	5.31×10^{-6}

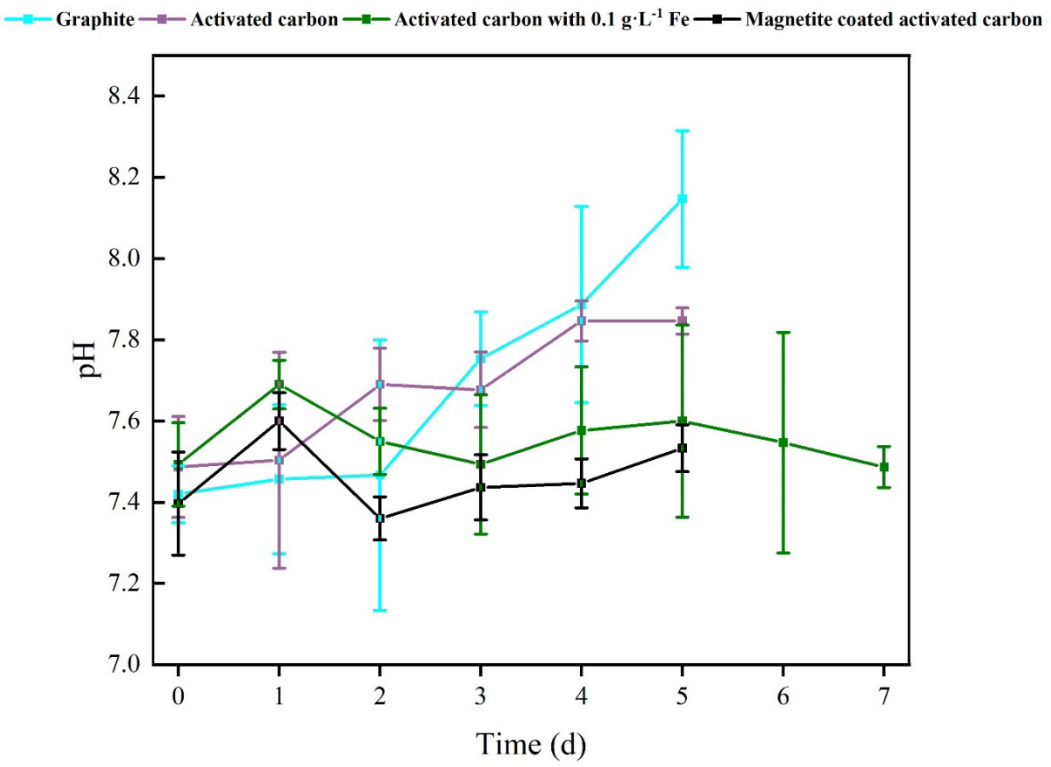


Figure S1: Measured pH during some of the BES experiments using graphite, activated carbon with and without added iron, and magnetite-coated activated-carbon anodes.

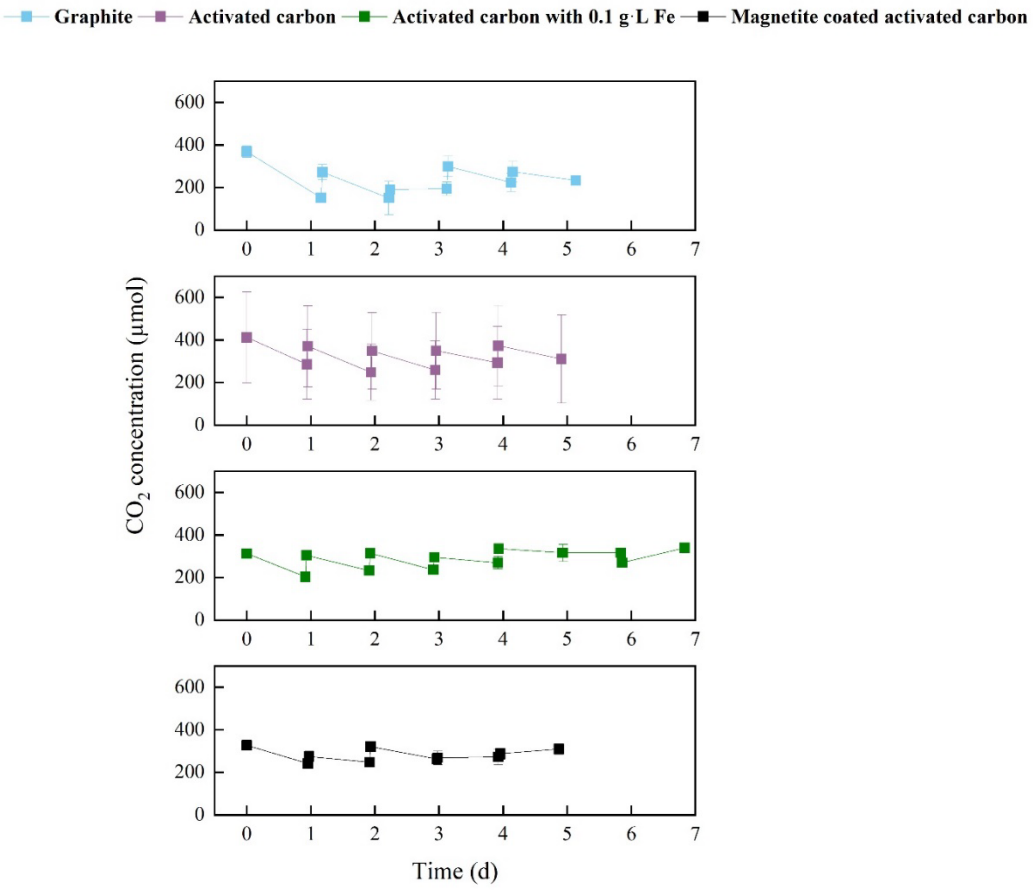


Figure S2: CO_2 concentration during batch experiments throughout time with the thermophilic archaeon *M. thermautotrophicus* ΔH. Graphite-rod and activated-carbon anodes were included with three treatments for activated carbon, including iron additions (soluble iron and magnetite). The error bars show the standard deviation for the average data from triplicate systems.

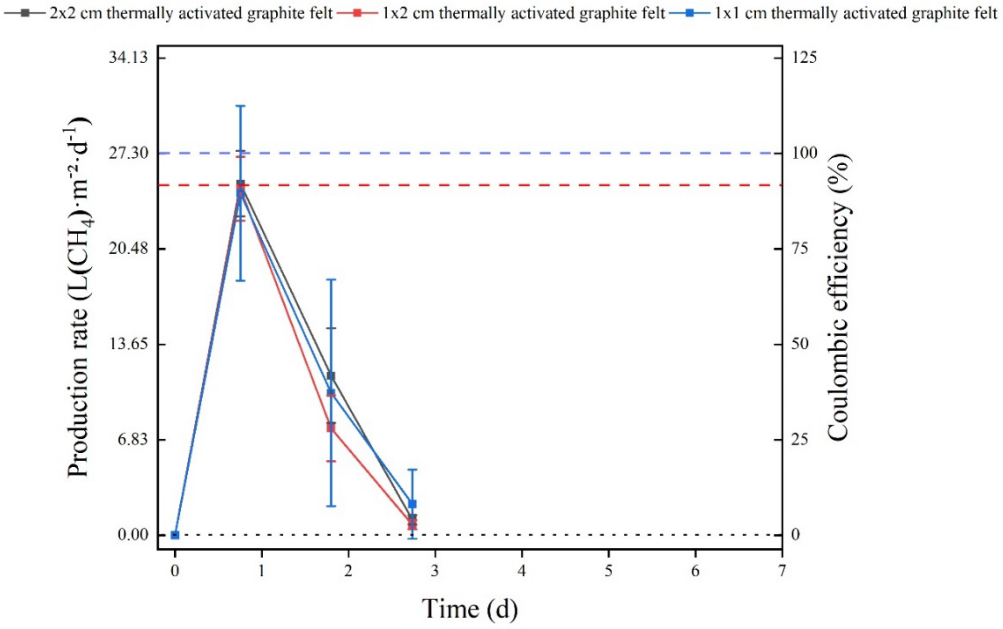


Figure S3: CH_4 production rates corrected to the cathode surface area and Coulombic efficiencies (at I = 1 A·cm^{-2}) during batch experiments in our BES throughout time with L-cysteine and with the thermophilic archaeon *M. thermautotrophicus* ΔH. Thermally activated graphite felt anodes were included with three different conditions (1x1 cm , 1x2 cm graphite felt, and 2x2 cm). The error bars show the standard deviation for the average data from triplicate systems. Carbon cloth was used as the cathode: **(**Y-axis 1) cathode-based geometric CH_4 production rates; and **(**Y-axis 2**)** Coulombic efficiencies.

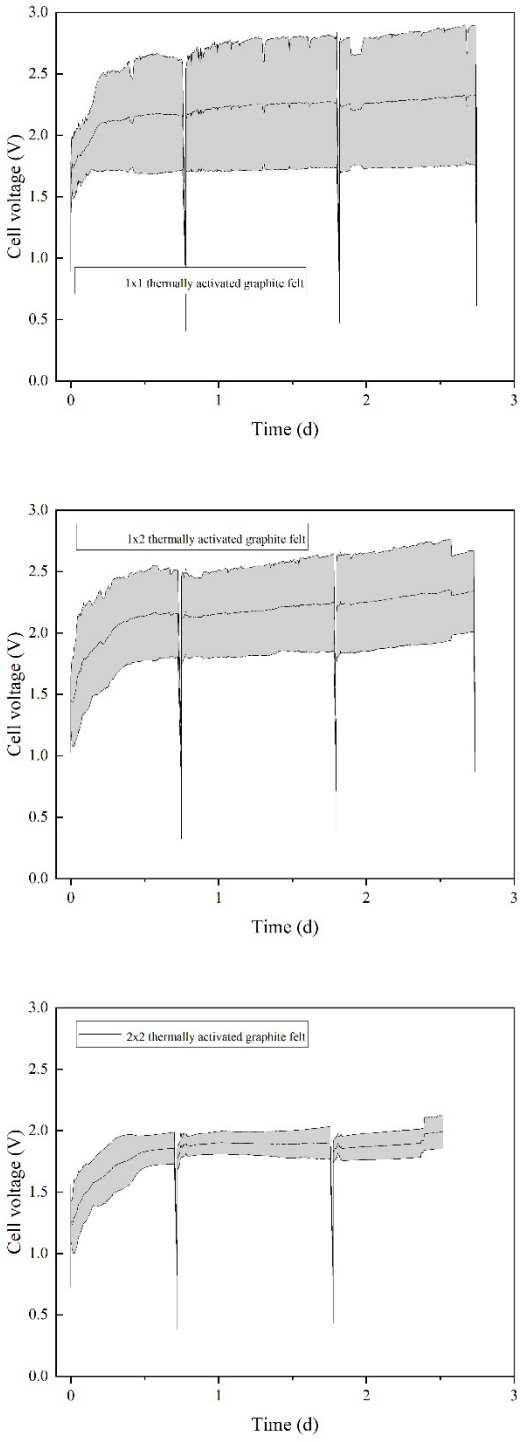


Figure S4: Cell voltages of the BES experiment performed in triplicates using three different sizes (1x1, 1x2, and 2x2 cm) of the thermally activated graphite felt as anode.

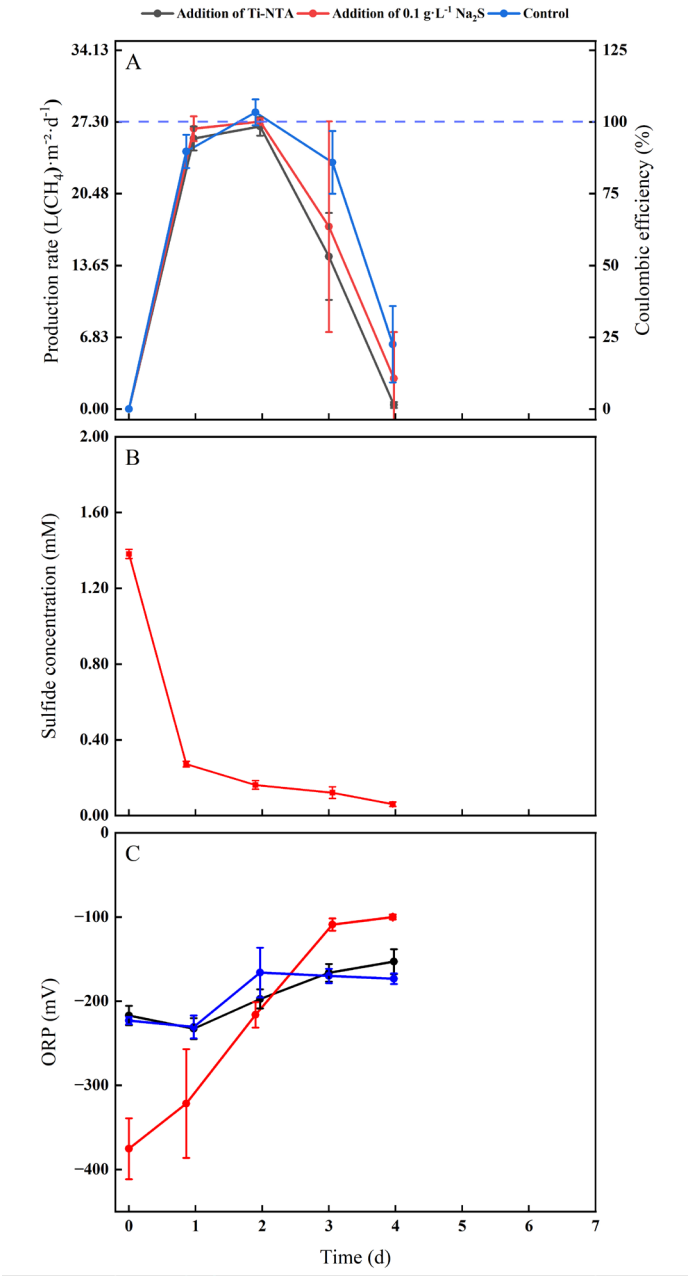


Figure S5: BES experiments with different reducing agents: (**A**) CH_4 production rates corrected to the cathode surface area and Coulombic efficiencies (at I = 1 A·cm^{-2}) during batch experiments throughout time with the thermophilic archaeon *M. thermautotrophicus* ΔH. Thermally activated graphite felt anodes were included with three different conditions (addition of Ti-NTA with L-cysteine, addition of 0.1 g·L^{-1} Na_2S without L-cysteine, and control with L-cysteine). Ti-NTA was supplied at a ratio of 1:1000 at the beginning and every sampling point. Each condition included iron additions of 0.1 g·L^{-1}. Carbon cloth was used as the cathode: **(**Y-axis 1) cathode-based geometric CH_4 production rates; and **(**Y-axis 2**)** Coulombic efficiencies; (**B**) Sulfide concentrations during the addition of 0.1 g·L^{-1} Na_2S batch experiment throughout time with the thermophilic archaeon *M. thermautotrophicus* ΔH; and (**C**) ORP measurement for all three conditions throughout time with the thermophilic archaeon *M. thermautotrophicus* ΔH. The error bars show the standard deviation for the average data from triplicate systems

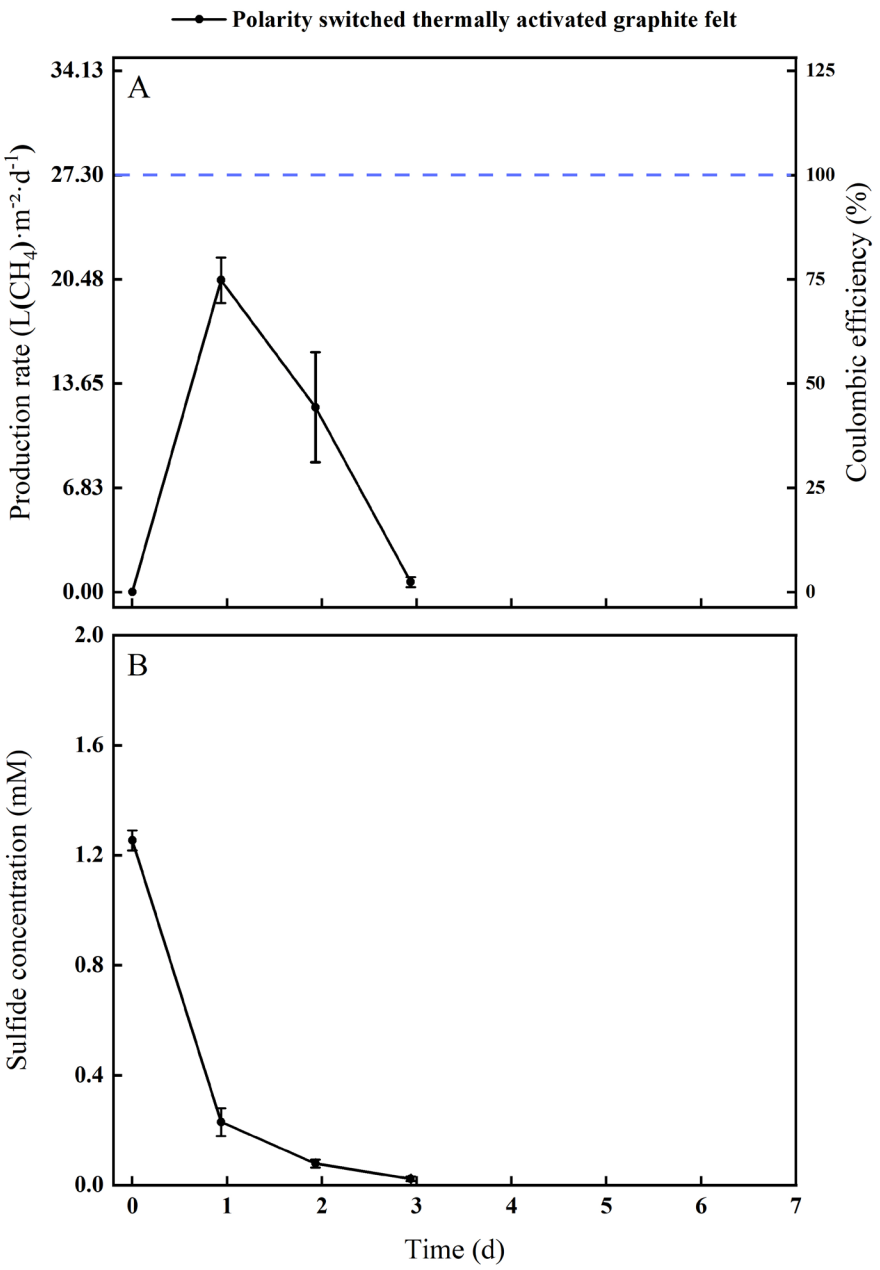


Figure S6: BES experiment with polarity switch: (**A**) CH_4 production rate corrected to the cathode surface area and Coulombic efficiency (at I = 1 A·cm^{-2}) during batch experiments throughout time with the thermophilic archaeon *M. thermautotrophicus* ΔH when the polarity of the thermally activated graphite felt anodes was switched every 4h. 0.1 g·L^{-1} Na_2S was supplied to the medium instead of L-cysteine; and (**B**) Sulfide concentrations during batch experiments throughout time. The error bars show the standard deviation for the average data from triplicate systems.

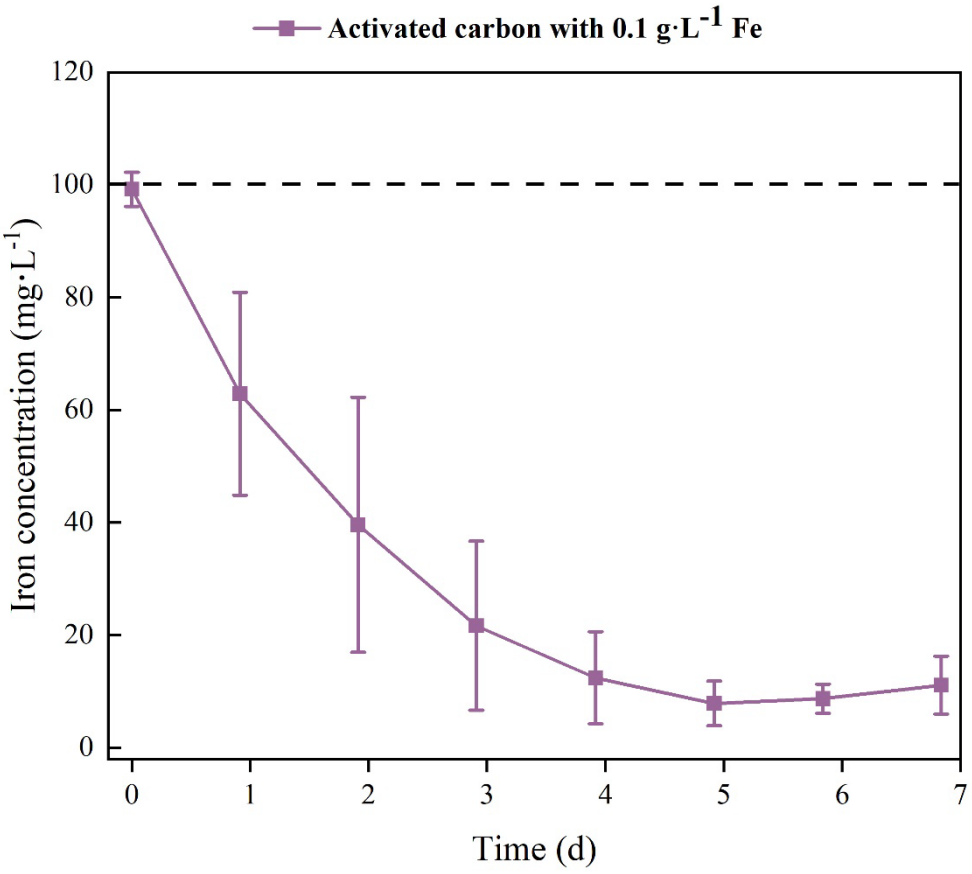


Figure S7: iron concentration during batch experiments of activated carbon-based anode with added iron throughout time with the thermophilic archaeon *M. thermautotrophicus* ΔH.



Figure S8: example of carbon exfoliation after the BES experiment. The exfoliated carbon turned the medium black.

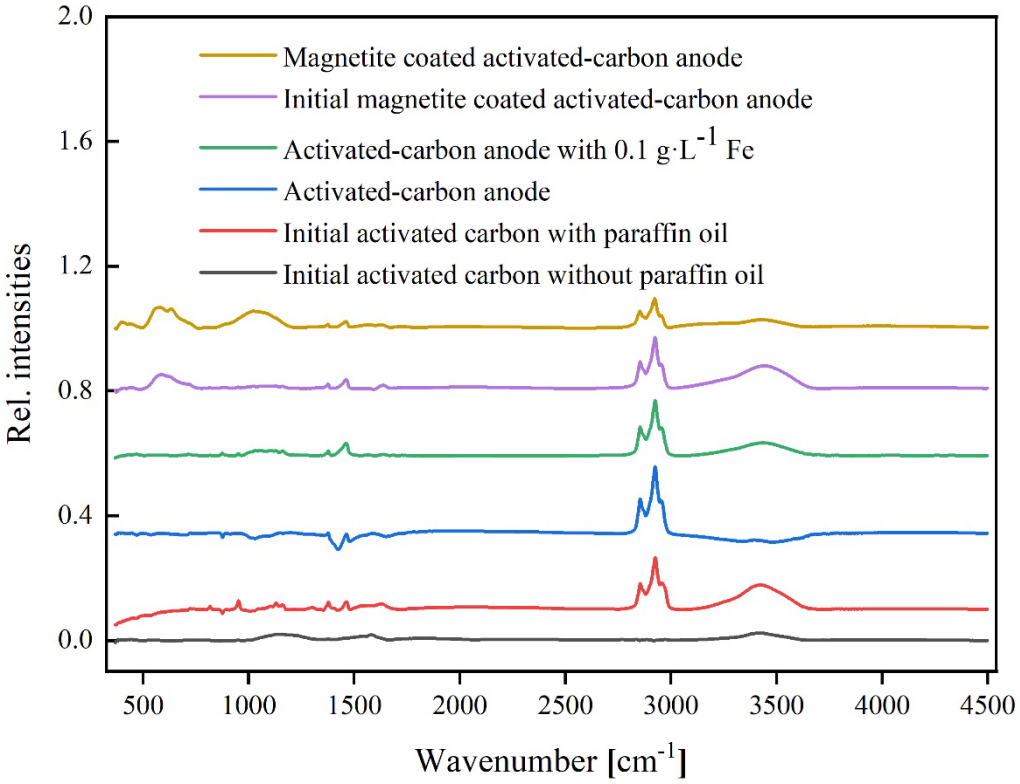


Figure S9: FTIR measurements of initial activated carbon with and without paraffin oil, activated-carbon anode, activated-carbon anode with 0.1 g·L^{-1} Fe, initial magnetite-coated activated-carbon anode, and magnetite-coated activated-carbon anode. Samples were taken from dried anodes after 5 days of oxidation.

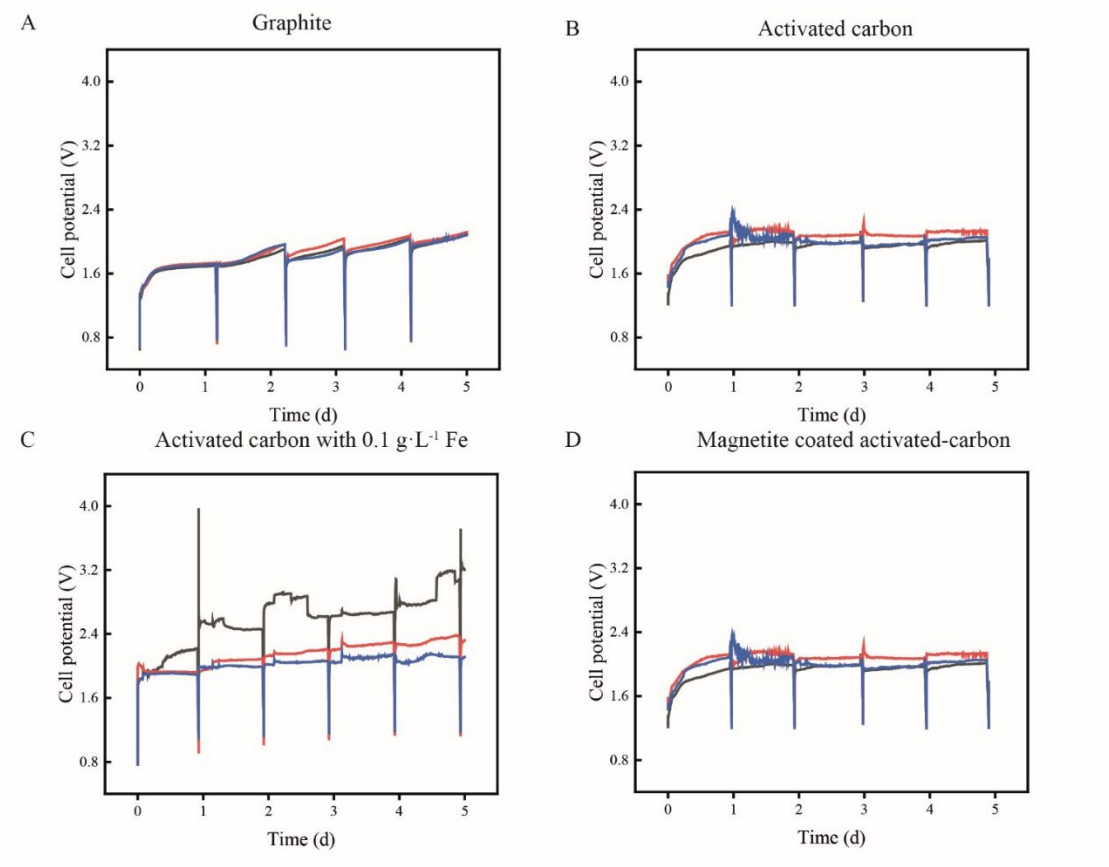


Figure S10: Cell potentials of the BES experiment performed in triplicates using different carbon based anodes: **(A)** graphite; **(B)** activated-carbon; **(C)** activated-carbon with 0.1 g·L^{-1} Fe; and **(D)** magnetite-coated activated-carbon.

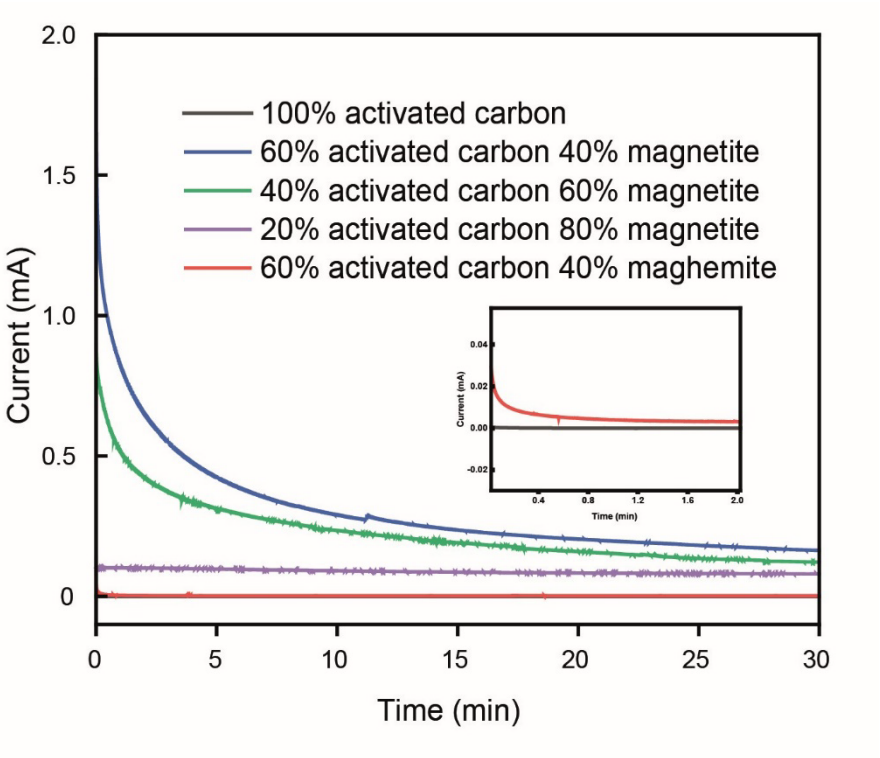


Figure S11: Chronoamperometic current traces of 100% activated carbon, 60% activated carbon & 40% magnetite, 40% activated carbon & 60% magnetite, 20% activated carbon & 80% magnetite, and 60% activated carbon & 40% maghemite at +0.6 V in 66 mM phosphate buffer.

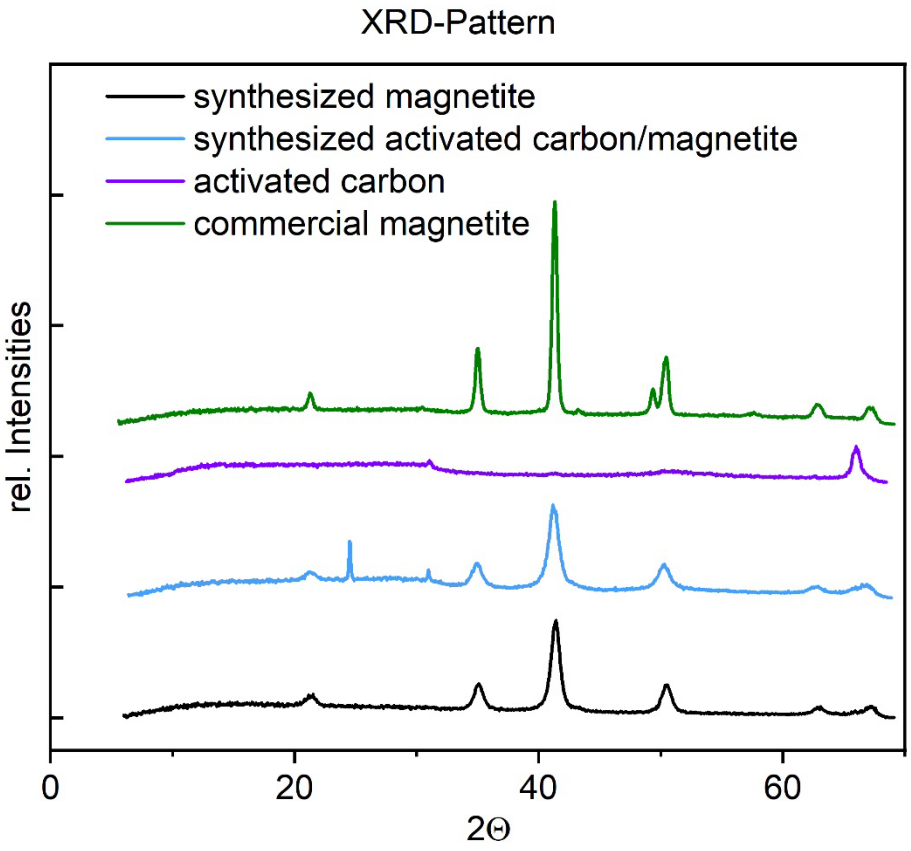


Figure S12: XRD pattern of synthesized magnetite, synthesized magnetite coated on activated carbon, activated carbon, and commercial magnetite.

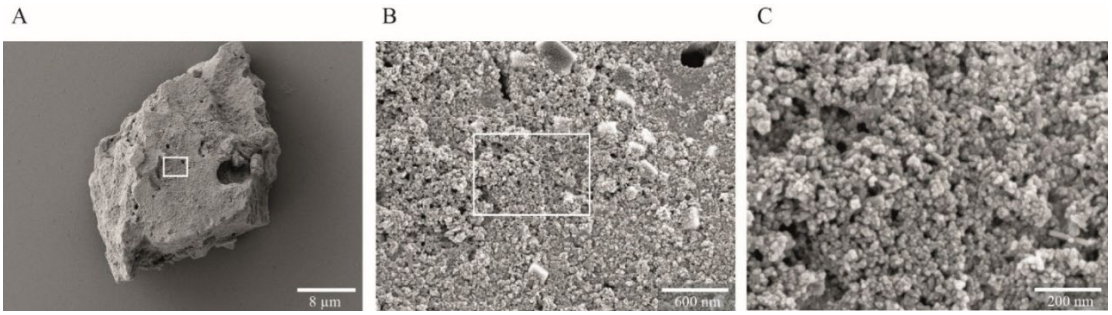


Figure S13: Scanning electron micrographs of magnetite-coated activated carbon: **(A)** Particle of magnetite-coated activated carbon with a 2300x magnification; **(B)** close-up from the rectangular-shaped area of (A) with a magnification of 35000x; and **(C)** close-up from the rectangular-shaped area of (B) with a magnification of 95000x.

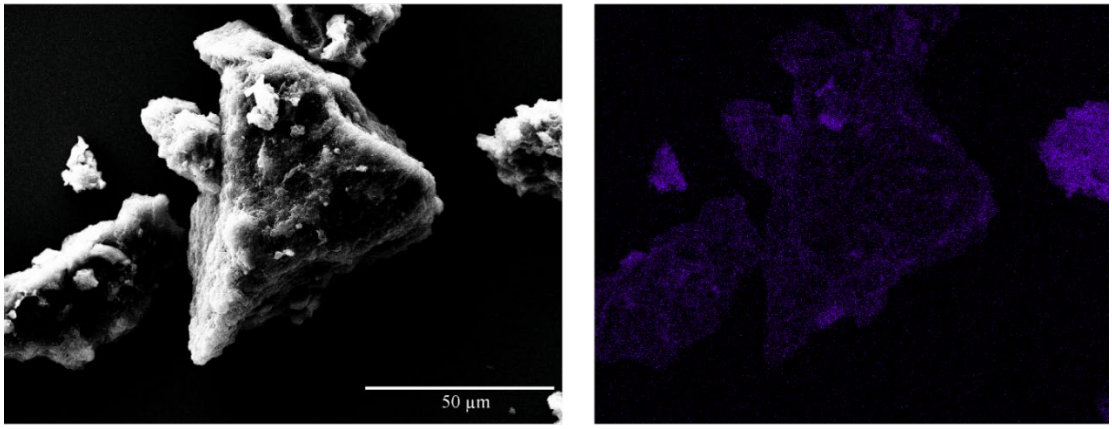


Figure S14: Scanning electron micrograph and its EDX Fe Kα elemental mapping (in violet).

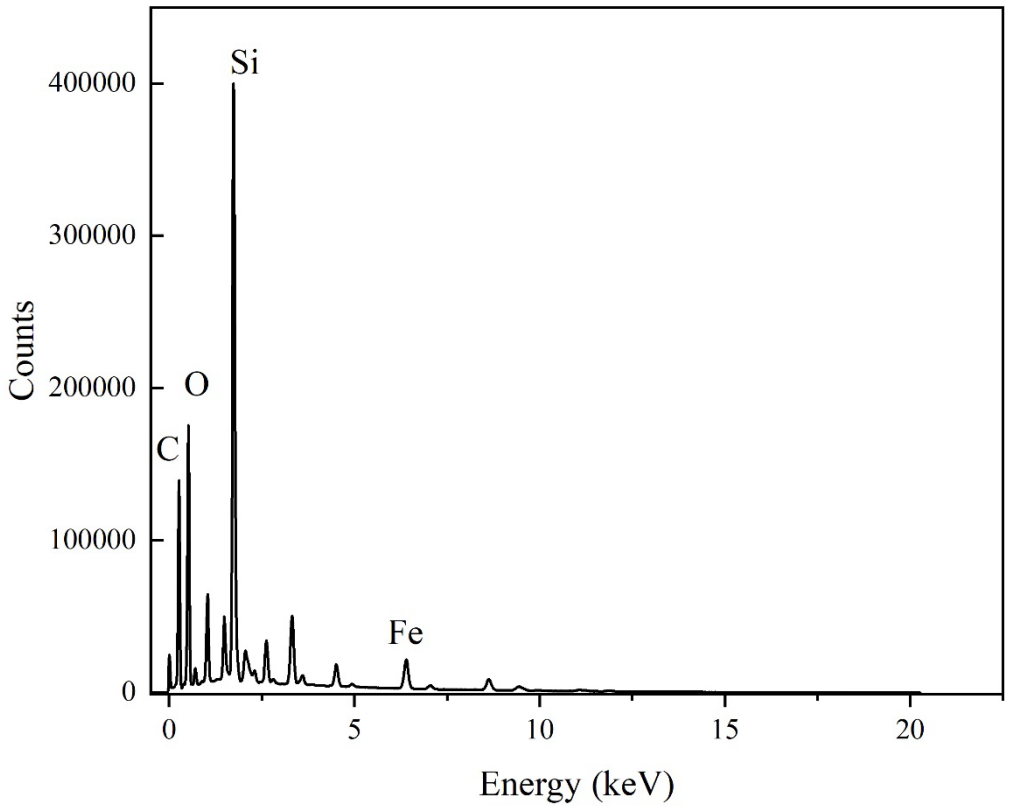


Figure S15: EDX Fe Kα elemental mapping spectrum from **Fig. S14**.

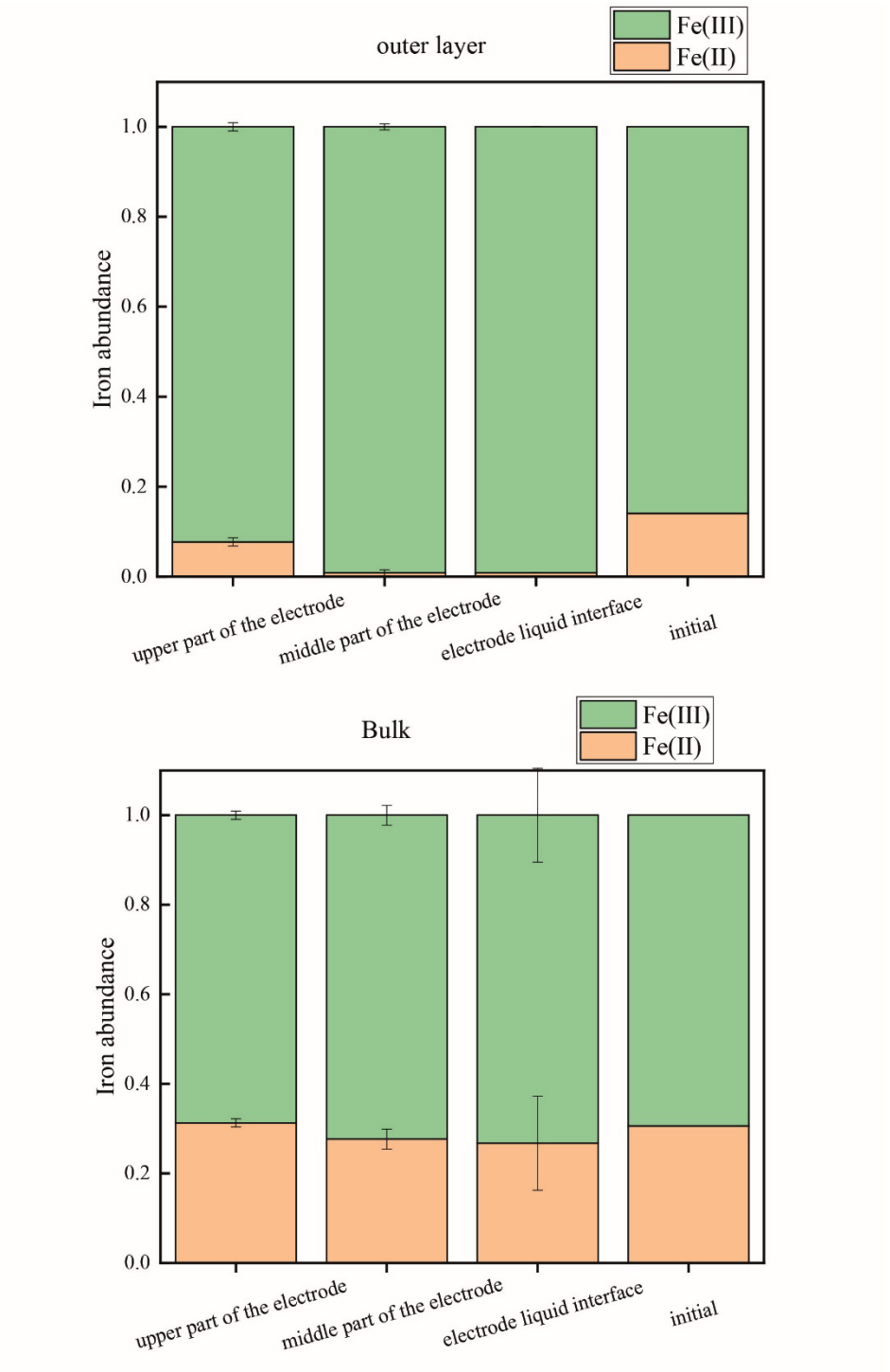


Figure S16: Oxidation state of magnetite. Measured Fe(II) and Fe(III) abundance from the outer layer and bulk from the upper part, middle part, and the electrode liquid interface.

Supplementary for Chapter 4

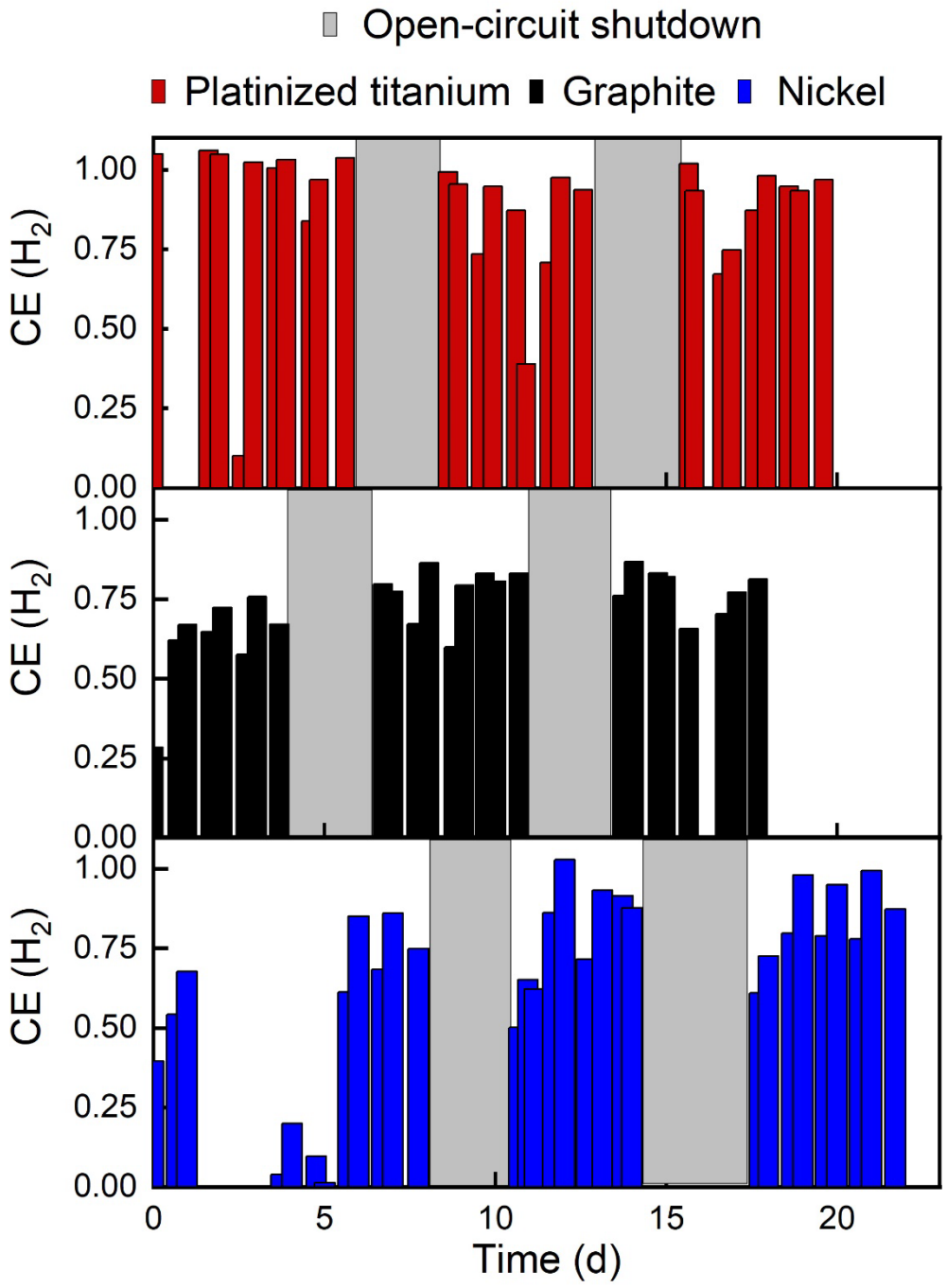


Figure S17: CE of H_2 during the microbial electrolysis cell experiments using graphite, nickel, and platinized titanium as cathode material. The light grey areas correspond to the open-circuit shutdown periods.

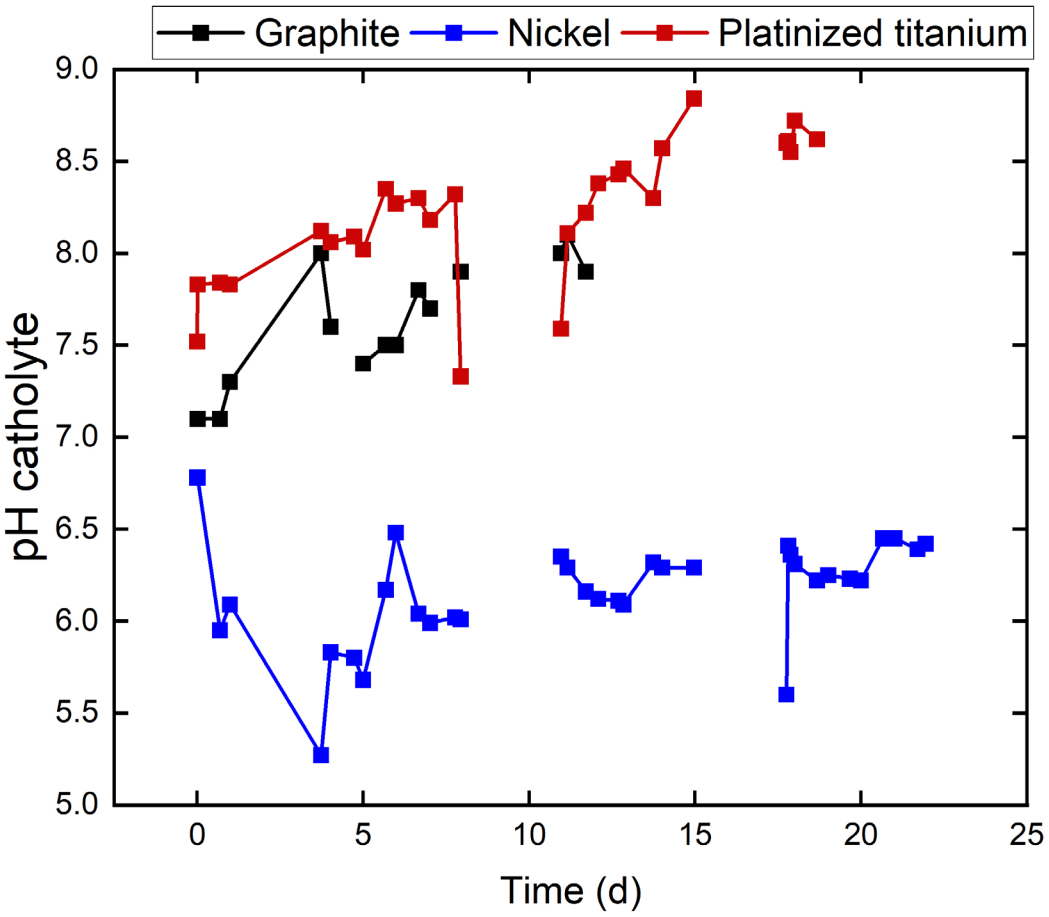


Figure S18: catholyte pH of microbial electrolysis cell experiments using graphite, nickel, and platinized titanium as cathode material. Interruptions in the line segments correspond to the open-circuit shutdown periods.

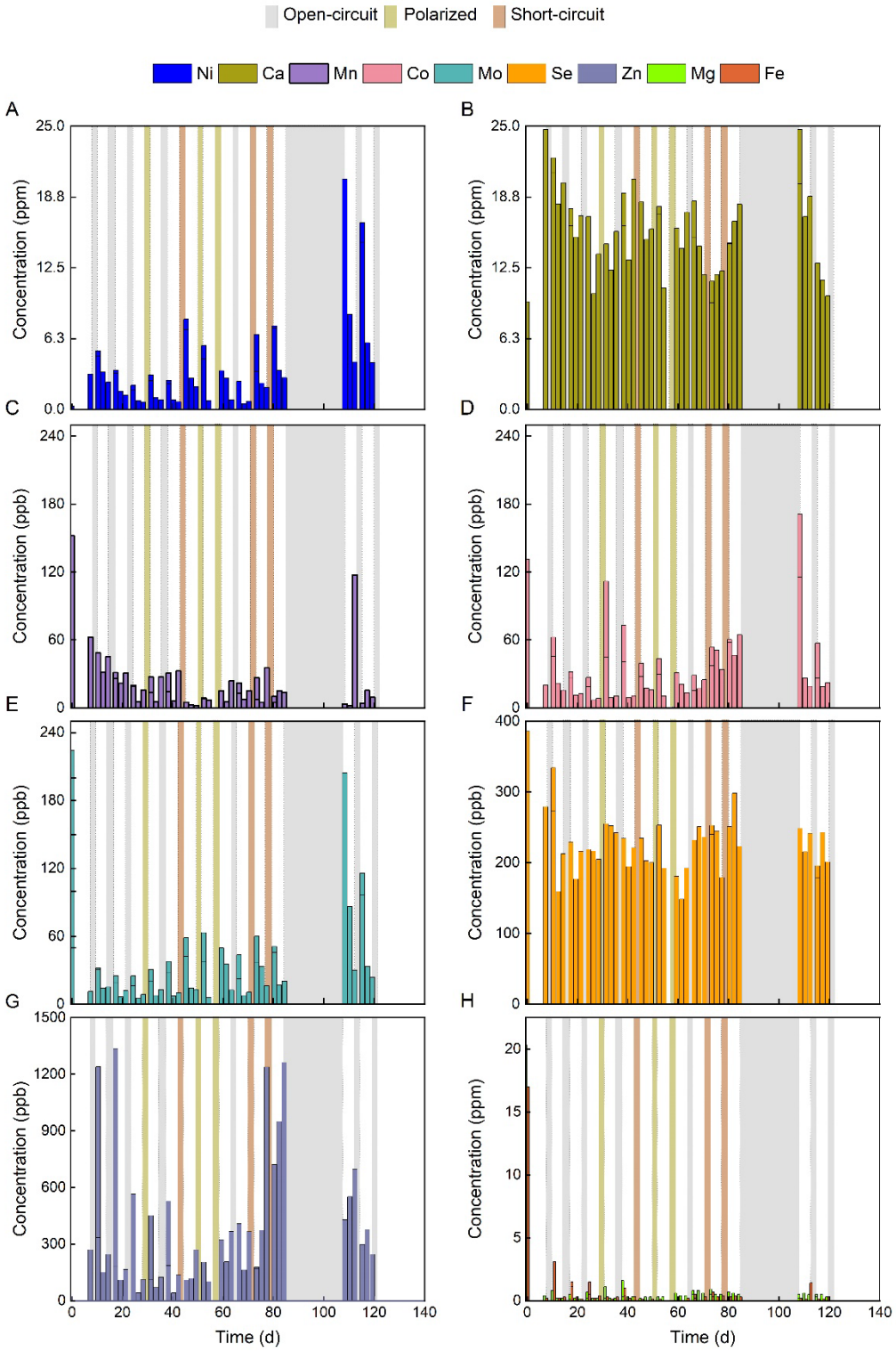


Figure S19: Element concentrations of Ni, Ca, Mn, Co, Mo, Se, Zn, Mg, and Fe in the catholyte measured with ICP-MS during the nickel electrode microbial electrolysis cell experiment. Samples were taken at the start, 2 hours, 3 days, and 5 days each week after and before a shutdown procedure. The different shutdown methods are coded in grey as open-circuit shutdown, light yellow as polarized shutdown, and light red as short-circuit shutdown.

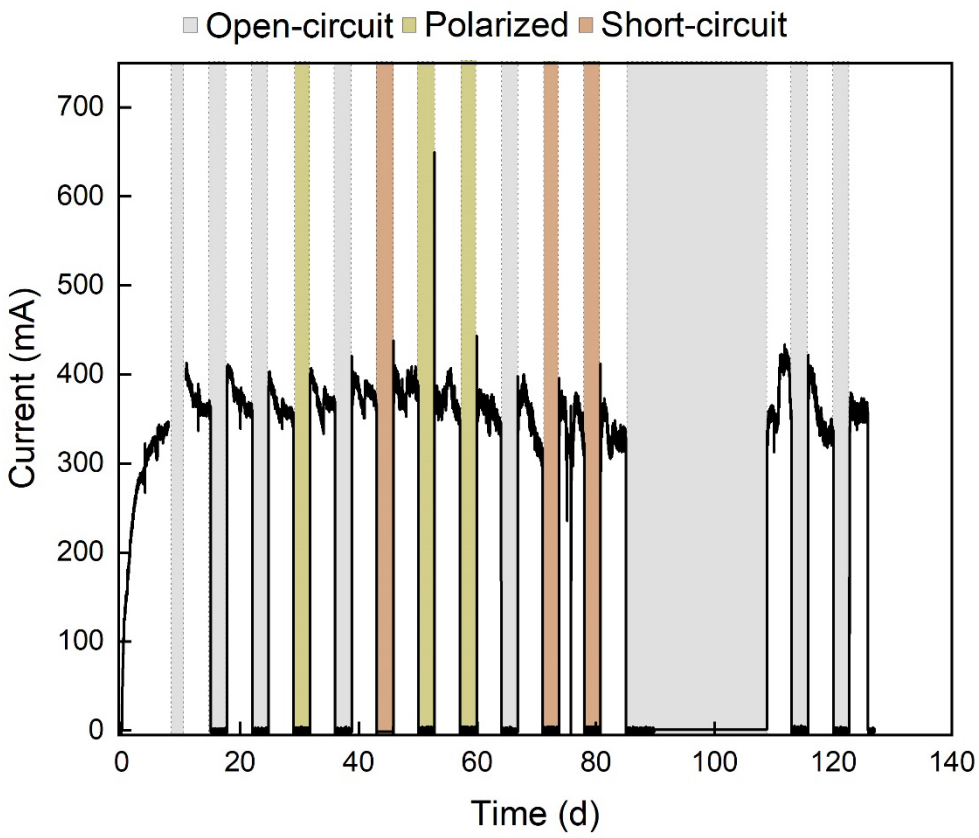


Figure S20: absolute current of the microbial electrolysis cell experiment using nickel as cathode with different shutdown methods coded in grey as open-circuit shutdown, light yellow as polarized shutdown, and light red as short-circuit shutdown.

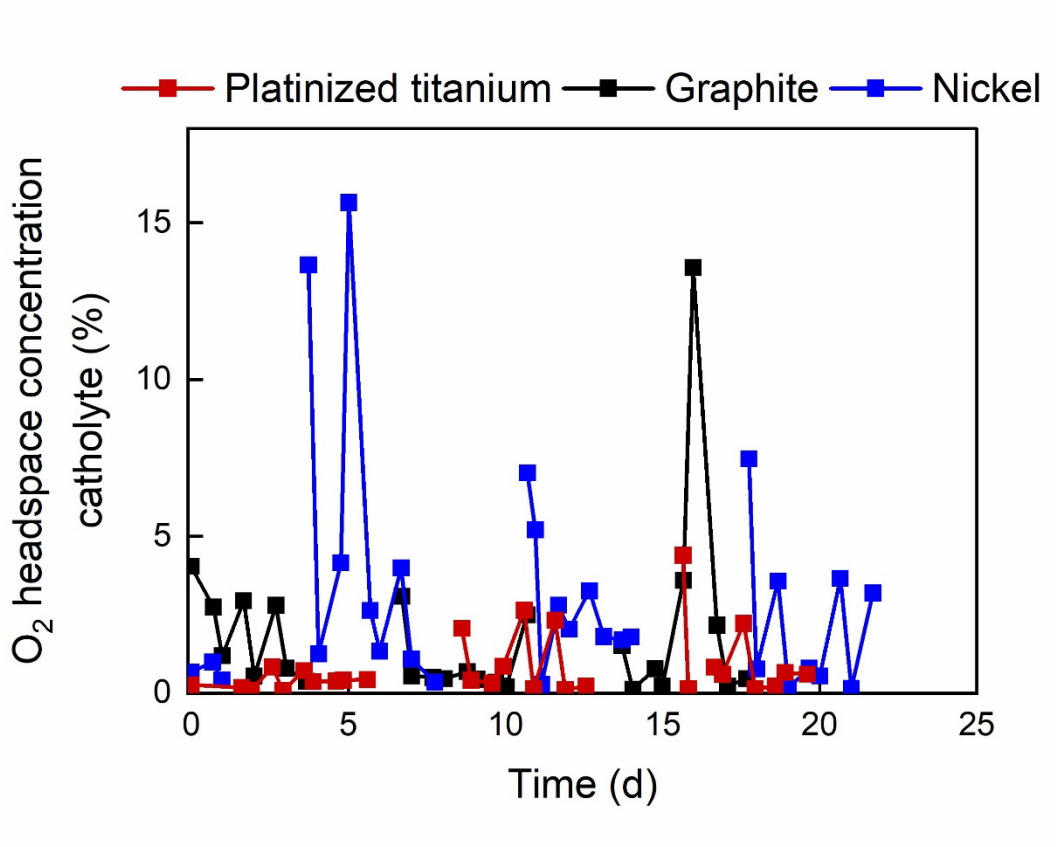


Figure S21: The percentage of cathode chamber headspace O2 concentration during the microbial electrolysis cell experiment using platinized titanium, graphite, and nickel cathodes.

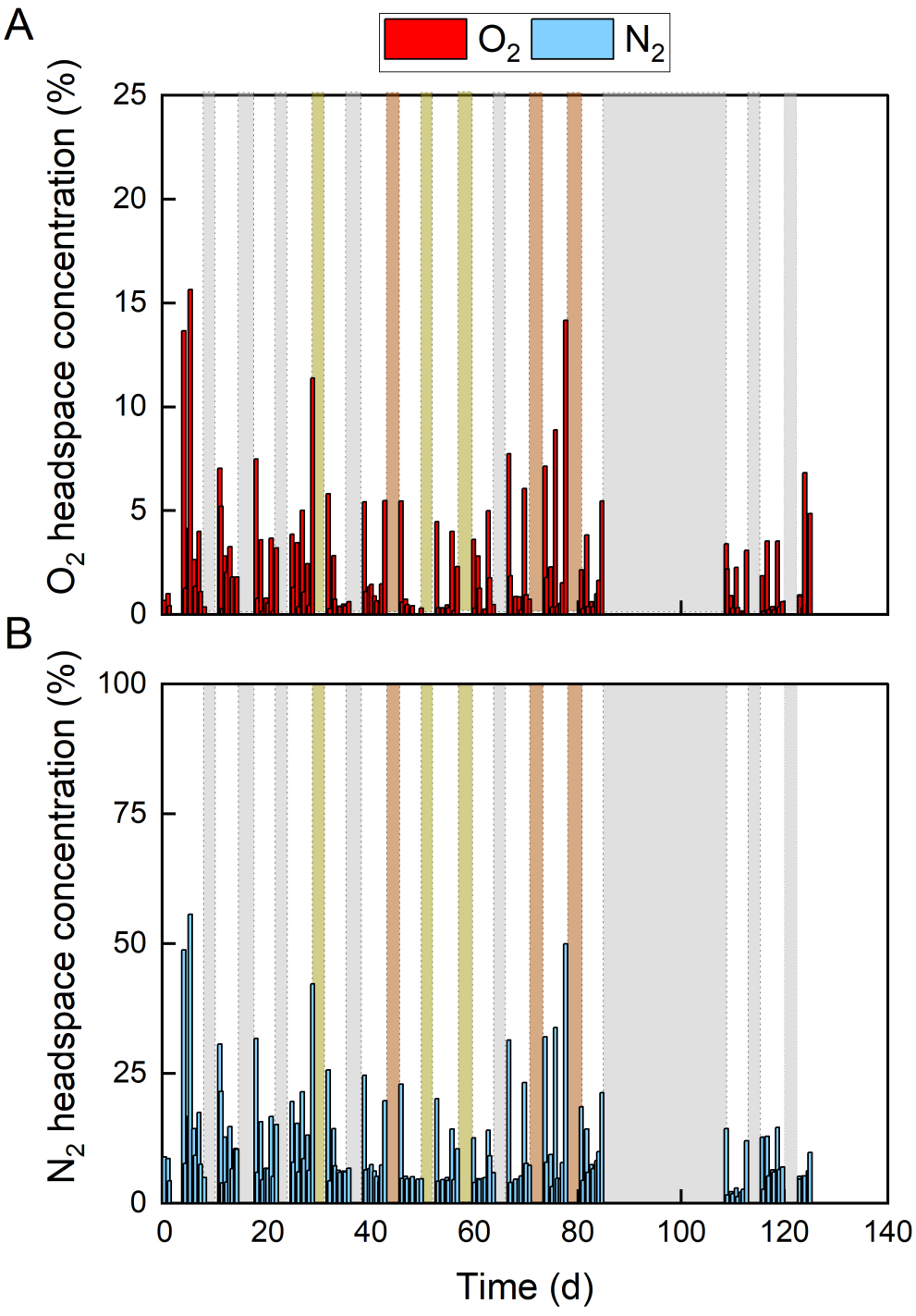


Figure S22: cathode chamber headspace concentration in percentage of (A) O_2 and (B) N_2 during the microbial electrolysis cell experiment using nickel as the cathode. The different shutdown methods are coded in grey as open-circuit shutdown, light yellow as polarized shutdown, and light red as short-circuit shutdown.

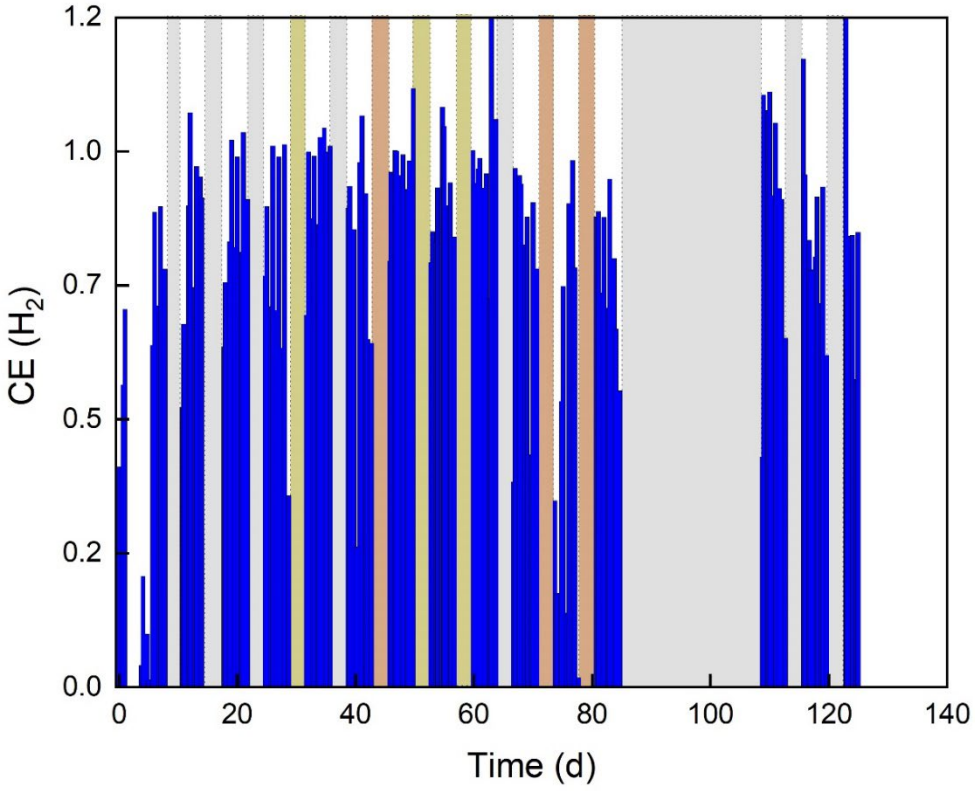


Figure S23: Coulombic efficiency (CE) of H_2 during the microbial electrolysis cell experiment using nickel as the cathode. The different shutdown methods are coded in grey as open-circuit shutdown, light yellow as polarized shutdown, and light red as short-circuit shutdown.

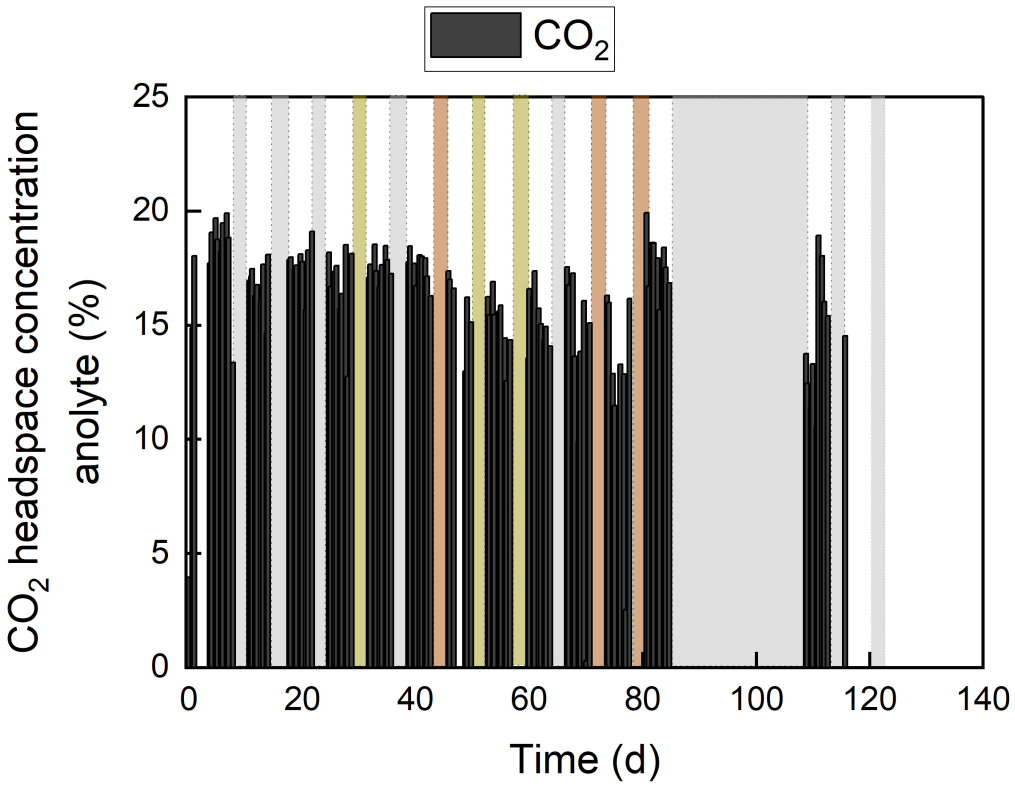


Figure S24: anode chamber headspace concentration in % of CO_2 during the microbial electrolysis cell experiment using nickel as the cathode. The different shutdown methods are coded in grey as open-circuit shutdown, light yellow as polarized shutdown, and light red as short-circuit shutdown.

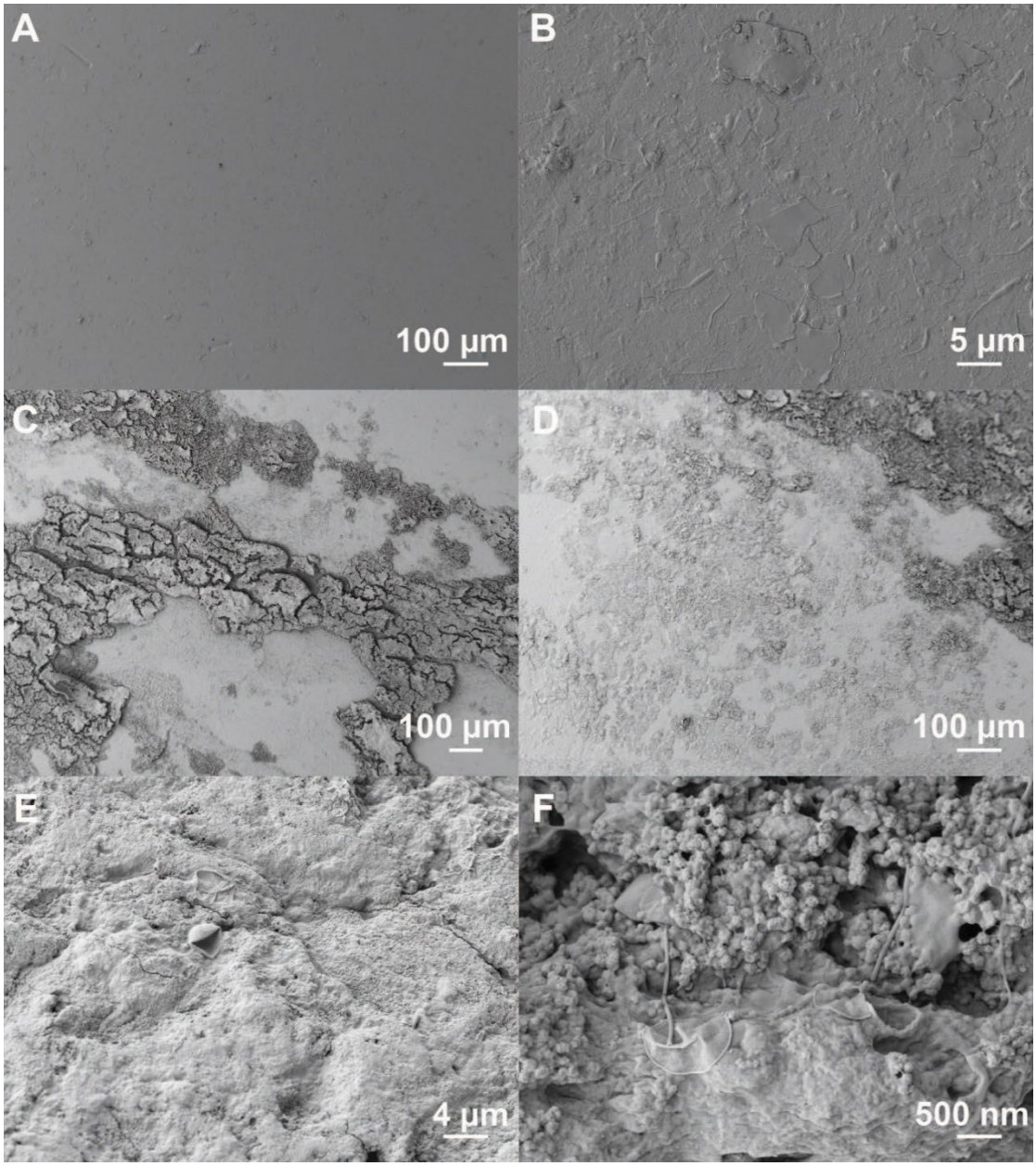


Figure S25: SEM micrographs of the (A) clean Nafion 117 ion-exchange membrane at 100x magnification, (B) close-up of the clean Nafion 117 ion-exchange membrane at 2020x magnification. (C) and (D) the Nafion 117 ion-exchange membrane post-experiment with precipitate at 100x magnification. (E) and (F) close-up of the Nafion 117 ion-exchange membrane post-experiment at 2260x and 20030x magnification, respectively.

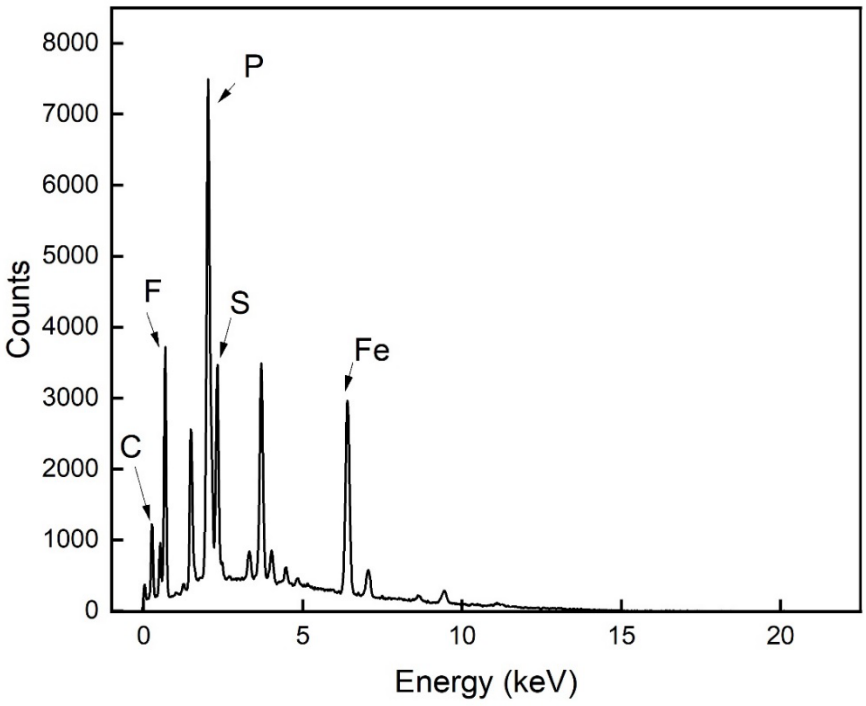


Figure S26: EDX Kα elemental mapping spectrum of the Nafion 117 ion-exchange membrane post-experiment.

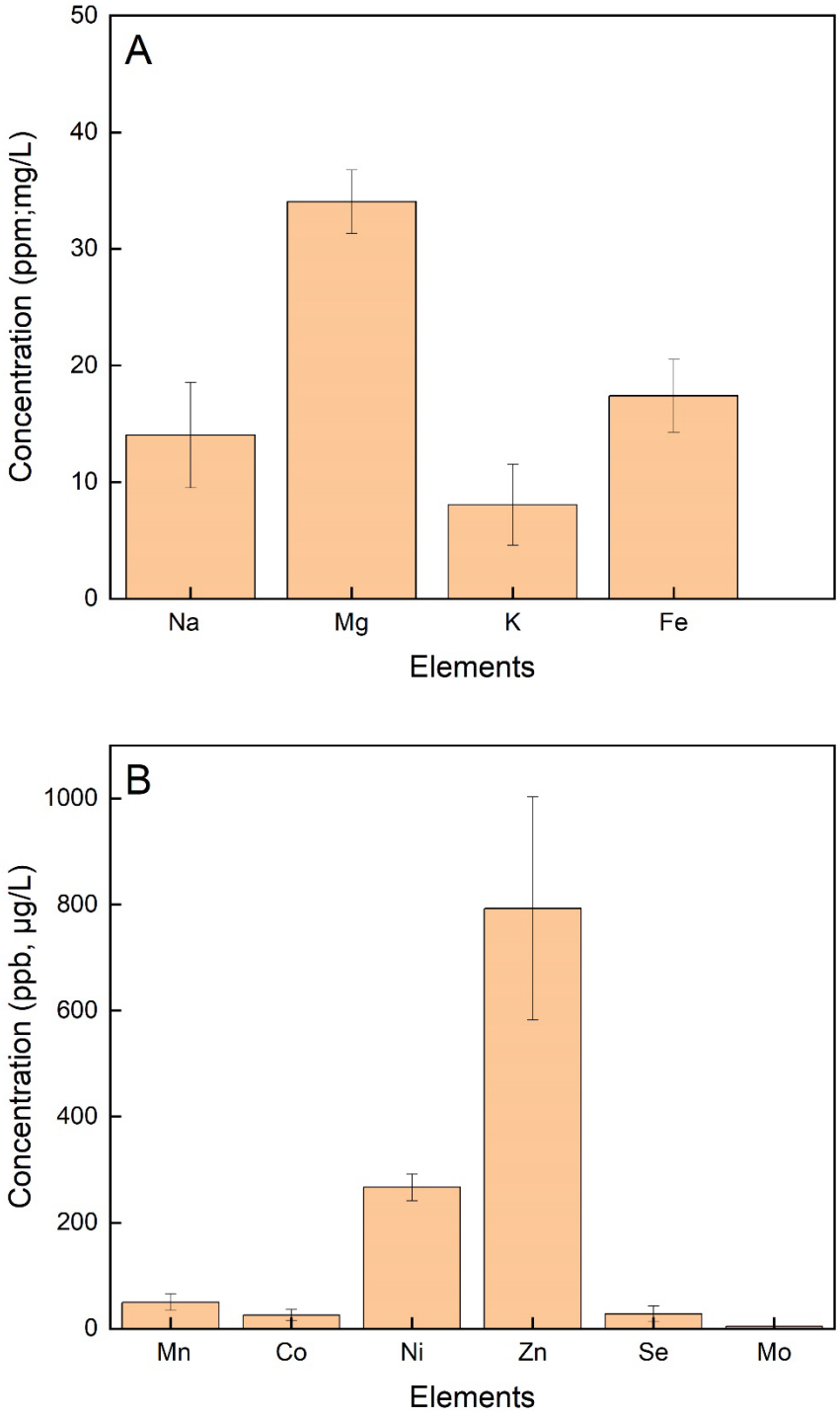


Figure S27: Element concentrations of Na, Mg, K, Fe, Mn, Co, Ni, Zn, Se, and Mo from a 1 cm² piece of Nafion 117 ion-exchange membrane calcinated. The sample was measured with ICP-MS.

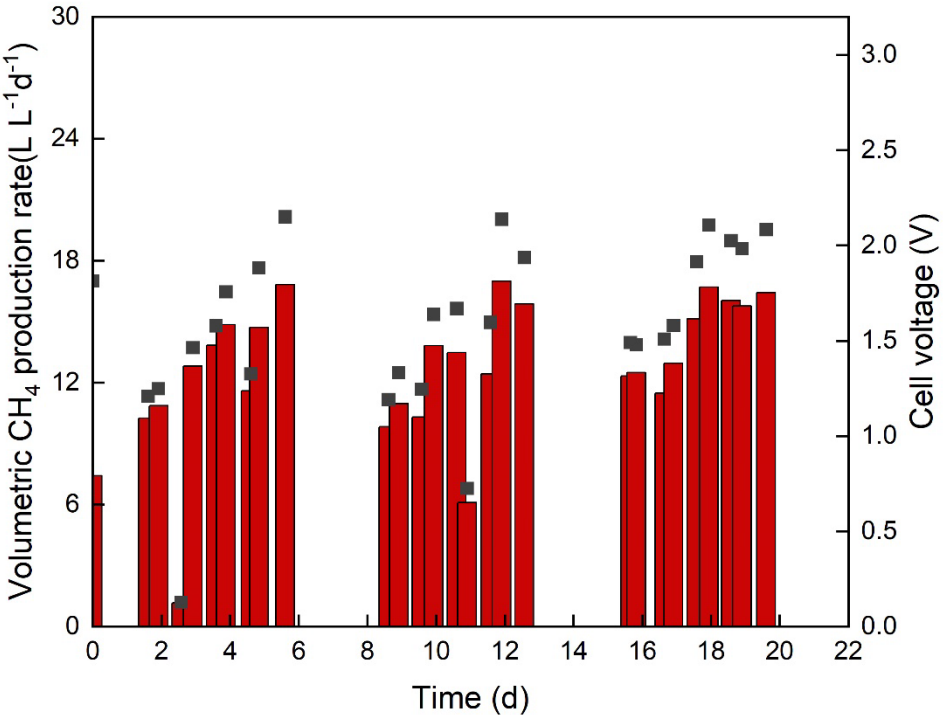


Figure S28: Volumetric production rate during the platinized titanium experiment and its hypothetical cell voltage if a minimum of 50% EE would be reached.

Supplementary for Chapter 5

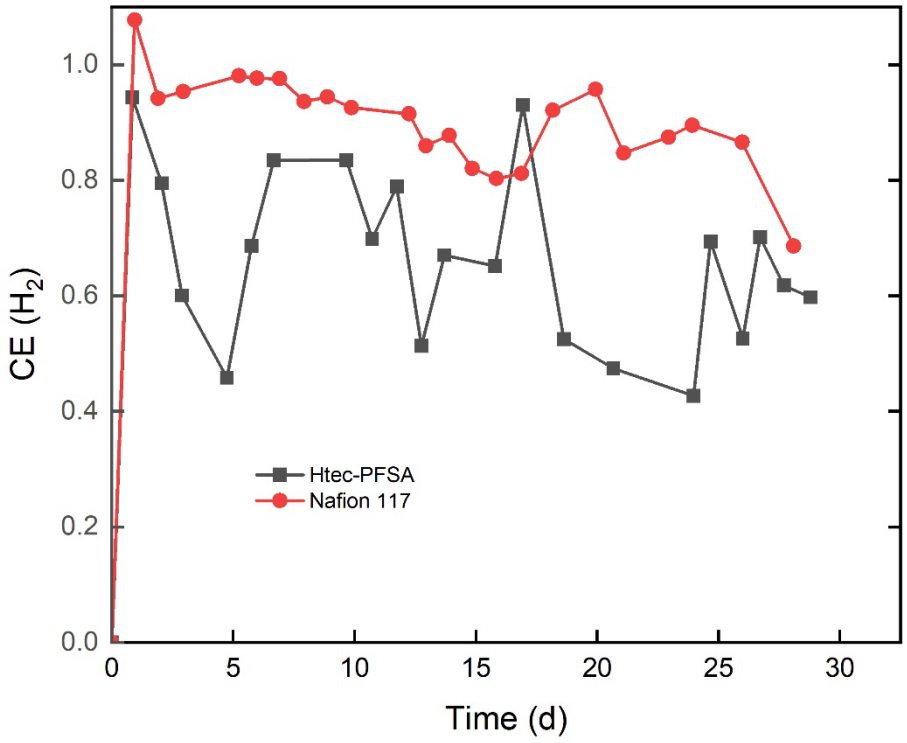


Figure S29: CE of H_2 during the liquid-fed zero-gap bioelectrochemical cell experiment using Htec-PFSA (dark grey) and Nafion 117 (red) as ion-exchange membrane.

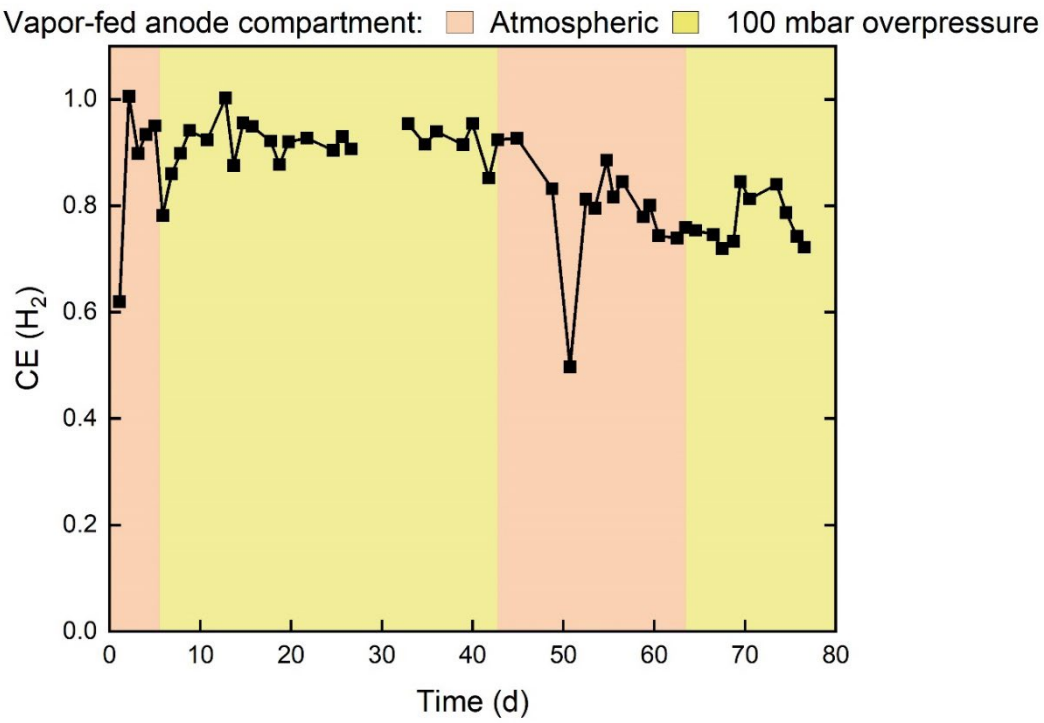


Figure S30: CE of H_2 during the liquid-fed zero-gap bioelectrochemical cell experiment using Nafion 117 as the ion-exchange membrane. The anode compartment of the bioelectrochemical cell was kept at atmospheric pressure (orange) or 100 mbar overpressure (yellow).

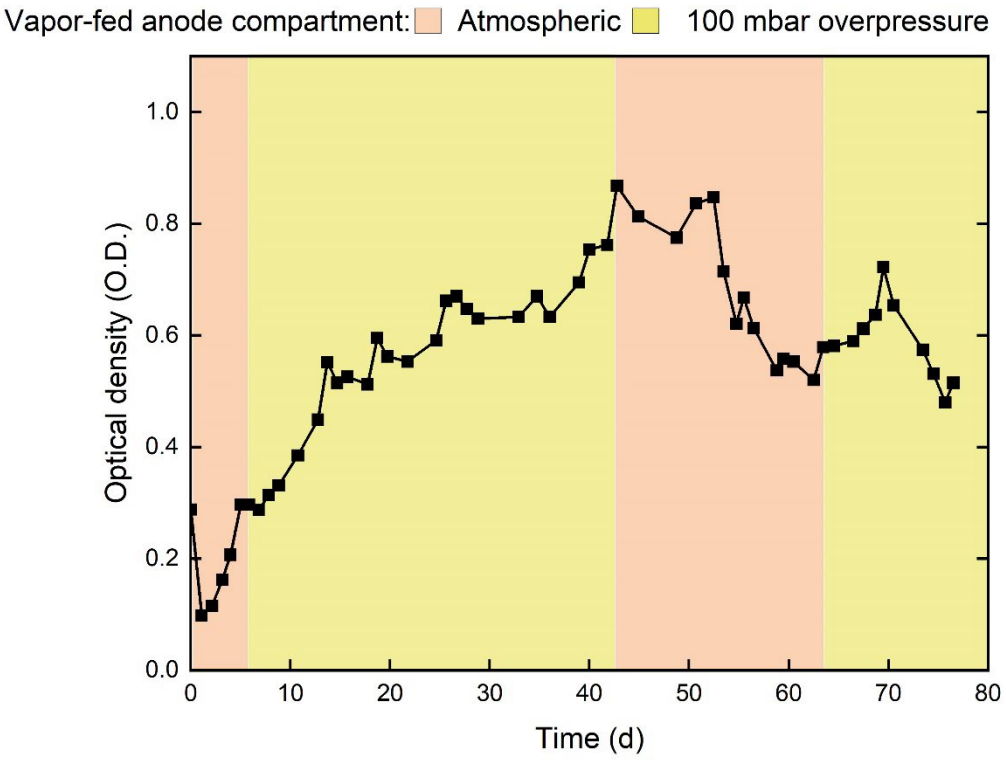


Figure S31: optical density (O.D.) during the liquid-fed zero-gap bioelectrochemical cell experiment using Nafion 117 as the ion-exchange membrane. The anode compartment of the bioelectrochemical cell was kept at atmospheric pressure (orange) or 100 mbar overpressure (yellow).

References

Abdollahi, Maliheh, Sara Al Sbei, Miriam A. Rosenbaum, and Falk Harnisch. 2022. 'The oxygen dilemma: The challenge of the anode reaction for microbial electrosynthesis from CO_2', *Frontiers in microbiology*, 13.

Al-Zahrani, Eman, M. Tahir Soomro, R. M. Bashami, Ateeq Ur Rehman, Ekram Danish, Iqbal M. I. Ismail, M. Aslam, and A. Hameed. 2016. 'Fabrication and performance of magnetite (Fe_3O_4) modified carbon paste electrode for the electrochemical detection of chlorite ions in aqueous medium', *Journal of Environmental Chemical Engineering*, 4: 4330–41.

Angenent, Largus T., and Miriam A. Rosenbaum. 2013. 'Microbial electrocatalysis to guide biofuel and biochemical bioprocessing', *Biofuels*, 4: 131–34.

Aulenta, Federico, Alessandro Catervi, Mauro Majone, Stefania Panero, Priscilla Reale, and Simona Rossetti. 2007. 'Electron transfer from a solid-state electrode assisted by methyl viologen sustains efficient microbial reductive dechlorination of TCE', *Environmental Science & Technology*, 41: 2554-59.

Baek, Gahyun, Ruggero Rossi, Pascal E. Saikaly, and Bruce E. Logan. 2022. 'High-rate microbial electrosynthesis using a zero-gap flow cell and vapor-fed anode design', *Water Research*, 219: 118597.

Bajracharya, Suman, Annemiek ter Heijne, Xochitl Dominguez Benetton, Karolien Vanbroekhoven, Cees J. N. Buisman, David P. B. T. B. Strik, and Deepak Pant. 2015. 'Carbon dioxide reduction by mixed and pure cultures in microbial electrosynthesis using an assembly of graphite felt and stainless steel as a cathode', *Bioresource Technology*, 195: 14-24.

Baker, Hugh S., Richard J. Millar, David J. Karoly, Urs Beyerle, Benoit P. Guillod, Dann Mitchell, Hideo Shiogama, Sarah Sparrow, Tim Woollings, and Myles R. Allen. 2018. 'Higher CO_2 concentrations increase extreme event risk in a 1.5 °C world', *Nature Climate Change*, 8: 604-08.

Bard, Allen J., and Larry R. Faulkner. 2000. *Electrochemical methods: Fundamentals and Applications, 2nd Edition* (Wiley: Hoboken, NJ, USA).

Boto, Santiago T., Bettina Bardl, Falk Harnisch, and Miriam A. Rosenbaum. 2023. 'Microbial electrosynthesis with *Clostridium ljungdahlii* benefits from hydrogen electron mediation and permits a greater variety of products', *Green Chemistry*, 25: 4375-86.

Bradley, Miranda J., and Paul G. Tratnyek. 2019. 'Electrochemical characterization of magnetite with agarose-stabilized powder disk electrodes and potentiometric methods', *ACS Earth and Space Chemistry*, 3: 688-99.

Byrne, James M., Nicole Klueglein, Carolyn Pearce, Kevin M. Rosso, Erwin Appel, and Andreas Kappler. 2015. 'Redox cycling of Fe(II) and Fe(III) in magnetite by Fe-metabolizing bacteria', *Science*, 347: 1473.

Byrne, James M., Gerrit van der Laan, Adriana I. Figueroa, Odeta Qafoku, Chongmin Wang, Carolyn I. Pearce, Michael Jackson, Joshua Feinberg, Kevin M. Rosso, and Andreas Kappler. 2016. 'Size dependent microbial oxidation and reduction of magnetite nano- and micro-particles', *Scientific Reports*, 6: 30969.

Cabrera, L., S. Gutierrez, N. Menendez, M. P. Morales, and P. Herrasti. 2008. 'Magnetite nanoparticles: Electrochemical synthesis and characterization', *Electrochimica Acta*, 53: 3436-41.

Cai, Wenfang, Kai Cui, Zhuangzhuang Liu, Xiaodan Jin, Qingyun Chen, Kun Guo, and Yunhai Wang. 2022. 'An electrolytic-hydrogen-fed moving bed biofilm reactor for efficient microbial electrosynthesis of methane from CO_2', *Chemical Engineering Journal*, 428: 132093.

Call, Douglas, and Bruce E. Logan. 2008. 'Hydrogen production in a single chamber microbial electrolysis cell lacking a membrane', *Environmental Science & Technology*, 42: 3401-06.

Carmo, Marcelo, David L. Fritz, Jürgen Mergel, and Detlef Stolten. 2013. 'A comprehensive review on PEM water electrolysis', *International Journal of Hydrogen Energy*, 38: 4901-34.

Cavalcante, Willame A., Tito A. Gehring, and Marcelo Zaiat. 2021. 'Stimulation and inhibition of direct interspecies electron transfer mechanisms within methanogenic reactors by adding magnetite and granular actived carbon', *Chemical Engineering Journal*, 415: 128882.

Ceballos-Escalera, Alba, Narcís Pous, M. Dolors Balaguer, and Sebastià Puig. 2024. 'Nitrate electro-bioremediation and water disinfection for rural areas', *Chemosphere*: 141370.

Ceballos-Escalera, Alba, Narcís Pous, Benjamin Korth, Falk Harnisch, M. Dolors Balaguer, and Sebastià Puig. 2024. 'Ex-situ electrochemical characterisation of fixed-bed denitrification biocathodes: A promising strategy to improve bioelectrochemical denitrification', *Chemosphere*, 347: 140699.

Chen, Chang-Hui, Adam Halford, Marc Walker, Colin Brennan, Stanley C. S. Lai, David J. Fermin, Patrick R. Unwin, and Paramaconi Rodriguez. 2018. 'Electrochemical characterization and regeneration of sulfur poisoned Pt catalysts in aqueous media', *Journal of Electroanalytical Chemistry*, 816: 138-48.

Chen, D., and R. Xu. 1998. 'Hydrothermal synthesis and characterization of nanocrystalline Fe_3O_4 powders', *Materials Research Bulletin*, 33: 1015-21.

Chen, Mingkun, Yi Zhang, Shezhan Liu, Changzhong Zhao, Shuang Dong, and Yongchen Song. 2023. 'CO_{-2} transport and carbonate precipitation in the coupled diffusion-reaction process during CO_2 storage', *Fuel*, 334: 126805.

Chen, Shuiliang, Sunil A. Patil, and Uwe Schröder. 2018. 'A high-performance rotating graphite fiber brush air-cathode for microbial fuel cells', *Applied Energy*, 211: 1089-94.

Cheng, Jun, Haiquan Dong, Haihua Zhang, Luyun Yuan, Hui Li, Liangchen Yue, Junjie Hua, and Junhu Zhou. 2020. 'Improving CH_4 production and energy conversion from CO_2 and H_2 feedstock gases with mixed methanogenic community over Fe nanoparticles', *Bioresource Technology*, 314: 123799.

Cheng, Shaoan, Defeng Xing, Douglas F. Call, and Bruce E. Logan. 2009. 'Direct biological conversion of electrical current into methane by electromethanogenesis', *Environ. Sci. Technol.*, 43: 3953-58.

Christgen, Beate, Martin Spurr, Edward M. Milner, Paniz Izadi, Clare McCann, Eileen Yu, Tom Curtis, Keith Scott, and Ian M. Head. 2023. 'Does pre-enrichment of anodes with acetate to select for *Geobacter spp*. enhance performance of

microbial fuel cells when switched to more complex substrates?', *Frontiers in microbiology*, 14.

Clauwaert, Peter, and Willy Verstraete. 2009. 'Methanogenesis in membraneless microbial electrolysis cells', *Applied Microbiology and Biotechnology*, 82: 829–36.

CLINE, JOEL D. 1969. 'Spectrophotometric determination of hydrogen sulfide in natrual waters 1', *Limnology and Oceanography*, 14: 454-58.

Coey, J. M. D., A. E. Berkowitz, Ll. Balcells, F. F. Putris, and F. T. Parker. 1998. 'Magnetoresistance of magnetite', *Applied Physics Letters*, 72: 734–36.

Contreras, G., J. Thomsen, M. Pfitzer, D. Hafenbradl, D. Kostner, D. Holtmann, R. A. Schmitz, M. Rother, and B. Molitor. 2022. 'New perspectives for biotechnological applications of methanogens', *Current Research in Biotechnology*, 4: 468-74.

Cornell, R. M., and U. Schwertmann. 2003. *The iron oxides: structure, properties, reactions, occurrence and uses* (Wiley: Weinheim, Germany).

Davis, Thomas A., J. David Genders, and Derek Pletcher. 1997. *A first course in ion permeable membranes* (Electrochemical Consultancy).

de Groot, Matheus T., Joost Kraakman, and Rodrigo Lira Garcia Barros. 2022. 'Optimal operating parameters for advanced alkaline water electrolysis', *International Journal of Hydrogen Energy*, 47: 34773-83.

de Smit, Sanne M., Thomas D. van Mameren, Yiduo Xie, David P. B. T. B. Strik, and Johannes H. Bitter. 2023. 'Trace metals from microbial growth media form in situ electro-catalysts', *Electrochimica Acta*, 462: 142722.

Deutzmann, Jörg S., Frauke Kracke, Wenyu Gu, and Alfred M. Spormann. 2022. 'Microbial electrosynthesis of acetate powered by intermittent electricity', *Environmental Science & Technology*.

Deutzmann, Jörg S., Merve Sahin, and Alfred M. Spormann. 2015. 'Extracellular enzymes facilitate electron uptake in biocorrosion and bioelectrosynthesis', *mBio*, 6.

Deutzmann, Jörg Stefan, Frauke Kracke, and Alfred Michael Spormann. 2023. 'Microbial electromethanogenesis powered by curtailed renewable electricity', *Cell Reports Physical Science*, 4.

Dinh, Hang T., Jan Kuever, Marc Mußmann, Achim W. Hassel, Martin Stratmann, and Friedrich Widdel. 2004. 'Iron corrosion by novel anaerobic microorganisms', *Nature*, 427: 829-32.

Długołęcki, Piotr, Piotr Ogonowski, Sybrand J. Metz, Michel Saakes, Kitty Nijmeijer, and Matthias Wessling. 2010. 'On the resistances of membrane, diffusion boundary layer and double layer in ion exchange membrane transport', *Journal of Membrane Science*, 349: 369-79.

Ennaoui, A., S. Fiechter, Ch Pettenkofer, N. Alonso-Vante, K. Büker, M. Bronold, Ch Höpfner, and H. Tributsch. 1993. 'Iron disulfide for solar energy conversion', *Solar Energy Materials and Solar Cells*, 29: 289-370.

Faivre, D., and D. Schuler. 2008. 'Magnetotactic Bacteria and Magnetosomes', *Chem. Rev.*, 108: 4875.

Farrell, James, William D. Bostick, Robert J. Jarabek, and Joseph N. Fiedor. 1999. 'Electrosorption and reduction of pertechnetate by anodically polarized magnetite', *Environmental Science & Technology*, 33: 1244-49.

Fink, Christian, Sebastian Beblawy, Andreas M. Enkerlin, Lucas Mühling, Largus T. Angenent, and Bastian Molitor. 2021. 'A shuttle-vector system allows heterologous gene expression in the thermophilic methanogen *Methanothermobacter thermautotrophicus* ΔH', *mBio*, 12: e02766-21.

Fink, Christian, Gines Martinez-Cano, Jeremiah Shuster, Aurora Panzera, Kim E. Rennhack, Nils Rohbohm, Largus T. Angenent, and Bastian Molitor. 2023. 'The targeted deletion of genes responsible for expression of the Mth60 fimbriae leads to loss of cell-cell connections in *Methanothermobacter thermautotrophicus* ΔH', *Applied and Environmental Microbiology*, 89: e00575-23.

Fornaciari, Julie C., Michael R. Gerhardt, Jie Zhou, Yagya N. Regmi, Nemanja Danilovic, Alexis T. Bell, and Adam Z. Weber. 2020. 'The role of water in vapor-fed proton-exchange-membrane electrolysis', *Journal of The Electrochemical Society*, 167: 104508.

Fornero, Jeffrey J., Miriam Rosenbaum, and Largus T. Angenent. 2010. 'electric power generation from municipal, food, and animal wastewaters using microbial fuel cells', *Electroanalysis*, 22: 832-43.

Freguia, Stefano, Seiya Tsujimura, and Kenji Kano. 2010. 'Electron transfer pathways in microbial oxygen biocathodes', *Electrochimica Acta*, 55: 813-18.

Gawel, Alina, Theresa Jaster, Daniel Siegmund, Johannes Holzmann, Heiko Lohmann, Elias Klemm, and Ulf-Peter Apfel. 2022. 'Electrochemical CO_2 reduction - The macroscopic world of electrode design, reactor concepts & economic aspects', *iScience*, 25: 104011.

Geppert, Florian, Dandan Liu, Mieke van Eerten-Jansen, Eckhard Weidner, Cees Buisman, and Annemiek ter Heijne. 2016. 'Bioelectrochemical power-to-gas: state of the art and future perspectives', *Trends in Biotechnology*, 34: 879-94.

Geppert, Florian, Dandan Liu, Eckhard Weidner, and Annemiek ter Heijne. 2019. 'Redox-flow battery design for a methane-producing bioelectrochemical system', *International Journal of Hydrogen Energy*, 44: 21464 - 69.

Giddings, Cloelle G. S., Kelly P. Nevin, Trevor Woodward, Derek R. Lovley, and Caitlyn S. Butler. 2015. 'Simplifying microbial electrosynthesis reactor design', *Frontiers in microbiology*, 6: 468-68.

Gilboa-Garber, Nechama. 1971. 'Direct spectrophotometric determination of inorganic sulfide in biological materials and in other complex mixtures', *Analytical Biochemistry*, 43: 129-33.

Gomez Vidales, Abraham, Guillaume Bruant, Sasha Omanovic, and Boris Tartakovsky. 2021. 'Carbon dioxide conversion to C1 - C2 compounds in a microbial electrosynthesis cell with in situ electrodeposition of nickel and iron', *Electrochimica Acta*, 383: 138349.

Gorski, Christopher A., and Michelle M. Scherer. 2010. 'Determination of nanoparticulate magnetite stoichiometry by Mössbauer spectroscopy, acidic dissolution, and powder X-ray diffraction: A critical review', *American Mineralogist*, 95: 1017–26.

Guo, Wei, Ya-Xia Yin, Sen Xin, Yu-Guo Guo, and Li-Jun Wan. 2012. 'Superior radical polymer cathode material with a two-electron process redox reaction promoted by graphene', *Energy & Environmental Science*, 5: 5221–25.

Guzman, Juan J. L., Meryem O. Pehlivaner Kara, Margaret W. Frey, and Largus T. Angenent. 2017. 'Performance of electro-spun carbon nanofiber electrodes with conductive poly(3,4-ethylenedioxythiophene) coatings in bioelectrochemical systems', *Journal of Power Sources*, 356: 331 - 37.

Hackbarth, Max, Johannes Gescher, Harald Horn, and Johannes Eberhard Reiner. 2023. 'A scalable, rotating disc bioelectrochemical reactor (RDBER) suitable for the cultivation of both cathodic and anodic biofilms', *Bioresource Technology Reports*, 21: 101357.

Hallenbeck, Patrick C., Melanie Grogger, and Donald Veverka. 2014. 'Recent advances in microbial electrocatalysis', *Electrocatalysis*, 5: 319–29.

Halley, J. W., A. Schofield, and B. Berntson. 2012. 'Use of magnetite as anode for electrolysis of water', *Journal of Applied Physics*, 111: 124911.

He, Yu-Ting, Qian Fu, Yuan Pang, Qing Li, Jun Li, Xun Zhu, Ren-Hao Lu, Wei Sun, Qiang Liao, and Uwe Schröder. 2021. 'Customizable design strategies for high-performance bioanodes in bioelectrochemical systems', *iScience*, 24: 102163.

Hegner, Richard, Katharina Neubert, Cora Kroner, Dirk Holtmann, and Falk Harnisch. 2020. 'Coupled electrochemical and microbial catalysis for the production of polymer bricks', *ChemSusChem*, n/a.

Heitner-Wirguin, Carla. 1996. 'Recent advances in perfluorinated ionomer membranes: structure, properties and applications', *Journal of Membrane Science*, 120: 1-33.

Hirano, S., N. Matsumoto, M. Morita, K. Sasaki, and N. Ohmura. 2013. 'Electrochemical control of redox potential affects methanogenesis of the hydrogenotrophic methanogen *Methanothermobacter thermautotrophicus*', *Letters in Applied Microbiology*, 56: 315-21.

Hodges, Aaron, Anh Linh Hoang, George Tsekouras, Klaudia Wagner, Chong-Yong Lee, Gerhard F. Swiegers, and Gordon G. Wallace. 2022. 'A high-performance capillary-fed electrolysis cell promises more cost-competitive renewable hydrogen', *Nature Communications*, 13: 1304.

Holubowitch, Nicolas E., Ayokunle Omosebi, Xin Gao, James Landon, and Kunlei Liu. 2019. 'Membrane-free electrochemical deoxygenation of aqueous solutions using symmetric activated carbon electrodes in flow-through cells', *Electrochimica Acta*, 297: 163-72.

Hu, Tianzhao, Yuzuo Wang, Juan Li, Shaorui Chen, Ying Shi, Zhuangnan Li, Dianbo Ruan, Qun Xu, and Feng Li. 2021. 'Progress in the regulation of electrode/electrolyte interfacial reactions toward high-voltage aqueous hybrid capacitors', *Batteries & Supercaps*, n/a.

Iwakura, Chiaki, Tsuyoshi Kawai, Masatomo Nojima, and Hiroshi Yoneyama. 1987. 'A new electrode-active material for polymer batteries: polyvinylferrocene', *Journal of The Electrochemical Society*, 134: 791.

Izadi, Paniz, Marten Niklas Gey, Nicolas Schlüter, and Uwe Schröder. 2021. 'Bidirectional electroactive microbial biofilms and the role of biogenic sulfur in charge storage and release', *iScience*, 24: 102822.

Janáky, Csaba, Csaba Visy, Ottó Berkesi, and Etelka Tombácz. 2009. 'Conducting polymer-based electrode with magnetic behavior: Electrochemical synthesis of Poly(3-thiophene-acetic-acid)/Magnetite nanocomposite thin layers', *Journal of Physical Chemistry C*, 113: 1352–58.

Jhong, Huei-Ru “Molly”, Sichao Ma, and Paul JA Kenis. 2013. 'Electrochemical conversion of CO_2 to useful chemicals: current status, remaining challenges, and future opportunities', *Current Opinion in Chemical Engineering*, 2: 191–99.

Ji, Sang Gu, Haesol Kim, Woong Hee Lee, Hyung-Suk Oh, and Chang Hyuck Choi. 2021. 'Real-time monitoring of electrochemical carbon corrosion in alkaline media', *Journal of Materials Chemistry A*, 9: 19834-39.

Jourdin, Ludovic, and Thomas Burdyny. 2021. 'Microbial electrosynthesis: where do we go from here?', *Trends in Biotechnology*, 39: 359-69.

Jourdin, Ludovic, Stefano Freguia, Bogdan C. Donose, Jun Chen, Gordon G. Wallace, Jurg Keller, and Victoria Flexer. 2014. 'A novel carbon nanotube modified scaffold as an efficient biocathode material for improved microbial electrosynthesis', *Journal of Materials Chemistry A*, 2: 13093–102.

Jourdin, Ludovic, Timothy Grieger, Juliette Monetti, Victoria Flexer, Stefano Freguia, Yang Lu, Jun Chen, Mark Romano, Gordon G. Wallace, and Jurg Keller. 2015. 'High acetic acid production rate obtained by microbial electrosynthesis from carbon dioxide', *Environmental Science & Technology*, 49: 13566-74.

Jourdin, Ludovic, Sanne M. T. Raes, Cees J. N. Buisman, and David P. B. T. B. Strik. 2018. 'Critical biofilm growth throughout unmodified carbon felts allows continuous bioelectrochemical chain elongation from CO_2 up to caproate at high current density', *Frontiers in Energy Research*, 6.

Jourdin, Ludovic, João Sousa, Niels van Stralen, and David P. B. T. B. Strik. 2020. 'Techno-economic assessment of microbial electrosynthesis from CO_2 and/or organics: An interdisciplinary roadmap towards future research and application', *Applied Energy*, 279: 115775.

Ju, HyungKuk, Sukhvinder Badwal, and Sarbjit Giddey. 2018. 'A comprehensive review of carbon and hydrocarbon assisted water electrolysis for hydrogen production', *Applied Energy*, 231: 502-33.

Kaster, Anne-Kristin, Meike Goenrich, Henning Seedorf, Heiko Liesegang, Antje Wollherr, Gerhard Gottschalk, and Rudolf K. Thauer. 2011. 'More than 200 genes required for methane formation from H_2 and CO_2 and energy conservation are present in *Methanothermobacter marburgensis* and *Methanothermobacter thermautotrophicus*', *Archaea*, 2011: 973848.

Kiener, A., and T. Leisinger. 1983. 'Oxygen sensitivity of methanogenic bacteria', *Systematic and Applied Microbiology*, 4: 305-12.

Kim, K. J., A. G. Fane, M. Nystrom, A. Pihlajamaki, W. R. Bowen, and H. Mukhtar. 1996. 'Evaluation of electroosmosis and streaming potential for measurement of electric charges of polymeric membranes', *Journal of Membrane Science*, 116: 149-59.

Kim, Yoona, Sang-Mun Jung, Kyu-Su Kim, Hyun-Yup Kim, Jaesub Kwon, Jinhyeon Lee, Hyun-Seok Cho, and Yong-Tae Kim. 2022. 'Cathodic protection system against a reverse-current after shut-down in zero-gap alkaline water electrolysis', *JACS Au*, 2: 2491-500.

Kracke, Frauke, Jörg S. Deutzmann, Wenyu Gu, and Alfred M. Spormann. 2020. 'In situ electrochemical H_2 production for efficient and stable power-to-gas electromethanogenesis', *Green Chemistry*, 22: 6194-203.

Kracke, Frauke, Jörg S. Deutzmann, Buddhinie S. Jayathilake, Simon H. Pang, Swetha Chandrasekaran, Sarah E. Baker, and Alfred M. Spormann. 2021. 'Efficient

hydrogen delivery for microbial electrosynthesis via 3D-printed cathodes', *Frontiers in microbiology*, 12.

Kracke, Frauke, Andrew Barnabas Wong, Karen Maegaard, Joerg S. Deutzmann, McKenzie A. Hubert, Christopher Hahn, Thomas F. Jaramillo, and Alfred M. Spormann. 2019. 'Robust and biocompatible catalysts for efficient hydrogen-driven microbial electrosynthesis', *Communications Chemistry*, 2: 45.

Kumar, Manoj, Srikanth Sandipam, Suresh Kumar Puri, Sankara Sri Venkata Ramakumar, Ludovicus Diels, Lambertus Bouwan, Karolien Vanbroekhoven, and Deepak Pant. 2020. "Membrane-less reactor and biotransformation of carbon dioxide. ." *European Patent, EP 3831983A1*. Germany.

Kumar, Yogendra, and Jitendra S. Sangwai. 2023. 'A perspective on the effect of physicochemical parameters, macroscopic environment, additives, and economics to harness the large-scale hydrate-based CO_2 sequestration potential in oceans', *ACS Sustainable Chemistry & Engineering*, 11: 10950-79.

Lai, Agnese, Federico Aulenta, Marina Mingazzini, Maria Teresa Palumbo, Marco Petrangeli Papini, Roberta Verdini, and Mauro Majone. 2017. 'Bioelectrochemical approach for reductive and oxidative dechlorination of chlorinated aliphatic hydrocarbons (CAHs)', *Chemosphere*, 169: 351-60.

Lalvani, S. B., and M. Shami. 1985. 'Pyrite-assisted water electrolysis', *International Journal of Hydrogen Energy*, 10: 447-52.

Lee, Hyunjun, Boreum Lee, Manhee Byun, and Hankwon Lim. 2020. 'Economic and environmental analysis for PEM water electrolysis based on replacement moment and renewable electricity resources', *Energy Conversion and Management*, 224: 113477.

Leong, Jun Xing, Wan Ramli Wan Daud, Mostafa Ghasemi, Kien Ben Liew, and Manal Ismail. 2013. 'Ion exchange membranes as separators in microbial fuel cells for bioenergy conversion: A comprehensive review', *Renewable and Sustainable Energy Reviews*, 28: 575–87.

Liang, Yanliang, Zhanliang Tao, and Jun Chen. 2012. 'Organic electrode materials for rechargeable lithium batteries', *Advanced Energy Materials*, 2: 742–69.

Lin, Hui-Wen, Caroline Kustermans, Eleni Vaiopoulou, Antonin Prévoteau, Korneel Rabaey, Zhiguo Yuan, and Ilje Pikaar. 2017. 'Electrochemical oxidation of iron and alkalinity generation for efficient sulfide control in sewers', *Water Research*, 118: 114-20.

Liu, Hao, Guoxiu Wang, Jiazhao Wang, and David Wexler. 2008. 'Magnetite/carbon core-shell nanorods as anode materials for lithium-ion batteries', *Electrochemistry Communications*, 10: 1879–82.

Liu, Rui-Ting, Zheng-Long Xu, Fu-Min Li, Fei-Yang Chen, Jing-Ya Yu, Ya Yan, Yu Chen, and Bao Yu Xia. 2023. 'Recent advances in proton exchange membrane water electrolysis', *Chemical Society Reviews*, 52: 5652-83.

Liu, Shujuan, Yujie Feng, Jiaojiao Niu, Jia Liu, Nan Li, and Weihua He. 2019. 'A novel single chamber vertical baffle flow biocathode microbial electrochemical system with microbial separator', *Bioresource Technology*, 294: 122236.

Liu, Xiaoqing, Wei Xu, Dezhou Zheng, Zhifeng Li, Yinxiang Zeng, and Xihong Lu. 2020. 'Carbon cloth as an advanced electrode material for supercapacitors: progress and challenges', *Journal of Materials Chemistry A*, 8: 17938-50.

Logan, Bruce E. 2009. 'Exoelectrogenic bacteria that power microbial fuel cells', *Nature Reviews Microbiology*, 7: 375-81.

Logan, Bruce E., Bert Hamelers, René Rozendal, Uwe Schröder, Jürg Keller, Stefano Freguia, Peter Aelterman, Willy Verstraete, and Korneel Rabaey. 2006. 'Microbial fuel cells: Methodology and technology', *Environmental Science & Technology*, 40: 5181-92.

Logan, Bruce E., Ruggero Rossi, Ala'a Ragab, and Pascal E. Saikaly. 2019. 'Electroactive microorganisms in bioelectrochemical systems', *Nature Reviews Microbiology*, 17: 307-19.

Logan, Bruce E., Maxwell J. Wallack, Kyoung-Yeol Kim, Weihua He, Yujie Feng, and Pascal E. Saikaly. 2015. 'Assessment of microbial fuel cell configurations and power densities', *Environmental Science & Technology Letters*, 2: 206-14.

Lohner, Svenja, Joerg Deutzmann, Bruce Logan, John Leigh, and Alfred Spormann. 2014. 'Hydrogenase-independent uptake and metabolism of electrons by the archaeon *Methanococcus maripaludis*', *The ISME journal*, 8.

Lovley, Derek R., and Kelly P. Nevin. 2012. "Microbial production of multi-carbon chemicals and fuels from water and carbon dioxide using electric current." *USA Patent, 9856449*. USA.

Lu, An-Hui, E. L. Salabas, and Ferdi Schüth. 2007. 'Magnetic nanoparticles: Synthesis, protection, functionalization, and application', *Angewandte Chemie International Edition*, 46: 1222-44.

Luna, Phil De, Christopher Hahn, Drew Higgins, Shaffiq A. Jaffer, Thomas F. Jaramillo, and Edward H. Sargent. 2019. 'What would it take for renewably powered electrosynthesis to displace petrochemical processes?', *Science*, 364: eaav3506.

Ma, Sichao, Masaaki Sadakiyo, Raymond Luo, Minako Heima, Miho Yamauchi, and Paul J. A. Kenis. 2016. 'One-step electrosynthesis of ethylene and ethanol from CO_2 in an alkaline electrolyzer', *Journal of Power Sources*, 301: 219-28.

Mac Dowell, Niall, Paul S. Fennell, Nilay Shah, and Geoffrey C. Maitland. 2017. 'The role of CO_2 capture and utilization in mitigating climate change', *Nature Climate Change*, 7: 243-49.

Mališ, Jakub, Martin Paidar, Tomas Bystron, Libuše Brožová, Alexander Zhigunov, and Karel Bouzek. 2018. 'Changes in Nafion® 117 internal structure and related properties during exposure to elevated temperature and pressure in an aqueous environment', *Electrochimica Acta*, 262: 264-75.

Mano, Nicolas, Fei Mao, and Adam Heller. 2004. 'A miniature membrane-less biofuel cell operating at +0.60 V under physiological conditions', *ChemBioChem*, 5: 1703-05.

Mao, Yingling, Benhu Zhou, and Sen Peng. 2020. 'Magnetite ultrafine particles/porous reduced graphene oxide in situ grown onto Ni foam as a binder-free electrode for supercapacitors', *RSC Advances*, 10: 20753-64.

Martin, Agate, Patrick Trinke, Boris Bensmann, and Richard Hanke-Rauschenbach. 2022. 'Hydrogen crossover in PEM water electrolysis at current densities up to 10 A cm^{-2}', *Journal of The Electrochemical Society*, 169: 094507.

Martin, Matthew R., Jeffrey J. Fornero, Rebecca Stark, Laurens Mets, and Largus T. Angenent. 2013. 'A single-culture bioprocess of *Methanothermobacter*

thermautotrophicus to upgrade digester biogas by CO_2-to-CH_4 conversion with H_2', *Archaea*, 2013.

Matula, R. A. 1979. 'Electrical resistivity of copper, gold, palladium, and silver', *Journal of Physical and Chemical Reference Data*, 8: 1147-298.

Mayer, Florian, Franziska Enzmann, Antonio Martinez Lopez, and Dirk Holtmann. 2019. 'Performance of different methanogenic species for the microbial electrosynthesis of methane from carbon dioxide', *Bioresource Technology*, 289: 121706.

McCrory, Charles C. L., Suho Jung, Ivonne M. Ferrer, Shawn M. Chatman, Jonas C. Peters, and Thomas F. Jaramillo. 2015. 'Benchmarking Hydrogen Evolving Reaction and Oxygen Evolving Reaction Electrocatalysts for Solar Water Splitting Devices', *Journal of the American Chemical Society*, 137: 4347-57.

McLaughlin, Hope, Anna A. Littlefield, Maia Menefee, Austin Kinzer, Tobias Hull, Benjamin K. Sovacool, Morgan D. Bazilian, Jinsoo Kim, and Steven Griffiths. 2023. 'Carbon capture utilization and storage in review: Sociotechnical implications for a carbon reliant world', *Renewable and Sustainable Energy Reviews*, 177: 113215.

Ménard, Isabelle, Evelyne Thiffault, Werner A. Kurz, and Jean-François Boucher. 2023. 'Carbon sequestration and emission mitigation potential of afforestation and reforestation of unproductive territories', *New Forests*, 54: 1013-35.

Mishra, Akanksha, Jean Nepomuscene Ntihuga, Bastian Molitor, and Largus T. Angenent. 2020. 'Power-to-protein: Carbon fixation with renewable electric power to feed the world', *Joule*, 4: 1142-47.

Moench, Thomas T., and J. G. Zeikus. 1983. 'An improved preparation method for a titanium (III) media reductant', *Journal of Microbiological Methods*, 1: 199-202.

Moreira, Fernanda, Edson Roberto Santana, and Almir Spinelli. 2020. 'Ionic liquid-supported magnetite nanoparticles as electrode modifier materials for estrogens sensing', *Scientific Reports*, 10: 1955.

Moscoviz, Roman, Javiera Toledo-Alarcón, Eric Trably, and Nicolas Bernet. 2016. 'Electro-fermentation: How to drive fermentation using electrochemical systems', *Trends in Biotechnology*, 34: 856-65.

Nevin, Kelly P., Trevor L. Woodard, Ashley E. Franks, Zarath M. Summers, and Derek R. Lovley. 2010. 'Microbial electrosynthesis: Feeding microbes electricity to convert carbon dioxide and water to multicarbon extracellular organic compounds', *mBio*, 1: e00103-10.

Nishimura, Norihiro, Shinko Kitaura, Akio Mimura, and Yoshimasa Takahara. 1992. 'Cultivation of thermophilic methanogen KN-15 on H_2-CO_2 under pressurized conditions', *Journal of Fermentation and Bioengineering*, 73: 477-80.

Oh, Sang-Eun, and Bruce E. Logan. 2006. 'Proton exchange membrane and electrode surface areas as factors that affect power generation in microbial fuel cells', *Applied Microbiology and Biotechnology*, 70: 162-69.

Ouboter, Heleen T., Tom Berben, Stefanie Berger, Mike S. M. Jetten, Tom Sleutels, Annemiek Ter Heijne, and Cornelia U. Welte. 2022. 'Methane-dependent extracellular electron transfer at the bioanode by the anaerobic archaeal methanotroph "*Candidatus Methanoperedens*"', *Frontiers in microbiology*, 13.

Oyaizu, Kenichi, and Hiroyuki Nishide. 2009. 'Radical polymers for organic electronic devices: A radical departure from conjugated polymers?', *Advanced Materials*, 21: 2339-44.

Park, D. H., M. Laivenieks, M. V. Guettler, M. K. Jain, and J. G. Zeikus. 1999. 'Microbial utilization of electrically reduced neutral red as the sole Electron donor for growth and metabolite production', *Applied and Environmental Microbiology*, 65: 2912.

Park, D. H., and J. G. Zeikus. 1999. 'Utilization of electrically reduced neutral red by *Actinobacillus succinogenes*: Physiological function of neutral red in membrane-driven fumarate reduction and energy conservation', *Journal of Bacteriology*, 181: 2403-10.

Pierson, Hugh O. 1994. *Handbook of carbon, graphite, diamonds and fullerenes* (William Andrew).

Prévoteau, Antonin, Jose M. Carvajal-Arroyo, Ramon Ganigué, and Korneel Rabaey. 2020. 'Microbial electrosynthesis from CO_2: forever a promise?', *Current Opinion in Biotechnology*, 62: 48-57.

Puig, Sebastià, Ramon Ganigué, Pau Batlle-Vilanova, M. Dolors Balaguer, Lluís Bañeras, and Jesús Colprim. 2017. 'Tracking bio-hydrogen-mediated production of commodity chemicals from carbon dioxide and renewable electricity', *Bioresource Technology*, 228: 201-09.

Rabaey, Korneel, and René A. Rozendal. 2010. 'Microbial electrosynthesis -- revisiting the electrical route for microbial production', *Nature Reviews Microbiology*, 8: 706-16.

Rad, Ramineh, Tito Gehring, Kevinjeorjios Pellumbi, Daniel Siegmund, Edith Nettmann, Marc Wichern, and Ulf-Peter Apfel. 2023. 'A hybrid bioelectrochemical system coupling a zero-gap cell and a methanogenic reactor for carbon dioxide reduction using a wastewater-derived catholyte', *Cell Reports Physical Science*, 4.

Ren, Guoping, Piao Chen, Jing Yu, Jianbo Liu, Jie Ye, and Shungui Zhou. 2019. 'Recyclable magnetite-enhanced electromethanogenesis for biomethane production from wastewater', *Water Research*, 166: 115095.

Renault, Stéven, Joaquin Geng, Franck Dolhem, and Philippe Poizot. 2011. 'Evaluation of polyketones with N-cyclic structure as electrode material for electrochemical energy storage: case of pyromellitic diimide dilithium salt', *Chemical Communications*, 47: 2414–16.

Roberts, Joseph J. P., John A. Westgard, Laura M. Cooper, and Royce W. Murray. 2014. 'Solution voltammetry of 4 nm magnetite iron oxide nanoparticles', *Journal of the American Chemical Society*, 136: 10783-89.

Rohbohm, Nils, Tianran Sun, Ramiro Blasco-Gómez, James M. Byrne, Andreas Kappler, and Largus T. Angenent. 2023. 'Carbon oxidation with sacrificial anodes to inhibit O_2 evolution in membrane-less bioelectrochemical systems for microbial electrosynthesis', *EES Catalysis*, 1: 972-86.

Rosenbaum, Miriam A., and Alexander W. Henrich. 2014. 'Engineering microbial electrocatalysis for chemical and fuel production', *Current Opinion in Biotechnology*, 29: 93–98.

Rosenbaum, Miriam, Federico Aulenta, Marianna Villano, and Largus T. Angenent. 2011. 'Cathodes as electron donors for microbial metabolism: Which

extracellular electron transfer mechanisms are involved?', *Bioresource Technology*, 102: 324-33.

Rosenbaum, Miriam, Michael A. Cotta, and Largus T. Angenent. 2010. 'Aerated *Shewanella oneidensis* in continuously fed bioelectrochemical systems for power and hydrogen production', *Biotechnology and Bioengineering*, 105: 880-88.

Rossi, Ruggero, Derek M. Hall, Le Shi, Nicholas R. Cross, Christopher A. Gorski, Michael A. Hickner, and Bruce E. Logan. 2021. 'Using a vapor-fed anode and saline catholyte to manage ion transport in a proton exchange membrane electrolyzer', *Energy & Environmental Science*, 14: 6041-49.

Rotaru, Amelia-Elena, Pravin Malla Shrestha, Fanghua Liu, Beatrice Markovaite, Shanshan Chen, Kelly P. Nevin, and Derek R. Lovley. 2014. 'Direct Interspecies Electron Transfer between *Geobacter metallireducens* and Methanosarcina barkeri', *Applied and Environmental Microbiology*, 80: 4599.

Rovira-Alsina, Laura, M. Dolors Balaguer, and Sebastià Puig. 2022. 'Transition roadmap for thermophilic carbon dioxide microbial electrosynthesis: Testing with real exhaust gases and operational control for a scalable design', *Bioresource Technology*, 365: 128161.

Rozendal, René A., Hubertus V. M. Hamelers, and Cees J. N. Buisman. 2006. 'Effects of membrane cation transport on pH and microbial fuel cell performance', *Environmental Science & Technology*, 40: 5206-11.

Rozendal, René A., Hubertus V. M. Hamelers, Gerrit J. W. Euverink, Sybrand J. Metz, and Cees J. N. Buisman. 2006. 'Principle and perspectives of hydrogen production through biocatalyzed electrolysis', *International Journal of Hydrogen Energy*, 31: 1632-40.

Rozendal, René A., Hubertus V. M. Hamelers, Redmar J. Molenkamp, and Cees J. N. Buisman. 2007. 'Performance of single chamber biocatalyzed electrolysis with different types of ion exchange membranes', *Water Research*, 41: 1984–94.

Rusmanis, Davis, Richard O'Shea, David M. Wall, and Jerry D. Murphy. 2019. 'Biological hydrogen methanation systems – an overview of design and efficiency', *Bioengineered*, 10: 604-34.

Sabareeswaran, S., R. Balaji, K. Ramya, N. Rajalakshmi, and K. S. Dhathathereyan. 2013. 'Carbon assisted water electrolysis for hydrogen generation', *AIP Conference Proceedings*, 1538: 43-47.

Sandfeld, Tobias, Louise Vinther Grøn, Laura Munoz, Rikke Louise Meyer, Klaus Koren, and Jo Philips. 2024. 'Considerations on the use of microsensors to profile dissolved H_2 concentrations in microbial electrochemical reactors', *PLOS ONE*, 19: e0293734.

Sandy, Moriah, and Alison Butler. 2009. 'Microbial iron acquisition: Marine and terrestrial siderophores', *Chemical reviews*, 109: 4580.

Santoro, Carlo, Catia Arbizzani, Benjamin Erable, and Ioannis Ieropoulos. 2017. 'Microbial fuel cells: From fundamentals to applications. A review', *Journal of Power Sources*, 356: 225-44.

Santoro, Carlo, Francesca Soavi, Catia Arbizzani, Alexey Serov, Sadia Kabir, Kayla Carpenter, Orianna Bretschger, and Plamen Atanassov. 2016. 'Co-generation of hydrogen and power/current pulses from supercapacitive MFCs using novel HER iron-based catalysts', *Electrochimica Acta*, 220: 672-82.

Schönheit, Peter, Johanna Moll, and Rudolf K. Thauer. 1979. 'Nickel, cobalt, and molybdenum requirement for growth of *Methanobacterium thermoautotrophicum*', *Archives of Microbiology*, 123: 105-07.

Schröder, Uwe, Falk Harnisch, and Largus T. Angenent. 2015. 'Microbial electrochemistry and technology: terminology and classification', *Energy Environ. Sci.*, 8: 513-19.

Sharma, Mohita, Yolanda Alvarez-Gallego, Wafa Achouak, Deepak Pant, Priyangshu M. Sarma, and Xochitl Dominguez-Benetton. 2019. 'Electrode material properties for designing effective microbial electrosynthesis systems', *Journal of Materials Chemistry A*, 7: 24420–36.

Shima, Seigo, and Rudolf K. Thauer. 2021. '*Methanothermobacter* — Biokatalysator für die Energiewende', *BIOspektrum*, 27: 14-17.

Shirakawa, Hideki, Edwin J. Louis, Alan G. MacDiarmid, Chwan K. Chiang, and Alan J. Heeger. 1977. 'Synthesis of electrically conducting organic polymers: halogen derivatives of polyacetylene, (CH)', *Journal of the Chemical Society, Chemical Communications*: 578–80.

Sleutels, Tom H. J. A., Annemiek Ter Heijne, Cees J. N. Buisman, and Hubertus V. M. Hamelers. 2012. 'Bioelectrochemical Systems: An Outlook for Practical Applications', *ChemSusChem*, 5: 1012-19.

Soleymani, Meysam, Solmaz Khalighfard, Saeed Khodayari, Hamid Khodayari, Mohammad Reza Kalhori, Mahmoud Reza Hadjighassem, Zhila Shaterabadi, and Ali Mohammad Alizadeh. 2020. 'Effects of multiple injections on the efficacy and cytotoxicity of folate-targeted magnetite nanoparticles as theranostic agents for MRI detection and magnetic hyperthermia therapy of tumor cells', *Scientific Reports*, 10: 1695.

Solomon, Susan, Gian-Kasper Plattner, Reto Knutti, and Pierre Friedlingstein. 2009. 'Irreversible climate change due to carbon dioxide emissions', *Proceedings of the National Academy of Sciences*, 106: 1704–09.

Song, Zhiping, and Haoshen Zhou. 2013. 'Towards sustainable and versatile energy storage devices: an overview of organic electrode materials', *Energy & Environmental Science*, 6: 2280-301.

Sorwat, Julian, Adrian Mellage, Andreas Kappler, and James M. Byrne. 2020. 'Immobilizing magnetite onto quartz sand for chromium remediation', *Journal of Hazardous Materials*, 400: 123139.

Steinbusch, Kirsten J. J., Hubertus V. M. Hamelers, Joris D. Schaap, Christel Kampman, and Cees J. N. Buisman. 2010. 'Bioelectrochemical ethanol production through mediated acetate reduction by mixed cultures', *Environmental Science & Technology*, 44: 513-17.

Stookey, Lawrence L. 1970. 'Ferrozine---a new spectrophotometric reagent for iron', *Analytical Chemistry*, 42: 779-81.

Stucki, S., G. G. Scherer, S. Schlagowski, and E. Fischer. 1998. 'PEM water electrolysers: evidence for membrane failure in 100kW demonstration plants', *Journal of Applied Electrochemistry*, 28: 1041-49.

Sun, Tianran, Barnaby D. A. Levin, Juan J. L. Guzman, Akio Enders, David A. Muller, Largus T. Angenent, and Johannes Lehmann. 2017. 'Rapid electron transfer by the carbon matrix in natural pyrogenic carbon', *Nature Communications*, 8: 14873.

Ter Heijne, Annemiek, Olivier Schaetzle, Sixto Gimenez, Francisco Fabregat-Santiago, Juan Bisquert, David P. B. T. B. Strik, Frédéric Barrière, Cees J. N. Buisman, and Hubertus V. M. Hamelers. 2011. 'Identifying charge and mass transfer resistances of an oxygen reducing biocathode', *Energy & Environmental Science*, 4: 5035-43.

Thauer, Rudolf K., Anne-Kristin Kaster, Meike Goenrich, Michael Schick, Takeshi Hiromoto, and Seigo Shima. 2010. 'Hydrogenases from methanogenic archaea, nickel, a novel cofactor, and H_2 storage', *Annual Review of Biochemistry*, 79: 507-36.

Thauer, Rudolf K., Anne-Kristin Kaster, Henning Seedorf, Wolfgang Buckel, and Reiner Hedderich. 2008. 'Methanogenic archaea: ecologically relevant differences in energy conservation', *Nature Reviews Microbiology*, 6: 579-91.

Thema, M., F. Bauer, and M. Sterner. 2019. 'Power-to-gas: Electrolysis and methanation status review', *Renewable and Sustainable Energy Reviews*, 112: 775-87.

Thoma, Christine, Monika Frank, Reinhard Rachel, Silvia Schmid, Daniela Näther, Gerhard Wanner, and Reinhard Wirth. 2008. 'The Mth60 fimbriae of *Methanothermobacter thermoautotrophicus* are functional adhesins', *Environmental Microbiology*, 10: 2785-95.

Tosun, Jale, Mile Mišić, and Nicole M. Schmidt. 2018. 'The public's perception of international climate leadership: Insights from the european union.' in, *Transformative Climates and Accountable Governance* (Palgrave Macmillan, Cham).

Tremblay, Pier-Luc, Largus T. Angenent, and Tian Zhang. 2017. 'Extracellular electron uptake: Among autotrophs and mediated by surfaces', *Trends in Biotechnology*, 35: 360-71.

Trinke, P., P. Haug, J. Brauns, B. Bensmann, R. Hanke-Rauschenbach, and T. Turek. 2018. 'Hydrogen crossover in PEM and alkaline water electrolysis: Mechanisms, direct comparison and mitigation strategies', *Journal of The Electrochemical Society*, 165: F502.

Umetsu, Masaki, Takaaki Sunouchi, Yasuhiro Fukuda, Hideyuki Takahashi, and Chika Tada. 2020. 'Functional group distribution of the carrier surface influences adhesion of *Methanothermobacter thermautotrophicus*', *Archaea*, 2020: 9432803.

Van Eerten-Jansen, Mieke C. A. A., Annemiek Ter Heijne, Cees J. N. Buisman, and Hubertus V. M. Hamelers. 2012. 'Microbial electrolysis cells for production of methane from CO_2: long-term performance and perspectives', *International Journal of Energy Research*, 36: 809-19.

Van Eerten-Jansen, Mieke C. A. A., Anna B. Veldhoen, Caroline M. Plugge, Alfons J. M. Stams, Cees J. N. Buisman, and Annemiek Ter Heijne. 2013. 'Microbial community analysis of a methane-producing biocathode in a bioelectrochemical System', *Archaea*, 2013.

Verhallen, P. T. H. M., L. J. P. Oomen, A. J. J. M. v d Elsen, J. Kruger, and J. M. H. Fortuin. 1984. 'The diffusion coefficients of helium, hydrogen, oxygen and nitrogen in water determined from the permeability of a stagnant liquid layer in the quasi-s', *Chemical Engineering Science*, 39: 1535-41.

Verwey, E. J. W. 1939. 'Electronic conduction of magnetite (Fe_3O_4) and its transition point at low temperatures', *Nature*, 144: 327–28.

Viggi, C. Cruz, S. Colantoni, F. Falzetti, A. Bacaloni, D. Montecchio, and F. Aulenta. 2020. 'Conductive magnetite nanoparticles enhance the microbial electrosynthesis of acetate from CO_2 while diverting electrons away from methanogenesis', *Fuel Cells*, 20: 98-106.

Villano, Marianna, Federico Aulenta, Costanza Ciucci, Tommaso Ferri, Antonio Giuliano, and Mauro Majone. 2010. 'Bioelectrochemical reduction of CO_2 to CH_4 via direct and indirect extracellular electron transfer by a hydrogenophilic methanogenic culture', *Bioresource Technology*, 101: 3085-90.

von Stockar, U., and J. S. Liu. 1999. 'Does microbial life always feed on negative entropy? Thermodynamic analysis of microbial growth', *Biochimica et Biophysica Acta (BBA) - Bioenergetics*, 1412: 191-211.

Vu, Mung Thi, Md Tabish Noori, and Booki Min. 2019. 'Conductive magnetite nanoparticles trigger syntrophic methane production in single chamber microbial electrochemical systems', *Bioresource Technology*: 122265.

Walspurger, Stéphane, Gerard D. Elzinga, Jan Wilco Dijkstra, Marija Sarić, and Wim G. Haije. 2014. 'Sorption enhanced methanation for substitute natural gas production: Experimental results and thermodynamic considerations', *Chemical Engineering Journal*, 242: 379-86.

Walz, F., L. Torres, K. Bendimya, C. de Francisco, and H. Kronmüller. 1997. 'Analysis of magnetic after-effect spectra in titanium-doped magnetite', *physica status solidi (a)*, 164: 805–20.

Wang, Heming, and Zhiyong Jason Ren. 2013. 'A comprehensive review of microbial electrochemical systems as a platform technology', *Biotechnology Advances*, 31: 1796 - 807.

Weng, Guoming, Yuzhi Su, Zhaoqing Liu, Jianhua Zhang, Wen Dong, and Changwei Xu. 2009. 'Electrochemical properties of novel organodisulfide poly 1,2-bis(thiophen-3-ylmethyl)disulfane as cathode material for secondary lithium batteries', *Energy*, 34: 1351-54.

White, Art F., Maria L. Peterson, and Michael F. Hochella. 1994. 'Electrochemistry and dissolution kinetics of magnetite and ilmenite', *Geochimica et Cosmochimica Acta*, 58: 1859-75.

Wu, Yiwen, Ronghua Zeng, Junmin Nan, Dong Shu, Yongcai Qiu, and Shu-Lei Chou. 2017. 'Quinone electrode materials for rechargeable lithium/sodium ion batteries', *Advanced Energy Materials*, 7: 1700278.

Xu, Juan, Guo-Ping Sheng, Hong-Wei Luo, Wen-Wei Li, Long-Fei Wang, and Han-Qing Yu. 2012. 'Fouling of proton exchange membrane (PEM) deteriorates the performance of microbial fuel cell', *Water Research*, 46: 1817-24.

Yahiro, Hidenori, Yamato Matsunaga, Makiko Asamoto, and Tsuyoshi Yamaji. 2019. 'Low potential electrolysis of aqueous glycerin using polymer electrolyte membrane', *ECS Transactions*, 25: 1943-49.

Yee, Mon Oo, Joerg Deutzmann, Alfred Spormann, and Amelia-Elena Rotaru. 2020. 'Cultivating electroactive microbes—from field to bench', *Nanotechnology*, 31: 174003.

Yekini Suberu, Mohammed, Mohd Wazir Mustafa, and Nouruddeen Bashir. 2014. 'Energy storage systems for renewable energy power sector integration and

mitigation of intermittency', *Renewable and Sustainable Energy Reviews*, 35: 499-514.

Yi, Hana, Kelly P. Nevin, Byoung-Chan Kim, Ashely E. Franks, Anna Klimes, Leonard M. Tender, and Derek R. Lovley. 2009. 'Selection of a variant of *Geobacter sulfurreducens* with enhanced capacity for current production in microbial fuel cells', *Biosensors and Bioelectronics*, 24: 3498-503.

Yi, Youngmi, Gisela Weinberg, Marina Prenzel, Mark Greiner, Saskia Heumann, Sylvia Becker, and Robert Schlögl. 2017. 'Electrochemical corrosion of a glassy carbon electrode', *Catalysis Today*, 295: 32-40.

Yin, Renhe, Yonggang Zhao, Shiyin Lu, Haomin Wang, Weimin Cao, and Qinbai Fan. 2009. 'Electrocatalytic oxidation of coal on Ti-supported metal oxides coupled with liquid catalysts for H_2 production', *Electrochimica Acta*, 55: 46-51.

Yuan, Ke, Eugene S. Ilton, Mark R. Antonio, Zhongrui Li, Peter J. Cook, and Udo Becker. 2015. 'Electrochemical and spectroscopic evidence on the one-electron reduction of U(VI) to U(V) on magnetite', *Environmental Science & Technology*, 49: 6206-13.

Yuan, Ke, Devon Renock, Rodney C. Ewing, and Udo Becker. 2015. 'Uranium reduction on magnetite: Probing for pentavalent uranium using electrochemical methods', *Geochimica et Cosmochimica Acta*, 156: 194-206.

Zebardast, H. R., S. Rogak, and E. Asselin. 2012. 'Use of EIS to measure the rate of H_2O_2 decomposition on a bulk magnetite electrode in alkaline solution', *Journal of The Electrochemical Society*, 159: B831–B38.

Zeppilli, Marco, Edoardo Dell'Armi, Lorenzo Cristiani, Marco Petrangeli Papini, and Mauro Majone. 2019. 'Reductive/oxidative sequential bioelectrochemical process for perchloroethylene removal', *Water*, 11: 2579.

Zhang, Tianyu, Weitao Li, Kai Huang, Huazhang Guo, Zhengyuan Li, Yanbo Fang, Ram Manohar Yadav, Vesselin Shanov, Pulickel M. Ajayan, Liang Wang, Cheng Lian, and Jingjie Wu. 2021. 'Regulation of functional groups on graphene quantum dots directs selective CO_2 to CH_4 conversion', *Nature Communications*, 12: 5265.

Zhang, Xiaoyuan, Shaoan Cheng, Xia Huang, and Bruce E. Logan. 2010. 'Improved performance of single-chamber microbial fuel cells through control of membrane deformation', *Biosensors and Bioelectronics*, 25: 1825–28.

Zhang, Yuanyuan, Fenpei Li, Xiangqing Liu, Jiaxing Lu, and Guirong Zhang. 2017. 'Promoting influence of activated carbon used in carbon paste electrode on platinum nanoparticles efficiency in methanol electrooxidation', *Electrochimica Acta*, 242: 165-72.

Zhao, Junjie, Zhengkai Tu, and Siew Hwa Chan. 2021. 'Carbon corrosion mechanism and mitigation strategies in a proton exchange membrane fuel cell (PEMFC): A review', *Journal of Power Sources*, 488: 229434.

Zhou, Min, Jianfeng Qian, Xinping Ai, and Hanxi Yang. 2011. 'Redox-active Fe(CN)64–-Doped conducting polymers with greatly enhanced capacity as cathode materials for Li-ion batteries', *Advanced Materials*, 23: 4913-17.

Zhou, Ming, Jie Ding, Li-ping Guo, and Qing-kun Shang. 2007. 'Electrochemical behavior of l-Cysteine and its detection at ordered mesoporous carbon-modified glassy carbon electrode', *Analytical Chemistry*, 79: 5328-35.

Zhu, Hao, Zhiwei Dong, Qiong Huang, Tian-shun Song, and Jingjing Xie. 2019. 'Fe_3O_4/granular activated carbon as an efficient three-dimensional electrode to enhance the microbial electrosynthesis of acetate from CO_2', *RSC Advances*, 9: 34095-101.